Synthesis and Crystallography of Cerium(IV) Bis Porphyrinates and Hafnium(IV) mono Porphyrinates; a Tool Box for Supramolecular Chemistry

by

Alexander Falber

A dissertation submitted to the Graduate Faculty in Chemistry
in partial fulfillment of the requirements for the degree of Doctor of Philosophy,
The City University of New York

2007

ProQuest Information and Learning Company
300 North Zeeb Road
P.O. Box 1346
Ann Arbor, MI 48106-1346

This manuscript has been read and accepted for the Graduate Faculty in Chemistry in satisfaction of the dissertation requirements for the degree of Doctor of Philosophy

12/06/06	Dr. Charles Michael Drain
Date	Chair of examining Committee
12/14/06	Dr. Michael Green
Date	Acting Executive Officer

Dr. L. Francesconi

Dr. A. Couzis

Dr. K. Grohmann

Dr. H. Matsui

Dr. L. Todaro

Supervisory Committee

THE CITY UNIVERSITY OF NEW YORK

Abstract

Synthesis and Crystallography of Cerium(IV) Bis Porphyrinates and Hafnium(IV) mono Porphyrinates; a Tool Box for Supramolecular Chemistry

by

Alexander Falber

Advisor: Professor Charles Michael Drain

Cerium(IV) bis tetra aryl porphyrinato "sandwich" complexes, CeP_2, were synthesized in a solvent mixture of 1,2,4 trichlorobenzene and 1-dodecanol. The porphyrin is deprotonated to the Na_2P species *in situ* using sodium dodecanate and then metalated with cerium, under argon at 205°C reflux, using the cerium (III) tris-acetylacetonate hydrate starting complex, $Ce(acac)_3 \bullet H_2O_x$. CeP_2 complex formation is achieved in 2-4 hours in yields equal to or higher than reported preparations. Structural studies of these complexes using NMR and crystallographic techniques have displayed asymmetric distortions of the porphyrin macrocycles not previously reported.

Hafnium(IV) mono porphyrinate complexes of the type $Hf(P)L_2$, where L = Cl^-, acetate (OAc^-), octinoate (oct), pentanoate (pent), para-amino benzoate (PABA), peroxo (O_2^{-2}), HPO_4^{-2}, and SO_4^{-2} have been synthesized according to four unique methods that cater to a wide variety of porphyrins not previously reported in hafnium porphyrinate chemistry. The methods use refluxing solvent mixtures of 1-chloronapthalene, dodecanol, and *o*-cresol under argon to metalate porphyrins with the hafnium (IV) ion from $HfCl_4$. A solventless method has also been developed using, hafnium (IV) bis

cyclopentadienyl dichloride, $Hf(cp)_2Cl_2$, in a melt with the porphyrins at 300°C. The compounds have been purified as the $Hf(P)OAc_2$ derivative using chromatography over silica. The other mentioned derivatives have been formed in quantitative yield by exchange of the acetate ligands and are also, in a large part, new to the field of hafnium porphyrinate chemistry . The crystal structure of the SO_4^{-2}, HPO_4^{-2}, and the O_2^{-2} complexes reveal bridged dimer crystal structures that also exist as dimers in solution according to spectroscopic evidence.

Stirring solutions of the $Hf(TPP)OAc_2$ and the $Hf(TPyP)OAc_2$ complexes with the Keggin lacunary polyoxometalate $H_3PW_{11}O_{39}[TBA]_4$, generates the ternary complexes, $(TPP)HfPW_{11}O_{39}[TBA]_5$ and $(TPyP)HfPW_{11}O_{39}[TBA]_5$, that have been isolated and characterized. The crystal structure for the TPyP ternary complex reveals that the POM draws the hafnium ion further away from the porphyrin core than its relative position in the crystal structure of the $Hf(TPyP)OAc_2$ complex. This results in spectroscopic shifts observed in the UV-Visible absorption, ^1H NMR, and ^{31}P NMR spectra.

ב' ד

רבות מחשבות בלב איש ועצת ד' היא תקום.

For Romy, this is only the beginning

Acknowledgements

I would like to thank my mentor, Dr. Drain for his guidance, but mostly for the creative freedom he has granted me in laboratory. I am also thankful for the opportunities he has given me for my research abroad in Tel Aviv University under the guidance of our collaborator, Dr. Israel Goldberg. I thank Dr. Goldberg for opening his lab to me and taking time to introduce me to crystallography. Our crystallographer at Hunter College, Dr. Louis Todaro, deserves a great deal of thanks for the many hours he committed to solving my crystal structures and doing so at an exhaustive pace.

I thank the rest of my committee, Dr. Grohmann, Dr. Francesconi, Dr. Matsui, and Dr. Couzis for their support and guidance over the past four years. Dr. Grohmann not only served on my doctoral committee, but advised me on many occasions and helped me with especially delicate reactions. Dr. Francesconi helped me link porphyrin and polyoxometalate chemistry; the finale of my work. I also thank my friend and colleague, Mikki Vinodu, for his guidance these past two years. Dr. Ben. P. Burton-Pye and Dr. Blumenstein are greatly appreciated for their guidance in NMR spectroscopy and Mike Favilla for his assistance in the lab.

My wife, Romy, deserves a lifetime of gratitude for her support and helping me through this challenge. You are my home and greatest reason to succeed.

I thank my parents, Cary and Kathy Falber, for teaching me how to learn and to know that nothing I truly want is beyond my reach.

Table of contents

List of figures

Introduction

Chapter 1

Chapter 1 appendix

Chapter 2

Chapter 2 appendix

Chapter 3

Chapter 3 appendix

List of schemes and tables

Chapter 1

Chapter 2

Chapter 3

Introduction:

In this work are presented a series of new methods and compounds in the synthesis of both cerium(IV) bis tetra aryl porphyrinate complexes, CeP_2, and hafnium (IV) mono tetra aryl porphyrinate complexes, $Hf(P)L_2$ where L is a counter ligand such as acetate as well as a series of other oxo-bearing ligands that generate a whole library of new complexes. The common factor between the cerium and hafnium complexes is that the large f-block metal ion rests outside of the porphyrin core as their respective ionic radii are far too large to fit inside the tetra-pyrrole ring (**Figure 1)**.

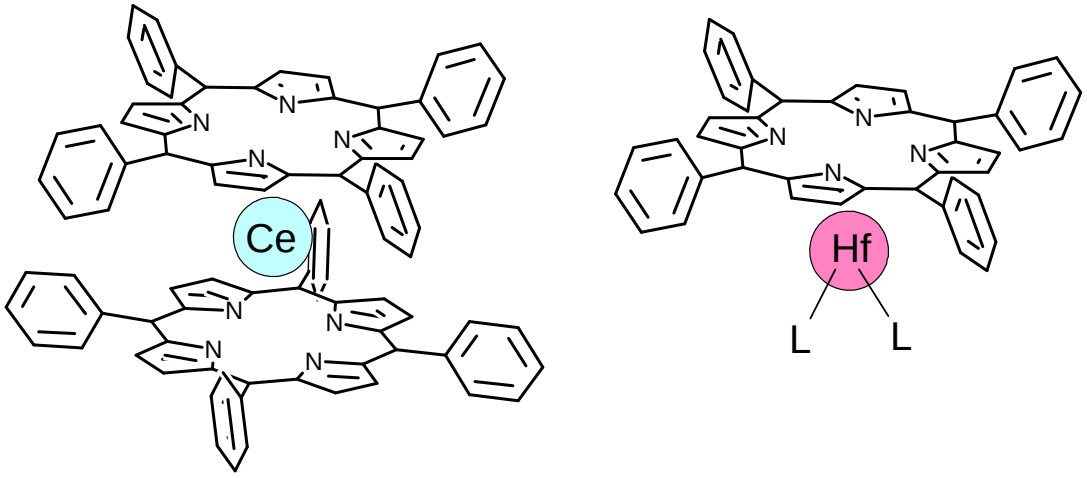

Figure 1. Basic CeP_2 and $Hf(P)L_2$ structures

For CeP_2 complexes this allows a "sandwich" complex where one cerium atom is bound to all eight pyrrolic nitrogens of two porphyrin macrocycles. The two porphyrins are found in a staggered conformation where the porphyrins assume a domed distortion as a result of the mutual repulsion of the two π-systems and the pyrrolic nitrogens being drawn out of the plane of the C_{20} ring by the cerium ion. These distortions alter the photophysical properties of the porphyrin complexes and offer wide variety of electronic

properties not found in the corresponding free-base porphyrins or metalloporphyrins of the first row transition metals[3].

Hafnium(IV) forms only mono-porphyrinate complexes though the porphyrin distortion is still quite prevalent. The advantage of these complexes is the highly diverse range of counter ligands that can be exchanged on the large coordination sphere of the hafnium ion, allowing a multitude of possible structural architectures.

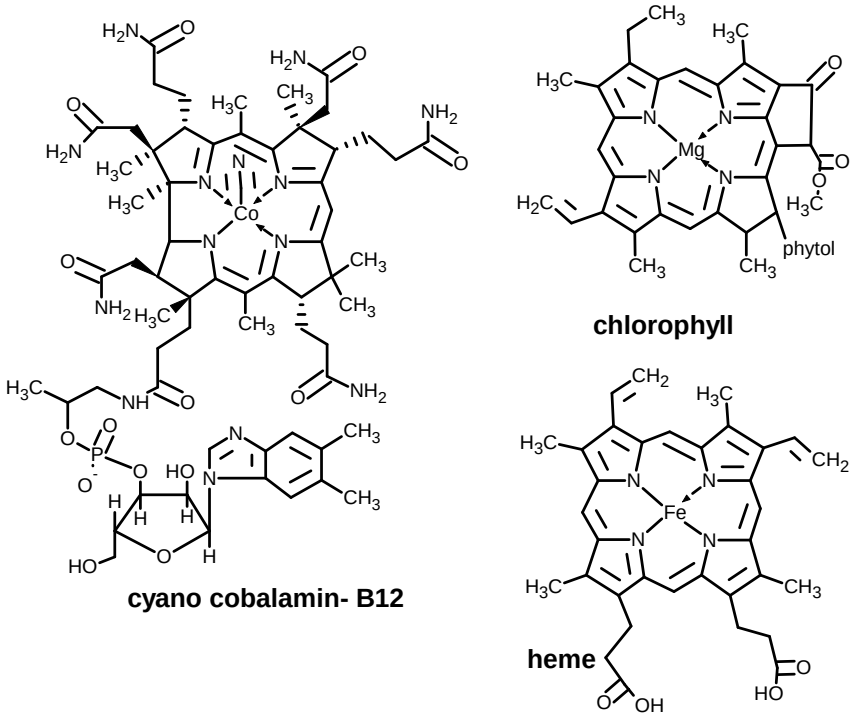

Figure 2. Common porphyrinoids found in nature

Porphyrins have been a crucial component of life on earth long before human beings evolved to study them. The magnesium porphyrinoid, chlorophyll, in photosynthetic organisms, is responsible for a complex series of electron transfers resulting from the excited state of a chlorophyll dimer that results in growth and carbohydrate production. The iron porphyrinoid, heme, carries oxygen through the body and releases it in a pH dependant cycle. The commonly known vitamin B_{12} is a

metalloporphyrin that is involved in complex, enzyme catalyzed reactions in animal biology; one of a very few organometallic mechanisms in biology[4] (**Figure 2**). A key factor to consider throughout the many examples of porphyrin functions in nature is that the porphyrins must be built into a larger hierarchical structure in order to fulfill their function. In photosynthesis, for example, the chlorophyll exists as a dimer which injects electrons from its excited state through a series of electron acceptors. Though the external organic substituents of porphyrins have varying degrees of stability, the porphyrin core is remarkably robust, as evidenced by its presence in various geochemical deposits such as shale oil.[5] Porphyrins show a natural tendency to form supramolecular architectures

It has been shown through countless reports, the multitude of applications and variations of the porphyrinoid macrocycle[4]. This work focuses on the potential for tetra aryl porphyrins to form hierarchal structures using the naturally self-organizing tendencies porphyrins display in nature and in the laboratory. More specifically, porphyrin structures reported by those such as C.M. Drain[6-11] and I. Goldberg[2, 11, 12] serve as motivational models for the porphyrinate complexes reported herein.

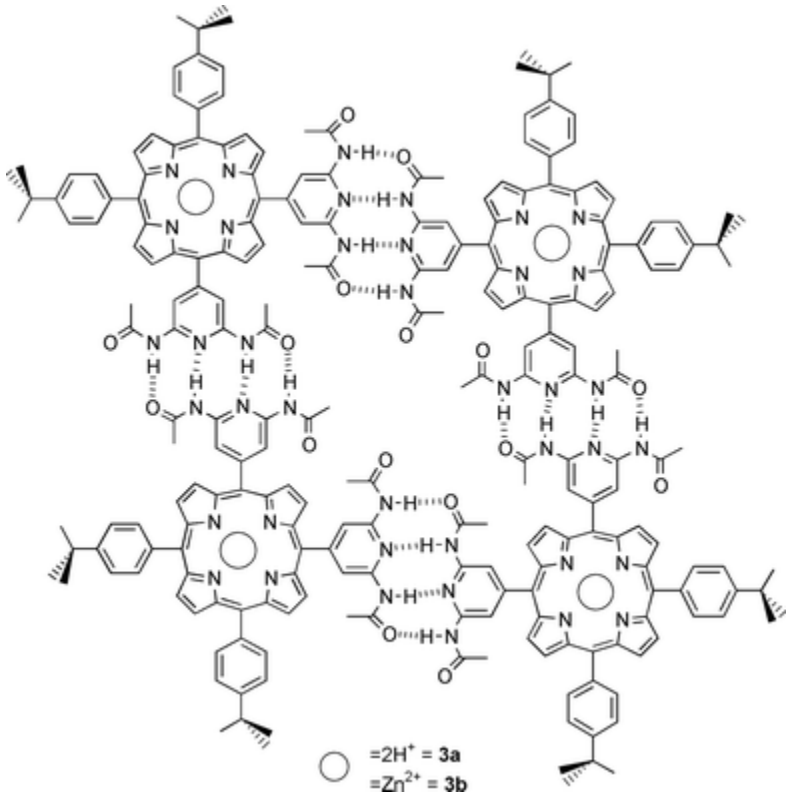

Figure 3 Porphyrin tetramer formed by H-bonding[1]

These models use porphyrins, with specially designed external substituents, to form discrete structures in solution,[6, 7] or crystallize into organized lattice structures in their solid form.[11, 13, 14] In large part, this past literature deals with free-base or metalloporphyrins coordinated to first or second row transitions metals. The porphyrins organize by hydrogen-bonding (**Figure 3**) or coordination of porphyrin substituents to metals ions (**Figure 4**). The metal ions may be auxiliary components linking *meso* substituents as found with the dimers, tetramers, nonamers, and polymers of porphyrins partially functionalized with pyridyl groups linked through metal coordination bonds with platinum or palladium.[8] These large porphyrin arrays have been shown to act as photonic

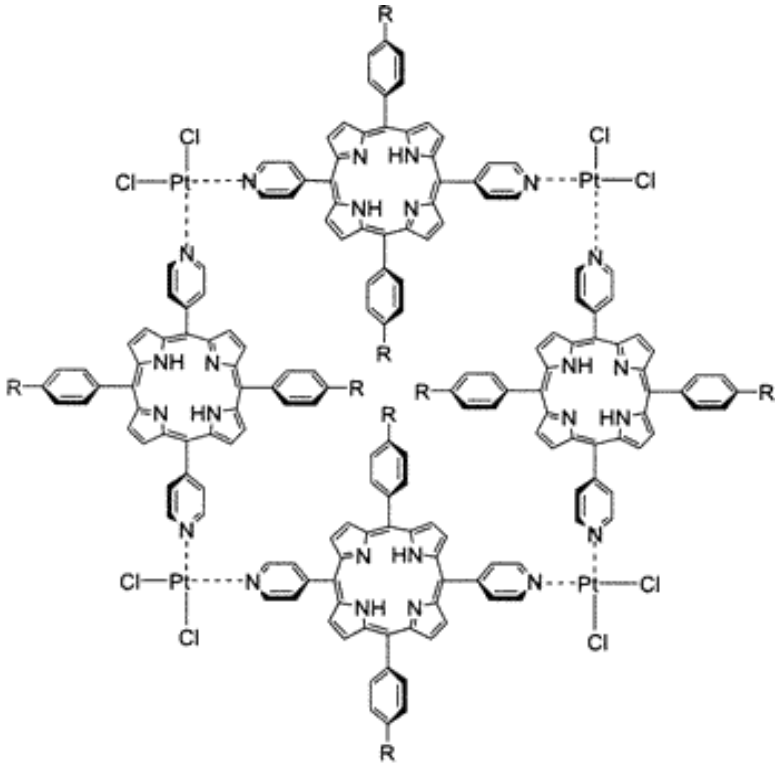

Figure 4. Pyridyl groups on porphyrins linked via Pt-N bonds in a tetrameric square.

that self-assemble in solution and on surfaces.[9] The metal ion can also be inserted into the porphyrin core and allow coordination of substituents perpendicular to the macrocycle.[15]

In their crystallography, porphyrin architectures can form large cavities of tailored sizes that act as hosts for specific molecules. These molecular sieves[15] are analogous to inorganic zeolites that have many applications including drug delivery, separation, and act as catalysts for reactions between encapsulated molecules.[15, 16] In designing these architectures certain porphyrin substituents have proven very versatile in forming strong coordination bonds that enable the formation of the observed crystal lattices. These include pyridyl, cyano-phenyl, hydroxyphenyl, and carboxyphenyl porphyrin substituents.[15] In the case of the protic groups, both hydrogen bonding and metal chelation have led to very interesting crystal designs (**Figure 5**).[15-17]

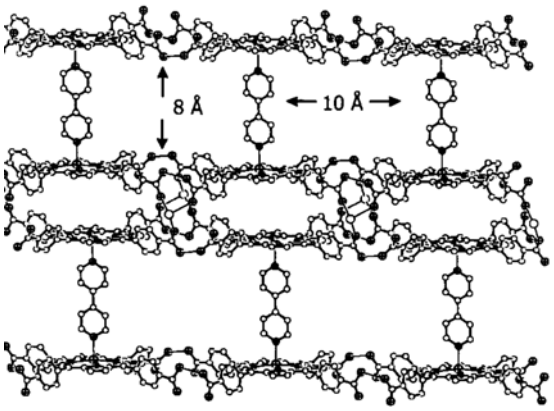

Figure 5. Crystal structure of a zinc tetracarboxyphenyl porphyrin interconnected by both chelation of the carboxylates around sodium ions as well as perpendicular coordination of bipyridyl ligands to the zinc ions in the center of the porphyrin macrocycles. [2]

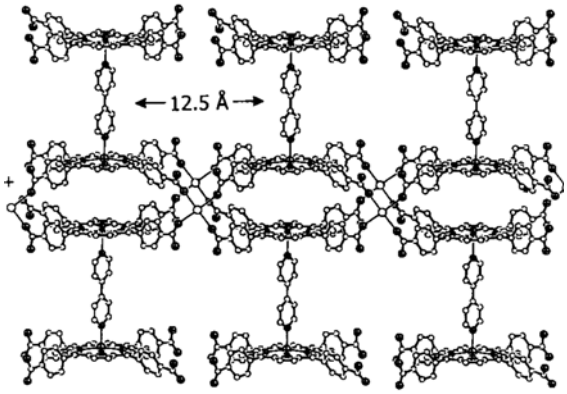

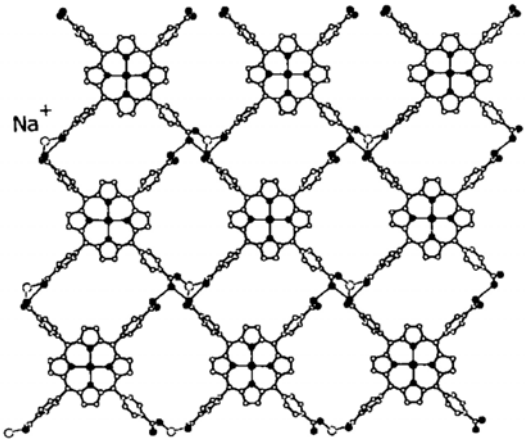

By using established crystallographic dimensions and tendencies of these porphyrin frameworks, the self-assembly of the larger f-block metalloporphyrinates could be explored. For CeP_2 complexes bearing pyridyl groups, for example, the two-layer structure and distortions of the macrocycles may lead to very interesting coordination structures with external metal ion such as Pt(II) and Pd(II). The electronic properties of these types of assemblies would be drastically different from their one dimensional predecesors due to their unique geometry and redox chemistry. The domed distortion of CeP_2 has already yielded interesting crystal structures (reported herein) that contain large, isolated cavities, akin to the molecular sieves reported by Goldberg.

For $Hf(P)L_2$ complexes, the large oxo-philic hafnium ion can accept up to four ligations of two negatively charged substituents such as two acetates. These have a very high potential for generating rigid crystallographic architectures as the hafnium acts as a built in chelating site for oxo-substituents on the periphery of the porphyrin.

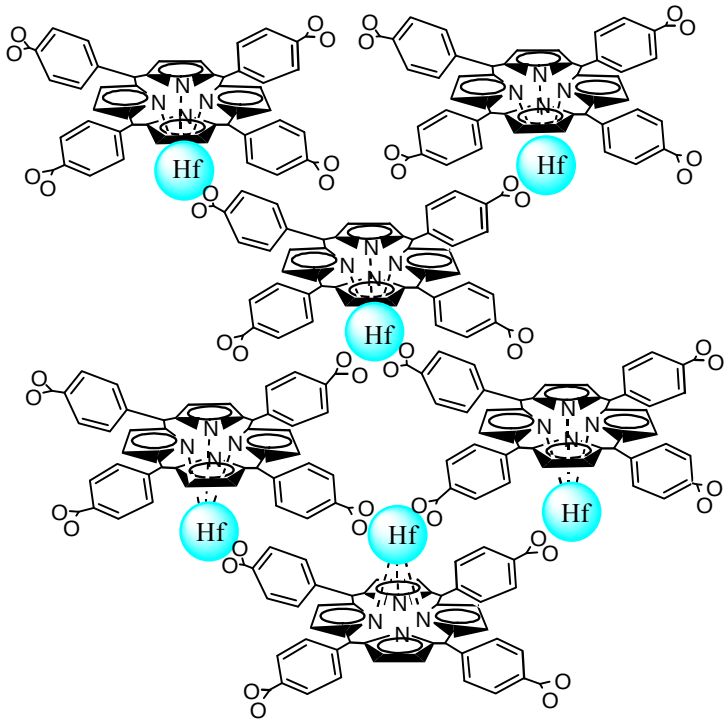

Figure 6 Possible coordination scheme for a self-complementary $Hf(TCPP)^{+2}$ complex where the carboxyphenyl substituents bond to neighboring hafnium ions.

For example, hafnium(IV) tetra carboxyphenyl porphyrinate, Hf(TCPP) has a self contained positively charge metal ion and four negatively charged carboxylates on its periphery (**Figure 6)**. This complex has a high potential for forming very rigid architectures akin to those reported by Goldberg. A route to this new hafnium complex is reported herein.

Finally, and perhaps most significantly, hafnium porphyrinates can also bind very strongly to oxide surfaces such as TiO_2. This may prove very useful in photovoltaic

research where organic dyes are bound to a semiconductor surface, such as TiO_2, through a carboxylate on the periphery of the complex to the surface Ti moeities.[18] The excited state of the dye injects electrons into the surface which then "percolate" through the semiconductor to generate an electrical current. Hafnium porphyrinates would bind to the surface *via* the oxygen moieties and use the hafnium ion as a conduit for electron transfer from the porphyrin into the oxide surface. We have generated numerous models for this by way of crystallographic structures of the hafnium porphyrinates bound to oxo-ligands. Most notably, the crystal structure of the hafnium porphyrinates bound to the Keggin polyoxometalate, $PW_{11}O_{39}^{-7}$, (reported herein) provides an insightful model for this type of potential surface chemistry.

References

1. Drain, C. M.; Shi, X.; Milic, T.; Nifiatis, F., *Chem. Commun.* **2001**, 287-288 (Adendum 1418).

2. Diskin-Posner, Y.; Dahal, S.; Goldberg, I., *Angew. Chem. Int. Ed.* **2000,** 39, (7), 1288-1292.

3. Buchler, J. W.; Ng, D. K. P., Metal Tetrapyrrole Double- and Triple-Deckers with Special Emphasis on Porphyrin Systems. In *The Porphyrin Handbook*, Kadish, K. M.; Smith, K. M.; Guilard, R., Eds. Academic Press:: San Diego, 2000; Vol. 3, pp 245-294.

4. Kadish, K. M.; Smith, K. M.; Guilard, R., *The Porphyrin Handbook*. Academic Press: San Diego, 2000.

5. Mauzerall, D. C., *Clin. Dermatol.* **998,** 16, (6), 195-201.

6. Drain, C. M.; Fischer, R.; Nolen, E.; Lehn, J. M., *Chem. Commun.* **1993**, 243-245.

7. Drain, C. M.; Lehn, J.-M., *Chem. Commun.* **1994**, 2313-2315 (correction 1995, p503).

8. Drain, C. M.; Nifiatis, F.; Vasenko, A.; Batteas, J. D., *Angew. Chem. Int. Ed.* **1998,** 37, (17), 2344-2347.

9. Milic, T.; Garno, J. C.; Smeureanu, G.; Batteas, J. D.; C. M. Drain, *Langmuir* **2004,** 20, 3974-3983.

10. Drain, C. M.; Goldberg, I.; Sylvain, I.; Falber, A., *Top. Curr. Chem.* **2005,** 245, 55–88.

11. Goldberg, I., *Chem. Comm.* **2005**, 1243-1254.

12. Goldberg, I., *Cryst. Eng. Comm.* **2002,** 4, 109-116.

13. Diskin-Posner; Patra, G. K.; Goldberg, I., *Eur. J. of Inorg. Chem.* **2001,** 2001, (10), 2515-2523.

14. Yael Diskin-Posner, G. K. P. a. I. G., *Cryst. Eng. Comm.* **2002,** 4, 296-301.

15. Goldberg, I., *Chem. Eur. J.* **2000,** 6, (21), 3863-3870.

16. Shmilovits, M.; Diskin-Posner, Y.; Vinodu, M.; Goldberg, I., *Cryst. Growth Des.* **2003,** 3, (5), 855-863.

17. Diskin-Posner, Y.; Dahal, S.; Goldberg, I., *Angew. Chem. Int. Ed.* **2000,** 39, (7), 1288-1292.

18. Nazeeruddin, M. K.; Pèchy, P.; Renouard, T.; Zakeeruddin, S. M.; Humphry-Baker, R.; Comte, P.; Liska, P.; Cevey, L.; Costa, E.; Shklover, V.; Spiccia, L.; Deacon, G. B.; Bignozzi, C. A.; Graetzel, M., *J. Am. Chem. Soc.* **2001,** 123, (1613-1624).

Chapter 1

New Methods for the Synthesis of Bis(tetra-aryl porphyrinato) Cerium(IV) Complexes: Crystal Structures and NMR Studies of Homoleptic and Heteroleptic Complexes

Abstract

New strategies for the synthesis of bis(porphyrinato)cerium (IV) sandwich complexes, **CeP_2**, are reported. **CeP_2** complexes, where **P**= 5,10,15,20-tetraphenylporphyrin (TPP), **P**= 5,10,15,20-tetrakis(4-pyridal)porphyrin (TPyP), and **P**= 5,10,15,20-tetrakis-(3-cyanophenyl)porphyrin (T-3-CNPP) are formed rapidly and in good yields in a mixed solvent solution of 1,2,4 trichlorobenzene (TCB) and 1-dodecanol. Activation of the porphyrins for metal insertion by deprotonation of the inner pyrroles, is accomplished in situ by the addition of 10 equivalents of sodium hydride to the dodecanol before addition to the reaction. After addition of five equivalents of $Ce(acac)_3 \cdot H_2O$ the solution is refluxed under argon for 3 to 6 hours. 55-80 % yields are obtained after chromatographic purification. Compared to previous methods that carry out metal insertion in neat TCB with excess *n*-butyl lithium, the solvent mixture affords greater solubility for the porphyrins, and the milder alkoxide base avoids the potential benzyne chemistry resulting from the reaction of *n*-butyl lithium with TCB. These conditions allow small scale reactions. Low temperature H^1-NMR and COSY spectra elucidate the structural dynamics of the complexes, especially in the analysis of peaks

arising from asymmetrical distortions in the porphyrin macrocycles. Crystallographic data for the homoleptic $Ce(TPyP)_2$ complex, in two different packing orders, and the heteroleptic Ce(TPP)(TPyP) complex are also reported.

Introduction

Synthetic strategies to form lanthanide and actinide porphyrinate complexes have been expanding recently due to growing interest in their unique photophysical and electrochemical properties, which significantly differ both from the free-base and the metalloporphyrinates of the first and second row transition metals. Metals with large ionic radii form double-decker and triple-decker complexes with porphyrins (P), phthalocyanines (Pc) and other porphyrinoids.[1] The physical chemistry of these complexes makes them suitable for many potential applications. For example, porphyrinoid double and triple-decker complexes are proposed as molecular electronic components in memory storage, wherein the potentials of up to eight reversible reduction/oxidation (redox) processes are tuned by the choice of both metal ion and the porphyrinoid (P, Pc).[2-5] Heteroleptic compounds are particularly attractive for these purposes because the macrocycles have different redox potentials, and contribute to the properties of the complex.[2] Heteroleptic CeP_2 and Ce(P)(Pc) complexes have been deposited on HOPG where they form ordered layers.[6] Triple-decker complexes of mixed P/Pc with cerium, europium and other lanthanides that are designed to covalently bond to Si(100) and other surfaces have been reported.[3, 4, 7] Monolayers of a Ce(TPyP)(Pc) have been reported to form extensive two-dimensional networks in the presence of metal ion auxiliaries.[8]

The cerium complexes are of interest for several reasons. The properties of CeP_2 complexes are partially due to the stability of the [Xe] electron configuration of Ce(IV), but metal-centered electrochemical processes are observed due to the Ce^{3+}/Ce^{4+} redox states that are unique among the lanthanides.[9] The $Ce(TPyP)_2$ complex has a low rotation barrier around the principal axis[10] and the luminescence is quenched by internal conversion, but ditopic substrates capable of binding to pyridyl moieties on each half of the sandwich, such as diacids and sugars, freeze the rotation and the complex luminesces.[11-13] The low rotation barrier of the $Ce(IV)P_2$ sandwich complexes are desirable properties for tectons in the construction of 2- and 3- dimensional supramolecular systems,[14-16] because the relative conformation of porphyrins bearing motifs for specific intermolecular interactions can adjust to optimize these interactions. For example, it may be possible to construct hierarchical arrays of sandwich complexes using pyridyl porphyrins matched to the coordination geometries of metal ion auxiliaries that are analogous to free base and first row metalloporphyrins arrays.[17-19] The closed shell electron configuration of Ce(IV) aids in NMR characterization of both the complex and the supramolecular systems.

To date, there are a few published synthetic routes for these types of complexes, and the application of each depends on the metal ion which is being inserted and on the specific porphyrinoid. For homoleptic lanthanide and actinide complexes, these generally fall into two categories: (1) extended reflux at high temperatures such as in TCB (bp ~205°C), (2) activation of the macrocycle by formation of lithium salts, Li_2P, for shorter reaction times in similar high boiling solvents.[1] Heteroleptic Ce(Pc)(TPyP) complexes have been reported in 69% yield by a stepwise reaction of $Ce(acac)_3 \cdot H_2O$ with the lithium

salt of the phthalocyanine in TCB and then addition of TPyP.[2] Typically, the porphyrinoid(s) and $Ce(acac)_3 \cdot H_2O$ are suspended in TCB and refluxed under an inert atmosphere for 24 hours, to give the Ce complex in 52% yield for porphyrazines,[20] 78% for oactaethylporphyrin[18], and 44% for tetra-tolyl porphyrin.[21] The $CePc_2$ can be made *in situ* during the macrocycle synthesis,[2] or refluxing the Pc with fresh $CeI[N(SiMe_3)_2]_2DME_2$ (DME = dimethoxyethyl ether) for 5-18 h gave the corresponding double and triple-decker complexes.[3] Refluxing a 2:1 octanol:toulene system with $Ce(acac)_3 \cdot H_2O$ and DBU to activate an aryl-porphyrin bearing liquid crystal groups yields the double decker after ca. 16 hours but in low yields.[6]

The relatively small ionic radius of Ce(VI), 0.97Å, results in strong π-π interactions between the macrocycles in CeP_2, and the steric interactions between the macrocycles and their substituents cause ring distortion as observed in crystal structures of $Ce(OEP)_2$ and $Ce(TPP)_2$.[1, 22] This steric interaction between the porphyrins also necessitates the higher temperature synthesis, and is a reason for the relatively low reported yields[1] of the tetra aryl porphyrins complexes such as $Ce(TPP)_2$. Analogous thorium, uranium, and hafnium complexes are typically formed in greater yields in lower boiling solvents such as toluene, and show less porphyrin ring distortion according to crystallographic data.[23, 24] Thus the charge and radius of the metal ions greatly influence the yield of sandwich complexes and the degree of macrocycle distortion: Hf(IV) 0.83Å, Th(IV)1.05Å, U(IV)1.00Å.[1] However, we found that these methods generally result in poor yields in small, <100 mg, scale preparations. The reduced yields may arise from complications from the n-butyl lithium, used to make the Li_2P, also reacting with the trichlorobenzene to form a benzyne[25] that may react with the macrocycle at the high

temperatures used in the reaction. The presence of trace amounts of water, from the cerium starting complex, or dioxygen, and other factors may also be detrimental especially for smaller scale reactions. We report herein a variation in the solvent system typically used for $Ce(P)_2$ synthesis that allows a variety of porphyrins to be used, works on a small scale, and affords the complex in good yields (scheme 1).

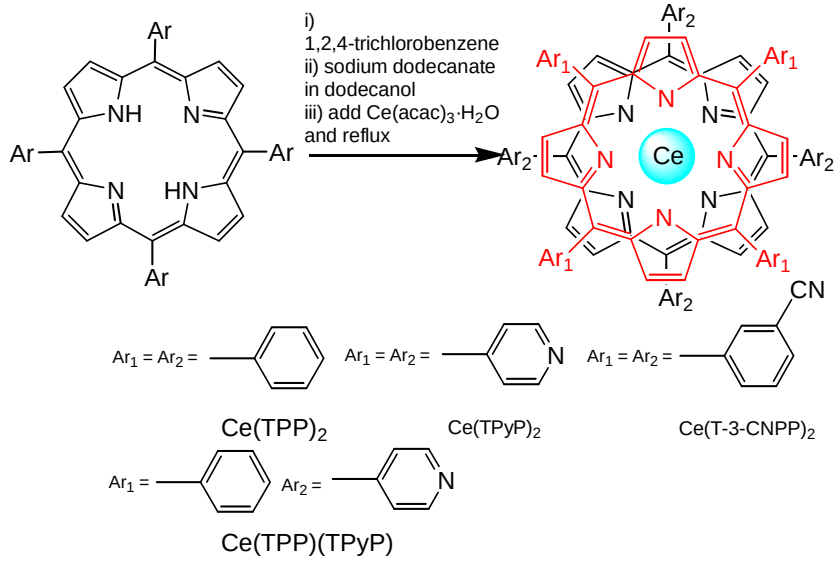

Scheme 1. Reactions are done under an argon atmosphere. For $Ce(TPP)_2$, (i) the porphyrin is dissolved 1,2,4-trichlorobenzene (10 mg/mL); (ii) a solution of 10 equivalents sodium dodecanate in ca. one quarter volume dodecanol is added; and (iii) the solution refluxed for 3-6 hours after addition of five equivalents of $Ce(acac)_3 \cdot H_2O$. For $Ce(T\text{-}3\text{-}CNPP)_2$,$Ce(TPyP)_2$, and Ce(TPP)(TPyP) a 1:1 v:v ratio of trichlorobenzene and dodecanol are used. The crude products are treated with DDQ or $K_2Cr_2O_7$ to fully oxidize the product from $Ce(III)P_2^-$ to $Ce(IV)P_2$.

Discussion

Synthesis

We had little success with methods employing *n*-butyl lithium in neat TCB reported previously,[26] especially for 50 mg scale reactions, and for the synthesis of porphyrin complexes bearing polar ligand groups that aggregate with the cerium starting material, such as $Ce(TPyrP)_2$ and $Ce(T\text{-}3\text{-}CNPP)_2$. Porphyrins bearing exocyclic ligands nearly quantitatively aggregate and precipitate after the addition of base and the $Ce(acac)_3{\cdot}H_2O$ starting material, and do not redissolve even when refluxed. Others have also reported low and erratic yields using this method.[27]

Based on the observation that H_2TPyP is soluble in high concentrations in mixed solvents such as CH_2Cl_2 and CH_3OH, we added a high boiling alcohol, dodecanol (bp 250 $^{\circ}$C), to the TCB and observed a drastic increase in the solubility of H_2TPyP. Addition of sufficient NaH to the dodecanol to form about 10 equivalents of sodium dodecanate, effectively deprotonates the macrocycle as judged by the consistent green color of the porphyrin dianion in the mixture. Afterwards, five equivalents of the $Ce(acac)_3{\cdot}H_2O$ complex were added, which is consistent with most reported synthetic methods.[1] The yield of $Ce(P)_2$ in all cases studied was optimal using ca. 50% dodecanol, and increasing the dodecanol to more than 50% does not improve the results. This method affords increased yields, especially of the $Ce(TPyrP)_2$ complex, and allows a reduction in solvent volume to less than 1 mL/10mg of porphyrin, which also reduces waste and makes purification easier. E.g. up to 100 mg of the $Ce(P)_2$ complex can be synthesized in a disposable 1.8 x 15.0 cm test tube.

During the purification of $Ce(TPyP)_2$, $Ce(T\text{-}3\text{-}CNPP)_2$, and Ce(TPP)(TPyP), we noted two distinct bands on TLC, rust-brown and green bands, in addition to the purple band of the unreacted porphyrin(s). UV-Vis spectroscopy reveals that the rust-brown is the $Ce(IV)P_2$ complex and is constant with reported spectra for this compound with a Soret maximum at 393 nm, while the green, reduced $Ce(III)P_2^-$ material has a Soret at 408-411 nm and a very small rf value on TLC.[1, 9, 28] The spectra suggest substantial delocalization of the electron between the metal and the macrocycles. The electron-donating pyridyl groups have been described as having a reductive effect on the cerium center, making the Ce(III) species more prevalent.[1] The reduced species is a significant product in our synthesis, which may be due to the use of argon instead of nitrogen (which has ca. 10ppm dioxygen). Isolation of the target compound is achieved by treatment of the reaction mixture with excess 2,6-dichloro-3,5-dicyanobenzoquinone (DDQ)[29] or a biphasic reaction with the $Ce(P)_2$ in the organic phase and dilute aqueous $K_2Cr_2O_7$. The reduced species can be reproduced by treatment of the complex with excess hydrazine.[28] These observations are consistent with previous reports. In general, the cerium sandwich complexes are 0.3 V to 0.5 V more easily oxidized than the free base, e.g. for a $Ce(porphyrazine)_2$.[20] The strong π–π interactions between the two porphyrins has been proposed to the origin of the shifts in the redox potentials,[1, 9, 28] the chemical reactivity, and photochemistry.[28, 30, 31]

The purification of the $Ce(T\text{-}3\text{-}CNPP)_2$ was complicated due to multiple bands (>20) of interdispersed rust-brown and green colors observed on TLC with nominally distinguished rf values. The green bands are not identified as the reduced, charged species since charged species do not move well on silica gel. When removed from the

silica and redissolved, these green bands appeared rust-brown and their UV-Vis spectra were that of the Ce(IV)P_2 complex. Since there are 21 possible atropomers of this complex, we assumed that the various fractions arise exclusively from atropomeric mixtures with different combinations of the eight 3-cyano groups in the *endo* and *exo* positions (*vide infra*). Conversely, the combined data (UV-Vis, TLC, NMR, and X-ray crystallography) from this and other complexes suggests that the Ce(T-3-CNPP)$_2$ molecule exists in more than one conformation at room temperature, wherein the porphyrin rings are distorted. The various conformations of the porphyrin macrocycles are also distinguished by preparative TLC, indicated by the varied colors of green and brown, concomitant with atropomer separation, resulting in very complex chromatography. The data suggest that the energy barrier between conformational isomers is greater than the rotational barrier of the aryl moieties. We are able to isolate a single conformer at room temperature from the preparative TLC but the atropomers re-equilibrate to a mixture favoring the 3-cyano groups in the *endo* position (see NMR studies below). As observed for porphyrins that are forced into nonplanar conformations by steric crowding of peripheral substituents,[32-34] the distortion of porphyrin macrocycles Ce(T-3-CNPP)$_2$ greatly influences their electronic spectra. Some of these conformers, coincidently to the reduced Ce(TPyP)$_2$ complex, appear green on silica, but appear rust-brown in solution.

Purifcation of the Ce(TPP)$_2$, Ce(TPyP)$_2$, and Ce(TPP)(TPyP) complexes were straight forward. After oxidation, the sandwich complexes elute from silica gel columns as one fraction. The purification of the heteroleptic Ce(TPP)(TPyP) complex exhibited a faint green fraction on TLC with an rf slightly lower than that of the target complex, and

the yield of this complex is low due to the competition between formation of all three possible sandwich complexes, $Ce(TPP)_2$, Ce(TPP)(TPyPP), and $Ce(TPyP)_2$. This approximately reduces the yield of the target complex in half, but the 33% yield is still within an acceptable range considering other synthetic methods.

Characterization

H^1- NMR and COSY spectra

The rotation of the macrocycles around the principle axis and the rotation of the aryl substituents at 22 °C results in significant line broadening in the ^{1}H NMR spectra,[21] but lower temperatures significantly sharpen the signals and allow high-quality COSY spectra to aid in peak assignments. The ^{1}H-NMR data for the CeP_2 complexes are given in **Table 1**. It is known that the formation of porphyrin sandwich complexes often causes a distortion of the porphyrin rings as a result of the electronic repulsion between the two π-systems.[21, 35] Our crystallographic data shows that the C_2-axis of the phenyl substituents is tilted ca. 13° from the average plane of the macrocycle. Using previous conventions,[21] the protons are assigned as *endo* or *exo* if the aryl tilt turns the protons toward the porphyrin ring current (deshielding) or away (shielding), respectively. The deshielding of the *endo* protons results in a downfield shift, while the shielding of the *exo* protons, tilted away from the macrocycle, produce the upfield shift. The reduced-temperature NMR spectra for all $Ce(P)_2$ are well resolved.

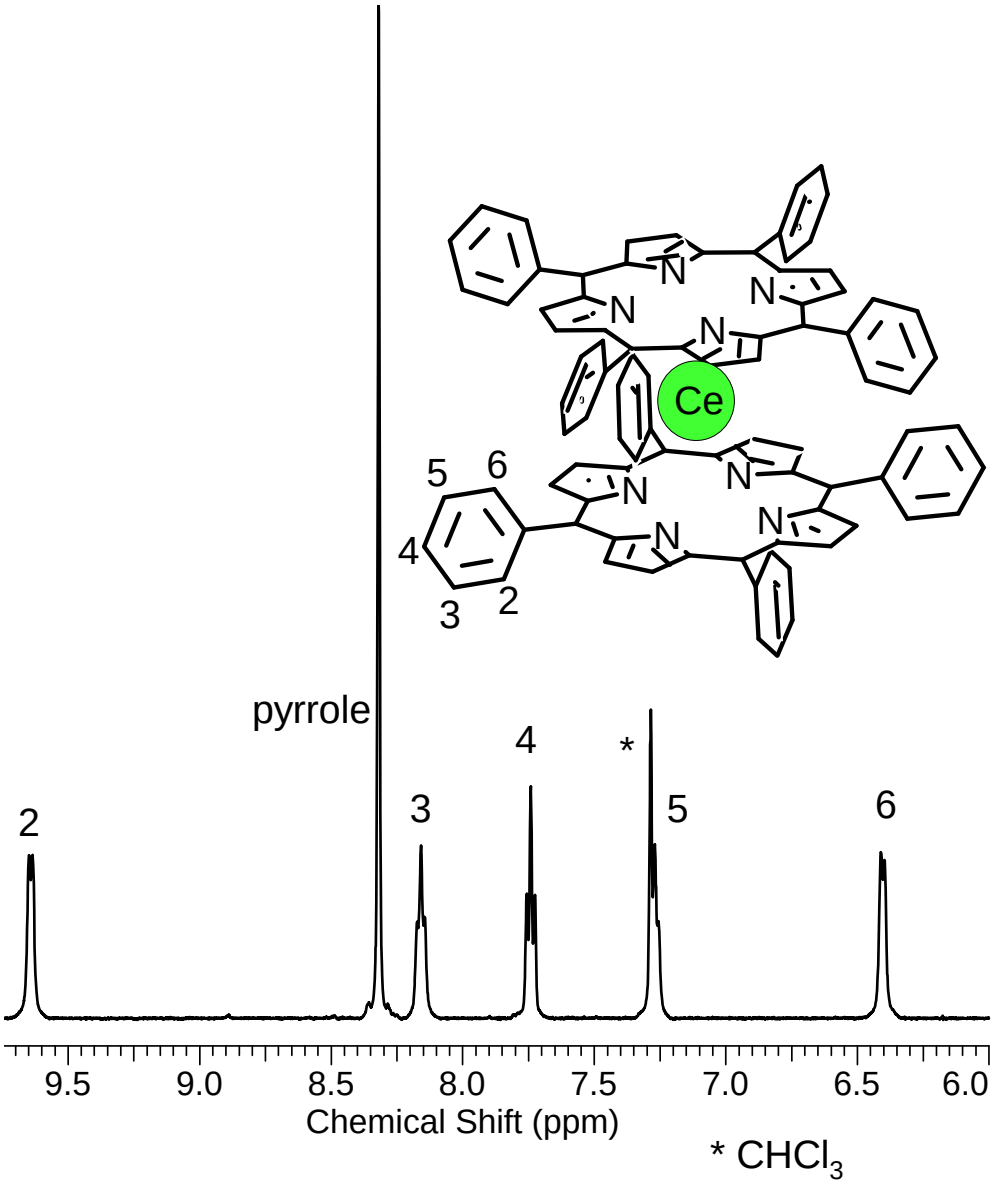

Figure 1. 1D ^{1}H-NMR of $Ce(TPP)_2$ at 3°C in $CDCl_3$

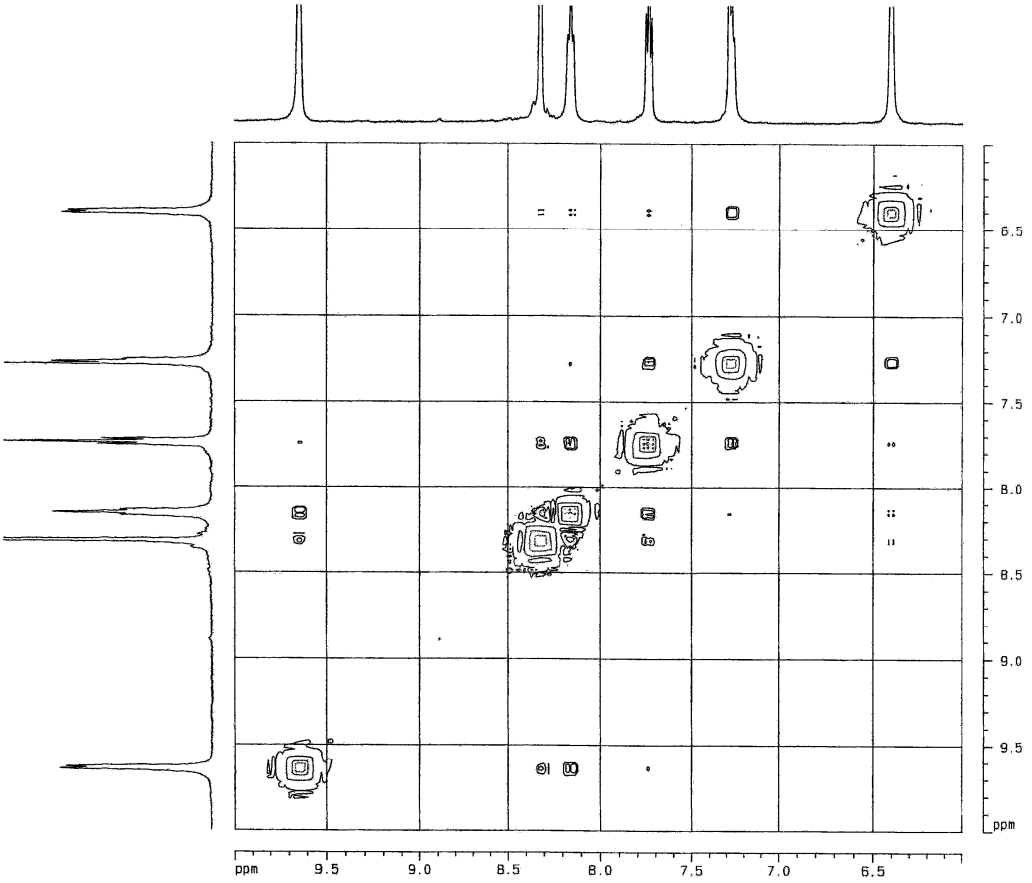

Figure 2. COSY spectrum of $Ce(TPP)_2$ at 3°C in $CDCl_3$

The COSY and 1D spectra of the $Ce(TPP)_2$ complex show clear phenyl coupling patterns with no equivalent protons and multiple-bond coupling around the phenyl ring. All five phenyl proton peaks are observed and show the expected multiplicity (**Figure 1 and 2)**.

The pyridyl nitrogens of the $Ce(TPyrP)_2$ complex separate the *endo* and *exo* protons resulting in two distinct sets of NMR peaks (**Figure 3 and 4)**. At 30 °C, both the *meta* and *ortho* -*endo* protons overlap in agreement with previous accounts,[26]

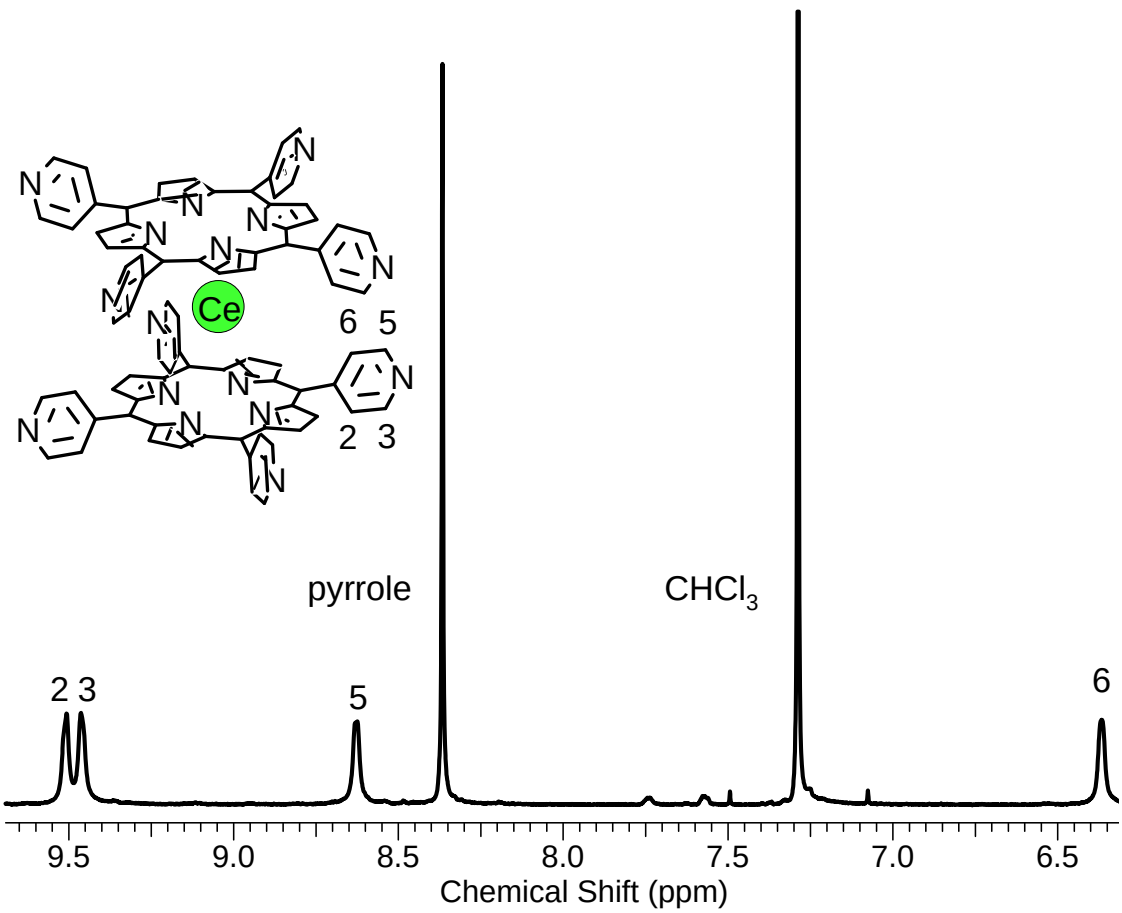

Figure 3 ^{1}H NMR of $Ce(TPyP)_2$ in 1:1 $CDCl_3$:CD_3OD at 3°C

but at 3 °C they are observed at 9.46 ppm and 9.51 ppm, respectively. In contrast, the *exo* protons are separated by nearly 3.5 ppm. Note that the NMR of this complex was taken in a 1:1 mixture of $CDCl_3$ and CD_3OD for greater solubility, which slightly alters the shifts of this complex taken in neat $CDCl_3$.

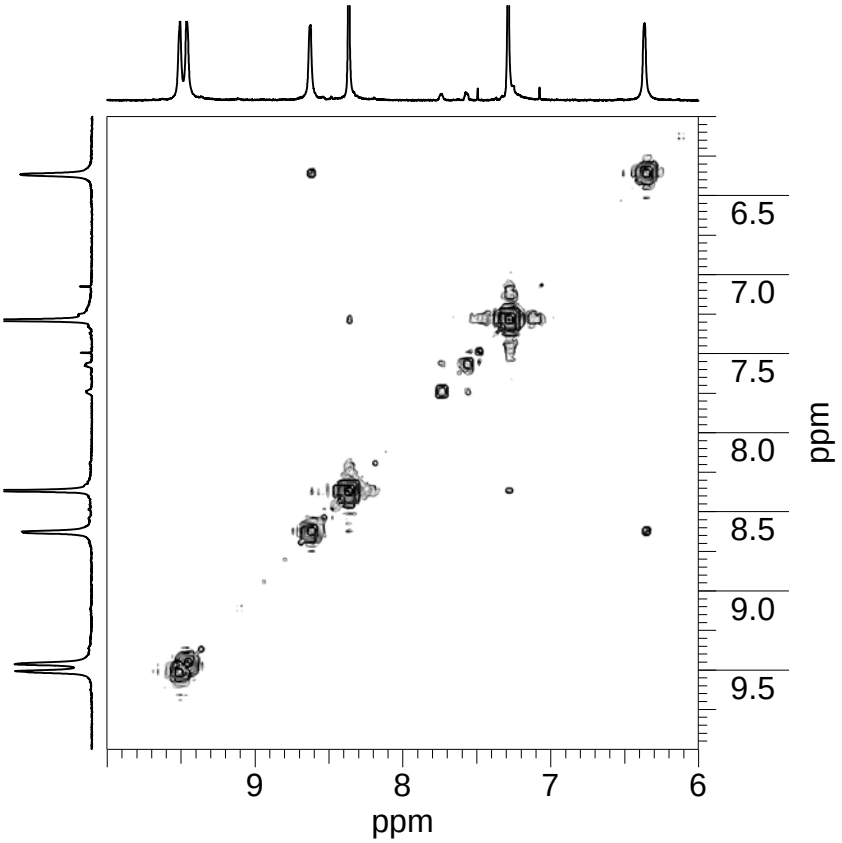

Figure 4. COSY NMR of $Ce(TPyP)_2$ at 3 ˚C

We observe a small doublet of doublets between 7.54 - 7.73 ppm in the H^1 NMR of the $Ce(TPyP)_2$ complex that are not due to the presence of the free base H_2TPyP and appear to sharpen slightly with lower temperatures in the same manner as the major peaks **(Figure.3)**. Since aryl CeP_2 complexes are distorted, these resonances are likely from a minor conformation in equilibrium,[33] *vide infra*. **Figure 5** illustrates the affect of temperature on the macrocycle rotation on the NMR time scale.

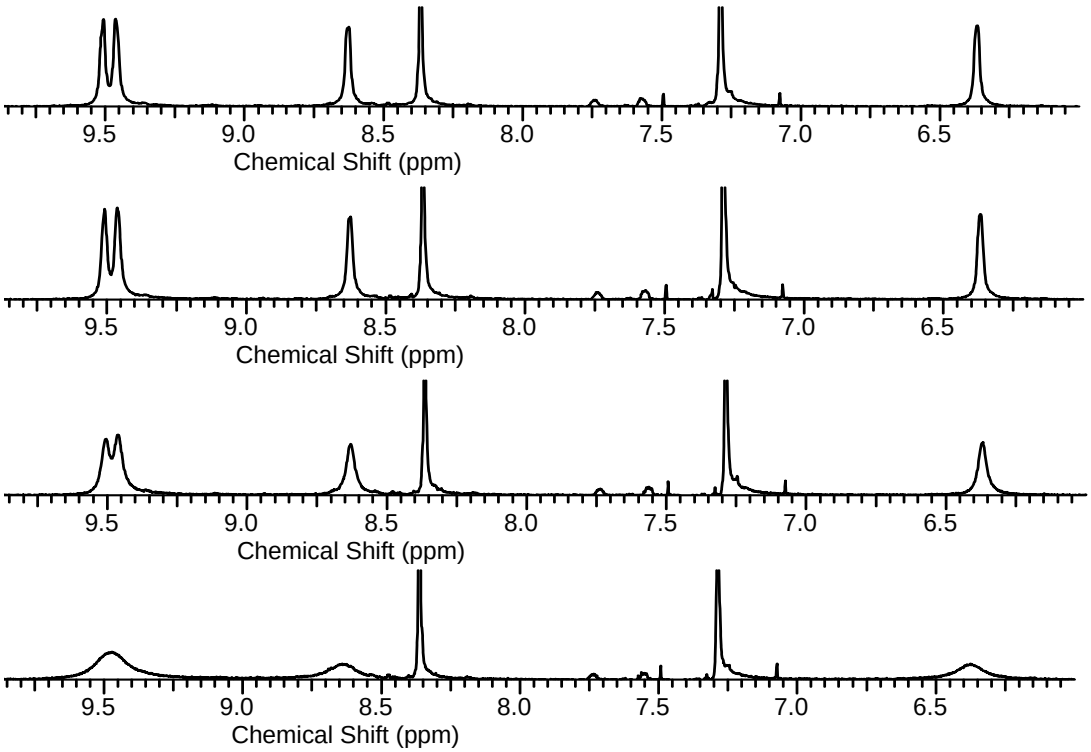

Figure 5. ^{1}**H** NMR spectra of $Ce(TPyP)_2$ in 1:1 $CDCl_3$:CD_3OD at 3°C(top), 6°C (middle), 15°C(middle), 30°C(bottom).

Table 1. ^{1}H-NMR resonances (ppm) for $Ce(TPP)_2$, $Ce(TPyrP)_2$, and $Ce(T\text{-}3\text{-}CNPP)_2$ at 3 °C

a- not resolved or assigned with certainty

Complex	**solvent**	**pyrrole**	**ortho-exo**	**meta-exo**	**para**	**meta-endo**	**ortho-endo**
$Ce(TPyP)_2$	1:1 $CDCl_3$:CD_3OD	8.37	6.37	8.62	NA	9.51	9.46
$Ce(TPP)_2$	$CDCl_3$	8.32	6.41	7.28	7.74	8.16	9.64
Ce(TPP)(TPyP)	$CDCl_3$						
major phenyl		8.33	6.35	7.28	7.77	8.19	9.52
major 4-pyridyl		8.35	6.42	8.60	NA	9.46	9.56
minor phenyl		*a*	6.06	7.28	7.64	8.05	8.98-9.17
minor 4-pyridyl		*a*	6.53-6.59	8.63		*a*	*a*
$Ce(T\text{-}3\text{-}CNPP)_2$ **at 30 °C**	$CDCl_3$	8.14	6.78	7.48	8.00	*a*	9.37
$Ce(T\text{-}3\text{-}CNPP)_2$ **at 3 °C**	$CDCl_3$	8.32	6.66	7.53	8.18	*a*	9.82

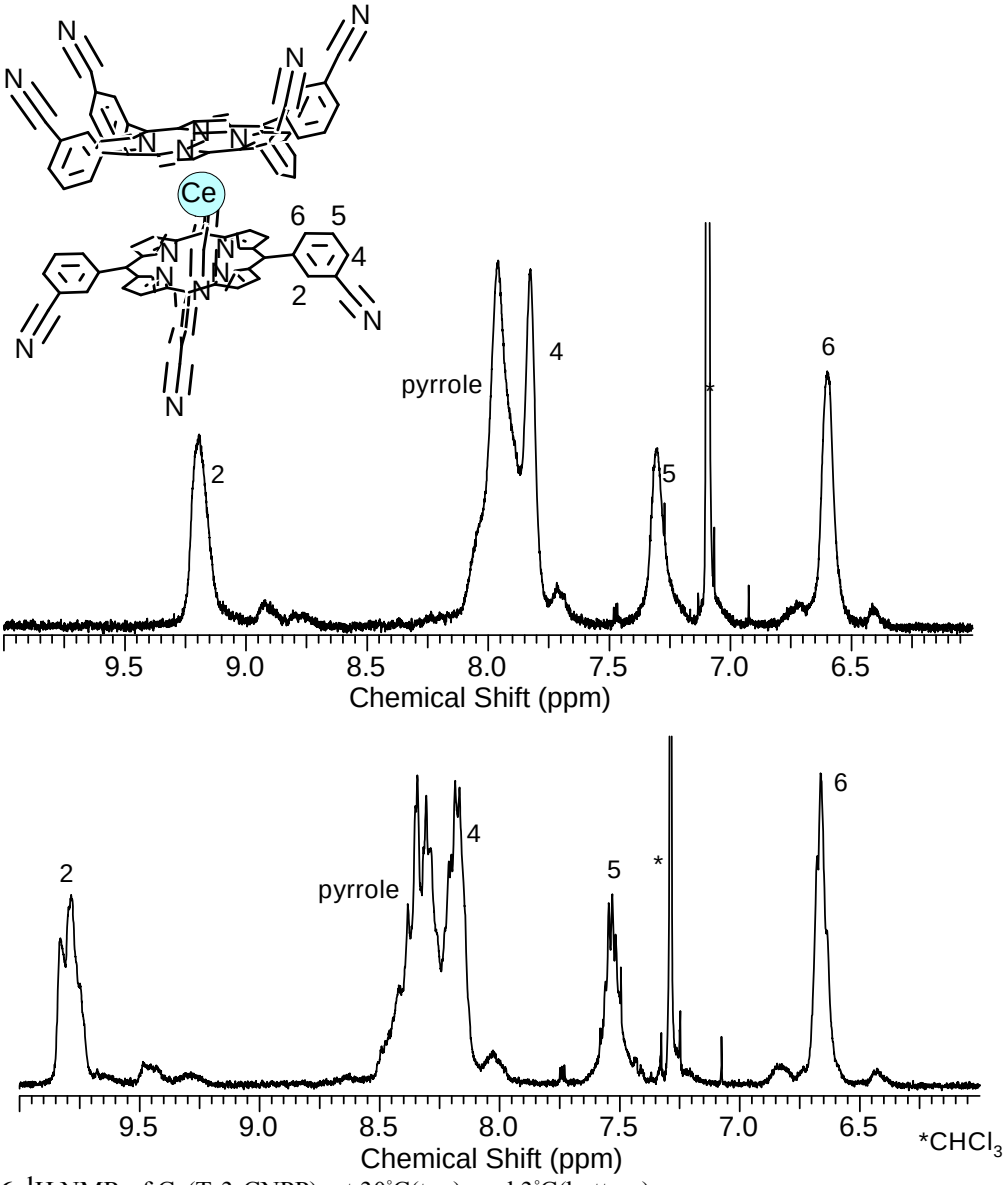

Figure 6. ^{1}H NMR of Ce(T-3-CNPP)$_2$ at 30°C(top), and 3°C(bottom)

For the Ce(T-3-CNPP)$_2$ complex, the UV-Vis spectrum indicates successful isolation of a sandwich complex, displaying a Soret band at 395 nm and the MALDI mass spectrum shows only a very strong peak at the predicted mass, both indicating a single product. NMR spectra of one major band from the preparative TLC, **A**, compared to the NMR spectra of the mixture of bands, **B,** suggest an equilibrium between different

macrocycle conformers, that do not interconvert at room temperature, rather than between atropomers which readily re-equilibrate in solution at room temperature. Fraction **A** re-equilibrates to **B** in refluxing $CHCl_3$ as observed by TLC while maintaining a constant UV-Vis spectrum throughout.

For the NMR of **A** (**Figure 6**), the four aryl peaks are broad and do not sharpen significantly at 3 °C compared to 30 °C, though poorly resolved splitting is observed, indicating the retardation of porphyrin rotation. The *endo* and *exo* proton resonances of the low temperature spectrum are shifted downfield and upfield respectively, compared to the spectrum at room temperature, indicating an interconversion of the porphyrin conformers (**Figure 6)**. Most significant is the pyrrole region which appears to be split into a poorly resolved doublet (or doublet of doublets) at low temperature. The COSY spectrum at 3 °C (**Figure 8**) indicates only one prevalent rotamer of the 3-cyano substituents where the cyano is facing in the *endo* position. Though smaller peaks, found buried on the downfield side of the pyrrolic region, are at the appropriate shift for the *endo*-meta proton, suggest a small population of the other rotamer not observed in the COSY.

The ^{1}H-NMR spectrum of **B,** at 3 °C, displays all the peaks found in both the 30 °C and 3 °C spectra of A **(Figure 7)**, showing the full mixture of conformers, but the 2D COSY spectra of both **A** and **B** similarly exhibit only one predominant rotameric pattern of the aryl protons of the 3-cyano groups in the endo position **(Figure 8)**. The relative difference in shifts between the 3 °C and 30 °C NMR resonances of **A** is similar those observed in reduced temperature NMR studies of dimeric porphyrin complexes[36, 37] that have been identified as the result of interconversion between conformers.

As observed in some other nonplanar porphyrins,[33] distortions in the porphyrin ring arising from different conformers are the most likely explanation for the non-equivalent pyrrolic protons. Small populations of other conformers in equilibrium may explain the presence of the minor resonances in the major fraction. Coupling between the ortho-*endo* peak and the pyrrolic region is found with $Ce(TPP)_2$ and $Ce(T\text{-}3\text{-}MePP)_2$,[38] but this type of coupling does not result in even slight splitting of the pyrrolic signal.

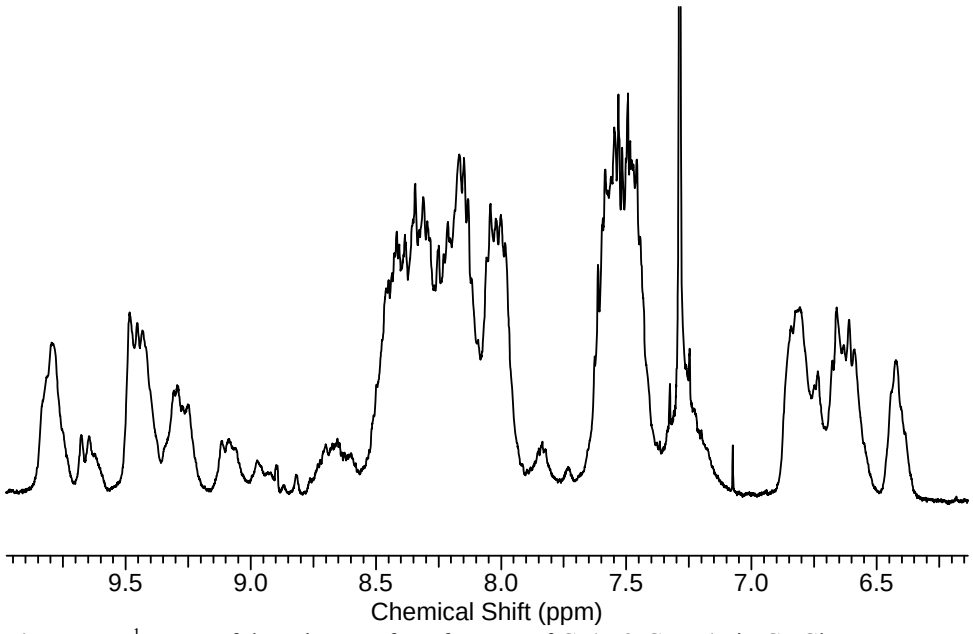

Figure 7. H^1 NMR of the mixture of conformers of $Ce(T\text{-}3\text{-}CNPP)_2$ in $CDCl_3$

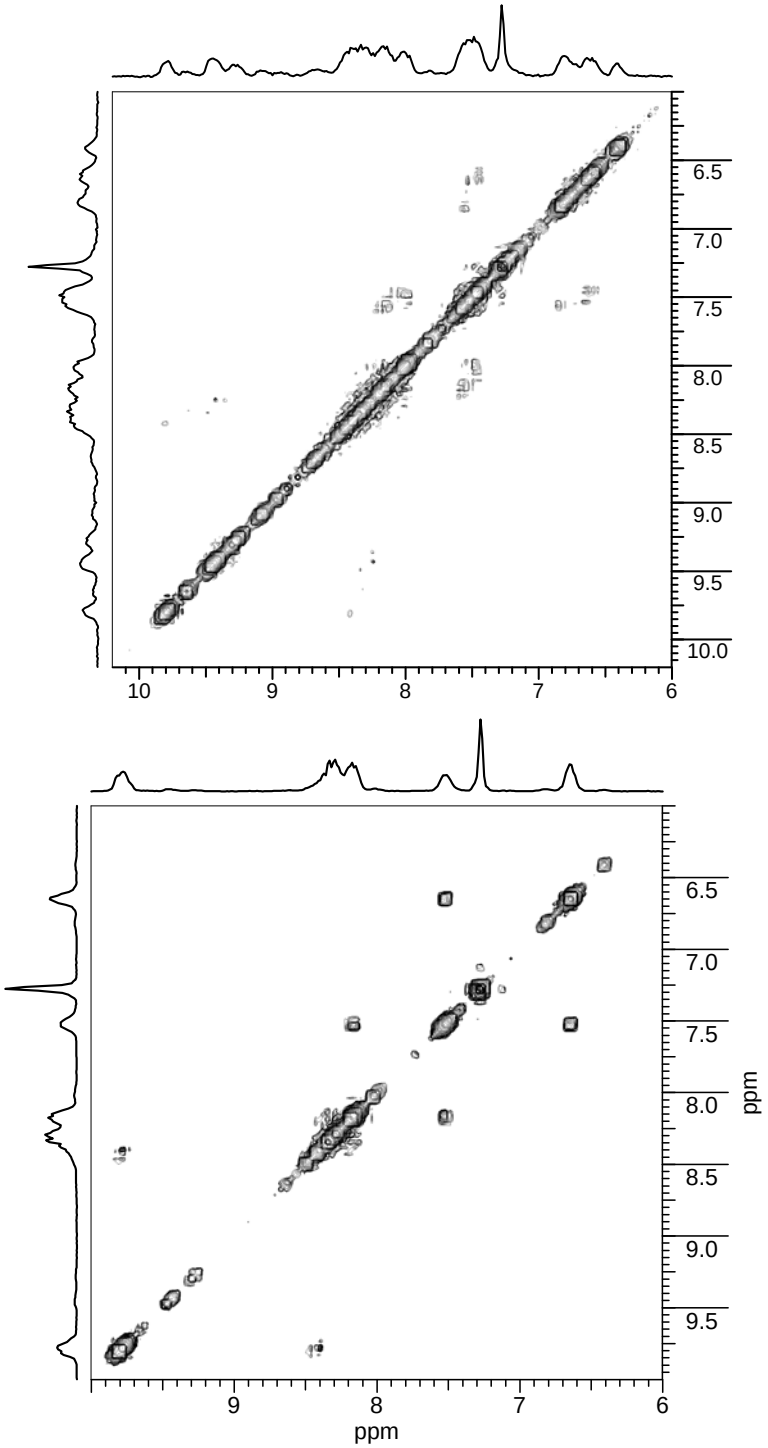

Figure 8 COSY of the mixture of conformers of $Ce(T\text{-}3\text{-}CNPP)_2$ (top) vs. the COSY spectrum of the isolated fraction(bottom).

Previous literature reports the synthesis and NMR spectroscopy of bis[(tetra-3-methylphenyl porphyrinate)]Ce(IV), Ce(T-3-MePP)$_2$.[38] This complex can also be a atropameric mixture, but complications during purification are not reported. The NMR displays two sets of aryl peaks, one for the methyl group *endo* and one for the methyl group *exo*. The pyrrole exhibits a sharp singlet peak for Ce(T-3-MPP)$_2$, indicating that the *exo-endo* atropomers of the methyl group does not perturb the pyrrolic shift and probably indicate a symmetrically domed macrocycle.

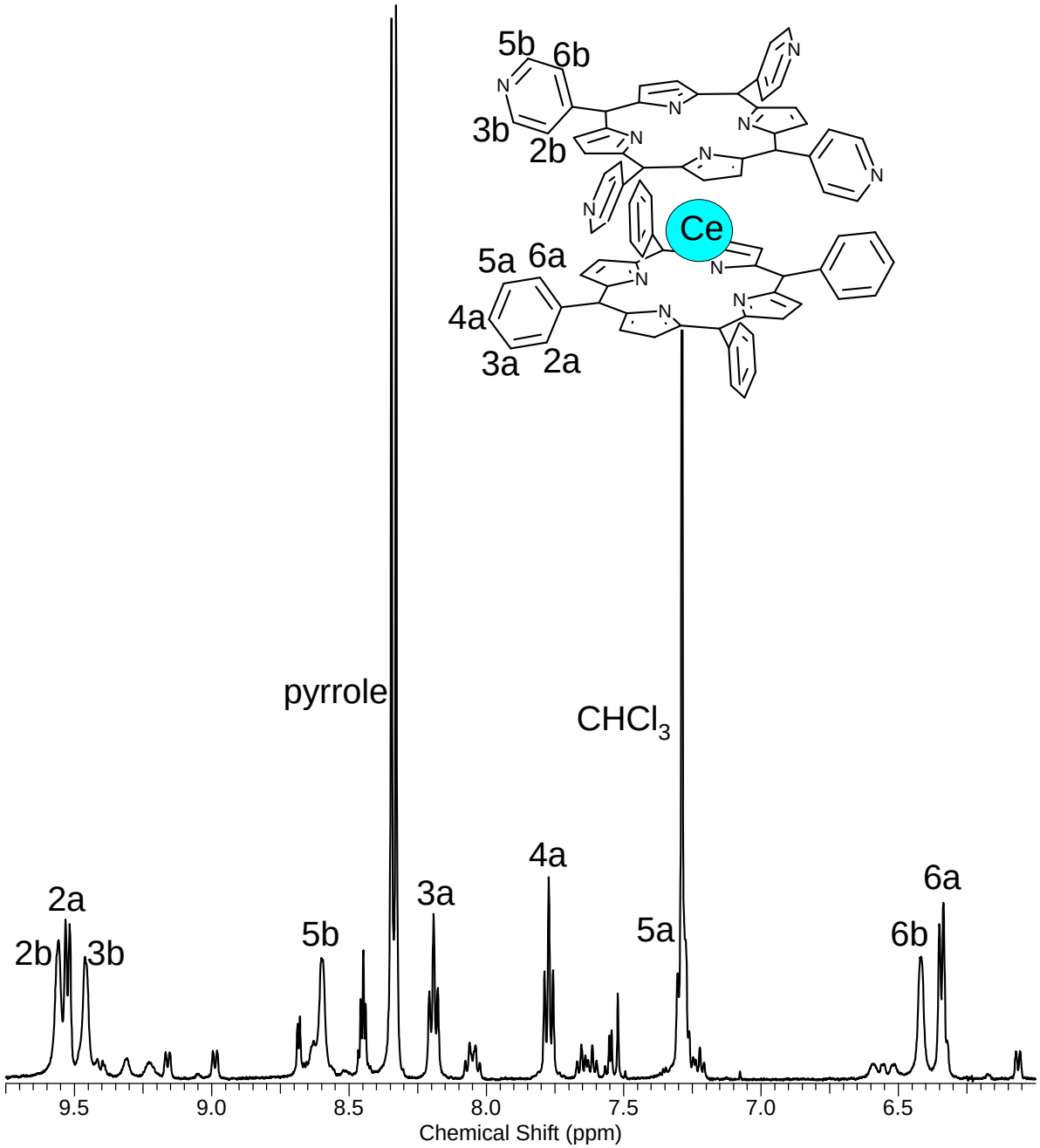

Figure 9. ^{1}H NMR of Ce(TPP)(TPyP) in $CDCl_3$ at 3°C; major aryl protons are assigned

Eventhough the ^{1}H-NMR of Ce(TPP)(TPyP) exhibits multiple peaks because the compound is less symmetric, the spectrum is reasonably resolved. The spectrum, measured at 3 $^{\circ}$C, consists of the five phenyl peaks and four pyridyl peaks in roughly the same positions as they are found in their respective homoleptic sandwich complexes **(Figure 9)**. These are labeled as *major phenyl* and *major 4-pyridyl* in **Table 1**. The existence of a minor conformation is indicated by the presence of an entire second set of minor peaks that mirror the coupling and chemical shifts of the major conformer. The entire phenyl-proton coupling pattern can be observed in the COSY **(Figure 10)** of these smaller peaks and are labeled as *minor phenyl* in **Table 1**. The smaller pyridyl peaks are also visible but only the *exo* protons can be assigned with reasonable certainty and are listed as *minor pyridyl* in **Table 1**. Unassigned resonances between 8.25 ppm and 8.75 ppm are most likely due to non equivalent pyrrolic protons arising from conformational distortion.

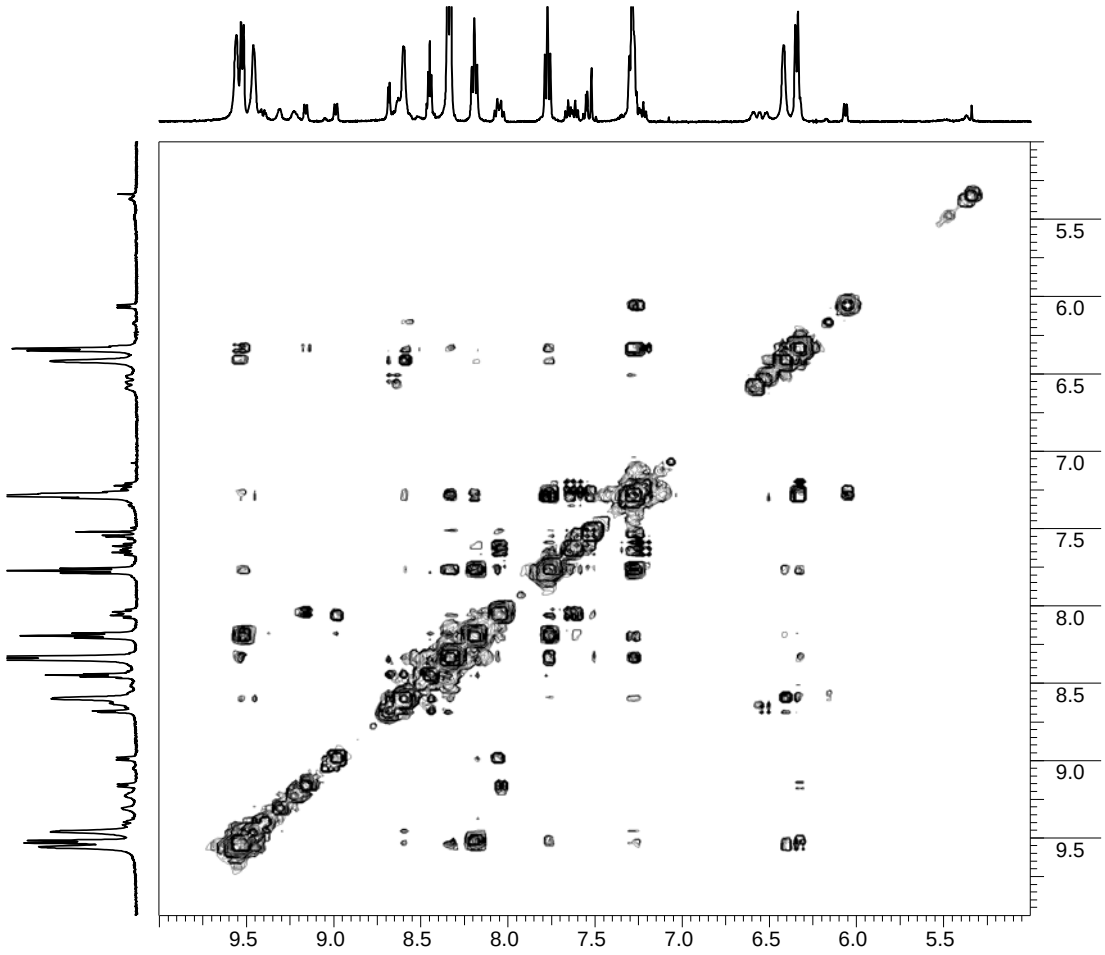

Figure 10. COSY spectrum of the Ce(TPP)(TPyP) complex.

Crystallography

Although both $Ce(TPP)_2$ and $Ce(TPyP)_2$ have been widely studied for their photophysical properties and various sensor/reporter applications, respectively,[10, 13, 39-42] the crystal structure of the latter has not been reported.

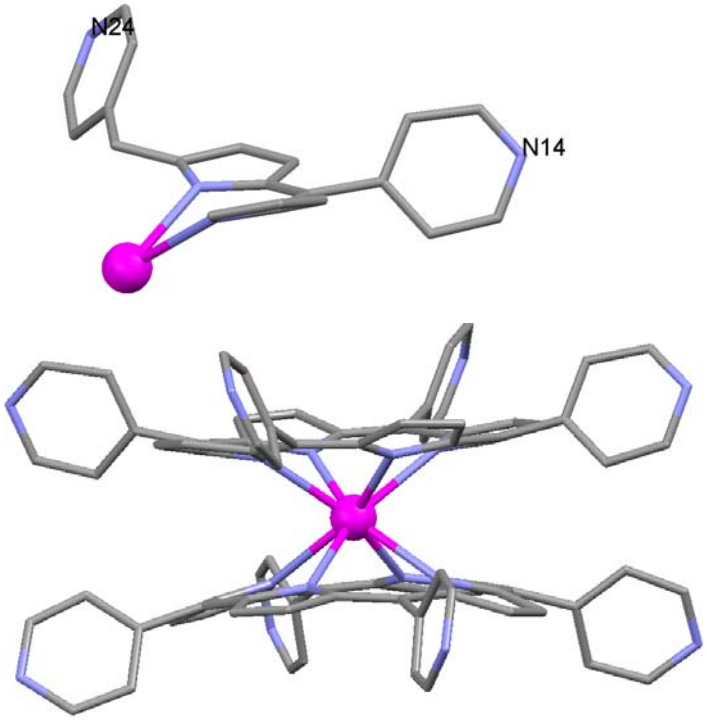

Figure 11. Asymmetric unit (top) and entire structure of $Ce(TPyP)_2$ (bottom)

There are a variety of factors that determine the degree of distortion of the otherwise planar porphyrinoid aromatic macrocycle in the sandwich complexes. First, coordination of the pyrrole nitrogens to the central metal ion involves doming of the two porphyrinoid rings towards the metal. Then, substituents on the macrocycle, such as the nominally orthogonal aryl moieties, can sterically crowd each other, and the interporphyrin distance is governed by the ionic radii of the metal ion and bond strength.[2] Strong π-π steric interactions also contribute to the non-planar distortions.[1, 22] E.g. alkyl-substituted

porphyrazine Ce(IV) sandwich complexes are distorted even though the substituents are alkanes,[20] similar distortions are found for the heteroleptic cerium compounds.[2]

Crystallographic data for the neutral Ce(IV)$(TPyrP)_2$ complex was obtained by crystallization from two 6 mg samples of the Ce$(TPyrP)_2$ complex dissolved in 4 mL of a 1:1 chloroform-methanol mixture. To one sample was added about 0.1 mL of nitrobenzene and 0.1 mL of ethyl benzoate was added to the other. The solutions were allowed to evaporate slowly. After three weeks, all but the nitrobenzene and the ethyl benzoate had evaporated and small dark crystals were found in the remaining solvent of each sample (labeled **1** and **2**, respectively). The dimensions of the Ce$(TPyP)_2$ complex are the same for both crystal structures which only differ in their respective packing arrangements and solvent molecules found in the unit cell. The complex exhibits high symmetry as the crystallographically unique fragment of its structure (excluding the solvent) is comprised of one half of one porphyrin unit bound to the cerium center, which resides on a special position **(Figure 11)**. Generally, the packing observed in both structures has neighboring complexes aligned in two dimensional sheets that are stacked vertically. The packing arrangement of crystal **1**, shown in **Figure 12**, displays widely spaced Ce$(TPyP)_2$ complexes with larger intermolecular cavities than that of **2** (**Figure 13**). The figures for the crystal packing arrangement of crystals **1** and **2** show the solvent in a space-filling mode while the Ce$(TPyP)_2$ complex is a simple framework in order to illustrate the distribution and size of the crystal cavities.

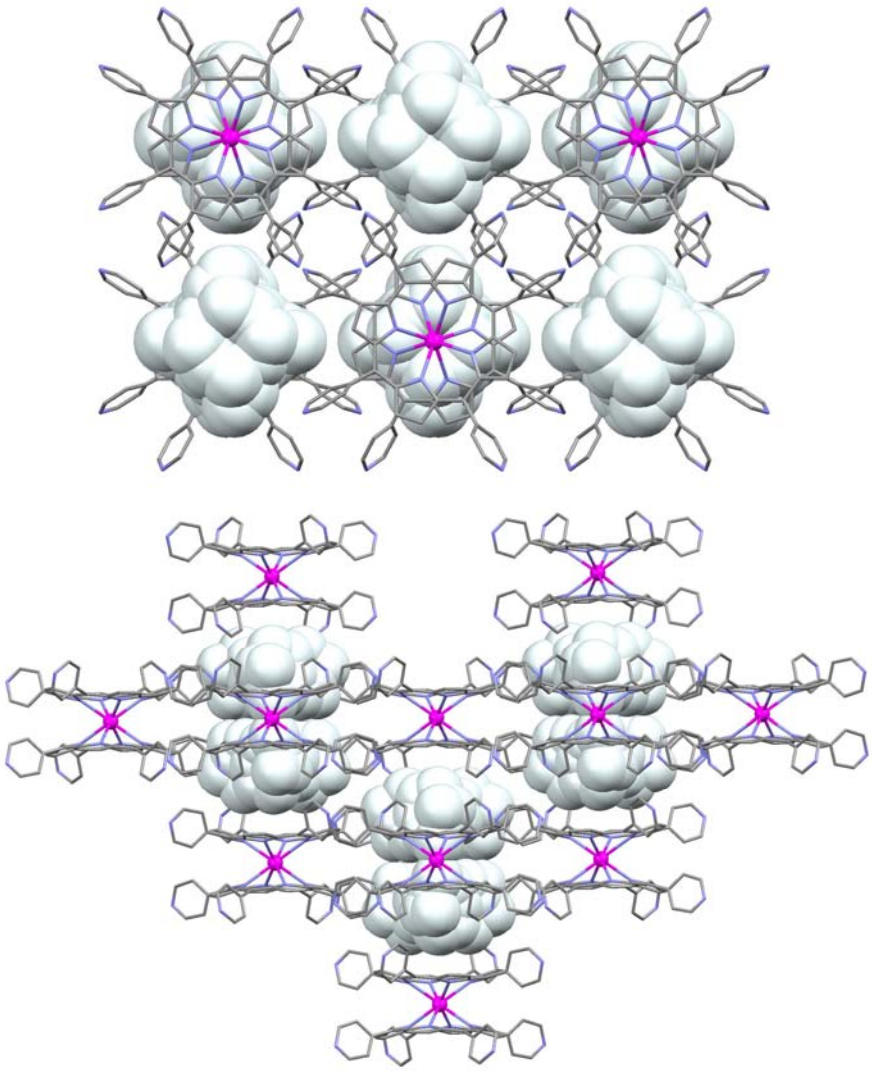

Figure 12. Packing diagrams of crystal **1** with large nitrobenzene filled cavities

We have analyzed the solvent accessible voids (between the sandwich complexes) in the corresponding crystals by using the PLATON software.[43] PLATON analysis of crystal **1** gave the following results: The solvent (nitrobenzene in this case) accessible inter-porphyrin void space amounts to 2777 $Å^3$, which consists nearly 34% of the unit-cell volume. These are isolated cavities (four per cell) centered at (0 1/4 3/4), (0 3/4 1/4),

(1/2 1/4 1/4) and (1/2 3/4 3/4). Each cavity is surrounded by six molecules of the double-decker porphyrin complex. Four complexes surround a wide cavity that is capped on the top and bottom by two more complexes to form an octahedron. Two disordered nitrobenzene molecules (disordered between four possible sites) are found in each cavity. The crystal consists of widely spaced 2D layers of the complex. Each layer is offset by ½ unit cell in the *b*-direction from the one above and below.

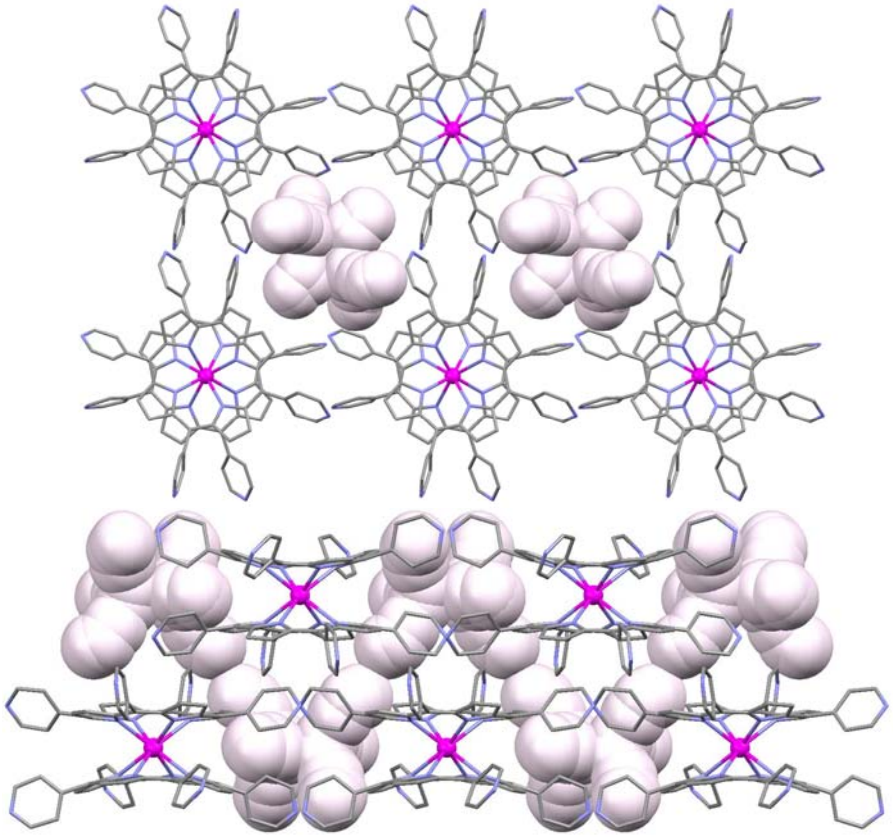

Figure 13. Packing diagrams of $Ce(TPyP)_2$ crystal **2** with smaller cavities filled with disordered methanol

The PLATON results for crystal **2** are as follows: The solvent accessible voids in this structure were assessed to be 1221 $Å^3$ and consist of about 18% of the unit-cell volume. This space is equally distributed among four different sites around (1/2 1/2 0), (1/2 0 1/4), (0 0 1/2) and (0 1/2 3/4) (with the Ce atom at 0 0 0 center). The packing design of this crystal consists of each solvent-filled cavity surrounded by four $Ce(TPyP)_2$ complexes. The *c*-axis follows through stacked layers of 2D arrays of this pattern. For each layer, the one above is offset by 1/4 unit cell in the *a* direction and the one below is offset by 1/4 unit cell in the *b* direction allowing more efficient packing than crystal **1**.

These are localized cavities, isolated from each other. As the total residual electron density was roughly estimated by PLATON to amount to about 84 electrons/unit-cell, and these residual electron-density peaks were rather low. It is reasonable to assume that in each of the four solvent sites resides 1-1.5 disordered molecule of MeOH (since from the other solvent components ethyl benzoate would be too big, and chloroform too heavy in terms of its high diffraction power).

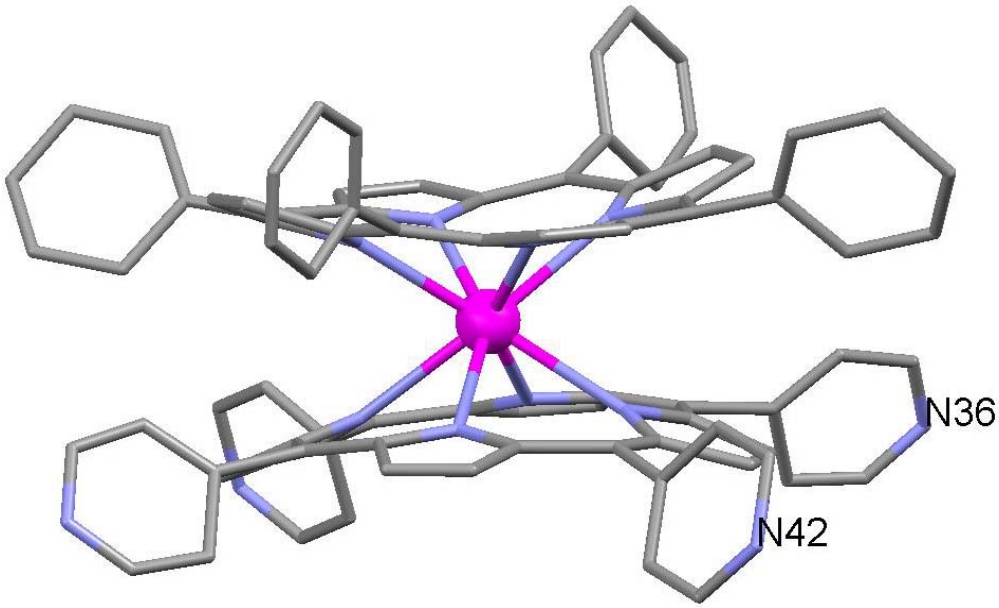

Figure 14. Crystal structure of the Ce(TPP)(TPyP) complex with pyridyl nitrogens labeled for clarity.

Crystals of the Ce(TPP)(TPyP) complex were formed by slow evaporation of a 4 mL of a 1:1; $CHCl_3$:MeOH solution of the complex with 3% v/v nitrobenzene . About 2mg of $Yb(OAc)_3 \bullet H_2O_x$ was added to observe any coordination affect the large Yb metal may have on the complex, though no Yb was observed in the final structure **3 (Figure 14)**. The space group is orthorhombic Fdd2, non-centrosymmetric, but the structure is heavily pseudo-centrosymmetric (the crystals being twinned) resembling space group Fddd. The decision to prefer Fdd2 over Fddd relies on two parameters: (1) knowledge that the compound is Ce(TPP)(TPyP) which is itself non-centrosymmetric, while in the Fddd solution it was forced to lie in a disordered manner on inversion; (2) the intensity statistics of the diffraction data clearly indicates a non-centrosymmetric distribution.

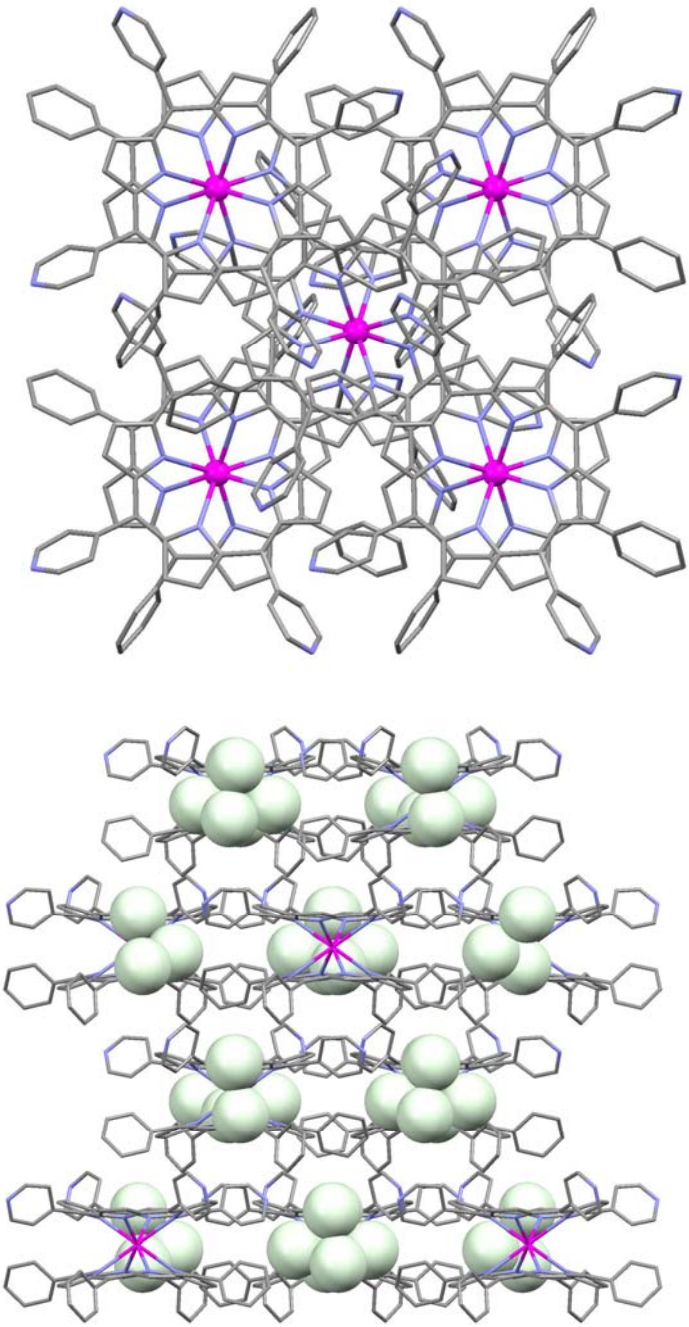

Figure 15. Packing diagrams of the Ce(TPP)(TPyP) crystal structure. Top-down view through *c*-axis (top) shows dense packing of the complex. Side view (bottom) shows small water filled cavities.

PLATON tells us that the total solvent accessible void amounts to 2350.4 A^3 per unit-cell, which consists 17.2% of the unit-cell volume (13641.9 A^3). This solvent accessible space is equally divided into 8 small local voids (294 A^3 each), in every one of

which are accommodated the 3 water species. Thus, we can say that this porphyrin compound packs much more efficiently in the lattice than the other ones **(Figure 15)**. Yet, this always depends on the crystallization conditions. Our first crystallization of this compound without the $Yb(OAc)_3 \bullet H_2O_x$, which indeed may have acted as an efficient "organizer" of the porphyrin molecules, led to a very fuzzy crystal structure with a lot of unidentified solvent included in the lattice in a disordered manner.

An important feature of this structure is the high level of distortion of the porphyrin framework. We observe ca. 10° variation in the C_2-axis tilt of the phenyl groups and a twisting of the macrocycle which lends itself to other visible distortions. The tetra pyridyl porphyrinate macrocycles also shows distortion where the deviation from planarity varies around the porphyrin macrocycle. This is in agreement with our NMR data as this would cause a variation in the shift of the phenyl protons. The *endo* and *exo* shifts are almost purely dependant on this tilt. In contrast the $Ce(TPyP)_2$ complex appears more evenly "domed" around the macrocycle which is reflected in its simpler NMR spectrum. The inherent twisting of the macrocycle having unevenly angled aryl groups, would surely affect the pyrrolic shift as we also see unassigned peaks in the NMR that may be attributed to the non-equivalent pyrrolic protons.

$Ce(TPyP)_2$ complex:

There has been some discussion in the literature regarding the dynamics of the $Ce(TPyP)_2$ species in regards to the origin of the allosteric effects upon binding of ditopic moieties to the pyridyl groups on the same, or opposite porphyrins.[11, 39-41] The discussion centers on whether the ditopic moieties inhibit rotation of the TPyP groups about the

principle axis, inhibit rotation of the pyridyl groups which then inhibits porphyrin rotation, or induces a torsional strain.[39] It has been assumed that the normally orthogonal pyridyl moieties must simultaneously rotate to nearly coplanar conformations to allow the porphyrins to rotate. The ^{1}H NMR and x-ray data provide insight into this discussion in that the NMR demonstrates that both the porphyrin and the pyridyl rotations occur at room temperature but are considerably slowed upon cooling to 3 $^{\circ}$C. The x-ray structure, at -173 $^{\circ}$C, reveals a significant domed distortion in the macrocycles such that the pyridyl groups actually point away from the cerium center (**Figure 8**). At room temperature in solution the distortions are likely greater, thus pyridyl group rotation may not be necessary for porphyrin rotation and inhibition of the pyridyl rotation an unlikely origin of the cooperativity. This is somewhat counter intuitive, but the small ionic radius of Ce(IV) results significant π-π interactions between the porphyrins and causes the domed distortion. This indicates that the relatively weak binding of the ditopic moieties are unlikely to significantly alter the conformation of the porphyrin macrocycles, or cause them to tilt to one side, or rotate the pyridyl groups to a conformation that inhibits macrocycle rotation.

Table. 2 Crystallographic data for CeP_2 complexes

Compound	1	2	3
emp formula	$C_{104}H_{68}Ce_1N_{20}O_8$	$C_{21.50}H_{18}Ce_{0.25}N_4O_{1.5}$	$C_{84}H_{52}Ce_1N_{12}O_3$
formula wt.	1865.90	391.43	1417.50
cryst. System	Orthorhombic	Tetragonal	orthorhombic
space group	Ccca	I4(1)22	Fdd2
unit cell			
a/ Å	21.023(4)	14.795(2)	20.5828(9)
b/ Å	21.077(4)	14.795(2)	21.1716(9)
c/Å	18.476(4)	30.747(6)	31.3053(14)
α/ Å	90	90	90
β/°	90	90	90
γ/°	90	90	90
V/ $Å^3$	8187.(3)	6730.7(19)	13641.9(10)
Z	4	16	8
ρ_{calcd} [gcm^{-3}]	1.514	1.545	1.380
μ(MoKα) mm^{-1}	0.635	0.751	0.729
T/°K	100	100	110
F(000)	3816	3224	5776
crystal size	0.50 X 0.44 X 0.34	0.40 X 0.40 X 0.12	0.25 X 0.25 X 0.20
Θ range[°]	2.93 to 27.52	3.06 to 27.49	1.41 to 27.88
index ranges	$-27 \le h \le 27$	$-19 \le h \le 19$	$-26 \le h \le 26$
	$-27 \le k \le 26$	$-19 \le k \le 19$	$-27 \le k \le 27$
	$-23 \le l \le 23$	$-39 \le l \le 39$	$-41 \le l \le 41$
reflns collected	55828	38838	24470
ind. reflections	4663	3850	7793
R(int)	0.1058	0.1150	0.0660
Completeness to Θ_{max} [%]	98.7	98.8	99.1
reflns gt	3998	3459	6062
data/restraints/parameters	4663/0/339	3850/0/275	7793/1/451
final R indices [$I > 2\sigma(I)$]			
*R*1	0.0785	0.0546	0.0705
*wR*2	0.1874	0.1166	0.1645
R indices (all data)			
*R*1	0.0898	0.0632	0.0971
*wR*2	0.1943	0.1202	0.1804
largest diff. peak and hol [$eÅ^{-3}$]	1.1569 and -0.831	1.989 and -0.556	1.567 and -0.682

Electronic Spectroscopy

In general, the formation of sandwich complexes results in blue shifts of the Soret band and three major Q bands, indicating strong pi-pi interactions and the increased symmetry of the chromophore, respectively. There are additional weak Q bands that are believed to arise from electron delocalization over the two porphyrinoids,[20] and this has been correlated with the ionic radii of the ligated metal.[2, 44]

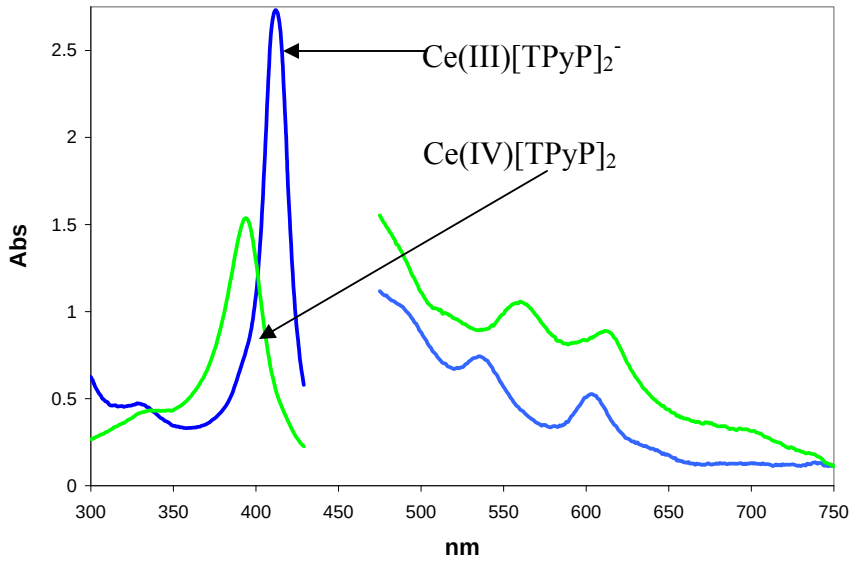

Figure 16. UV-Vis of a solution of $Ce(TPyP)_2$ before(green) and after(blue) treatment with excess hydrazine to form the $Ce(III)(TPyP)_2^{-1}$ complex in chloroform, 50% methanol. Note the large red shift of the Soret as well as the two lower energy Q-bands. The extinction coefficient nearly doubles for the reduced species having a narrower band width.

Comparison of the $Ce(IV)[TPyP]_2$ before and after treatment with excess hydrazine displays the known red shifts of the Soret band as well as the two low energy Q-bands for the formation of the $Ce(III)[TPyP]_2^{-1}$ complex. Interestingly, a large increase in the extinction coefficient of the Soret band is observed after reduction as the absorption band narrows significantly.

Experimental

Reagents and methods. 1,2,4 trichlorobenzene, 1-dodecanol, H_2TPP, H_2TPyrP and sodium hydride were obtained from Aldrich and used without further purification. Sodium hydride was in a 60% dispersion in mineral oil; it was weighed and used as found. $Ce(acac)_3 \cdot H_2O$ was obtained from Strem chemicals. H_2T-3-CNPP was synthesized according to literature methods by condensation of pyrrole and 3-cyano benzaldehyde in proprionic acid.[45] ^{1}H NMR spectra were run on a 500 MHz Varian Inova. UV-Vis spectra were recorded on a Carey Bio-1 spectrophotometer. Mass spectroscopy measurements were taken on an Agilent Mass Spectrometer, or as a service of the University of Illinois Mass Spectrometry Center.

Synthesis:

Bis(5,10,15,20-tetraphenylporphyrinato)cerium(IV) **Ce(TPP)$_2$.** 50 mg (0.08mmol) of H_2TPP was dissolved in 4 mL of 1,2,4 TCB in a 50 mL three necked round bottom flask, fitted with a condenser, under a stream of argon. In a separate 1.0 cm X 75cm tt, 35 mg (0.88 mmol) of NaH was fully reacted with 1 mL of neat dodecanol by heating briefly to a boil, and the resulting sodium dodecanate solution was decanted into the reaction vessel. The solution turned green, indicating the formation of the Na_2TPP, and was heated in a sand bath to a gentle boil under argon before the addition of 175 mg (0.40 mmol) of $Ce(acac)_3 \cdot H_2O$ suspended in 1 mL of TCB. After refluxing six hours, the reaction was allowed to cool to room temperature under an increased flow of argon. The mixture was diluted with 50 mL of CH_2Cl_2 and excess base was neutralized with three washings with distilled water in a separatory funnel. The solvent was then removed under high vacuum. The residue was dissolved in chloroform:methanol, 95:5, and passed

over a short column of silica (30 g, 4 cm x 4 cm) to remove metal impurities. The eluted fraction was a mixture of H_2TPP and $CeTPP_2$ which are difficult to separate by chromatography. The sandwich complex was isolated by evaporation of this fraction to dryness followed by multiple recrystallizations from a 1:1 toluene/hexane solution wherein the solution was heated, sonicated briefly, and then cooled by refrigeration. The target sandwich complex precipitates and unreacted porphyrin was decanted in the supernatant. The process was repeated five times until no free base was detected by UV-Vis spectroscopy. Purity was determined by UV-Vis and TLC to yield 33mg, (59%) $Ce(TPP)_2$. Spectroscopic characterization is consistent with the literature values.[26] UV-Vis spectrum in $CHCl_3$ λ_{max} nm (log ϵ): 337(4.65),396(5.33), 486(4.10), 540 (3.99), 631(3.40). negative ES MS m/z calcd. for M^{-1} 1364.38 found 1364.37

Bis[5,10,15,20-tetrakis(-4-pyridyl)porphyrinato]cerium(IV) **$Ce(TPyP)_2$**. Preparation of the $Ce(TPyP)_2$ complex was similar to that of the $Ce(TPP)_2$. Increasing the proportion of dodecanol to 50% of the total reaction solvent volume helped in the solvation of H_2TPyP, which is poorly soluble in TCB. The reaction vessel was a 18 X 150 mm disposable borosilicate test tube fitted with a rubber septum and embedded approximately 5 cm into a hot sand bath. Argon was introduced and vented via syringe needles through the septum. 50 mg (0.08mmol) of H_2TPyP was dissolved and heated just below reflux in a mixture of 2 mL of TCB and 2 mL of dodecanol under a stream of argon. In a separate test tube 35 mg (0.88 mmol) of NaH was fully reacted with 1 mL dodecanol by heating, and the resulting dodecanate solution was decanted into the porphyrin solution which turned green under a flow of argon. The reaction mixture was

heated to a gentle reflux under a strong stream of argon just before 176 mg of $Ce(acac)_3 \cdot H_2O$ suspended in 1 mL of TCB was added via pipette. The reaction was refluxed for 2.5 hours under argon and allowed to cool. A crude product precipitated from the reaction mixture upon addition of ca. 300 mL of hexanes, 1% v/v acetic acid (to neutralize excess base) and subsequently filtered. The precipitate was washed with three additional 10 mL portions of hexanes. The filtrate, containing a dilute amount of the H_2TPyP and reaction solvents, was discarded. The precipitate was dried in an oven at 120 $^{\circ}$C overnight to evaporate trace amounts of solvent. UV-Vis spectra of the crude precipitate indicated that the reaction products contained a large fraction of a green reduced sandwich complex nominally ascribed to $Ce(III)(TPyP)_2H^+$ with a broad UV-Vis Soret band at 408 nm, consistent with literature values.[26] Two different oxidation methods were used to treat the mixture of the sandwich complexes with the (III/IV) cerium valences to obtain a neutral, brown-colored solution of the Ce(IV) complex.

Oxidation procedure 1. A 1:1 $CHCl_3$:MeOH solution of the crude product was refluxed with excess DDQ for 2 hours. Oxidation was monitored by UV-Vis spectra until the 393 nm Soret band of the sandwich complex was maximized compared to a small fraction of unreacted porphyrin with a Soret absorbance at 417 nm. The DDQ was removed by evaporating the reaction mixture to dryness and suspending the residue in methanol with 10% H_2O. After sonication, the solution was centrifuged and the DDQ was decanted in the supernatant. This procedure was repeated three times such that the UV-Vis spectra and TLC indicated the DDQ had been completely removed. The solid was dissolved in chloroform and loaded onto a silica column (2.5 cm x 20 cm). The first fraction containing the free base H_2TPyP was eluted with 90:10 (v/v) CH_2Cl_2:MeOH,

while the second fraction containing a mixture of $Ce(TPyP)_2$ and H_2TPyP was eluted with 85:15 (v/v) CH_2Cl_2:MeOH. A third, brown-orange fraction of $Ce(TPyP)_2$ was eluted with 80:20 CH_2Cl_2:MeOH. The second fraction was purified to remove the trace amounts of H_2TPyP by a second column and combined with the products of the first column to yield 31 mg of the $Ce(TPyP)_2$ complex, 56% yield.

Oxidation procedure 2. 200 mg of Na_2TPyP was generated *in situ* and reacted with five equivalents $Ce(acac)_3 \cdot H_2O$ in the same manner as above. The total solvent volume was 15 mL of a 1:1 (v/v) TCB:dodecanol mixture. The crude product was precipitated with 500 mL hexane with 1% CH_3COOH. The dried, crude precipitate was dissolved in 200 mL of a 1:1 (v/v) $CHCl_3$:MeOH solution and stirred over an aqueous layer, 300 mL, of excess $K_2Cr_2O_7$ (0.2M) for one hour. The oxidation to the cerium IV species was monitored by UV-Vis spectroscopy as above. The $K_2Cr_2O_7$ method is more efficient due to the shorter reaction time and by the fact that the oxidant does not remain in the organic phase. The mixture was transferred to a separatory funnel and the chloroform layer was removed. A layer of white insoluble material (most likely cerium salts) between the chloroform and aqueous layers was excluded from the chloroform solution. The complex was then purified over silica as outlined above, to yield 176 mg of the sandwich complex, 80% yield, after two silica gel columns (2.5 cm x 30 cm) purifications.

All spectroscopic data were identical for the products of both preparations and consistent with literature values.[26] UV-Vis in 1:1 $CHCl_3$:MeOH λ_{max} nm (log ϵ) 332(4.73), 393(Soret, 5.28), 488(4.12), 535(3.96), 602(3.76).. negative ES MS m/z calcd. for M^{-1} 1373.5 found 1373.2.

Bis[5,10,15,20-tetrakis(3-cyanophenyl)porphyrinato]cerium(IV), **Ce(T-3-CNPP)$_2$** was prepared in the same manner as Ce(TPyP)$_2$. 70 mg of NaH dispersion was fully reacted with 2 mL of dodecanol and added to100 mg of porphyrin pre-dissolved in 8 mL of a 5:3 TCB:dodecanol mixture. 340 mg Ce(acac)$_3$ ·H$_2$O was added and the mixture refluxed for 3 hours under a stream of argon. After precipitation by addition of 400 mL of hexanes with 1% CH_3COOH and filtration, the solid was dried in an oven overnight. The crude product was then dissolved in a minimum of $CHCl_3$ and treated with an aqueous layer of $K_2Cr_2O_7$ until the Ce(IV) species was the major species detected by UV-Vis spectra. Unreacted porphyrin was the first fraction from a silica gel column (2.5 cm x 150 cm) using neat CH_2Cl_2 as the eluent. Ce(T-3-CNPP)$_2$ was eluted as a broad second fraction with 2:98 MeOH:CH_2Cl_2. 10 mL of MeOH was added to the second fraction (ca. 100 mL) and the CH_2Cl_2 was removed by heating the flask, at which point the product precipitated, and was filtered from the remaining methanol. The precipitate was dried and weighed to yield 76 mg of the sandwich complex, 68% yield. UV-Vis in $CHCl_3$, λ_{max} nm (log ϵ): 334(sh, 4.69), 397(Soret, 5.33), 486(4.13), 539(4.01), 604(3.69). MALDI MS m/z calcd. for M+H$^+$ 1566.67 found 1567.

(5,10,15,20-tetraphenylporphyrinato)(5,10,15,20-tetrakis(-4pyridyl)porphyrinato)cerium (IV) **Ce(TPP)(TPyP)** was prepared in the same manner as Ce(TPyP)$_2$, but on a larger scale. The synthesis forms a statistical mixture of Ce(TPP)$_2$, Ce(TPyP)$_2$, and Ce(TPP)(TPyP) by reacting equal amounts of the free base porphyrins with the Ce(III)(acac)$_3$ starting complex. 200mg of H$_2$TPP and 200mg of H$_2$TPyP was dissolved in 40 mL of a 1:1 mixture of TCB and dodecanol in a 100 mL

three- necked, round bottom flask fitted with a condenser. The vessel was placed in a hot sand bath (ca.300 $^{\circ}$C) so that the level of the sand was just below the solvent level. In a separate test tube, 280 mg (6.51 mmol) of NaH 60% dispersion was fully reacted with 5 mL of dodecanol by heating, and the resulting dodecanate solution was decanted into the porphyrin solution which turned green under a flow of argon. After the reaction chamber was purged with sufficient argon, 1.421g of $Ce(acac)_3 \cdot H_2O$ was added to the mixture. After four hours of reflux, the reaction mixture was precipitated with 500 mL of hexanes. The precipitate was filtered and washed with 4, 10 mL portions of hexane. The filtrate contained reaction solvents, unreacted porphyrins, and trace amounts of $Ce(TPP)_2$. The filtrate was discarded and the precipitate was dissolved in chloroform. The chloroform solution was treated with aqueous $K_2Cr_2O_7$ as described in *oxidation procedure 2* (above). The chloroform layer was isolated and preloaded onto 20g of silica by evaporation of the solvent. The preloaded silica was added to a silica column of neat CH_2Cl_2. 1% MeOH in CH_2Cl_2 eluted trace amounts of unreacted H_2TPP as frac **1** and about 50mg, determined spectroscopically by UV-Vis, of $Ce(TPP)_2$ as frac **2**. Increasing the MeOH on a slow gradient to 4% eluted the target complex, Ce(TPP)(TPyP) as frac. **3** followed closely by unreacted H_2TPyP as frac.**4** with 5-7% MeOH. About 65mg, determined spectroscopically by UV-Vis, of $Ce(TPyP)_2$ was eluted with 10-15% MeOH as frac.**5**. Frac. **3,** Ce(TPP)(TPyP), was dried and weighed to yield 117mg, 33%. UV-Vis in $CHCl_3$, λ_{max} nm (log ϵ): 332(sh, 4.71), 395(Soret, 5.32), 490(4.08), 537(3.99), 607(2.16). MALDI MS m/z calcd. for $M+H^+$ 1368.3 found 1368.1

Conclusions

The synthetic strategies presented here allow small-scale reactions in good yields and quick purification of $Ce(IV)P_2$ complexes. Many applications of lanthanide and actinide porphyrinoid sandwich complexes have been proposed based on their optical, mechanical, and oxidation/reduction chemistry. By analogy to the well-known supramolecular chemistry of the various isomers of the mixed meso phenyl/pyridyl porphyrins,[16-19, 46-50] precise nanoarchitectures of sandwich complexes may afford a variety of other applications that are unobtainable from the single molecule or amorphous aggregates. Thus, the cyano and pyridyl moieties on these compounds may facilitate the self-assembly or self-organization of these systems into new materials. However it should be noted that the crystallographic data reveals that the distortions in the porphyrins significantly alter the orientation of the exocyclic pyridyl and cyano ligands, such that these molecular geometries are unlikely techtons for planar arrays in of themselves.

References

1. Buchler, J. W.; Ng, D. K. P., Metal Tetrapyrrole Double- and Triple-Deckers with Special Emphasis on Porphyrin Systems. In *The Porphyrin Handbook*, Kadish, K. M.; Smith, K. M.; Guilard, R., Eds. Academic Press:: San Diego, 2000; Vol. 3, pp 245-294.

2. Bian, Y.; Jiang, J.; Tao, Y.; Choi, M. T. M.; Li, R.; Ng, A. C. H.; Zhu, P.; Pan, N.; Sun, X.; Arnold, D. P.; Zhou, Z. Y.; Li, H. W.; Mak, T. C. W.; Ng, D. K. P., *J. Am. Chem. Soc.* **2003,** 125, (40), 12257-12267.

3. Gross, T.; Chevalier, F.; Lindsey, J. S., *Inorg. Chem.* **2001,** 40, (18), 4762-4774.

4. Gryko, D.; Li, J.; Diers, J. R.; Roth, K. M.; Bocian, D. F.; Kuhr, W. G.; Lindsey, J. S., *J. Mat. Chem.* **2001,** 11, (4), 1162-1180.

5. Clausen, C.; Gryko, D. T.; Yasseri, A. A.; Diers, J. R.; Bocian, D. F.; Kuhr, W. G.; Lindsey, J. S., *J. Org. Chem.* **2000,** 65, (22), 7371-7378.

6. Otsuki, J.; Kawaguchi, S.; Yamakawa, T.; Asakawa, M.; Miyake, K., *Langmuir* **2006,** 22, (13), 5708-5715.

7. Li, Q. L.; Surthi, S.; Mathur, G.; Gowda, S.; Zhao, Q.; Sorenson, T. A.; Tenent, R. C.; Muthukumaran, K.; Lindsey, J. S.; Misra, V., *Appl. Phys. Lett.* **2004,** 85, (10), 1829-1831.

8. Qian, D. J.; Liu, H. G.; Jiang, J., *Colloids Surf., A* **2000,** 163, (2-3), 191-197.

9. Buchler, J. W.; Scharbert, B., *J. Am. Chem. Soc.* **1988,** 110, (13), 4272-4276.

10. Ikeda, M.; Takeuchi, M.; Shinkai, S.; Tani, F.; Naruta, Y.; Sakamoto, S.; Yamaguchi, K., *Chem. Eur. J.* **2002,** 8, (24), 5541-5550.

11. Shinkai, S.; Ikeda, M.; Sugasaki, A.; Takeuchi, M., *Acc. Chem. Res.* **2001,** 34, (6), 494-503.

12. Takeuchi, M.; Imada, T.; Shinkai, S., *Angew. Chem. Int. Ed.* **1998,** 37, (15), 2096-2099.

13. Sugasaki, A.; Ikeda, M.; Takeuchi, M.; Shinkai, S., *Angew. Chem. Int. Ed.* **2000,** 39, (21), 3839-3842.

14. Goldberg, I., *Chem. Comm.* **2005**, 1243-1254.

15. Goldberg, I., *Cryst. Eng. Comm.* **2002,** 4, 109-116.

16. Drain, C. M.; Goldberg, I.; Sylvain, I.; Falber, A., *Top. Curr. Chem.* **2005,** 245, 55–88.

17. Drain, C. M.; Lehn, J.-M., *Chem. Commun.* **1994**, 2313-2315 (correction 1995, p503).

18. Drain, C. M.; Nifiatis, F.; Vasenko, A.; Batteas, J. D., *Angew. Chem. Int. Ed.* **1998,** 37, (17), 2344-2347.

19. Drain, C. M.; Hupp, J. T.; Suslick, K. S.; Wasielewski, M. R.; Chen, X., *J. Porph. Phthal.* **2002,** 6, (4), 241-256.

20. Montalban, A. G.; Michel, S. L. J.; Baum, S. M.; Vesper, B. J.; White, A. J. P.; Williams, D. J.; Barrett, A. G. M.; Hoffman, B. M., *J. Chem. Soc. Dalton Trans.* **2001**, 3269-3273.

21. Buchler, J. W.; Kapellmann, H.-G.; Knoff, M.; Lay, K.-L.; Pfeifer, S., *Z. Naturforsch* **1983,** 38b, 1339-1345.

22. Buchler, J. W.; DeCian, A.; Fischer, J.; M.Kihn-Botulinski; Paulus, H.; Weiss, R., *J. Am. Chem. Soc.* **1986,** 108, 3652-3659.

23. Girolami, G. S.; Milam, S. N.; Suslick, K. S., *J. Am. Chem. Soc.* **1988,** 110, 2012-2013.

24. Girolami, G. S.; Milam, S. N.; Suslick, K. S., *Inorg. Chem.* **1987,** 26, (3), 343-344.

25. Roberts, J. D.; Hammond, G. S.; Cram, D. J., *Annu. Rev. Phys. Chem.* **1957,** 8, 299-330.

26. Buchler, J. W.; Nawra, M., *Inorg. Chem.* **1994,** 33, 2830-2837.

27. Jiang, J.; Machida, K.-i.; Adachi, G.-y., *J. Alloys Compd.* **1993,** 192, (1-2), 296-299.

28. Buchler, J. W.; Dippell, T., *Eur. J. Inorg. Chem.* **1998**, (4), 445-449.

29. Bernstein, P. A.; Lever, A. B. P., *Inorg. Chem.* **1990,** 29, (4), 608-616.

30. Tashiro, K.; Konishi, K.; Aida, T., *J. Am. Chem. Soc.* **2000,** 122, (33), 7921-7926.

31. S.Radzki; Giannotti, C., *J. Chem. Soc., Dalton Trans.* **1993**, 675 - 679.

32. Drain, C. M.; Kirmaier, C.; Medforth, C. J.; Nurco, D. J.; Smith, K. M.; Holten, D., *J. Phys. Chem.* **1996,** 100, (29), 11984-11993.

33. Drain, C. M.; Gentemann, S.; Roberts, J. A.; Nelson, N. Y.; Medforth, C. J.; Jia, S.; Simpson, M. C.; Smith, K. M.; Fajer, J.; Shelnutt, J. A.; Holten, D., *J. Am. Chem. Soc.* **1998,** 120, (15), 3781-3791.

34. Retsek, J. L.; Drain, C. M.; Kirmaier, C.; Nurco, D. J.; Medforth, C. J.; Smith, K. M.; Sazanovich, I. V.; Chirvony, V. S.; Fajer, J.; Holten., D., *J. Am. Chem. Soc.* **2003,** 125, 9787-9800.

35. Bilsel, O.; Rodriguez, J.; Milam, S. N.; Corlin, P. A.; Girolami, G. S.; Suslick, K. S.; Holten, D., *J. Am. Chem. Soc.* **1992,** 114, 6528-6538.

36. Borovkov, V. V.; Lintuluoto, J. M.; Fujiki, M.; Inoue, Y., *J. Am. Chem. Soc.* **2000,** 122, (18), 4403-4407.

37. Ponomarev, G. V.; Borovkov, V. V.; Sugiura, K.; Sakata, Y.; Shul'ga, A. M., *Tetrahedron Lett.* **1993,** 34, (13).

38. Davoras, E. M.; Spyroulias, G. A.; Mikros, E.; Coutsolelos, A. G., *Inorg. Chem.* **1994,** 33, 3430-3434.

39. Ercolani, G., *Org. Lett.* **2005,** 7, (5), 803-805.

40. Sugasaki, A.; Ikeda, M.; Takeuchi, M.; Koumoto, K.; Shinkai, S., *Tetrahedron* **2000,** 56, (27), 4717-4723.

41. Takeuchi, M.; Imada, T.; Ikeda, M.; Shinkai, S., *Tetrahedron Lett.* **1998,** 39, (43), 7897-7900.

42. Tashiro, K.; Fujiwara, T.; Konishi, K.; Aida, T., *Chem. Comm.* **1998**, (10), 1121-1122.

43. Spek, A. L., *J. Appl. Crystallogr.* **2003,** 36, (1), 7-13.

44. Gorbunova, Y. G.; Lapkina, L. A.; Martynov, A. G.; Biryukova, I. V.; Tsivadze, A. Y., *Russ. J. Org. Chem.* **2004,** 30, (4), 245-251.

45. Adler, A. D.; Longo, F. R.; Finarelli, J. D.; Goldmacher, J.; Assour, J.; Korsakoff, L., *J. Org. Chem.* **1967,** 32, 476-480.

46. Drain, C. M., *Proc. Natl. Acad. Sci., USA* **2002,** 99, 5178-5182.

47. Drain, C. M.; Batteas, J. D.; Flynn, G. W.; Milic, T.; Chi, N.; Yablon, D. G.; Sommers, H., *Proc. Natl. Acad. Sci., USA* **2002,** 99, 6498-6502.

48. Drain, C. M.; Chen, X., Self-Assembled Porphyrinic Nanoarchitectures. In *Encyclopedia of Nanoscience & Nanotechnology*, Nalwa, H. S., Ed. American Scientific Press: New York, 2004; Vol. 9, pp 593-616.

49. Milic, T. N.; Chi, N.; Yablon, D. G.; Flynn, G. W.; Batteas, J. D.; Drain, C. M., *Angew. Chem., Int. Ed.* **2002,** 41, 2117-2119.

50. Drain, C. M.; Bazzan, G.; Milic, T.; Vinodu, M.; Goeltz, J. C., *Israel J. Chem.* **2005,** 45, 255-269.

Cerium(IV) Porphyrinate appendix

I. $Ce(TPP)_2$

- A. UV-Vis
- B. Mass spec

II. $Ce(TPyP)_2$

- A. UV-Vis
- B. Mass spec

III. $Ce(T\text{-}3\text{-}CNPP)_2$

- A. UV-Vis
- B. Mass spec

IV. Ce(TPP)(TPyP)

- A. UV-Vis
- B. Mass spec

Figure 1. $Ce(TPP)_2$ UV-Vis 50 μM in $CHCl_3$ in a 1 mm cuvette Q-band region taken in a 1 cm cuvette

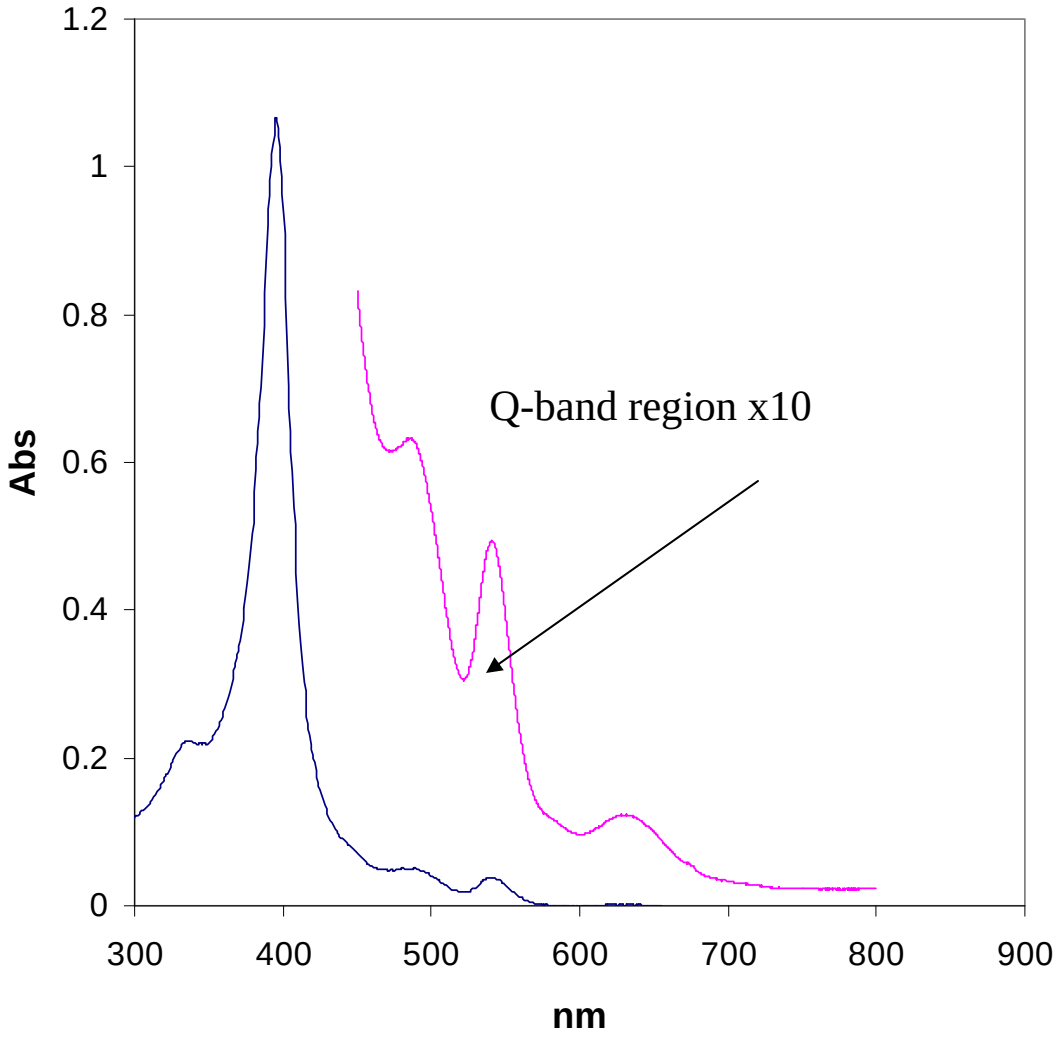

Figure 2. $Ce(TPP)_2$
negative ESI- MS

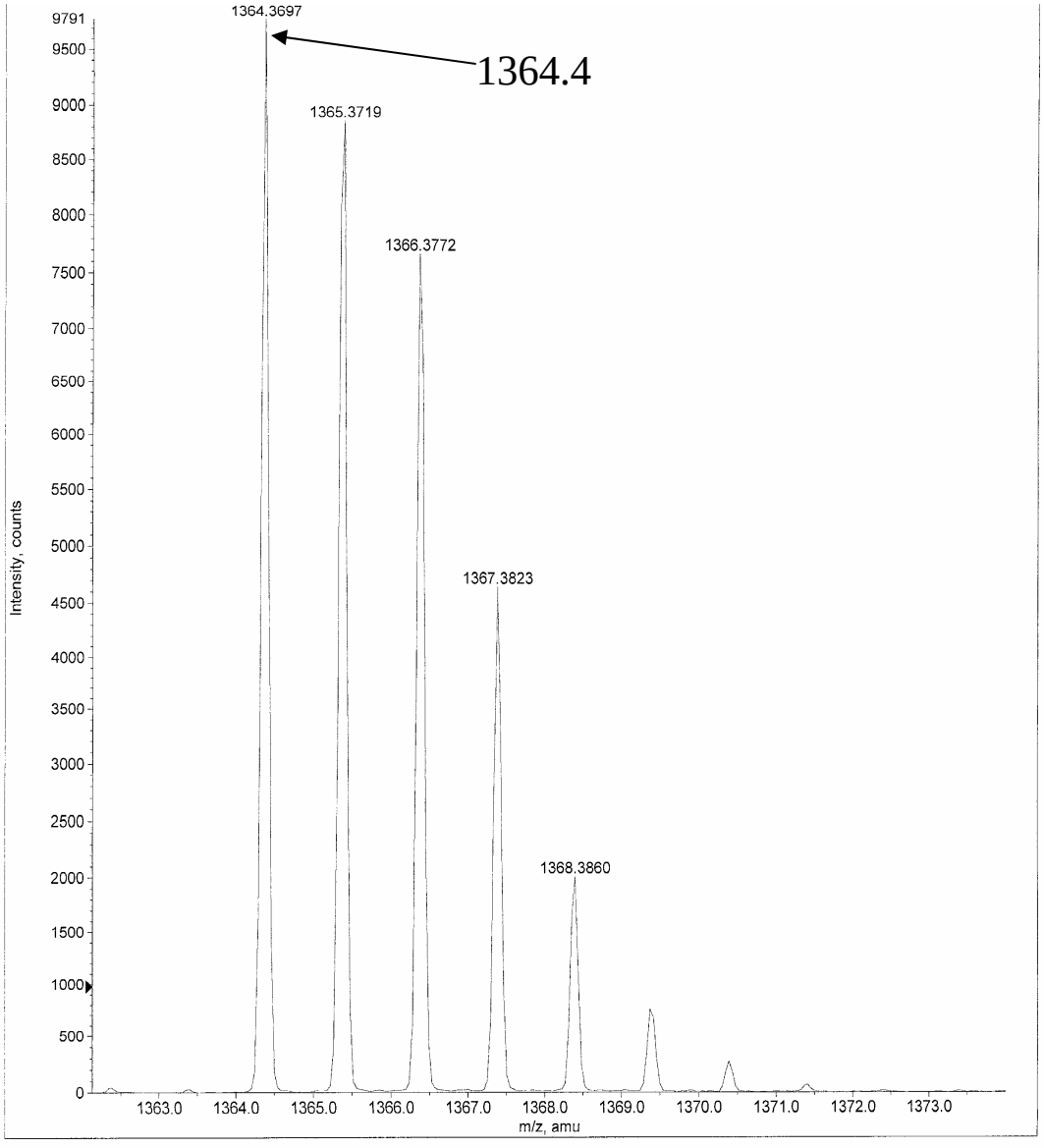

Figure 3. $Ce(TPyP)_2$ UV-Vis 50 μM in $CHCl_3$, 50% MeOH in a 1mm cuvette Q-band region taken in a 1 cm cuvette

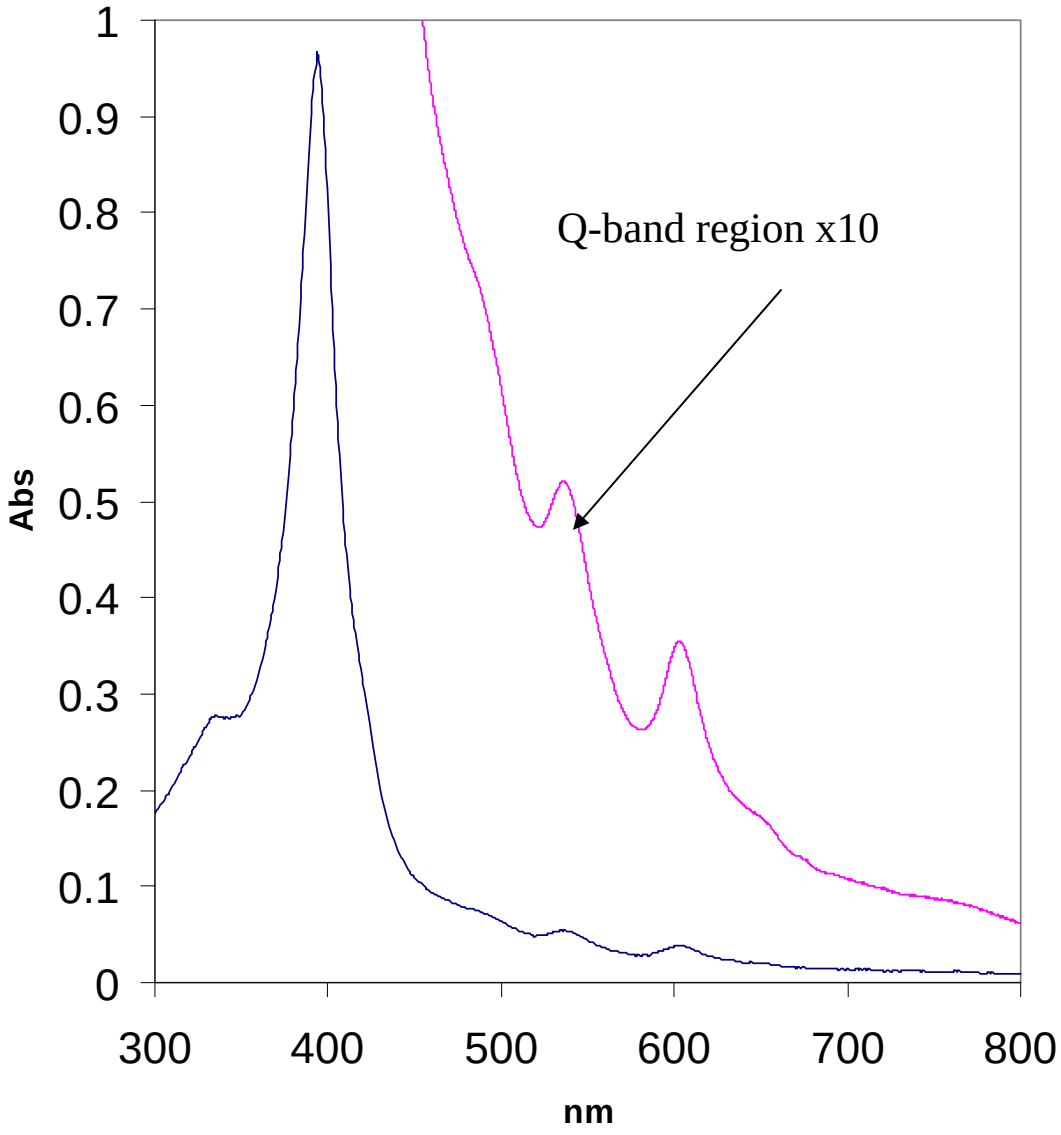

Figure 4. $Ce(TPyP)_2$
positive ESI MS

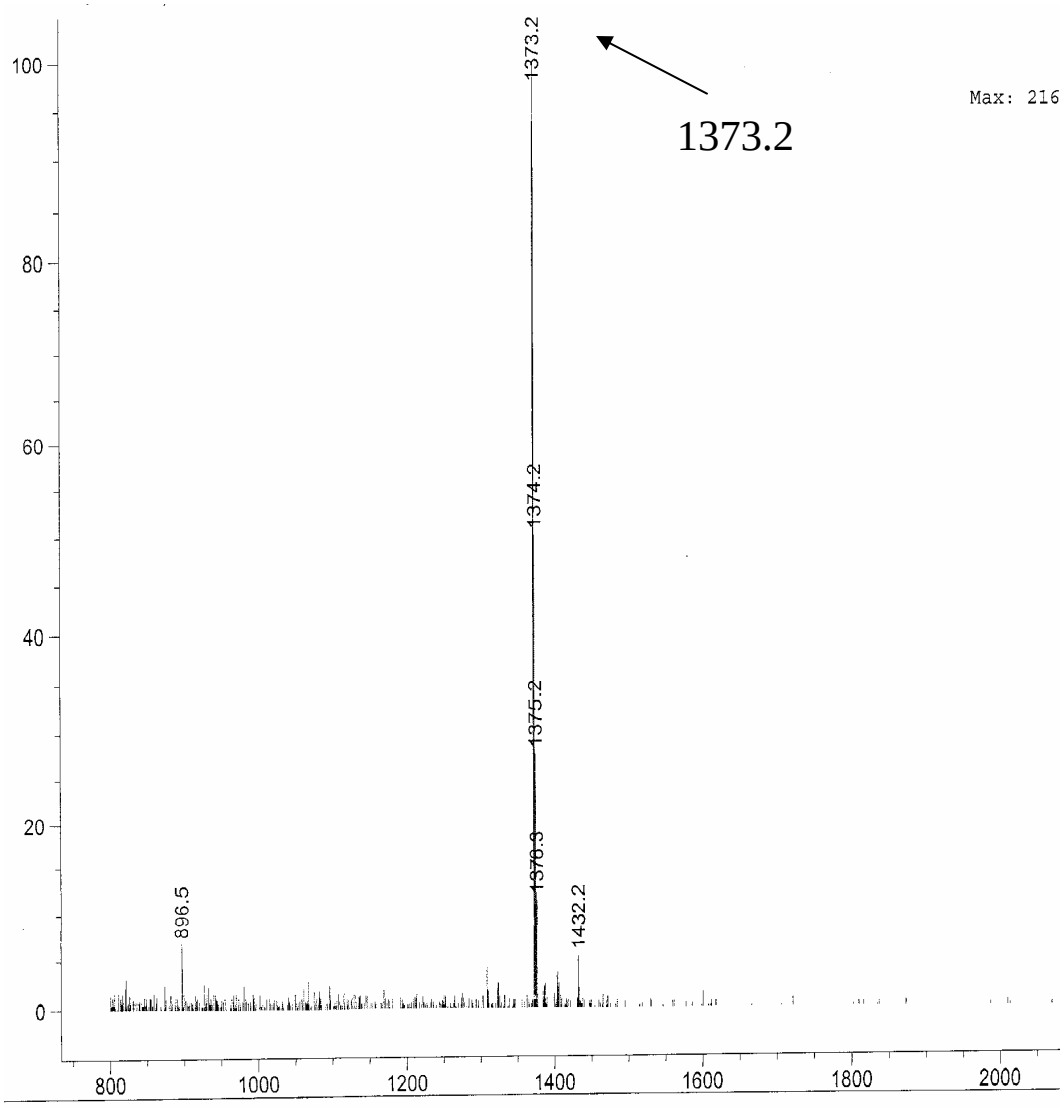

Figure 5. Ce(T-3-CNPP)$_2$ UV-Vis 50 μM in $CHCl_3$ in a 1 mm cuvette Q-band region taken in a 1cm cuvette

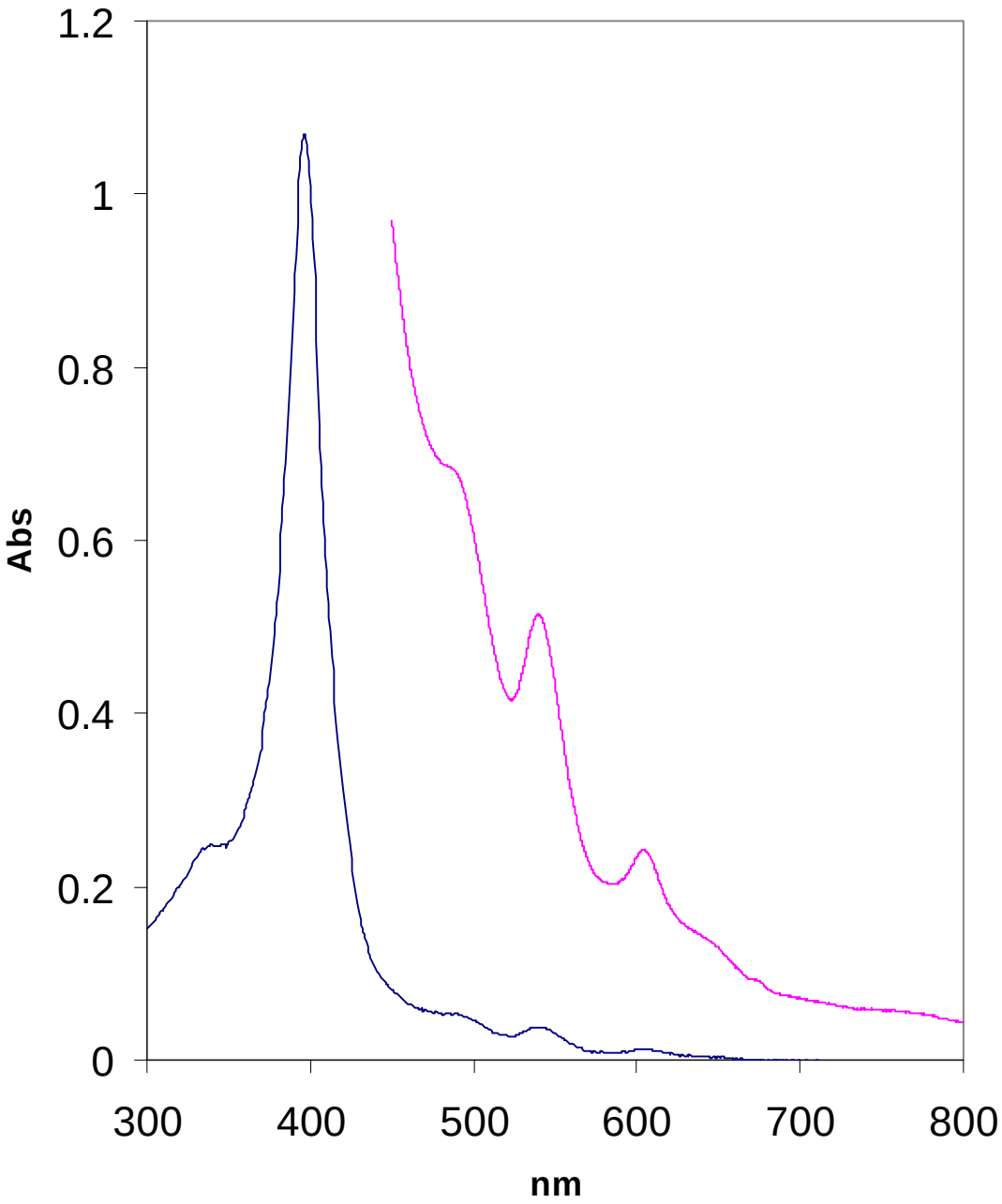

Figure 6. $Ce(T\text{-}3\text{-}CNPP)_2$ negative MALDI MS

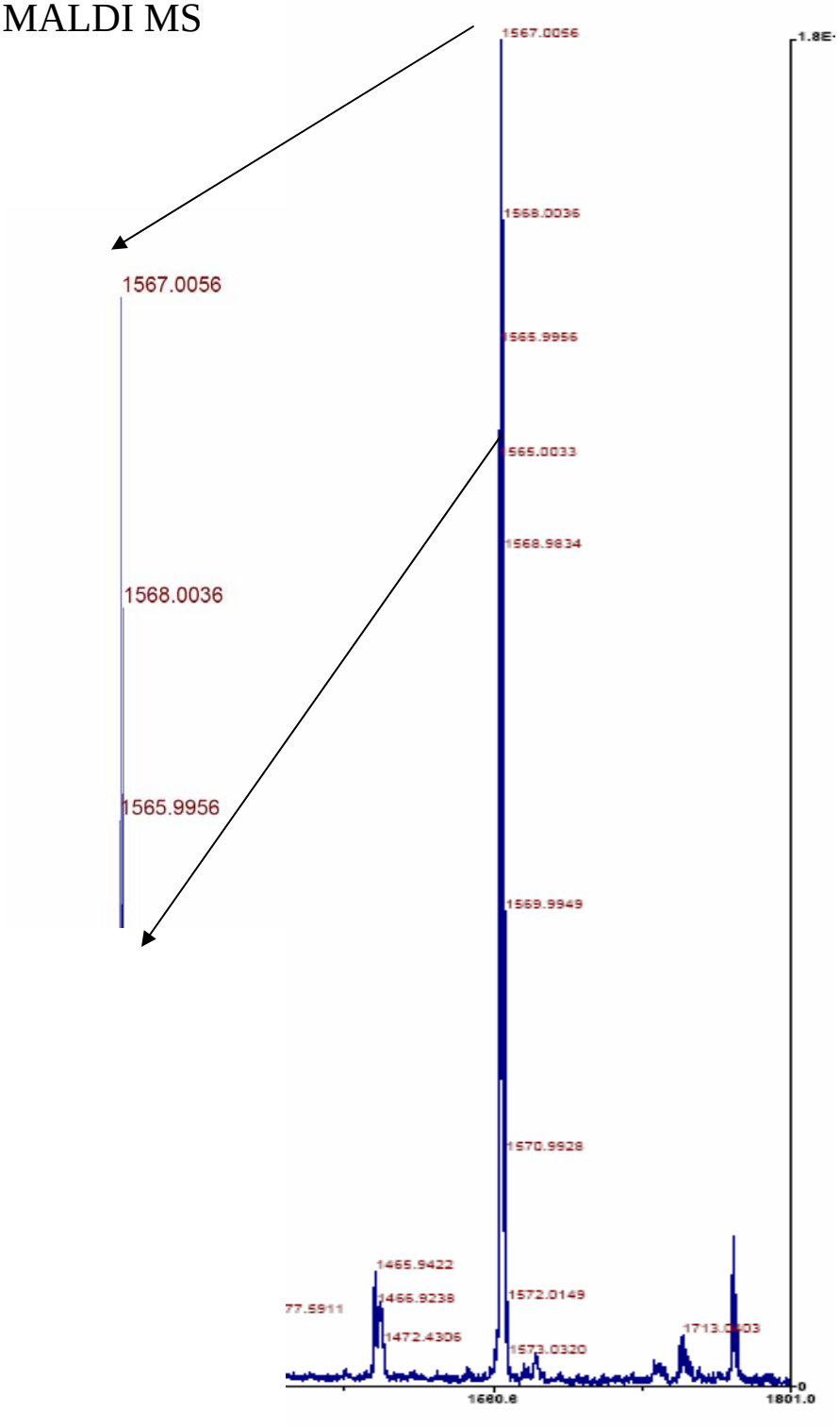

Figure 7. Ce(TPP)(TPyP) UV-Vis 36 μM in $CHCl_3$ in a 1mm cuvette Q-band region taken in a 1 cm cuvette

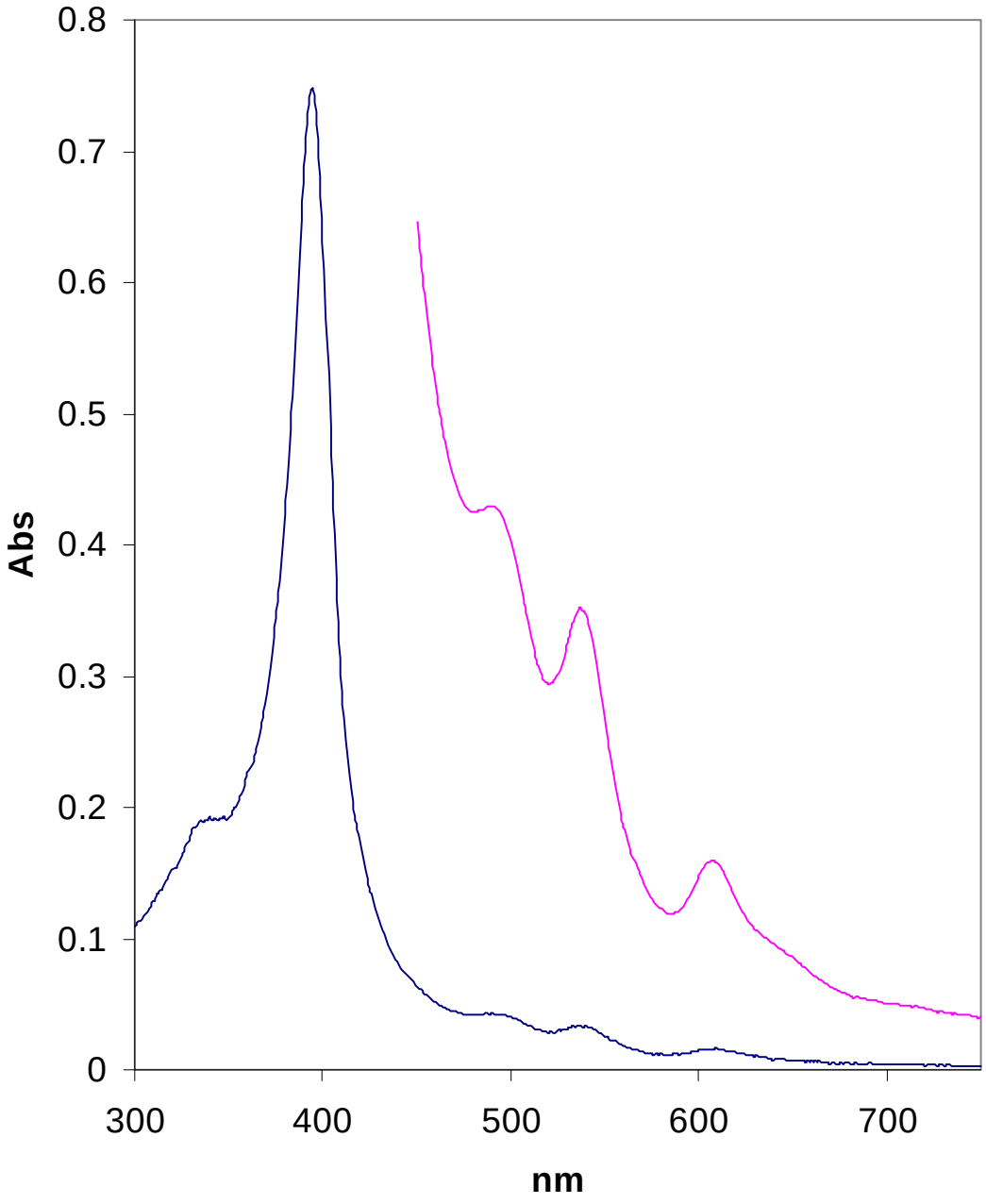

Figure 8.
Ce(TPP)(TPyP) negative MALDI MS

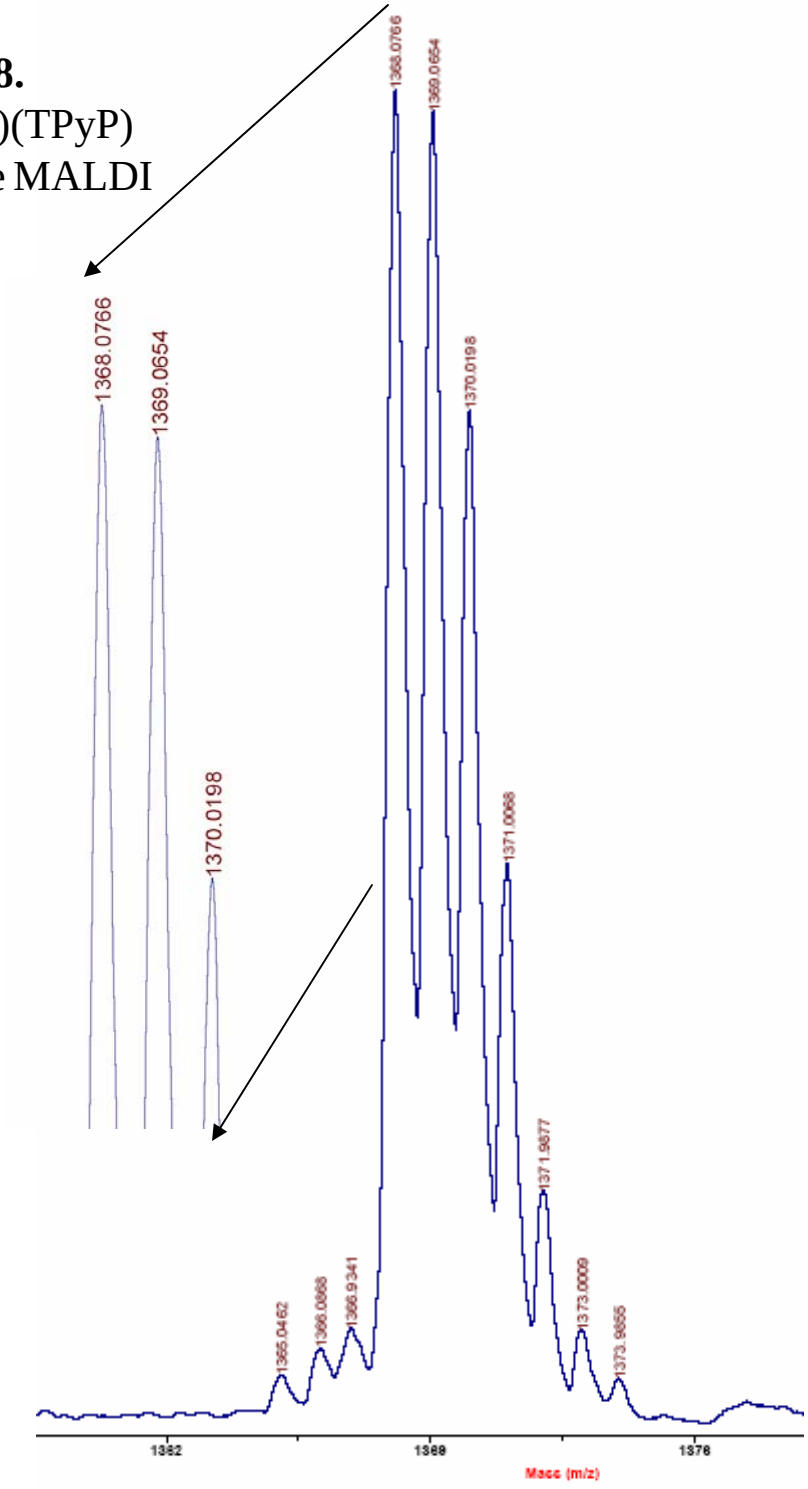

Chapter 2

Synthesis, Characterization, and Crystallography of mono Tetra-aryl Porphyrinato Hafnium(IV) Complexes

Abstract:

New strategies for the synthesis of mono tetra-aryl porphyrinato Hafnium (IV) complexes are reported. Porphyrinates, namely tetraphenyl porphyrin (TPP), tetra-(4-pyridyl) porphyrin (TPyP), tetra-tolyl porphyrin (TTP), tetra-(perfluoro)-phenyl porphyrin ($TPPF_{20}$), tetra(4-methyl ester)-phenyl porphyrin (TMeCPP), and tetra-(4-carboxy phenyl porphyrin (TCPP), have been metalated with the hafnium(IV) ion using a series of methods that cater to the solubility and reactivity of the above mentioned porphyrins. The synthesis is accomplished by refluxing the porphyrin with $HfCl_4$ in 1-chloronaphthalene or in a mixed solvent of 1-chloronaphthalene and *o*-cresol. A solventless method is also reported wherein the porphyrin is melted with $Hf(cp)_2Cl_2$ for a high yield of metalated porphyrin. Purification of the complexes over silica using 3-5% acetic acid yields the porphyrinato hafnium(IV) diacetate complexes, $Hf(P)OAc_2$. Exchange of the acetate ligands for other oxo-bearing ligands, namely para-amino benzoate (PABA), pentanoate (pent), octinoate (oct), peroxo (O_2^{-2}), SO_4^{-2}, and HPO_4^{-2} has generated a library of complexes, of which we report the crystal structures.

Introduction:

To date, the chemistry of hafnium (IV) porphyrinates[2-17] remains undeveloped, being limited to octaethyl porphyrin (OEP) and TPP, with a small variety of derivatives with different anions to balance the remaining 2+ charge and ligands to satisfy the 7-8 coordination sphere. These derivatives have the general formula $Hf(P)L_2$ where L= Cl, OAc, C_6H_4Bu[18], CH_3, *n*-butyl[10], and $P_2O_7^2$. The synthesis for hafnium(IV) and zirconium(IV) porphyrinates is similar; reported procedures are carried out in refluxing benzonitrile, DME, or toluene with the $HfCl_4$ starting complex with 80-85% yield for the $M(P)L_2$ complex. These complexes are oxophilic, thus the preference for carboxylate or other oxygen bearing anion ligands. In analogy to the zirconium (IV) porphyrinates,[18-29] which also are almost entirely OEP and TPP derivatives, much of the research on $Hf(P)L_2$ compounds has centered on the organometallic chemistry[3, 18, 21, 30] and the potential catalytic properties. Zr(IV) has an electron configuration of [Kr], and Hf (IV) has that of [Xe] 4f,[14] so both are closed shell metal ions. Because of the lack of functional groups on the porphyrin moieties, there is a paucity of supramolecular Zr(P) or Hf(P) materials with designed, hierarchical structures. Hafnium(IV) porphyrinates have an excellent potential for constructing robust supramolecular architectures for several reasons: (1) Hf is strongly bound to the porphyrin, being resistant to acids, bases, and high temperature, (2) the large coordination sphere and charge of the hafnium ion allows a great variety of ligands which can also be designed to direct intermolecular interactions, and (3) the expanded repertoire of porphyrins allows functional groups on this part of the complex to be exploited for self-assembly.

Herein, we focus on new synthetic strategies that allow the synthesis of meso tetraaryl porphyrins bearing functional groups that can serve as tectons for the construction of hierarchically structured materials, works on small scales, and minimizes solvent use in both synthesis and purification. These methods take advantage of the oxophilic nature of the Hf(IV) center and use the stable $Hf(P)OAc_2$ as a starting point for a variety of other derivatives.

Results and Discussion:

Synthesis and purification

We report a series of methods for the hafnium(IV) metalation of a range of tetra aryl porphyrinoids which differ in their respective aryl substituents, namely TPP, TTP, $TPPF_{20}$, TPyP, T-Me-CPP, and TCPP. All methods are designed to use simple apparatus such that Schlenk-ware or nitrogen boxes are not necessary, thus simplifying the preparations. The reaction vessels were disposable test tubes fitted with rubber septums

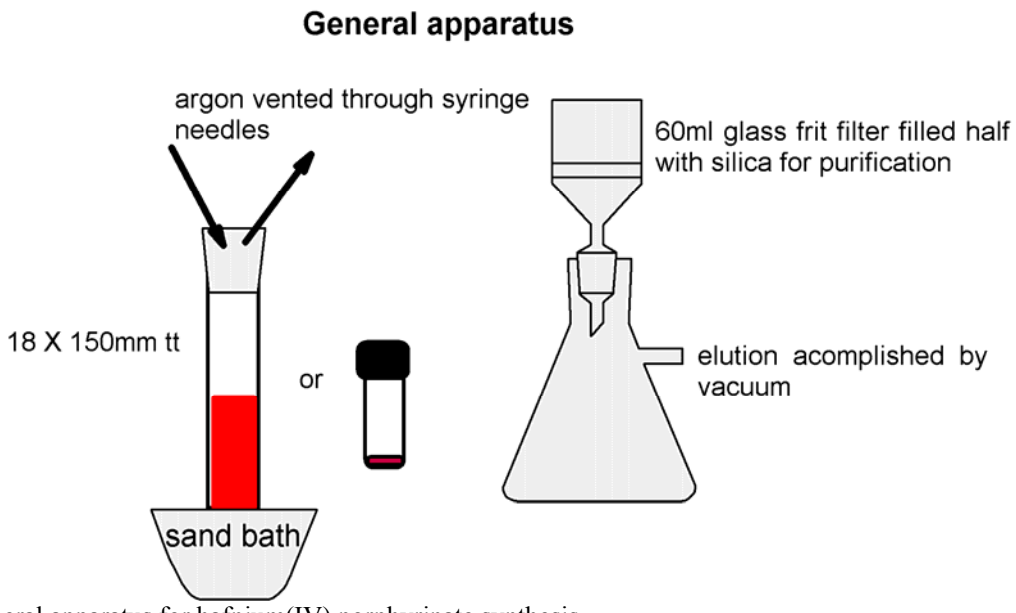

Figure 1. General apparatus for hafnium(IV) porphyrinate synthesis

or screw cap vials (**figure 1**). The new strategy for the purification over silica affords the $Hf(P)OAc_2$ derivative, which has been shown to be a favorable entry to a diverse array of derivatives.[10]

Method 1 (**figure 2**) proceeds in a similar manner to other reported methods and in similar yields, though we use 1-chloronapthalene as our reaction solvent rather than

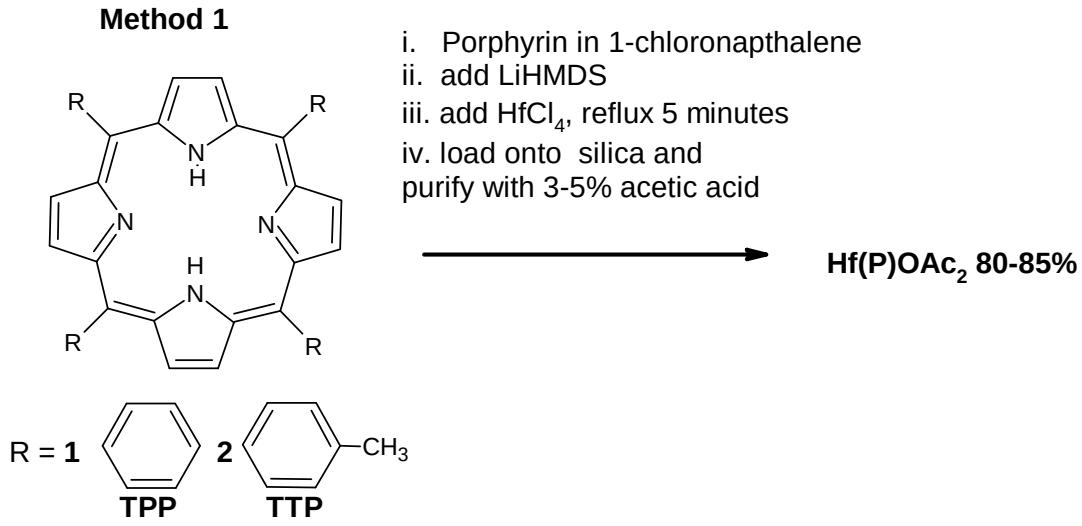

Figure 2. Method 1 for Hf(IV) porphyrinate synthesis

toluene or benzonitrile.[10]

The porphyrin is dissolved and the Li_2P is generated *in situ* with the highly hindered amide base, lithium hexamethyldisilazane (LiHMDS), in a 1.8 x 15.0 cm test tube (**figure 1)**. Then, two equivalents of hafnium tetrachloride, $HfCl_4$, is added and the solution is allowed to reflux for five minutes. It is assumed that the impure reaction mixture contains the $Hf(P)Cl_2$ species, but we have not isolated this product since the chlorides are exchanged for less labile, oxo-ligands during purification (*vide infra)*.

There are some significant advantages to this system. First, the use of 1-chloronapthalene, which is often used in phthalocyanine synthesis[31], allows direct use of

$HfCl_4$ without the need to first prepare and isolate the more soluble THF or DME adduct.[21] Second, the high boiling point and significantly increased porphyrin solubility allows much greater concentrations to be used and much shorter reaction times compared to reported methods.[10] Additionally, this method establishes 1-chloronapthalene as a useful solvent for hafnium metalation reactions for tetra aryl porphyrins; and is versatile enough to work with a large range of aryl substituents especially when combined with high boiling alcohols as cosolvents (*vide infra*).

As is the case for the planar OEP and phthalocyanines, high boiling solvents and extended reaction times can lead to a large fraction of the bis porphyrinoid hafnium(IV) sandwich complex.[32] This is not a concern for the tetra- aryl porphyrinates whose aryl substituents, being orthogonal to the macrocycle, prohibit sandwich complex formation using the $HfCl_4$ starting complex. The $Hf(NEt_2)_4$ starting complex is the only reagent reported which has lead to appreciable yields, about 50%, of the $Hf(IV)TPP_2$ complex.[33] Even at extended reflux (24 hours) the sandwich complex was not observed using our methods reported here.

Purification of the hafnium porphyrinates has been typically accomplished by recrystallization to isolate the $Hf(P)Cl_2$ as the THF or toluene adduct.[18, 19] The lability of the dichloride complex toward hydrolysis or chloride substitution by other ligands makes this a poor derivative for isolation and characterization; e.g. water and/or oxygen containing solvent molecules that bind to the Hf metal center in complex equilibriums are observed in the NMR spectra. The exchanging ligands and counter ions that fill the Hf coordination sphere are also observed in subtle changes in the UV-visible spectra.

The $Hf(P)Cl_2$ complex binds very tightly to silica and cannot be eluted even with neat methanol. As hafnium is quite oxophilic, we assume this is due to the exchange of chloride ligands for the available oxygens on the surface of the silica, and is observed as a bright red band at the top of the silica column. With the metalated product bound so tightly, reaction solvents and unreacted porphyrin can be eluted easily and quickly by using a glass-frit filter funnel filled with silica, where elution is accomplished by vacuum filtration on a filtering flask (**figure 1).** Once all unwanted material has be eluted, a solvent combination of CH_2Cl_2, MeOH and a small percentage of acetic acid quickly and cleanly elutes the product as the $Hf(P)OAc_2$ complex. The product can then be isolated as a bright pink powder by removal of the solvent and precipitation with distilled water. The acetates do not exchange for water and can be stored and handled easily as has been shown in previous accounts.[10] Also, the acetates can be easily exchanged for other oxo-ligands making it a suitable entry to other derivatives.

However, when a CH_2Cl_2 solution of the pure, $Hf(TPP)OAc_2$ complex is passed over silica gel a portion of the acetate ligands exchange for the silica gel oxygens during chromatography and the $Hf(TPP)^{+2}$ complex binds tightly after considerable streaking. When the acetate derivative is dried onto silica before chromatography, none of the acetates remain and the product will bind strongly without streaking. These chromatographic properties allow a fast, high yield exchange of counter ions by using other oxygen-bearing acids to elute the corresponding derivatives. This leads to the variety of other derivatives reported in this work.

Method 2 (Figure 3) was developed as a rapid, solventless method to synthesize hafnium porphyrinates by melting three equivalents of the $Hf(cp)_2Cl_2$ starting complex

with the free base porphyrin. This method provides the highest yield reported for $Hf(TPP)L_2$ and affords a moderate yield of $Hf(TPPF_{20})$ complex. No other method reported herein formed the $Hf(TPPF_{20})L_2$ complex without substitution of the highly reactive *para*-fluoro group. Up to 200 mg of H_2TPP can be metalated with hafnium using only a 2 mL screw cap vial in under 2 minutes. The resulting film in the vial is dissolved in CH_2Cl_2, loaded onto silica, and purification is then accomplished as described in **Method 1.**

Method 2 is unsuccessful with porphyrins bearing coordinating or protic substituents such as TPyP, TMeCPP (where the esters can cleave during the melt), or TCPP; the result is an insoluble film that cannot be solublized with any common solvent, acid, or base. Also, porphyrins bearing alkyl-oxy-phenyl ether substituents, such as tetra(4-octyl-oxy-phenyl)porphyrin, are subject to cleavage at the ether resulting in a mixture of products as we observed in preliminary work. It is somewhat surprising that

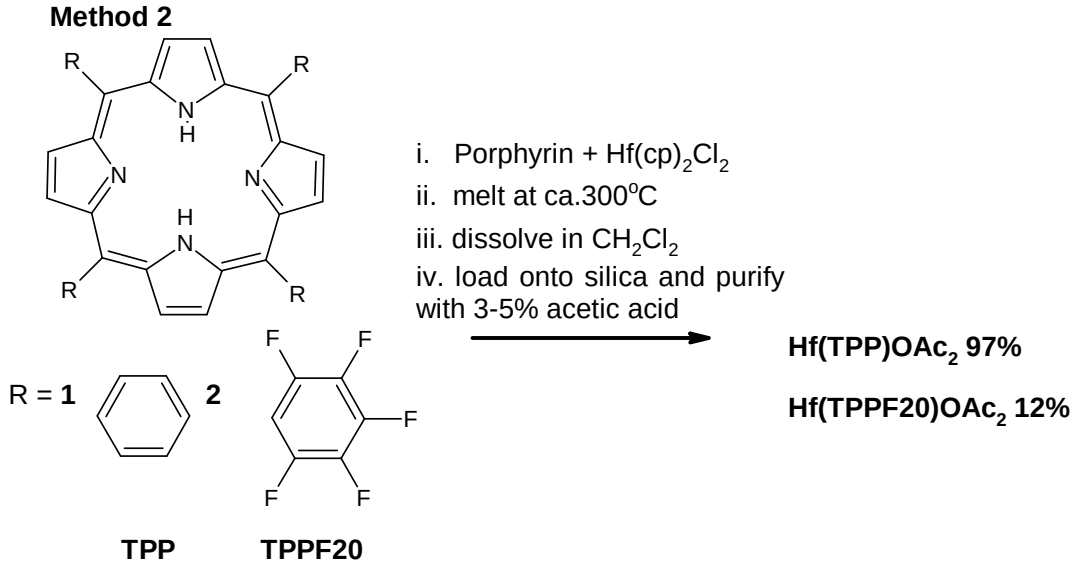

Figure 3. Method 2 for Hf(IV) porphyrinate synthesis

the fluoride on the para-position of $TPPF_{20}$ is not subject to any sort of substitution in this method.

Method 2 brings with it, two minor complications for both the Hf(TPP) and Hf($TPPF_{20}$) complexes: 1) The formation of a small fraction of a reduced Hf(P) complex identified as a chlorin complex formed by a 2 electron reduction of the macrocycle. The presence of this compound is marked by a low energy visible absorbance around 630 nm. 2) The excess cyclopentadienyl hafnium salts can polymerize during the melt and are difficult to separate from the product as they are charged and elute with the acetic acid solution. Both these problems can be greatly minimized by not overheating the vial and its contents.

Oxidation of the reduced product was accomplished, after purification, by a diphasic reaction of the Hf(P)OAc_2 fraction in CH_2Cl_2 with excess aq. $K_2Cr_2O_7$ over the course of three hours. The organic layer is then reduced in volume and the product precipitated with water as described above in method 1. The oxidation process does not perturb the acetate ligands or the non-reduced portion of the complex.

We also observed rapid oxidation (under five minutes) of the reduced complexes using $SOCl_2$, which has been shown to be a chemical oxidant in some applications.[34, 35] Oxidation of the reduced Hf($TPPF_{20}$)L_2 did not proceed cleanly, so that extra care in not over heating the reaction was the best way to avoid this complication.

The troublesome, cyclopentadienyl polymeric material was best separated from the product by first adding a few drops of concentrated HCl to the dissolved residue, in CH_2Cl_2, from the vial before purification over silica. The excess hafnium ions binds

irreversibly to the silica, allowing degraded cyclopentadiene to be eluted from the column with CH_2Cl_2.

Method 3 (**Figure 4**) was developed as a means to metalate porphyrins bearing polar and/or coordinating substituents, namely TPyP and TMeCPP. It begins with the same apparatus used in the **method 1**; the porphyrin is first dissolved in a mixed solvent of 1-chloronapthalene and freshly distilled *o*-cresol. As observed in our cerium(IV) bis porphyrinate synthesis, addition of a high boiling alcohol helps solvate and allow metalation of polar porphyrins. Cresol was chosen because phenols are less reactive in the trans-esterification of esters compared to straight chain alcohols, thus methyl esters, such as the methyl benzoate substituents on TMeCPP remain in tact.

To make the porphyrin solution more alkaline, to encourage metalation, a portion of the cresol is heated and reacted, separately, with 10 equivalents of NaH to form an 8-10% solution of the sodium cresolate. This is added to the predissolved porphyrin. After the chamber is fully purged with argon, five equivalents of $HfCl_4$ are added, and the solution refluxed for 30 minutes. This method results in over 70% metalation of the porphyrin.

Purification then proceeds over silica described above with some minor variations. The cresol solvent is difficult to remove from the silica column as it contains a large portion of the sodium cresolate base, $Na^+(C_7H_7O)^-$. In addition, we suspect that the unpurified reaction mixture contains the hafnium porphyrinate bearing cresolate ligands, $Hf(P)(C_7H_7O)_2$, which are more difficult to dissociate from the complex than chlorides. For both Hf(TPyP) and Hf(TMeCPP) a mixture of water and methanol was required to entirely clean the silica of residual cresol. It presence and absence was

monitored simply by its strong, distinctive odor. With the reaction solvents removed, solvents mixtures of 4% and 50% v/v acetic acid, for TMeCPP and TPyP respectively, were then used to elute the corresponding acetate derivatives of the two complexes.

For (TMeCPP), a portion of the esters had been cleaved as indicated by a complex NMR spectrum and mass spectroscopy. This resulted in complicated chromatography where unreacted porphyrins bearing more than two free carboxylates co-eluted with the metalated product. To obtain the target complex, the reaction mixture of a second attempt was precipitated with hexanes so that only the complexes bearing mostly intact esters remained in the supernatant. The precipitate was put aside and the hexane solution was purified over silica. The metalated fraction from the hexane solution still contained some cleaved esters and was combined with the impure precipitate. This combined material was then subjected to a diazomethane reaction to reform the methyl esters. Purification of the resulting products, after diazomethane, over silica gel resulted in two major fractions. The first fraction of free-base porphyrin was identified as H_2TMeCPP. TLC indicated a

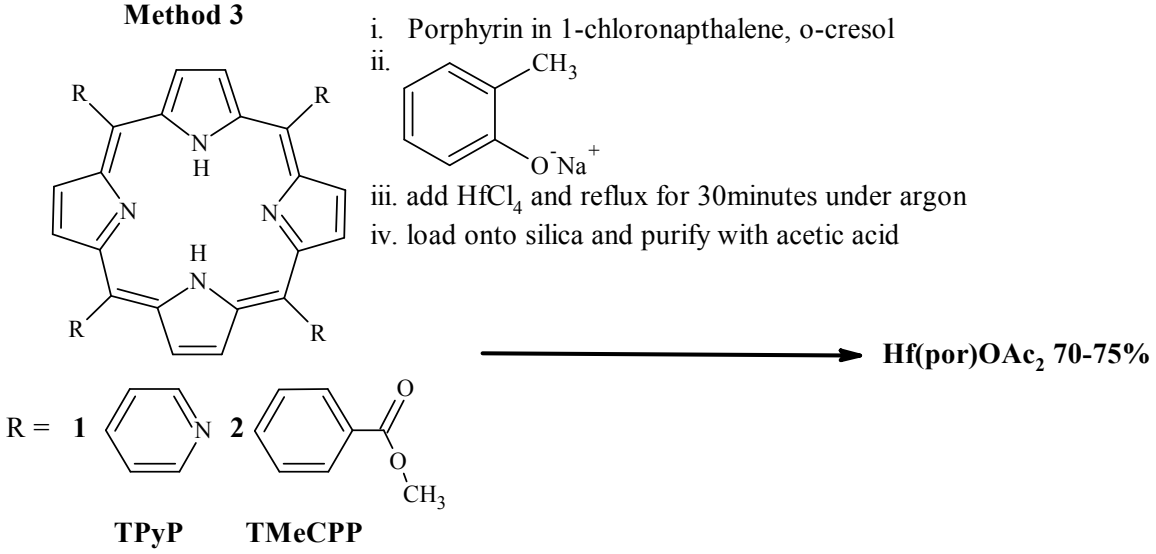

Figure 4. Method 3 for Hf(IV) porphyrinate synthesis

single product with no cleaved ester groups, which confirmed the successful diazomethane reaction. The metalated fraction still contained some cleaved esters indicating that either some esters were cleaved during purification after the diazomethane reaction, which seems unlikely, or more likely that the metalated porphyrins with benzoic acid groups were not soluble enough in ether for the diazomethane reaction to proceed effectively. A minimal number of cleaved esters after the diazomethane treatment allows the spectroscopic characterization of this product, but since the Hf(TMeCPP)L_2 complex serves only as a precursor to the Hf(TCPP)L_2 complex, which can be used to design hierarchical materials, this product was used without further purification. Once the esters are cleaved by refluxing in NMP with pyridinium hydrochloride for 2 hours, the resulting Hf(TCPP)L_2 is sparingly soluble in common solvents requiring 10% NH_4OH in methanol for moderate solubility.

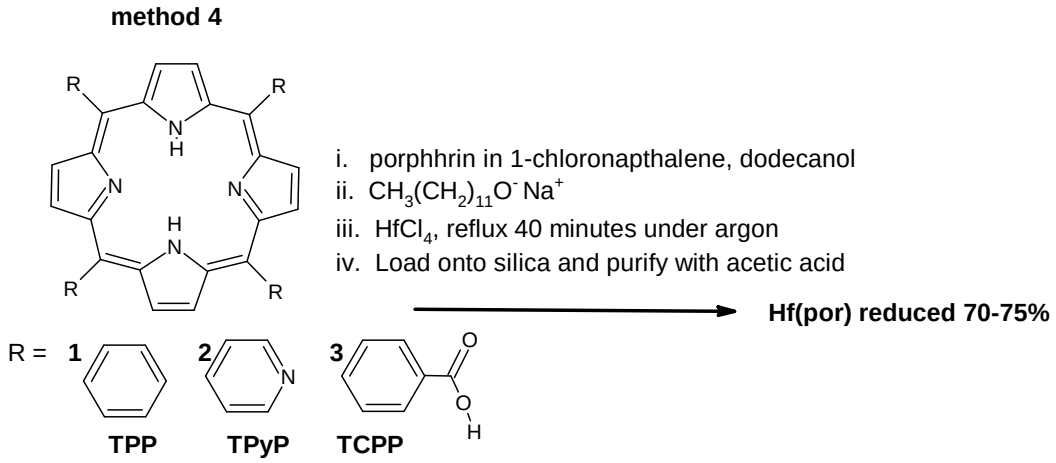

Figure 5. Method 4

To elute the Hf(TPyP)OAc_2 complex, a solution of 1:1 water:acetic acid was required. This allows solvation of the four protonated pyridiniums on the porphyrin that form upon exposure to acid, so that the producted is collected as the [Hf(H_4TPyP)OAc_2]OAc_4 complex. A large excess of sodium acetate is added to the eluted fraction, ca. 200 mg,

and the solution is evaporated. As the acetic acid is evaporated the solution becomes more basic, and the pyridinium substituents are neutralized to pyridyls. The resulting Hf(TPyP)OAc_2 complex is not water soluble and can be precipitated from distilled water to remove excess salts as described for the other hafnium porphyrinates.

Method 4 (**Figure 5**) was attempted first before **method 3** was developed. Using dodecanol as a co-solvent and sodium dodecanate as a base, in direct analogy to our Ce(IV)P_2 synthetic methods, we found mixed results. We have listed this method last as it produces an almost entirely reduced hafnium porphyrinate product; the same chlorin complex found as only a small fraction of the product from **method 2**. The results from this method lead us to change the alcohol co-solvent to cresol as described above.

When the dodecanol, with 10 equivalents of the sodium dodecanate salt, is refluxed with the porphyrin and $HfCl_4$ under argon, two side reactions occur in addition to metalation: 1) under these conditions the excess $HfCl_4$ acts as a chlorinating agent forming 1-chloro-dodecane; 2) the hafnium porphyrinate complex is reduced to a chlorin showing the red absorbance band near 630 nm. The mechanism of reduction is unclear but it is conceivable that 1-chloro-dodecane can act as a reducing agent in the presence of a the reactive Hf(IV) ion at high temperatures. The resulting Hf(IV) chlorin complex can be oxidized using the methods described above.

Method 4 was attempted with TPP, TPyP, and TCPP as the tetra-acid. The presence of the 1-chloro-dodecane was indicated by the resulting products. Though the TPyP was metalated, the reduced species is the dominant product as indicated by UV-visible spectra, and ESI-MS reveals that there is substantial pyridyl alkylation by dodecyl groups (appendix). Not surprisingly, the TCPP became unusually soluble during the

course of reaction, and showed that the resulting metalated and reduced porphyrin had been also esterified by dodecyl chains as observed by ESI-MS (appendix). From this we conclude that at least some 1-chloro-dodecane had formed in solution.

Significantly, **method 4** using TPP resulted in only a reduced hafnium porphyrinate solution with no other side reactions, thus is a good way to make the reduced complex. Under the assumption that 1-chloro-dodecane was indeed forming and that it was responsible for alkylation, esterification, and reduction of our porphyrins we turned to using cresol in **method 3**. By using cresol as a solvent, we observe no alkylation or reduction of the porphyrins.

Reduction by magnesium metal

As an indication of the nature of the chlorin species, the porphyrin of the Hf(TPP)OAc_2 complex can be reduced using magnesium metal and a protic acid, but with near complete loss of the hafnium ion. The Hf(TPP)OAc_2 complex is dissolved in a solution of CH_2Cl_2, 25% acetic acid and magnesium metal turning are added. As hydrogen gas evolves, the solution turns from reddish-pink to purple, then finally blue-green within 20 minutes at room temperature; the very same color changes observed during the course of **method 4**. The low energy absorbance band appears intensely in the UV-Vis spectrum, though we find it near 604 nm for the free base chlorin compared to 630 nm for the Hf complexes. The chlorin structure and demetalation is verified by UV-Visible spectra and positive mode ESI-MS (see appendix).

Since the free-base porphyrin does not reduce to the chlorin using magnesium under the same conditions, we speculate that there may be some mechanism which reduces the porphyrin through the hafnium center before demetalation occurs. In fact, the

methods used to reduced porphyrins to chlorins are usually much lower yielding and use more expensive reagents than this procedure. This may be useful the preparation of chlorins.

Derivatives

In general, the hafnium porphyrinates bearing acetate or chloride ligands are quite useful as starting materials to exchange the counter ion ligands on the hafnium ion for a great variety of other oxo ligands. Many different compounds are accessible, and the ligands can bring functionality to the complexes in of themselves. We have shown a straight forward method to functionalizing the $Hf(TPP)L_2$ and $HF(TTP)L_2$ complexes with a broad spectrum of oxygen-bearing counter ligands. **Figure 6** shows the general methods for derivatives we have synthesized for the reported the crystal structures below.

Starting from the acetate derivatives, formed during purification, other derivatives can be formed by exchange of the acetates. Organometallic alkyl derivatives have been formed from the $Hf(TPP)OAc_2$ using *n*-butyl lithium[10] or methyl[36] lithium. We have restricted our work to bidentate oxo-ligands, namely carboxylates and polyatomic oxo-anions to satisfy both the charge and the large hafnium coordination sphere. When dealing with mono-dentate anionic ligands, coordinating solvents fill the empty coordination sites, which easily exchange and results in different spectroscopic signatures. Since mono-dentate ligands do not bind as strongly, the resultant complexes are not as convenient to handle as those with bi- and multi- dentate ligands.

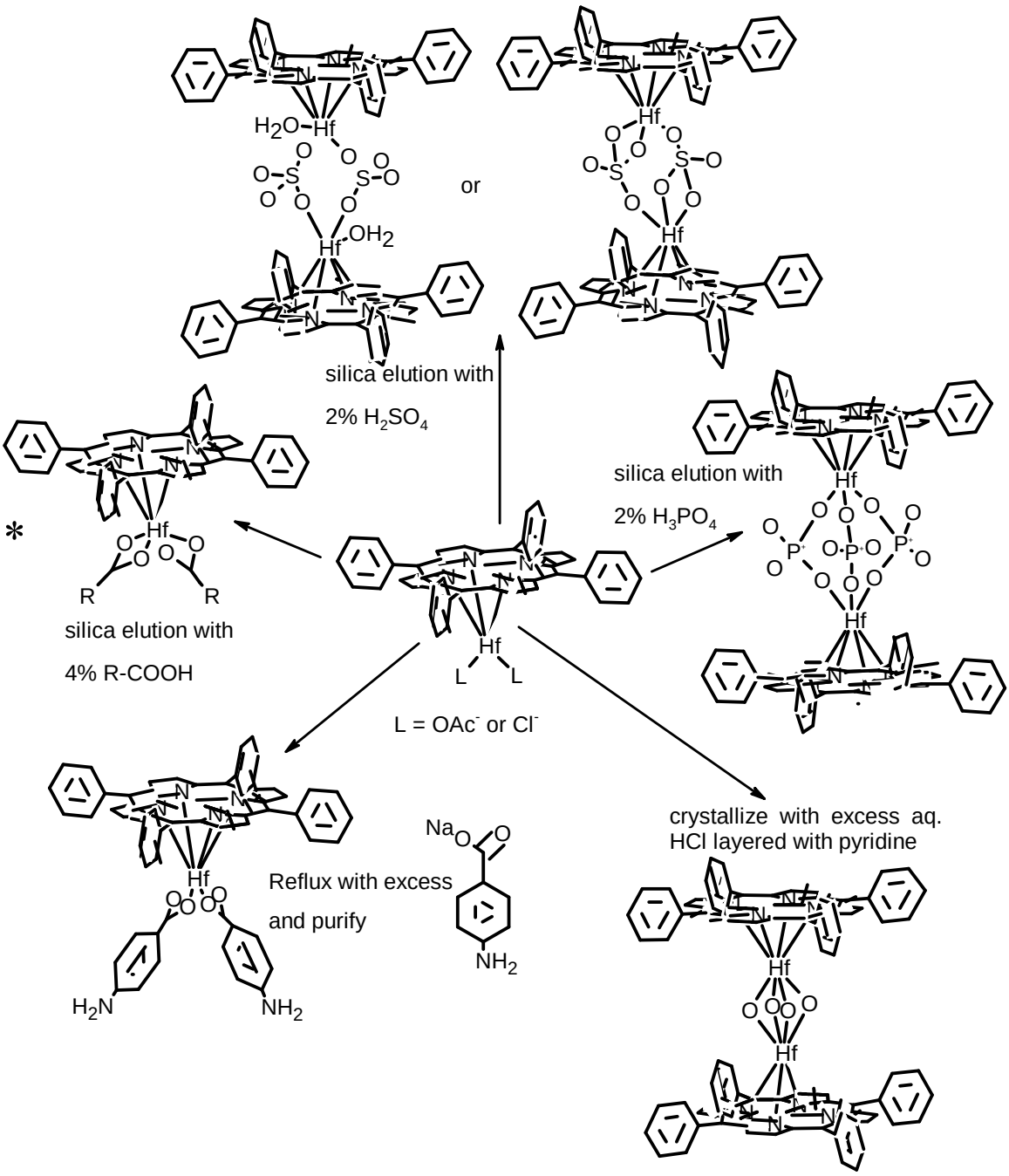

Figure 6. Formation of derivatives from the Hf(TPP)OAc_2, Hf(TPP)Cl_2, or Hf(TTP)Cl_2 complexes preloaded on silica
*the octinoate and pentanoate derivatives were made from the Hf(TTP)Cl_2 complex only

Most derivatives were formed by similar methods that are akin to the purification over silica using acetic acid; i.e. simply using a different acid in the CH_2Cl_2:CH_3OH solvent mixture affords the corresponding derivative. For example, elution of the Hf(TPP) complex from silica gel with 2% concentrated H_2SO_4 results in the sulfate derivative. If starting with an impure reaction mixture, the unreacted porphyrin and reaction solvents are eluted first with the organic solvents, followed by elution with the solvent system containing the acid. For the most part these derivatives are stable to precipitation and centrifugation from water. This strategy produces the sulfate, phosphate, and octinoate derivatives of the Hf(TPP) and/or the Hf(TTP) complexes.

When the carboxylic ligand is solid, such as *para*-amino benzoic acid (PABA), refluxing the Hf(TPP)OAc_2 or Hf(TPP)Cl_2 complex for 30 minutes with an excess of the carboxylate, as the sodium salt, in a toluene:methanol solution affords the desired complex. The PABA derivative is also stable to water which is useful in washing excess salts from the precipitated complex.

The sulfate, phosphate, and oxo- bridged dimers are a unique set of compounds compared to the monomeric, carboxylic derivatives. The oxo-bridged dimer is favored in various solvents and a range of pH values. In reported zirconium(IV) porphyrinate oxo-bridged crystal structures, the structure forms by hydrolysis of the Zr(por)Cl_2 or Zr(por)R_2 where R = CH_3[36] or $(CH_2)_3$-CH_3,[10] by simple exposure to atmosphere. When bidentate oxo-ligands are bound to the hafnium such as carboxylates (benzoic or alkyl) and acetylacetonate (acac), the complex is much more resistant to hydrolysis as observed previously[10] which is consistent with our results (precipitation from water does not hydrolyze the acetate derivatives). The same aqueous precipitation on the Hf(P)Cl_2

complex causes immediate hydrolysis of a large portion of the sample as shown by a large absorbance peak near 401 nm in the UV-Vis spectrum; a large blue shift in the porphyrin Soret is consistent with literature values for the oxo-bridged species.[18]

Starting from the acetate derivative we have found a convenient method to produce an oxo-bridged species, $[Hf(TPP)]_2(\mu\text{-}\eta^2\text{-}O_2)_2$. We represent this compound as peroxo-bridged ($\mu\text{-}\eta^2\text{-}O_2^{-2}$) dimer rather than a simple hydroxyl/oxo bridged dimer, in contrast to previous accounts[4, 7, 37] due to spectroscopic and crystallographic evidence, *vide infra*. As shown in **Figure 6**, a sample of the $Hf(TPP)OAc_2$ is treated with a small quantity of dilute HCl to dissociate the acetate ligands. Then by layering pyridine over the acidic solution, the acid is neutralized and the water in solution affords the oxo-bridged dimeric complex as a crystalline product after the solvent is allowed to evaporate. Previous accounts have also shown the formation of the oxo-bridged dimer, is facilitated by the presence of pyridine.[18]

The hafnium (IV) tetraphenyl porphyrinate sulfate bridged complex, $[Hf(TPP)]_2(SO_4)_2$, and the phosphate derivative, $[Hf(TPP)]_2(HPO_4)_3$ dianion (water bridges to the phosphate and/or H_3O^+ counter ions) are a second class of bridged dimers and the first of their kind to be reported for either hafnium or zirconium porphyrinates. The sulfate bridged dimer was also found for the Hf(TTP) complex (see crystallographic section). The dimeric structures are observed by crystallography using crystals from multiple, independent preparations. Evidence for the bridged dimer structures in solution are also observed in the electronic spectra of these complexes when compared to the monomeric bis carboxylate derivatives.

Structurally, the 104° angle between the oxygens on a tetrahedral sulfate or phosphate anion tends to result in one oxygen from each anion coordinated to each hafnium, but one of the crystal structures of the sulfate dimers does not follow this trend, (**Figure 6** and crystallographic section). The bridges consist of three phosphate, or two sulfates, where the remaining coordination site on each Hf in the latter are occupied by a solvent molecule (**Figure 6**). Considering that there is a large excess of the phosphate and sulfate ions during the preparation and crystalization, and that only the dimeric structures are found rather than the monomers, the sulfate and phosphate bridged dimers must be thermodynamically favored products. In addition, only the dimer structures are found in our crystallographic studies even when the complex is crystallized from a solution with 2% v/v of H_2SO_4 or H_3PO_4, (see cystallographic section).

These complexes are also somewhat resistant to hydrolysis, since precipitation from water to remove excess salts results in only partial hydrolysis to a presumably aquo species as indicated by a poorly defined high energy shoulder of the Soret band in the UV-Vis spectra. A sample from one of the sulfate preparations used for crystallization was precipitated from water and dried for elemental analysis to assure the identity of the S in the bridge (as opposed to Si). While sulfur was indeed present, the low elemental analysis of sulphur, 2.7%, compared to the calculated 3.4% for the complex only also suggests some hydrolysis. A crystal structure obtained with a partially hydrolyzed sample of the sulfate derivative still displays the sulfate bridged dimer as the water solvate.

Spectroscopy

Mass spectroscopy

Samples of the diacetate or dichloride derivatives of the hafnium porphyrinate complexes were submitted for mass spectroscopy using positive mode ESI-MS and/or MALDI. For samples submitted as the diacetate, we observed a number of mass peaks in the positive electrospray spectrum relating to the acetate complex with a high degree of exchange with methanol and water ligands. When the Hf(TPP) complex was submitted as the dichloride derivative, from a sample of filtered reaction mixture from **Method 1**, the chloride derivative was not observed. Rather, the major peaks observed indicate that the oxo-bridged species formed from the $Hf(TPP)Cl_2$ in the ESI-MS which uses a methanol with 1% formic acid solvent systems (see synthesis and appendix). Notably, the observed m/z peak at 1631 for the oxo-bridged Hf(TPP) dimer complex is consistent with a peroxo bridge (generically, O_2^{2-}) rather than a combination of H_2O, OH^-, or μ-oxo (O^{-2}) species (see appendix). The calculated weight of a mono-cationic complex as $[Hf(TPP)]_2[(OH)_3]^{+1}$ is 1633. Coordinated or bridging methanol molecules are not consistent either. Thus the m/z of 1631 suggests the formula $[Hf(TPP)]_2(\mu\text{-}\eta^2\text{-}O_2)(OH^-)]^+$, which derives from the bis ($\mu\text{-}\eta^2\text{-}O_2$) bridged species. Previous examples of oxo-bridged porphyrinate complexes also indicate an oxide bridging unit observed by mass spectroscopy, e.g. the $Sc(OEP)]_2[\mu\text{-}O]^{+1}$ species[37] where the bridging oxygen was formally assigned as an O^{2-} anion, but the given mass peak indicates an $O\bullet^{-1}$ bridge . Various ionization mechanisms occur in mass spectroscopy that are not representative of the complex in ambient conditions. However the electronic

spectra of the $[Hf(TPP)]_2(\mu\text{-}\eta^2\text{-}O_2)_2$ complex indicates this structure persists in solution in addition to the solid state crystal.

MALDI mass spectroscopy gave more consistent results compared to the electrospray methods. The MALDI data serves to characterize the hafnium-porphyrinate portion of the complex, while the counter ligands are quantitatively replaced by the matrix solvent, dithranol ($C_{14}O_3H_{10}$), FW 226 g/mol. Thus the Hf(P)($C_{14}O_3H_9$) adducts are observed where a deprotonated dithranol molecule is bound to the hafnium. The MALDI spectrum of the $Hf(TPPF_{20})OAc_2$ complex is an exception, where the loss of one acetate gives the $Hf(TPPF_{20})OAc^{+1}$ observed at the expected m/z of 1250 (see appendix).

Reduction of the $Hf(TPP)OAc_2$ complex with magnesium and acetic acid, results in prominent mass peaks indicative of two types of metal-free chlorins, a dihydro and a dihydroxy-chlorin (**Figure 7**), as well as a small fraction of dihyroxychlorin with the hafnium coordination retained.

NMR

The NMR spectra of the $Hf(P)OAc_2$ complexes verify sample purity, and verifies the 2:1 stoichiometry of OAc:porphyrin (e.g. the acetate methyl proton resonance near 0.2 ppm and the pyrrolic proton resonance near 9.1 ppm integrate to ca. 6:8). The ortho and meta positions are not equivalent due to the asymmetry a caused by coordination of the hafnium ion to one face of the macrocycle. Also, the pyrrole and the aryl proton resonances appear broad at room temperature, indicating rotation of the porphyrin around the hafnium center and possible interconversion between distorted macrocycle conformations found in the crystal structures.

For the Hf(TTP)oct_2 complex, the aliphatic region displays a clear set of peaks that depict the methylene peaks of the octyl chains starting at 4.37 ppm and ending with the terminal methyl group at 0.34 ppm. These peaks integrate well with the porphyrin resonances including the methyl protons of the tolyl substituents at 2.73 ppm.

The NMR spectra of the phosphate and sulfate bridged complexes are generally shifted upfield by about 0.2 ppm compared to the corresponding acetate derivatives, which may be an indication of the dimeric structure[38]. One distinct set of peaks for the porphyrin pyrrole and aryl protons indicates one species and the lack of an equilibrium between a dimeric and monomeric forms of the complexes.

The Hf(TPyP)OAc_2, Hf(TPP)OAc_2, and Hf(TTP)OAc_2 complexes all show similar ^{1}H-NMR spectra. For Hf(TPyP)OAc_2, the chemical shift of the two meta-proton resonances overlap and are downfield relative to those of the ortho protons due to the proximity to the pyridyl nitrogen in contrast to the meta protons of the TPP and TTP hafnium(IV) complexes which are observed upfield from the ortho proton resonances. The chemical shifts of the two ortho resonances, for all three complexes, do not overlap and are distinguishable. The acetate peak is broad for Hf(TPyP)OAc_2 and Hf(TPP)OAc_2, and poorly defined though it integrates well with the porphyrin pyrrole resonances. This broadness may be due to proton exchange between the acetates and trace amounts of water in the NMR solvent or excess acetates. The acetate peak for the Hf(TTP)OAc_2 complex was well defined (see appendix).

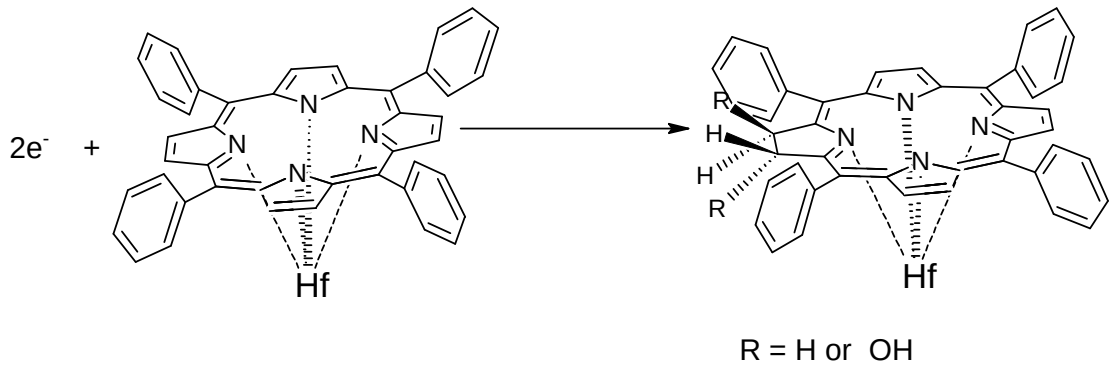

Figure 7. The reduction of Hf(TPP)OAc_2 results in the formation of chlorins. The two hydrogen atoms indicated are *trans* and therefore non-equivalent, resulting in a diagnostic mutliplet near 4.15 ppm. The nucleophiles, labeled as **R**, that are added across the bond can vary according to the reduction mechanism.

The NMR spectrum of the reduced Hf(TPP)OAc_2 obtained from **method 4** is complex and difficult to assign except for some key features (see appendix). The protons on the pyrroles adjacent to the reduced double bond in the chlorin are observed as a doublet of doublets centered at ca. 8.2 ppm while there is a singlet for the two protons on the opposite pyrrole at 9.12 ppm. In formation of a chlorin complex, two substituents are added across one of the pyrrolic carbon double bonds. Depending on the mechanism of chlorin formation, the protons on the macrocycle can be in a *cis* or *trans* orientation, the latter is diastereotopic with the Hf bound to one face of the porphyrin. We observe a multiplet centered around 4.15 ppm that intergrates equally with the pyrrole singlet at 9.12 ppm (which is coincident to the pyrrole chemical shift for the parent Hf(TPP)OAc_2, see the appendix). This 4.15 ppm multiplet is typical of diastereotopic pyrrolic resonances found for the methylenes protons in the Hf(OEP)Cl_2 complex.[18] **Figure 7** illustrates the formation of a chlorin complex by reduction of the porphyrin, and how the

two *trans* protons of the saturated methyelene carbons are diasterotopic due to the asymmetry caused by the out-of-plane complexation to the hafnium ion.

Electronic spectroscopy

UV-Vis absorption

The UV-Vis spectra for the hafnium porphyrinate dicarboxylate complexes are generally characterized by a large Soret band between 414-416 nm and a Q-band at about 15-fold less intense near 540 nm, flanked on either side by smaller Q-bands of even lesser intensity (see appendix and synthesis). These spectral features are common to many metalloporphyrinates and are consistent with reported spectra for hafnium porphyrinate complexes.[5]

The spectra of the sulfate and phosphate bridged dimer complexes generally have blue shifted Soret bands near 408 nm and nominally blue shifted Q-bands compared to the monomeric carboxylic derivatives. We view this blue shift as evidence for dimer formation as blue shifted absorption bands are often found with other metalloporphyrin dimer systems[39]. The inorganic anions, SO_4^{-2} and HPO_4^{-2}, may cause of this blue shift simply by donation of electron density into the porphyrin core via the Hf without dimer formation, but the previously reported Hf(TPP)($P_3O_9^{-3}$)[TBA] (TBA= tetrabutyl ammonium cation), which has a Soret band at 412 nm[2], is not significnatly blue shifted compared to the dichloride starting complex. This electron-rich, $P_3O_9^{-3}$ ligand is incapable of bridging two porphyrin units, has a Soret band more typical of monomeric hafnium porphyrinates, and is found to be a monomer in the crystal structure.

The $[Hf(TPP)]_2(\mu\text{-}\eta^2\text{-}O_2)_2$ complex has a significantly blue shifted Soret band near 401nm, and the aquo $Hf(TPP)(OH)_2$ species has a Soret near 416 nm. The latter is often found in small quantities in solution. The blue shifted Soret is consistent with previous accounts and the dimer/monomer equilibrium has been documented by others.[40] We interpret the blue-shifted peak at 401 nm as a result of dimer formation and as evidence of the peroxo, rather hydroxy, bridging ions in solution, i.e. $[Hf(TPP)]_2(\mu\text{-}\eta^2\text{-}O_2)_2$. In previous reports, the formation of a peroxo-bridged dimer from an oxo- (O^{2-}) or hydroxy (OH^-) porphyrin complex is characterized by a large blue shift, ca. 20 nm, in the Soret absorption band.[41]

Absorption spectra of the metalated chlorin from **method 4** and the mostly metal-free chlorin differ in the relative energies of their respective Q-bands though the relative intensities are similar. The largest difference is found in the intense low energy absorption band. The metalated product displays a peak at 630 nm while the metal free complex has an absorption band near 604. Also, the mass spectrum (appendix) indicated the free base chlorin exists mostly as the dihydro-chlorin while the NMR of the metalated complex suggests only two hydrogens at the reduced site, while the other positions are occupied most likely by hydroxides or chloride (appendix).

Fluorescence

Fluorescence spectra of the $Hf(TPP)OAc_2$, $[Hf(TPP)]_2(SO_4)_2$, $[Hf(TPP)]_2(HPO_4)_3$, and the $[Hf(TPP)]_2(\mu\text{-}\eta^2\text{-}O_2)_2$ complexes were taken in CH_2Cl_2 at concentrations where there is a ca. 0.6 absorbance in the UV-visible Soret band, in 1 cm path quartz cuvettes, and using right angle geometry. For comparison ZnTPP emission peaks are at ca. 600 nm and 650 nm with $\Phi = 0.03$, and free base TPP has emission peaks ca. 650 nm and 710

nm with Φ = 0.11. Hf is a closed shell group (IV) metal so ligand to metal charge transfer, and excited state metal electron configurations as observed for Ni(II)P[42, 43] are unlikely. Hf(TPP)OAc_2 in degassed toluene is reported[6] to have a weak fluorescence with an emission maximum at 633 nm, Φ_f = 0.001, with a weak shoulder to the red arising from heavy atom enhanced phosphorescence at 718 nm $\Phi_p = 8 \times 10^{-5}$. For a dissolved crystal of Hf(TPP)OAc_2 in degassed CH_2Cl_2 we observe three fluorescence peaks λ_{max} (relative intensity): 550 nm (1), 582 nm (3.5), and 634 nm (9.4) but not the phosphorescence bands. For the $[Hf(TPP)]_2(\mu\text{-}\eta^2\text{-}O_2)_2$ λ_{max} (relative intensity): 551 nm (1), 579 nm (3.1), and 633 (9.2). For the $[Hf(TPP)]_2(HPO_4)_2$ λ_{max} (relative intensity): 549 nm (1), 581 nm (3.7), and 633 (9.4). For the $[Hf(TPP)]_2(SO_4)_2$ λ_{max} (relative intensity): 549 nm (1), 579 nm (3.4), and 632 (7.9). The excitation spectra for the three larger emission peaks reveals only the absorption spectra of the starting Hf(P)L_2 or $[Hf(P)]_2$ dimers. The weak fluorescence emission spectra for all the Hf porphyrinate complexes are remarkably similar.

Crystallographic procedures and discussion:

Solvent condition for compounds 1-10

1. Hf(TPyP)OAc_2-Crystals of the Hf(TPyP)OAc_2 complex were obtained by slow evaporation (2 weeks) of the complex in a 1:1 solution of MeOH:$CHCl_3$, 2% v/v nitrobenzene.

2. Hf(TPP)$PABA_2$- Single crystals of the Hf(TPP)$PABA_2$ complex came from slow evaporation of the complex in a 1:1 solution of MeOH:$CHCl_3$, 2% v/v nitrobenzene.

3. Hf(TTP)pent$_2$ - The crystal structure of the pentanoate derivative, Hf(TTP)pent$_2$, was found as a result of a small sample of Hf(TTP)Cl$_2$ crystallized with trace amounts of pentanoic acid (see supporting information) in a mixed solvent of THF and $CHCl_3$. This further illustrates the ease of derivatization of these complexes and the hafnium affinity for oxo-ligands. The pentanoate derivative was not characterized apart from its crystal structure.

4. [Hf(TPP)]$_2$(μ-η^2-O$_2$)$_2$ – The Hf(TPP)OAc$_2$ complex was dissolved in a chloroform:methanol mixture with an small excess of conc. aq. HCl. Methanol with 10% pyridine was layered over the solution that was allowed to slowly diffuse into the lower layer. After the layers were mixed over the course of three days, the solution was allowed to evaporate slowly over a two week period, yielding x-ray diffraction quality single crystals. (see appendix)

5. [Hf(TTP)]$_2$(μ-η^2-O$_2$)$_2$ (chloroform solvate) & 6. Hf(TTP)]$_2$(μ-η^2- O$_2$)$_2$ (nitrobenzene solvate) - The Hf(TTP) peroxo bridged dimers formed from preliminary experiments in eluting the Hf(TTP) using dilute HCl. The samples from silica elution were allowed to evaporate, one with and one without 2% v/v nitrobenzene, affording single crystals of the corresponding compounds.

7 & 8 [Hf(TPP)]$_2$[SO$_4$(H$_2$O)]$_2$ and **[Hf(TTP)]$_2$[SO$_4$(CH$_3$OH)]$_2$** Crystals of both the solvated sulfate derivatives were obtained by slow evaporation of the complexes in a 1:1 solution of MeOH:$CHCl_3$.

9. [Hf(TPP)]$_2$[SO$_4$]$_2$ Crystals of the Hf(TPP) sulfate lacking any coordinating solvents display a structure where more of the oxygens from the bridging sulfates participate in coordination to the hafnium ions to fulfill the large coordination sphere.

The sample was dried thoroughly in an oven for three days before being dissolved for NMR spectroscopy (spectrum not used in this paper) in $CDCl_3$. Nitrobenzene and acetonitrile were added; the solvents were allowed to slowly evaporate to form good-quality crystals.

10. $[Hf(TPP)]_2[HPO_4]_3^{-2}$ The phosphate derivative was crystallized from a $CHCl_3$:MeOH, 2% v/v nitrobenzene. The dimer complex has a formal negative charge most likely compensated by protons and hydronium ions associated with unbound phosphate oxygens.

Crystallographic Discussion:

Single crystals suitable for x-ray diffraction analysis were obtained with (TPP), (TPyP) and (TTP) scaffolds, which exhibit similar metal coordination features of their central macrocyclic core. Crystallographic data for all 10 structures are given in **Tables 1-3**. Hafnium(IV) d^0 ions are often characterized by high coordination numbers of 7-8[44] with a square-antiprismal coordination environment in the latter case. They readily complex with porphyrin tetra-dentate ligands in 1:1 ratio.[3, 5, 21] However, t metal ion is too large to fit into the porphyrin core, and therefore when coordination to the four N-pyrrole sites takes place, the metal lies above the macrocycle with its coordination sphere completed by other small oxo or aza ligands, adapting a “piano-stool” type geometry.

Table 1. Crystallographic data for 1-3

Compound	**1**	**2**	**3**[a]
empirical formula	$C_{44}H_{30}HfN_8O_4$	$C_{70}H_{52}HfN_8O_9$	$C_{58}H_{54}HfN_4O_4$
	X1590	X1594	X1579
Formula wt.	913.25	1327.69	1049.54
cryst. System	monoclinic	monoclinic	monoclinic
space group	C2/c	$P2_1/n$	$P2_1/c$
unit cell			
a / Å	14.797(3)	14.622 (3)	16.191(3)
b / Å	16.384(3)	31.050 (6)	23.452(5)
c / Å	14.984(3)	14.712 (3)	16.340(3)
α / °	90	90	90
β / °	93.24(3)	119.58 (3)	116.88(3)
γ / °	90	90	90.00
V/ Å^3	3626.9(13)	5809 (2)	5534.3(24)
Z	4	4	4
ρ_{calcd} [gcm^{-3}]	1.672	1.518	1.261
μ(MoKα) mm^{-1}	2.935	1.865	1.930
T / K	100	100	100
F(000)	1816	2688	2136
crystal size [mm^3]	0.56 x 0.07 x 0.07	0.40 x 0.36 x 0.18	0.40 x 0.12 x 0.10
Θ range[°]	3.23 to 27.53	2.07 to 27.48	2.96 to 27.48
index ranges	$-19 \le h \le 19$	$-12 \le h \le 18$	$-21 \le h \le 20$
	$-21 \le k \le 21$	$-38 \le k \le 40$	$-30 \le k \le 30$
	$-19 \le l \le 19$	$-18 \le l \le 10$	$-21 \le l \le 20$
reflns collected	26545	25788	59134
unique reflections	4159	11570	12600
R(int)	0.094	0.064	0.065
completeness to Θ_{max} [%]	99.3	87.0	99.4
reflns with [$I > 2\sigma(I)$]	3620	8999	9144
data/restraints/parameters	4159/0/259	11570/0/793	12600/0/745
final R indices [$I > 2\sigma(I)$]			
*R*1	0.034	0.040	0.049
*wR*2	0.064	0.082	0.113
R indices (all data)			
*R*1	0.046	0.061	0.074
*wR*2	0.068	0.088	0.121
largest diff. peak and hole [eÅ^{-3}]	1.03 and -1.43	0.74 and -1.14	1.53 and -0.69

[a] Excluding the severely disordered THF solvent, which could not be modeled reliably by discrete atoms. Its contribution was subtracted from the diffraction data by the Squeeze procedure with the aid of the Platon software. [1]

Table 2. Crystallographic data for 4-7

Compound	**4**	**5**	**6**	**7**
empirical formula	$C_{44.25}H_{29}HfN_4O_{2.25}$	$C_{49}H_{37}Cl_3HfN_4O_2$	$C_{54}H_{41}HfN_5O_4$	$C_{47}H_{39}Cl_3HfN_4O_7S$
	X1572	X1592	X1595	X1588
formula wt.	831.20	998.67	1002.41	1088.72
crystal system	monoclinic	monoclinic	monoclinic	triclinic
Space group	$P2_1/n$	$P2_1/c$	$P2_1/c$	P-1
unit cell				
a / Å	13.460(3)	14.192 (3)	14.056 (3)	11.951(2)
b / Å	12.954(3)	19.046 (4)	19.193 (4)	14.653(3)
c / Å	20.811(4)	15.641 (3)	16.056 (3)	14.865(3)
α / °	90	90	90	66.15(3)
β / °	107.87(3)	94.27 (3)	94.74 (3)	86.36(3)
γ / °	90	90	90	67.92(3)
V/ $Å^3$	3553.5(14)	4216.1 (14)	4316.7 (15)	2194.2(12)
Z	4	4	4	2
ρ_{calcd} [gcm^{-3}]	1.597	1.573	1.542	1.648
M(MoKα) mm^{-1}	3.067	2.710	2.472	2.665
T /K	100	100	100	100
F(000)	1646	1992	2016	1088
crystal size [mm^3]	0.2 x 0.16 x 0.12	0.18 x 0.18 x 0.02	0.20 x 0.20 x 0.09	0.40 x 0.24 x 0.10
Θ range[°]	2.06 to 27.52	1.79 to 27.48	1.80 to 27.49	1.85 to 27.64
index ranges	$-17 \le h \le 17$	$-18 \le h \le 13$	$-11 \le h \le 18$	$-15 \le h \le 15$
	$-16 \le k \le 16$	$-24 \le k \le 23$	$-24 \le k \le 23$	$-19 \le k \le 19$
	$-27 \le l \le 26$	$-19 \le l \le 20$	$-20 \le l \le 20$	$-19 \le l \le 19$
Reflns collected	26629	37708	34675	23739
unique reflections	7888	9630	9879	9648
R(int)	0.048	0.128	0.048	0.082
completeness to Θ_{max} [%]	99.2	99.5	99.7	94.3
Reflns with [$I > 2\sigma(I)$]	7140	6049	8109	8976
data/restraints/parameters	7888/0/485	9630/0/536	9879/0/581	9648/0/572
final R indices [$I > 2\sigma(I)$]				
*R*1	0.050	0.058	0.038	0.044
*wR*2	0.100	0.090	0.087	0.106
R indices (all data)				
*R*1	0.058	0.108	0.052	0.048
*wR*2	0.102	0.123	0.094	0.108
largest diff. peak and hole [$eÅ^{-3}$]	1.48 and -0.96	1.10 to –0.83	0.97 and -0.90	2.66 and -2.43

Table 3. Crystallographic data for 8-10

Compound	**8**	**9**	**10**
empirical formula	$C_{50.50}H_{40}Cl_{4.5}HfN_4O_5S$	$C_{53}H_{33}HfN_{6.50}O_6S$	$C_{89.5}H_{57}Cl_3Hf_2N_8O_{16.5}P_3$
	X1580	X1570	X1600
formula wt.	1152.94	1067.41	2064.67
crystal system	monoclinic	triclinic	monoclinic
Space group	$P2_1/c$	P-1	C2/c
unit cell			
a / Å	14.624 (3)	13.244(3)	21.067(4)
b / Å	21.489 (4)	13.505(3)	15.382(3)
c / Å	15.044 (3)	13.567(3)	55.378(11)
α / °	90	74.91(3)	90
β / °	91.37 (3)	67.62(3)	91.60(3)
γ / °	90	79.54(3)	90
V/ $Å^3$	4726.3 (16)	2157.1(10)	17938(6)
Z	4	2	8
ρ_{calcd} [gcm^{-3}]	1.620	1.643	1.529
M(MoKα) mm^{-1}	2.558	2.530	2.525
T /K	100	100	100
F(000)	2302	1065	8176
crystal size [mm^3]	0.13 x 0.10 x 0.02	0.22 x 0.18 x 0.15	0.08 x 0.08 x 0.02
Θ range[°]	2.94 to 25.00	3.06 to 27.48	2.94 to 25.00
index ranges	$-17 \le h \le 17$	$-17 \le h \le 16$	$-25 \le h \le 25$
	$-25 \le k \le 25$	$-17 \le k \le 17$	$-18 \le k \le 18$
	$-17 \le l \le 17$	$-17 \le l \le 17$	$-65 \le l \le 65$
Reflns collected	67862	35670	93550
unique reflections	8292	9842	15751
R(int)	0.154	0.065	0.155
completeness to Θ_{max} [%]	99.7	99.4	99.5
Reflns with [$I > 2\sigma(I)$]	5817	8806	10581
data/restraints/parameters	8292/0/628	9842/0/644	20425/0/1145
final R indices [$I > 2\sigma(I)$]			
*R*1	0.069	0.034	0.087
*wR*2	0.112	0.069	0.173
R indices (all data)			
*R*1	0.111	0.042	0.140
*wR*2	0.126	0.072	0.195
largest diff. peak and hol [$eÅ^{-3}$]	1.23 and –0.81	1.51 and -0.95	1.59 and -1.60

Thus formed entities exist either as monomeric complexes, or as dimers wherein the exo-cyclic ligands bridge between two inverted Hf-porphyrin units. The high oxophilicity of early transition metals (as e.g., Hf or Zr) facilitates their complexation with a variety of organic as well as inorganic O-containing anions, which are used also to balance the net (2+) charge of the Hf-porphyrin adduct. Structural examples with the various $Hf(P)(L)_n$ complexes (L= oxo-ligand, n = 2 or 3) are provided below.

The $Hf(TPyP)(OAc)_2$ compound (**1**) (**Figure 8)** represents the first kind of monomeric complexes. It is characterized by a domed structure, residing in the crystal on axes of two-fold rotational symmetry at 0,y,¼. The porphyrin core adopts a distorted "saddle conformation" and the four inner pyrrole N-atoms deviate from the C_{20}-macrocycle towards the Hf ion, which lies above the ring. The distance of the hafnium ion from the mean N_4-plane is 1.036 Å. From the other side the metal cation is approached by the four O-sites of the two acetate counter-ions, at an average distance of 1.437 Å below the corresponding O_4-plane (**Table 4**). Thus, the coordination number (CN) of the Hf ion is 8. In the crystal, molecules of the complex are arranged next to one another in flat layers (parallel to the b-axis of the crystal), as frequently observed earlier for other metalloporphyrin compounds, exhibiting typical antiparallel face-to-face (at about 3.5 Å) or edge-to-face dispersion interactions between the peripheral aryl substituents of adjacent species.[45] Neighboring layers, displaced along the b-axis in an offset manner, are related to each other by crystallographic inversion. Their convex $Hf(OAc)_2$ surfaces interpenetrate in order to optimize the crystal packing and minimize void space at the interface, thus forming bi-layer domains. The interface between these bi-layers is lined with the concave surfaces of the domed porphyrin moieties (**Figure 9**).

Replacement of the acetate ligands by either *p*-aminobenzoic acid or pentanoic acid anions leads to similarly structured complexes **2** Hf(TPP)$(PABA)_2$ and **3** Hf(TTP)$pent_2$ irrespective of the different identity of the porphyrin building block in each case (**Figure 10**). While located in general positions, **2** and **3** are still characterized by the C_2 symmetry. The Hf ion is coordinated to the four pyrrole N-atoms from below at a distance of *ca.* 1.0 Å and the four carboxylate O-atoms from above at a distance of *ca.* 1.4 Å (CN=8, **Table 4**). However, presence of the amino functionality on the ligand in **2**, provides potential sites for specific intermolecular interaction of hydrogen bonding (as H-atom donors). This feature combined with the larger size of the anionic ligands induces co-crystallization with additional polar solvent species (water and nitrobenzene to fill effectively intermolecular space and balance the number of effective H-atom donors and acceptors) in this case. In the crystal, molecules of the solvent insert between the convex surfaces of inversion-related porphyrin layers, and bridge by continuous (though weak) hydrogen bonding between the individual complexes (**Table 5**). The overall crystal packing arrangements in **2** and **3** of stacked metalloporphyrin layers (along the b-axis of the unit-cell) remains similar to that observed in **1** (**Figures 11** and **12**), but with larger spacing between the inward-turning porphyrin layers. Due to the lipophilic character of the ligand alkyl residue in **3**, successful crystallization of this complex could be obtained with less polar solvent (than in **2**) as tetrahydrofuran. Molecules of the latter are inserted between the axial ligands in a disordered manner within the space between the inversion-related layers.

When the oxo ligands that interact with the Hf ions are accessible from opposite directions, formation of bridged dimeric metalloporphyrin moieties becomes feasible. [3, 5,

[21] This is the case with the bis-peroxo bridged porphyrin dimers, $[Hf(TPP)]_2(\mu\text{-}\eta^2\text{-}O_2)_2$ (**4**) and $[Hf(TTP)]_2(\mu\text{-}\eta^2\text{-}O_2)_2$ (**5** and **6**), which represent the second class of compounds in this study (**Figure 13**). Previous accounts have reported such oxo-bridged dimers as each oxygen existing as a OH^-, and or divalent O^{-2} for Zr(IV) and Hf(IV).[3, 4, 10, 22, 36] In structures **4**-**6**, the four oxygens take on a rectangular geometry with bonding O-O and non-bonding O···O distances of ca. 1.6 and 2.5 Å, respectively. Though in complex **4** we do find disorder within these sites, which allows us to construe the geometry to be the expected square, it would require a proposed structure involving 2 oxygens of low occupancy (0.25) and 2 oxygens of high occupancy (0.75); this is not a sound interpretation from a crystallographic standpoint. The two pairs of high occupancy oxygen atoms are within the upper range of appropriate distance for O-O peroxide bonds, ca. 1.56Å. The fact that we have observed this geometry in three independent crystal structures differing in both solvent and/or porphyrin unit, coupled with the data from our mass spectroscopy and absorption spectra lead us to believe these are appropriately viewed as peroxo-bridged dimers rather than hydroxy-bridged.

In previous accounts of a tri-oxo bridged zirconium structure[22], the oxygens are disordered, and the structure is presented as nearly equally spaced geometries of the bridging oxygens according to their respective occupancies. Additional structures of equal probability could also be proposed for this complex where two of the bridging oxygens are close enough to be bonded as peroxo molecule, suggesting a $[Zr(OEP)]_2[(\mu\text{-}\eta^2\text{-}O_2)(\mu\text{-}O)]$ complex. The IR spectra display stretches of $3740cm^{-1}$ for the Zr(TPP) oxo-bridged crystals which can more reasonably be interpreted as a peroxide IR stretch as this is a fairly high wavenumber for a (OH^-). [46] We have not observed a tri-oxo bridged

species for the hafnium analogue; this may be due to the larger coordination sphere of hafnium and/or differences in experimental conditions. We do not propose to argue with the reported analysis given by the authors; we only intend to suggest another possible interpretation that has not been discussed. Unfortunately, the diffraction data cannot define the presence or absence of hydrogens, but the mass spectra we have of our complexes clearly indicate that the bridging oxygens must be peroxides or oxygen radicals in order to justify charge and mass.

Most interesting, is the report of disulfide and selenium bridged dimers of Hf(TPP).[11] Here the rectangular geometry is also observed between the sulfur and selenium atoms, and they are correctly assigned as disulfide and diselenide bridges respectively, not as mono-atomic bridging ions.

In our three bridged structures, **4, 5,** and **6**, molecules of the dimeric units reside on centers of crystallographic inversion. The two peroxo-bridges balance the charge of the two metalloporphyrin species. These structures are characterized by two approximate square-antiprismatic environments about each of Hf centers, with the four bridging O-atoms forming one, common, four-sided face where the peroxo pairs form a rectangle rather than a square. The four N-atoms of the porphyrin ring comprises the other face on both sides (**Table 4**). As observed earlier for the Zr analogs of TPP,[22] the porphyrins are eclipsed. In **4**, the oxygen atoms are disordered, and traces of the methanol solvent are present in the crystal lattice. Compounds **5** and **6** crystallized as a chloroform and nitrobenzene solvates, respectively. This group of iso-structural TPP and TTP compounds is represented in Figure 6 by the molecular structure of **6**. The two peroxo ligands reside on a median plane between, and at an equal distance from, the two

metalloporphyrin components. The dimer molecules in **4-6** form layered arrangements perpendicular to the longest axis of the corresponding unit-cell (**Figure 14**). Adjacent layers are stacked in an offset manner, the individual porphyrin moieties in them adopting slightly different orientations (**Figure 14**). The crystallization solvent (traces of methanol in **4**, chloroform in **5**, and nitrobenzene in **6**) is accommodated in the interface between adjacent porphyrin molecules.

An interesting expansion of the above concept involves replacement of the peroxo moieties by SO_4^{2-} anions. The latter oxo ligands are also accessible to simultaneous Hf-coordination from different directions due to their tetrahedral geometry, thus providing another useful bridging element for the formation of the metalloporphyrin dimers. The successful synthesis of the corresponding materials of this third class, $[(TPP)Hf]_2[SO_4(H_2O)]_2$, (**7**) and $[Hf(TTP)]_2[SO_4(CH_3OH)]_2$ (**8**) is demonstrated in **Figure 15**. Two sulfate ions are used in this case for the dimer formation to account for the charge balance, each directing only one O-site at every adjacent Hf ion at *ca.* 2.05-2.15 Å. The coordination sphere of the hafnium is supplemented (to CN=7) by attracting an additional neutral water (in **7**) or methanol (in **8**) molecule from the crystallization mixture at a Hf-O(water/methanol) coordinating bond distance of *ca.* 2.25-2.29 Å. In **7**, the O-sites of the sulfate ions that do not coordinate to Hf are solvated by, via hydrogen bonds, molecules of methanol solvent (four methanols per dimer). In **8**, the methanol ligand hydrogen bonds also to the adjacent sulfate anion (**Figure 15**, **Table 5**). The larger size of the bridging sulfate ions (as compared to the peroxo bridges in **4-6**), results in a considerably larger Hf···Hf distance within the dimer (**Table 4**). In spite of the larger size of the dimeric complex, the crystal-packing modes in **7** and **8** are generally similar to

the motif observed in earlier examples (**Figure 16** and **17**). It can be best described as composed of layered arrangements of the complex entities $[(TPP)Hf(SO_4)(H_2O)]_2 \cdot 4MeOH$ or $[(TTP)Hf(SO_4)(MeOH)]_2$, which are then stacked one on top of the other along the third axis (Figures 9 and 10). Packing of these molecules is not self-complementary in three dimensions. Correspondingly, the formation of stable crystals is facilitated by inclusion of chloroform solvent within the interstitial space in an ordered manner in **7** and a disordered manner in **8**.

Another variant of this type of compounds is represented by dimer **9** $[(TPP)Hf(SO_4)]_2$, obtained from a non-aqueous environment (nitrobenzene and acetonitrile served as crystallization solvents in this case). Again, two sulfate anions accessible to coordination from opposite sites serve as bridges (as well as suitable counter ions) between two monomeric $[Hf^{IV}(TPP)]^{2+}$ entities (**Figure 18**). However, in the present example these ions serve also as the only ligands to the Hf metal (as no other oxo ligands were present in the reaction mixtures). Thus, in order to preserve the 7-coordination environment around it (as in **7** and **8**) two O-atoms of one sulfate and one O-atom of the second sulfate associate with each Hf at 2.08-2.18 Å (**Table 4**). Slightly longer bonding distances within this range characterize the former, while the latter represents the shortest distance. The crystal packing of **9** is depicted in **Figure 19**, revealing a layered intermolecular organization as in the previous examples. Molecules of the nitrobenzene and acetonitrile (disordered) solvent are accommodated in the lattice between the metalloporphyrin moieties.

In all three structures **7-9** the dimer complexes reside on centers of crystallographic inversion, with identical geometries of the two monomeric Hf-TPP

constituent parts. Moreover, dimers **4-8** exhibit an approximate C_{2h} symmetry with the twofold axis and the pseudo-mirror plane (the two porphyrin rings assuming an eclipsed orientation) passing through the Hf ions and the median plane of the bridging ligands, respectively. Although the actual identity of the porphyrin scaffold (whether TPP, TPyP or TTP) has negligible effect on the molecular structures described above, it does influence to some extent the layered organization of the monomeric or dimeric complexes. TPP- or TPyP-based compounds organize conveniently in space in a parallel fashion, within as well as between the layers. On the other hand, TTP-based materials with larger molecular framework pack in a herringbone manner, while preserving the layered organization. The molecular units in subsequent layers are slightly tilted with respect to the mean plane of the given layer. This seems to be required by the need to optimize condensed packing of the additional peripheral methyl substituents on the phenyl residues.

Additional reaction of the Hf(TPP) moiety with excess phosphoric acid yielded yet a differently structured dimer, **10** - $[Hf(TPP)]_2(HPO_4)_3^{-2}$, (hydronium ions are assumed to balance the negative charge of the parent complex) which involves three phosphate ions as bridging units (Figure 13). This is the only product in the series of the Hf-porphyrin dimers, which deviates from the axial two-fold symmetry and therefore does not contain an inversion center (**Figure 20**). The entire dimer represents the asymmetric unit (in which the bridging phosphates suffer from partial disorder) of this structure. The minimal coordination requirements of each Hf ion are satisfied by its bonding to the four pyrrole N-atoms of TPP and the O-atoms of the three tetrahedral phosphate bridges (CN = 7), without the need to coordinate another ligand from the

solvent environment. Noteworthy are the relatively short deviation of the Hf ion from the mean plane of the coordinating O-atoms and the Hf-O distances in this structure (**Table 4**) due to the stronger electrostatic attraction between the metal and the phosphate ions. In the resulting structure the two/four-fold symmetry of the porphyrin rings is incommensurate with the three-fold symmetry of the bridged Hf-$(PO_4)_3$-Hf fragment. As a result, the fully eclipsed orientation of the porphyrin components of a given dimer in **4-9** is not preserved any longer. Rather, the two porphyrin macrocycles are partly staggered, which has also an apparent effect on the crystal packing (see below). The outer, non-coordinating, O-sites of the phosphate ions are solvated by molecules of water and methanol solvents, each of the latter hydrogen-bonding simultaneously to, and interlinking between, two phosphate species (**Table 5**). The crystal packing of this compound also differs from that observed in the other dimers (**Figure 21**). It consists of bilayers of similarly oriented species, while crystal packing of these bilayers along the c-axis is in a herringbone manner. A considerable amount of partly disordered solvent (CH_2Cl_2, CH_3OH, H_2O and H_3O^+) is trapped between the metalloporphyrin units in the crystal lattice.

Table 4. Geometry of coordination interactions in solids **1-10**.[a]

Coordination bonding distance range (Å)

Compounds:	**1**[b]	**2**[b]	**3**[b]	**4**[b]	**5**[b]
Hf–N(pyrrole)	2.262-2.267	2.238-2.275	2.231-2.260	2.220-2.253	2.220-2.257
Hf–O(ligand)[a]	2.238-2.243	2.237-2.256	2.232-2.286	2.177-2.181	2.137-2.150

Compounds:	**6**[b]	**7**[c]	**8**[c]	**9**[d]	**10**[e]
Hf–N(pyrrole)	2.229-2.263	2.229-2.251	2.215-2.234	2.198-2.234	2.250-2.279
Hf–O(ligand)[a]	2.143-2.154	2.084-2.249	2.087-2.293	2.084-2.185	2.044-2.124

(Table 4 cont'd)

Deviation of Hf from the mean plane of the N_4(pyrrole) and O_3/O_4 (ligand) sites (Å).

Compounds:	**1**[b]	**2**[b]	**3**[b]	**4**[b]	**5**[b]
N_4 (pyrrole)	1.036	1.027	1.004	0.967	0.964
O_4 (ligand)	1.437	1.430	1.452	1.564	1.559

Compounds:	**6**[b]	**7**[c]	**8**[c]	**9**[d]	**10**[e]
N_4 (pyrrole)	0.978	0.994	0.971	0.938	1.048, 1.054
O_3/O_4 (ligand)	1.551	1.459	1.456	1.518	1.374, 1.340

Hf ···Hf distance in the dimeric structures (Å).

Compounds:	**1**[b]	**2**[b]	**3**[b]	**4**[b]	**5**[b]
	-	-	-	3.129	3.118

Compounds:	**6**[b]	**7**[c]	**8**[c]	**9**[d]	**10**[e]
	3.103	5.496	5.462	5.179	5.166

---

[a] The O-ligating anionic sites that balance the excessive charge on Hf consist of two acetyl (**1**), two benzoate (**2**), two pentanoate (**3**) four hydroxy (**4**, **5** and **6**), two SO_4^{2-} (**7**, **8** and **9**), and three phospate (**10**) species.

[b] In **1**-**6** each of the Hf ions is characterized by coordination number of 8, coordinating to four pyrrole N-atoms of the porphyrin and four O-sites of the two carboxylate or four hydroxy ligands.

[c] In **7** and **8** the Hf ion has a coordination number of 7, coordinating to four pyrrole N-atoms of the porphyrin, two O-sites (one from each sulfate ion) at *ca.* 2.08-2.15 Å and an additional water/methanol ligand at a slightly longer distance of *ca.* 2.25-2.29 Å.

[d] In **9** the Hf ion has a coordination number of 7, coordinating to four pyrrole N-atoms of the porphyrin, two O-sites of one sulfate ion and one O-site of the second sulfate species.

[e] In **10** the Hf ions have a coordination number of 7, coordinating to four pyrrole N-atoms of the porphyrin, and single O-sites of the three phosphate species. The two halves of **10** are crystallographically independent.

Detailed information on individual contacts is given in the supplementary CIF files.

Table 5. Hydrogen bonding interactions in 2, 7, 8 and 10.

D-H	A	D-H (Å)	H···A (Å)	D···A (Å)	D-H···A (º)
Complex **2**					
NHa(64)[a]	O90 (1-x, -y, 2-z)[b]	0.88	2.34	3.110	171
NHb(64)[a]	O82 (1-x, -y, 1-z)[c]	0.88	2.48	3.349	171
NHa(74)[d]	O81 (-x, -y, 1-z)[c]	0.88	2.27	3.101	158
NHb(74)[d]	O90 (-x, -y, 2-z)[b]	0.88	2.35	3.095	143
OHa(90)[b]	O91[e]	0.85	2.19	2.977	153
OHb(90)[b]	O62[f]	0.85	2.21	2.934	143
Complex **7**					
OHa(5)[g]	O71(-x, 1-y, 1-z)[h]	0.84	1.81	2.619	162
OHb(5)[g]	O4[i]	0.85	1.93	2.698	149
OH(71)[h]	O81[h]	0.84	1.88	2.717	178
OH(81)[h]	O3[i]	0.84	1.95	2.781	170
Complex **8**					
OH(11)[j]	O4(-x, 1-y, 1-z)[i]	0.84	1.78	2.617	176
Complex **10** (solution of this structure was not adequately precise to allow the location of the H-atoms)					
OHa(41)[b]	O23[k]			2.544	
OHb(41)[b]	O34[k]			2.802	
OHa(43)[b]	O24(x-½, y-½, z)[k]			2.678	
OHb(43)[b]	O14(x-½, y-½, z)[k]			2.849	
OH91[h]	O13[k]			2.899	
OH91[h]	O33[k]			2.774	

[a] NH_2 function of 1st ligand; [b] water solvent; [c] 1st nitrobenzene solvent;
[d] NH_2 function of 2nd ligand; [e] 2nd nitrobenzene solvent; [f] COO group of 1st ligand;
[g] water coordinated to Hf; [h] methanol solvent; [i] sulfate ion; [j] methanol coordinated to Hf;
[k] phosphate ion.

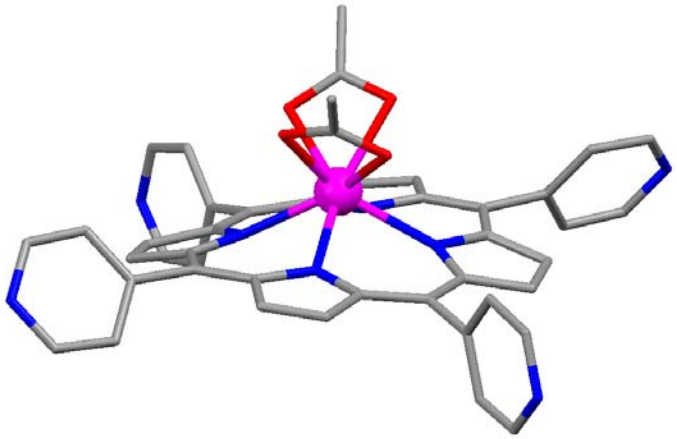

Figure 8. Crystal structure of **1**, showing its domed shape (H-atoms are omitted).

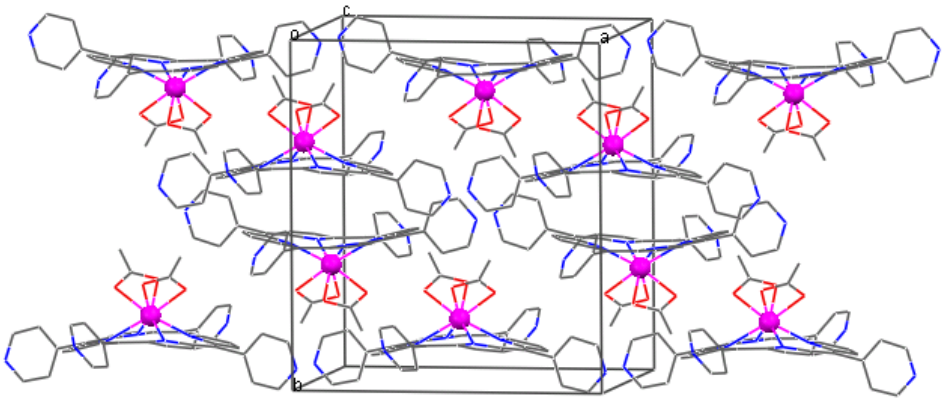

Figure 9. Crystal packing in **1**. Note the layered arrangement of the molecular units and the efficient packing of the convex surfaces of inversion-related layers.

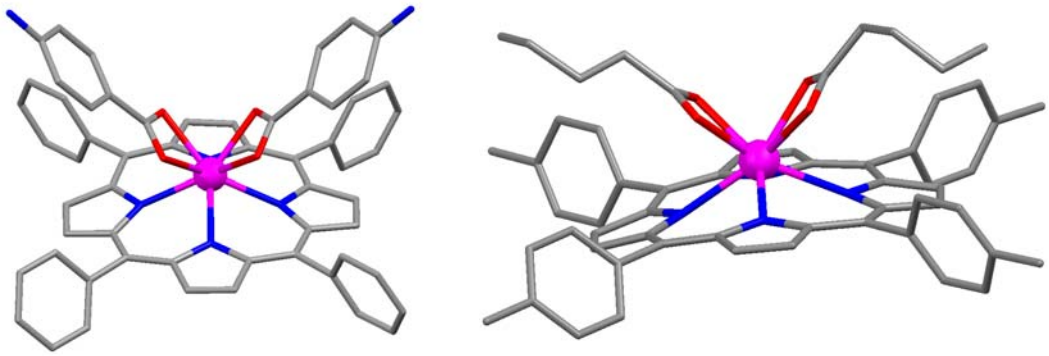

(a) **(b)**

Figure 10. Crystal structures of (a) **2** and (b) **3**.

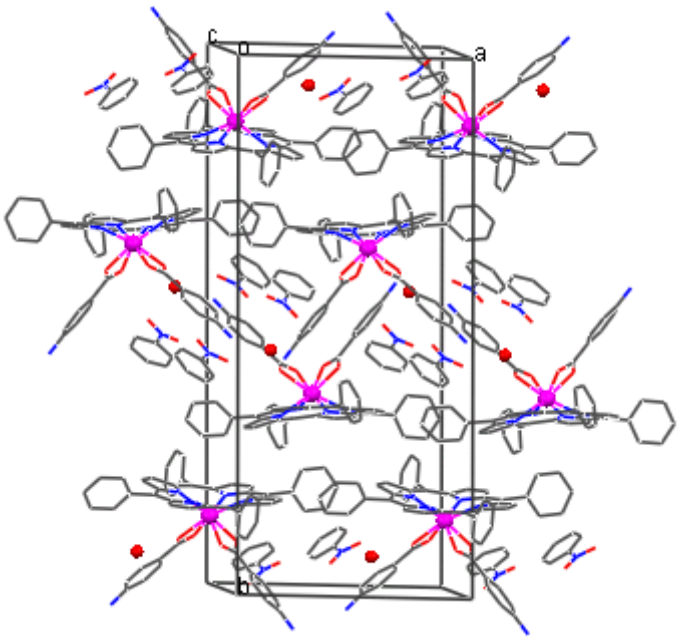

Figure 11. Crystal packing of **2**. Note the water (red spheres) and nitrobenzene solvent species intercalated between the inversion-related porphyrin layers.

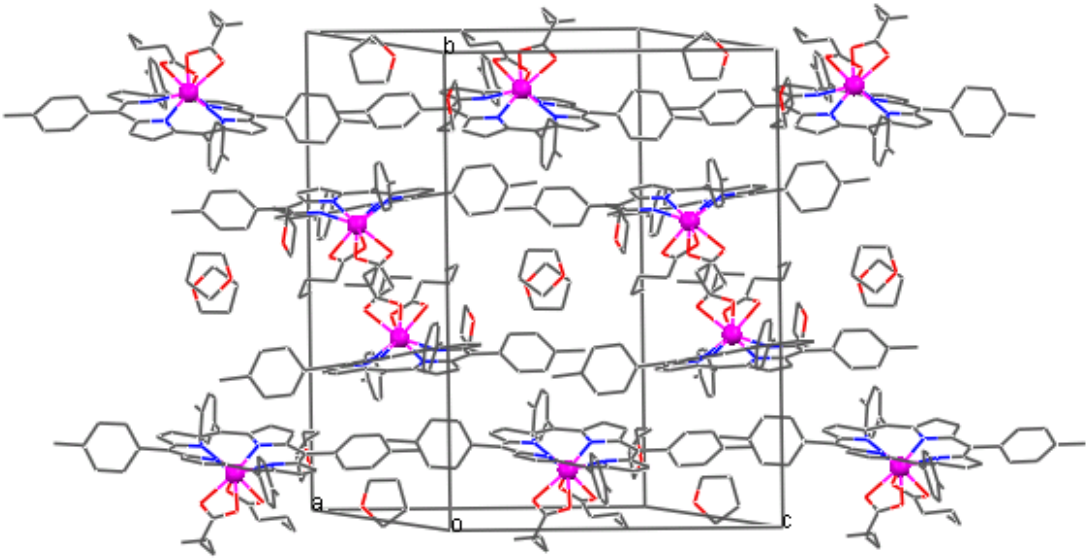

Figure 12. Crystal packing of **3**. Note the approximate positions of the disordered THF solvent intercalated within the inversion-related layers of the porphyrin units.

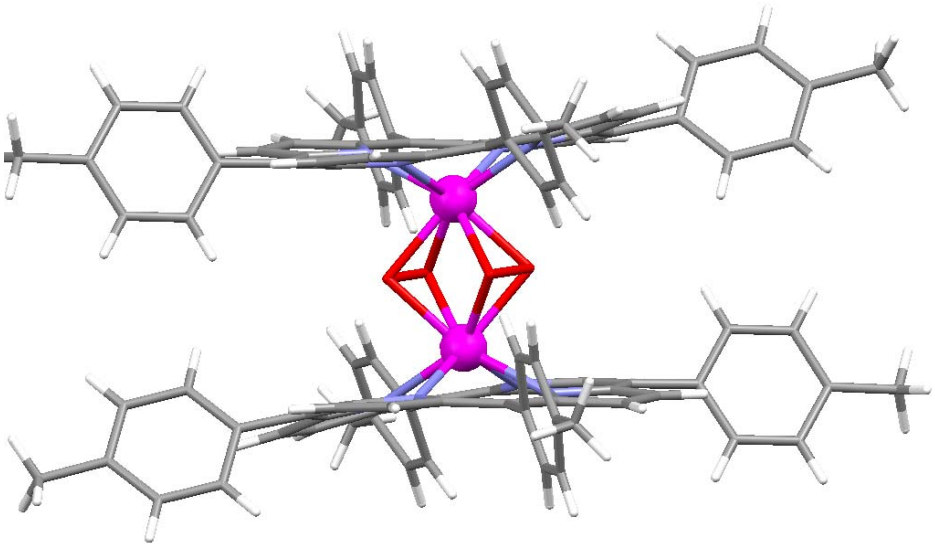

Figure 13. Crystal structure of the peroxo-bridged eclipsed dimer **6** shown with the O-O bonds of the peroxo bridging molecules. The analogous compounds **4** and **5** are characterized by similar inter-coordination features.

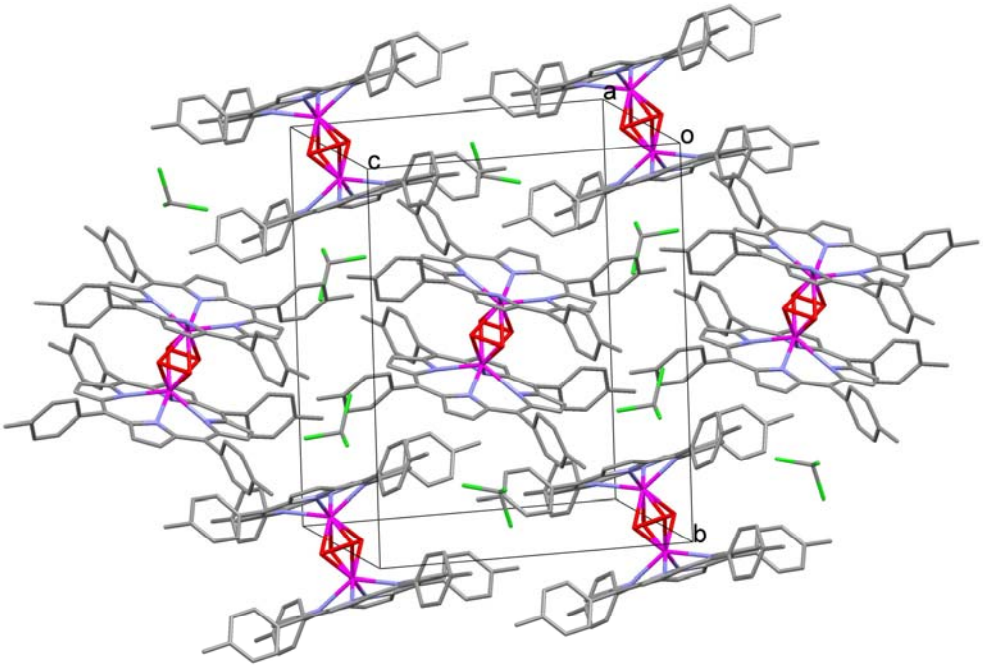

Figure 14. Crystal packing of the chloroform solvate of **5**. Note the corrugated layers of the metallo-porphyrin entities, and the chloroform solvent species intercalated between them. Neighboring layers contain units of the complex oriented in slightly different directions (in a herringbone style) to efficiently accommodate the peripheral methyl groups of the tolyl residues.

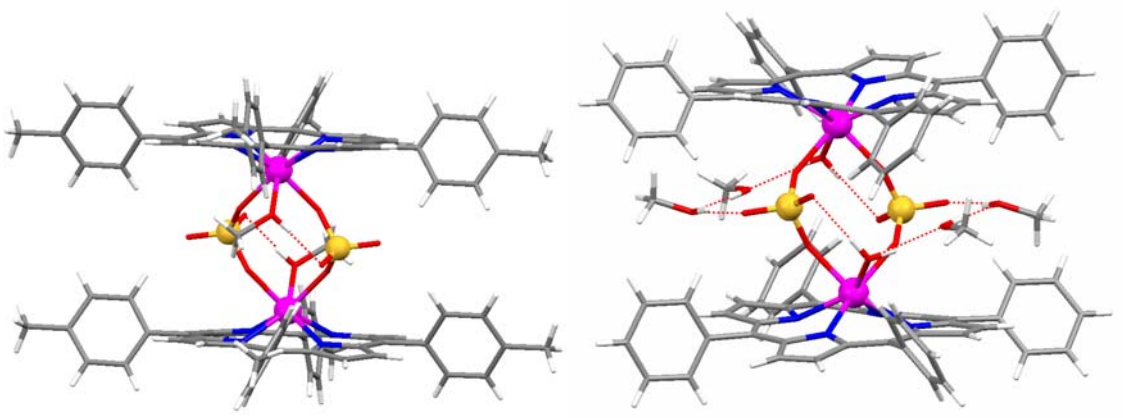

(a) **(b)**

Figure 15. Crystal structures of dimers (a) **7** and (b) **8**, sustained by two SO_4^{2-} bridges. Note in **7** the additional water ligand coordinated to the Hf-ions, and the four molecules of the methanol solvent that interlink by hydrogen-bonding (dotted lines) between the sulfate and water ligands. In **8** a molecule of methanol is coordinated directly to each Hf ion, forming simultaneously a hydrogen bond to the proxime sulfate anion. The hydrogen bonds are marked by dotted lines.

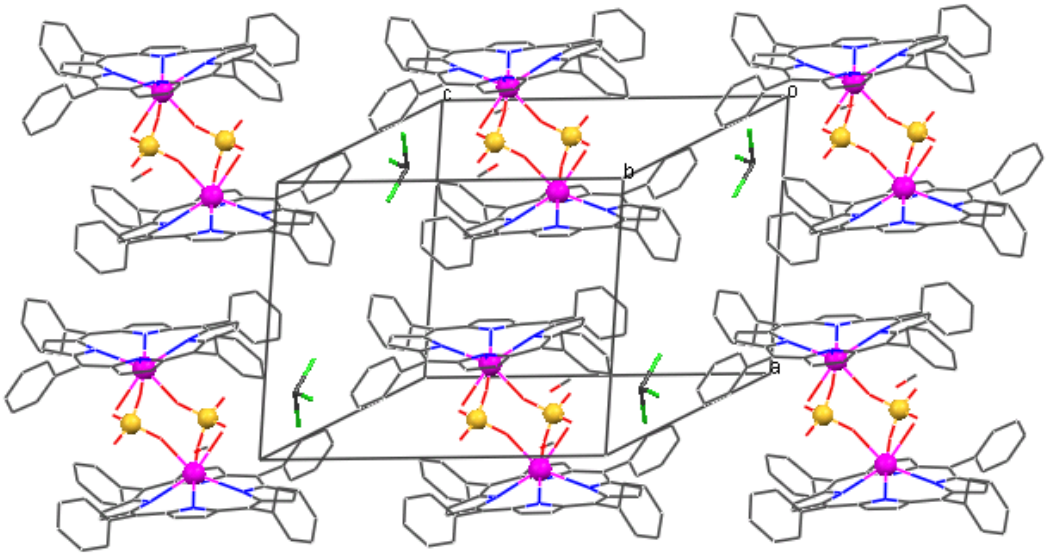

Figure 16. Intermolecular molecular organization in the crystals of **7**. Note the parallel layered organization of the solvated metalloporphyrin dimers, and intercalation of additional chloroform solvent species between them.

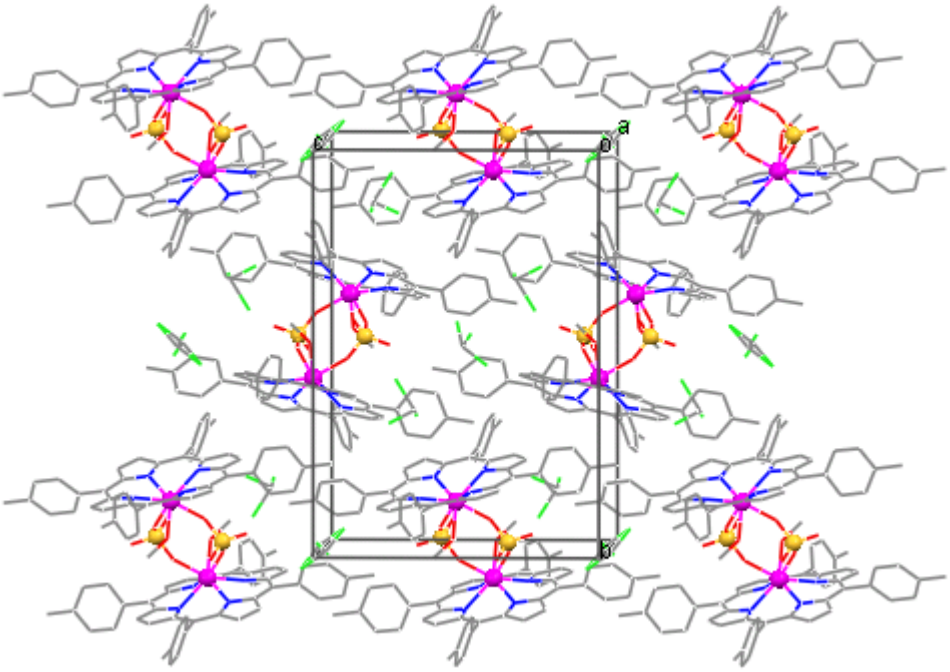

Figure 17. Intermolecular organization in the crystals of **8**. Note the layered organization of the metalloporphyrin dimers, and intercalation of additional chloroform solvent species between them. The larger size of the porphyrin units imparts a herringbone nature to the intermolecular organization to optimize condensed packing.

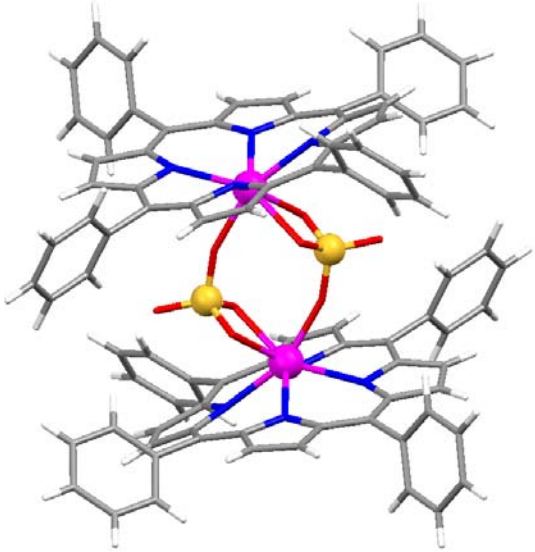

Figure 18. Molecular structure of dimer **9**, with the asymmetric coordination of the two SO_4^{2-} bridges to the Hf ions.

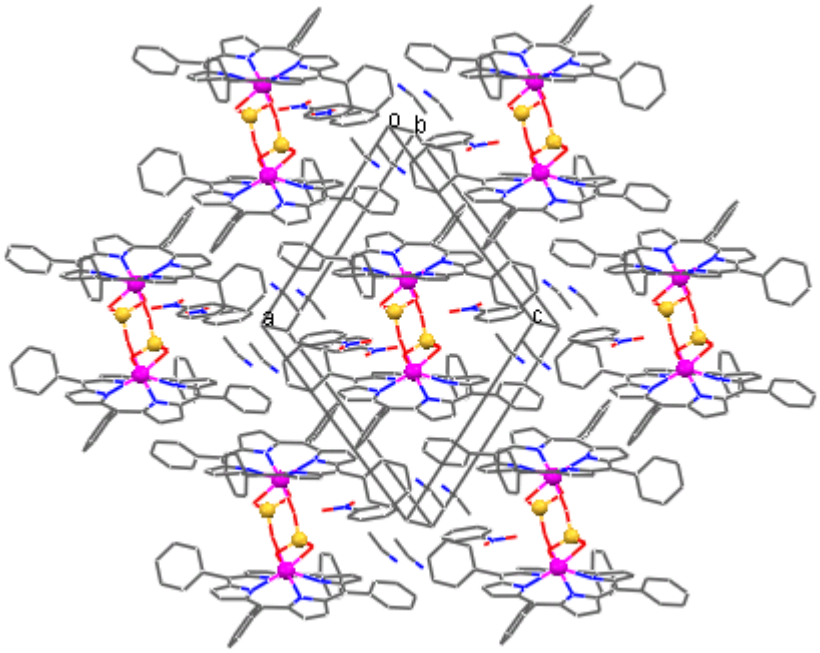

Figure 19. Crystal packing diagram of **9**. Note the interstitial occlusion of the nitrobenzene and acetonitrile solvents.

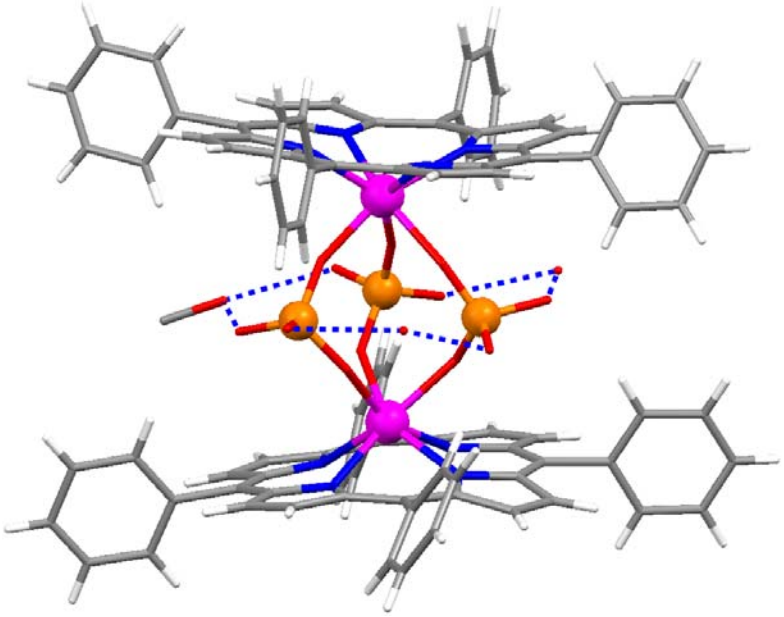

Figure 20. Molecular structure of dimer **10**, sustained by intercoordination through three (partly disordered) PO_4^{3-} bridges. The latter are farther interlinked on the periphery to one another by H-bonds (dotted lines) through MeOH and water species.

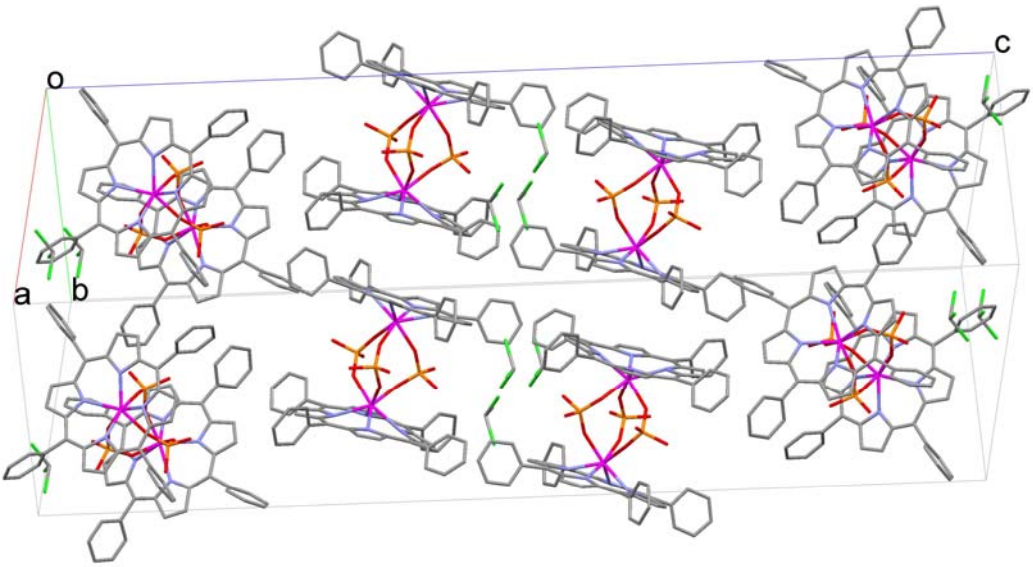

Figure 21. Crystal packing diagram of **10**. Only the chloroform solvent occluded within the bilayers is shown, the additional (partly disordered) water and methanol solvent species being omitted for clarity.

Metalation and Purification Methods

All UV-Visible spectra were taken in 1 cm quartz or glass cuvettes unless otherwise indicated, on a Carey Bio 3 spectrophotometer. Mass spectrometry was done as a service by the University of Illinois, Urbana-Champaign or on an Agilent 1100 LC/MSD instrument. NMR were run on a 500 MHz Varian Inova. Fluorescence spectra were taken on a Spex Tau-3 fluorometer in 1 cm quartz cuvettes. Gasses, reagents, and solvents were used as received unless otherwise noted. $HfCl_4$ and $Hf(cp)_2Cl_2$ were obtained from Strem Chemicals. Porphyrins were obtained from Aldrich or from Frontier Scientific. All solvents and other reagents were from Aldrich. Disposable vials and test tubes were used once.

Method 1: 1-chloronapthalene as solvent

Hafnium (IV) meso-tetraphenylporphyrinato diacetate **Hf(TPP)OAc$_2$** 100 mg (0.16 mmol) of H_2TPP was dissolved in 4 mL of hot 1-chloronapthalene, ca. 150 °C, in a 1.8 x 15.0 cm disposable test tube. The solution was allowed to cool to room temperature and 0.32 mL of 1M lithium hexamethyl disilizane, LiHMDA, in hexanes was added. The reaction mixture turned a dark green indicating the formation of Li_2TPP *in situ*. The resulting amines were evaporated by heating the solution. 208 mg (0.65 mmol) of $HfCl_4$ was added and the mixture was allowed to reflux for 5 minutes. After the solution cooled, it was diluted in 50 mL of CH_2Cl_2 and loaded directly onto 30 g of silica in a glass frit filter, 4.25 cm x 4.25 cm, 60 cm^3, placed on a filtering flask and vacuum filtered. The first fraction**,** along with reaction solvent, was eluted with neat CH_2Cl_2 and was identified as unreacted porphyrin by UV-Vis. The second fraction**,** Hf(TPP)OAc_2**,** was eluted with CH_2Cl_2:MeOH:CH_3COOH, 3:1:1, and reduced to 1 mL of mostly acetic acid by rotary-evaporation. The product was precipitated by the addition of 10 mL of distilled water and then centrifuged. The bright pink solid was dried and weighed to yield 122 mg (82%), of the Hf(TPP)OAc_2 complex.

Hafnium(IV) meso-tetra-4-tolylporphyrinato diacetate **Hf(TTP)OAc$_2$** was synthesized by reacting of 100 mg of H_2TTP with 190 mg $HfCl_4$ according to **Method 1**. A small portion, about 1 mL, of the reaction mixture was taken from the vessel to purify as the acetate derivative. The portion was loaded onto silica and unreacted porphyrin, H_2TTP, was eluted with neat toluene as the first fraction. The second fraction, Hf(TTP)OAc_2**,** was eluted with a solution of CH_2Cl_2:MeOH:CH_3COOH, 3:1:1 and reduced to 1 mL of mostly acetic acid by rotary evaporation. The product was

precipitated by the addition of 10 mL of distilled water and then centrifuged. The purple solid was dried and weighed to yield 25 mg of the Hf(TPP)OAc_2 complex. The relative spectroscopic yield compared to the free-base fraction was about 80%. The remainder of the reaction mixture was used for the formation of other derivatives (see below)

Method 2: Solventless $Hf(cp)_2Cl_2$ melt

Hafnium (IV) meso-tetraphenylporphyrinato diacetate **Hf(TPP)OAc_2**: To a dry, screw-cap, 2 mL glass vial was added 200 mg (0.3 mmol) of H_2TPP and 370 mg of $Hf(cp)_2Cl_2$ (0.9mmol). The hafnium starting complex was crushed to a fine powder before it was added to ensure even distribution. The contents of the vial were mixed thoroughly by gently turning the vial. The cap was sealed and the vial was heated in a hot sand bath (ca. 300 $^{\circ}$C) just on the bottom surface so that the sand level was never above that of the vial's contents. The $Hf(cp)_2Cl_2$ melted and solvated the porphyrin forming a dark, molten paste. White salts and cyclopentadiene sublimed from the paste and deposited on the upper walls of the vial over the course of 30 seconds. The vial was allowed to cool for a few moments before removing the cap. The vial was then fully embedded in the hot sand for only a few moments while argon was blown gently into the vial to remove the remaining cyclopentadiene before allowing the vial to cool to room temperature.

The film in the vial was dissolved in 30 mL of CH_2Cl_2 and filtered of any insoluble material. The solution was pre-loaded onto 10 g of silica gel powder and dried to ensure efficient binding of the product to the silica. A large glass frit filter, 4.25 x 4.25 cm, 60cm^3, was filled with 30 g of silica gel powder slurried in CH_2Cl_2 and placed on a filter flask. The preloaded silica was slurried in CH_2Cl_2 and added to the make-shift

column followed by rapid elution accomplished by vacuum filtration. Neat CH_2Cl_2 eluted the first fraction consisting of trace amounts of H_2TPP. A solution of CH_2Cl_2:MeOH:CH_3COOH, 77:20:3, was passed over the silica to remove the Hf(TPP)OAc_2 complex as the second fraction**.**

The initial UV-Vis spectrum of the Hf(TPP)OAc_2 fraction displayed an absorbance band at 634 nm at half the intensity of the normal Q-band which appears at 540 nm. This was identified as a fraction of a reduced Hf(TPP) complex. Thus, the crude Hf(TPP)OAc_2 was then stirred over 100 mL of 2.5 M aqueous potassium dichromate, $K_2Cr_2O_7$, for 3 hours. The oxidation was monitored by UV-Vis until the absorbance band at 634 nm no longer appeared. The organic layer was isolated and evaporated to 1 mL. The product was precipitated with 20 mL of distilled water and centrifuged. A brownish polymeric material (most likely from excess cyclopentadienyl salts from the melt) was found in the supernatant and was discarded. The solid was sonicated briefly and centrifuged twice more in 2:1:1, H_2O:MeOH:acetone washes to remove the last of this material. The pink solid was dried in an oven at 100 $^{\circ}$C to yield 291 mg (97%) of the Hf(TPP)OAc_2 complex.

Hafnium (IV) meso-tetra-perfluorophenylporphyrinato diacetate **Hf(TPPF_{20})OAc_2** was synthesized in a similar solventless method as in **Method 2.** 97 mg of H_2TPPF_{20} (0.1 mmol) was reacted with 114 mg of $Hf(cp)_2Cl_2$ (0.3mmol) as described above**.** Extra care was taken not to over heat the sample to minimize the amount of reduced Hf(TPPF_{20}) complex; as oxidation procedures are not as effective with this complex. The vial was not embedded into the sand further than 1 cm and only heated

enough to melt the mixture and observe the formation of white crystalline deposits on the walls of the vial.

The residue from the vial was sonicated in CH_2Cl_2 in a 200 mL conical flask; 0.1 mL of conc. aq. HCl was added to the solution which turned green from the formation of $H_4TPPF_{20}^{2+}$. The solution was added to a silica column in a glass frit filter, 4.5 cm X 4.5 cm and eluted by vacuum filtration. Neat CH_2Cl_2 eluted a small initial fraction of unreacted porphyrin. Then a solution of CH_2Cl_2, 2% v/v triethylamine eluted the remainder of the unreacted porphyrin, followed by $CHCl_2$:MeOH, 1:1 v/v to remove the last of the unreacted material. $CHCl_3$:MeOH:CH_3COOH, 77:20:3, eluted the metalated porphyrin as $Hf(TPPF_{20})OAc_2$. The product was dried and weighed, 18 mg of $Hf(TPPF_{20})OAc_2$, ca. 12% yield. Some polymeric material still remained in H^1- NMR and MALDI MS spectra (supporting information).

Method 3: 1-chloronapthalene, cresol method

Hafnium(IV) meso-tetra-4-pyridyporphyrinato diacetate **$Hf(TPyP)OAc_2$.** 100 mg of H_2TPyP was dissolved in a 1.8 x 15.0 cm test tube in 5 mL of a 3:1 mixture of dry 1-chloronapthalene and freshly distilled *o*-cresol. In a separate 1.2 x 7.5 cm test tube, 70 mg of NaH (60% dispersion in mineral oil) was added to 2 mL of *o*-cresol and heated until fully reacted to form a ca. 8.5% solution of the sodium cresolate salt; this was decanted into the solution of dissolved porphyrin. A rubber septum was placed on the test tube and argon was vented via syringe needles until the vessel was fully purged. The solution was heated under argon close to reflux. 260 mg of $HfCl_4$ (5 eq.) was added and the mixture was allowed to reflux for 20 minutes under a strong flow of argon. The reaction turned a deep red color and the UV-Vis indicated only small amounts of

unreacted porphyrin. The reaction mixture was loaded directly onto 35 g of silica in a 4.5 cm x 4.5 cm glass frit filter and vacuum filtration using CH_2Cl_2 as eluent to remove most of the reaction solvent.

Then an eluent of CH_2Cl_2 containing 10% MeOH removed unreacted porphyrin as the first fraction. The column was then eluted with neat methanol, followed by MeOH:H_2O 1:1 v/v to remove trace amounts of cresol while the metalated product remained unmoved at the top of the silica gel. The $[Hf(H_4TPyrP)OAc_2][OAc]_4$, wherein the pyridyl groups are protonated, was eluted with 1:1 distilled H_2O: CH_3COOH. While the elution with acetic acid affords the acetate derivative, it also protonates the pyridyl groups on the porphyrin. Though atypical, this was the only solvent system that eluted the product cleanly, as it solvates the pyridinium substituents. 100 mg of sodium acetate was dissolved in this fraction and the solvent was removed by evaporation under reduced pressure. While the solvent is removed, the $NaCH_3COO$ deprotonates the pyridinium ions. The residue was suspended in water and centrifuged. The supernatant contained excess salts and was decanted. The solid was suspended again in fresh, distilled H_2O and collected on a filter. Two 4 mL washings of distilled water removed residual salts. The pink solid was dried and weighed to yield 130 mg (73%) of the $Hf(TPyP)OAc_2$ complex.

Hafnium(IV) meso-tetra(4-methylbenzoyl)porphyrinato diacetate **Hf(TMeCPP)OAc$_2$** was synthesized according to **Method 3.** 200 mg of H_2TMeCPP (0.24 mmol) was dissolved in 8 mL of a 1:1 mixture of 1-chloronapthalene and *o*-cresol in a 1.8 x 15.0 cm disposable test tube fitted with a rubber septum. In a separate test tube 3 mL of cresol was thoroughly reacted with 96 mg of NaH (2.4mmol, 60%dispersion in mineral oil) and the resulting solution was added to the reaction chamber as described

above**.** After purging the vessel with argon via syringe needles, 380 mg (1.2 mmol) of $HfCl_4$ was added and the reaction was refluxed under a strong flow of argon for 30 minutes. The solution was allowed to cool to room temperature and was precipitated with 300 mL of hexanes. The mixture was filtered, collecting most of the product as a solid, and the supernatant was added directly to a silica column, 35 g, 4.25 cm x 4.25 cm, in a glass frit filter. Once the solution had been passed through the column, a bright pink band formed at the top and the clear elute was discarded. Neat CH_2Cl_2 was passed over the column, eluting a dark purple band of unreacted porphyrin and trace amounts of reaction solvent. Further elution of increasing proportions of MeOH up to 100% eluted more unreacted porphyrin with partially cleaved ester groups as indicated by TLC. Then 100 mL of 1:1, MeOH: H_2O, cleanly removed trace amounts of cresol from the silica. This was followed by neat methanol to remove the water from the column. The metalated porphyrin was eluted cleanly with CH_2Cl_2:MeOH:CH_3COOH, 3:1:1. This last fraction was reduced to 1 mL by rotary evaporation and precipitated with 20 mL of distilled water. The mixture was centrifuged and the clear supernatant was decanted. H^1-NMR of the dry solid indicated that the methyl esters had been partially cleaved and was combined with the initial precipitate.

The initial precipitate was determined by UV-Vis to be more than 85% metalated porphyrin bearing a mixture of partially cleaved esters. Rough estimates from the MALDI spectrum of this mixture (appendix) indicated the following proportions: tris/tetra carboxyphenyl 7%, cis/trans-carboxyphenylporphyrin 12%, mono-carboxyphenylporphyrin 24%, and the target tetra-methyl ester 57%. The carboxylate groups were re-esterified to the methyl esters by reaction of the products with

diazomethane prepared and distilled in diethyl ether according to standard literature procedures.

The crude product was dissolved in 120 mL of THF, 20% MeOH. The diazomethane solution was added to the porphyrin solution and allowed to react for several minutes after which the ether and diazomethane were evaporated from the solution in a warm water bath. The remaining solution was diluted with 100 mL of CH_2Cl_2 and 15 g of silica powder was added to the flask. The mixture was evaporated to dryness to efficiently bind the product to the silica. The preloaded sample was added to a silica column, 3 cm x 25 cm, suspended in CH_2Cl_2. Neat CH_2Cl_2 eluted a small fraction of unreacted porphyrin as H_2T-MeCPP. The Hf(T-MeCPP)OAc_2 complex was eluted with CH_2Cl_2:MeOH:CH_3COOH, 3:1:1 and reduced to 5 mL of acetic acid by rotary evaporation. 50 mL of distilled water was added and the product precipitated. The solid was centrifuged and dried to yield 194 mg, 72% of the Hf(T-MeCPP)OAc_2 complex. ESI-MS and ^{1}H-NMR still indicated some portion of cleaved esters after the diazomethane reaction. This was not pursued as the Hf(T-MeCPP)OAc_2 complex is only a precursor to the Hf(TCPP) complex which has many more applications to our purpose. (See synthesis of derivatives below)

Method 4: 1-chloronapthalene, dodecanol

Synthesis of reduced Hafnium(IV) porphyrinates

100 mg of TPP, TPyP, and tetra-4-carboxyphenyl porphyrin (TCPP) were individually reacted with $HfCl_4$ (5 equivalents) in the precise manner as described in **Method 3** using dodecanol in place of cresol in the same quantities and procedure under a strong stream of argon. The rate and yield of metalation for all three porphyrins was similar.

Within five minutes of reaction, the UV-Vis indicated a large portion of the porphyrin had been metalated. After which time the solution began to darken to a purple then blue after 30 minutes of reaction at reflux under argon. After 45 minutes the result was a dark marine-blue product that was identified by UV-Vis and chemical oxidation reduction reactions as a reduced Hf(P)complex. The absorption spectra contained a strong band around 630 that was also found in a fraction of the product from **Method 2.**

All three reaction mixtures were purified over silica using CH_2Cl_2, 20% MeOH to elute reaction solvents and unreacted porphyrin. The unreacted porphyrins displayed typical UV-Vis spectra for the corresponding free-base porphyrins. CH_2Cl_2:MeOH:CH_3COOH, 3:1:1, eluted the metalloporphyrin products as described above. The major product was the reduced, deep blue band of chlorin, and only a small fraction of the pink, non-reduced species remaining as indicated by TLC. The yield of metalated porphyrin was determined spectroscopically to be ca. 75% for all three reactions.

The reduced Hf(TPP) complex was purified and isolated as a blue powder. H^1-NMR was not useful for complete characterization of the products, due to poorly resolved peaks, though the large difference between the reduced and non-reduced NMR spectra clearly show a structural alteration of the porphyrin macrocycle (appendix). UV-Vis displayed an intense red absorbance at 634 nm, reminiscent of a chlorin absorption spectrum (appendix). The products from this method were oxidized to the neutral $Hf(TPP)OAc_2$ using $K_2Cr_2O_7$ as described in **Method 2**.

Rapid oxidation of the reduced complex, without demetalation, was observed by treatment of a 5 mg sample dissolved in 4 mL of CH_2Cl_2 with 0.2 mL of $SOCl_2$ which has been known to be a powerful oxidant.[34, 35] After stirring at room temperature for five minutes, the color of the solution turned from blue-purple to red and the absorbance at 634 disappeared. The solvent was evaporated to remove excess $SOCl_2$ and HCl.

For TPyP, a large fraction of the pyridyl substituents were alkylated to form dodecyl pyridinium in addition to metalation of the porphyrin by hafnium, as vaguely indicated by ESI-MS (appendix). The alkylation likely arises from the formation of 1-chloro-dodecane under the high temperatures used and the presence of an excess of $HfCl_4$. There was less reduced product observed by UV-Vis for the Hf(TPyP) alkylated product, indicated by a less intense 630 nm absorbance band.

In the case of TCPP, the dodecyl chloride esterified a large fraction of the free carboxylates to form dodecyl ester phenyl substituents as well as metalating and reducing the porphyrin to a blue-purple product. The distinctive low energy absorbance band near 630 nm was observed The esterification was observed by large mass peaks in ESI-MS (appendix). These results show that this method is a poor route to the hafnium (IV) tetra-

carboxyphenyl porpyyrinate complex. Cleavage of the methyl ester substituents to the carboxylic acid of Hf(T-Me-CPP)OAc_2 was deemed a superior method to achieve the Hf(TCPP) complex as outlined below.

Synthesis and Characterization of Hafnium(IV) Porphyrinate derivatives:

Hafnium IV Porphyrinato diacetates:

The acetate derivatives were made for all hafnium porphyrinate complexes in this work as a product of purification. The spectroscopic characterization for the Hf(TPP)OAc_2 complex is consistent with previous literature.[5, 10] The acetate compounds readily serve as a precursor for all other derivatives with other carboxylate ligands, which can be formed in virtually quantitative yields by simple exchange of the acetate ligands. These latter derivatives, characterized spectroscopically, include the octinoate (oct), pentanoate (pen), para amino benzoate (PABA), peroxo-bridged dimers (μ-η^2-O_2), sulfate (SO_4), and phosphate (HPO_4) derivatives.

Hf(TPP)OAc_2 ^{1}H NMR (500 MHz $CDCl_3$) δ ppm 9.04 (s, 8H, pyrrole), 8.38 (br s, 4H, phen-*o*), 8.13 (br. s, 4H phen-*o*), 7.83 (m, 4H, phen-*p*), 7.79 (br. s, 8H phen-*m*), 0.39 (br. s, 6H CH_3) UV-Vis CH_2Cl_2 λ_{max} nm(log ϵ): 393(4.61), 414(5.70), 498(3.52), 540(4.39), 572(3.44) Positive ESI-MS m/*z* Hf(TPP)$OAc_2(H_3O)^{+1}$ calc. 928.3, found 928.2 MALDI-MS dithranol ($C_{14}H_{10}O_3$) m/*z* Hf(TPP)$(C_{14}H_9O_3)^{+1}$ calc. 1017.5, found 1017.1.

Hf(TPP)OAc_x-*reduced by method 4* UV-Vis CH_2Cl_2 λ_{max} nm (relative intensities) 393(0.11), (414(1), 509(0.02), 538(0.34), 579(0.27), 605(0.038), 628(0.14)

H_2TPP-*reduced to chlorin by magnesium.* 20mg of the Hf(TPP)OAc_2complex was dissolved in a 1:1 CH_2Cl_2:CH_3COOH solution. 1 gram of magnesium turnings was added and hydrogen gas evolution was observed. After 30minutes the color of the solution turned purple, then a deep marine blue. The reaction was monitored by U-Vis until no further change was observed. UV-Vis CH_2Cl_2 λ_{max} nm(relative intensities) 373 (0.351), 392(0.28), (414(1), 463(0.032), 535(0.0646), 558(0.043), 603(0.139), 628(0.042) *see ESI-MS in appendix*

Hf(TTP)OAc_2 ^{1}H NMR (500MHz $CDCl_3$) δppm 9.05 (s, 8H, pyrrole), 8.25 (br s, 4H phen-*o*), 8.02 (br s, 4H, phen-*o*), 7.59 (br s, 8H, phen-*m*), 2.75 (s, 12H, Ph-CH_3), 0.22 (6H, OAc-CH_3). UV-Vis CH_2Cl_2 λ_{max} nm(log ϵ): 395(4.63), 416(5.71), 500(3.60), 539(4.43), 574(3.47). MALDI mass spec in dithranol matrix ($C_{14}H_{10}O_3$) found Hf(TTP)$(C_{14}H_9O_3)^{+1}$ 1074, calc. 1073

Hf(TPPF_{20})OAc_2 ^{1}H NMR (500MHz $CDCl_3$) δppm 9.13 (s, 8H, pyrrole), 0.24 (s, 6H OAc-CH_3). UV-Vis nm in CH_2Cl_2 λ_{max} nm (rel. intensities) 387(0.13), 408(1.0), 535(0.051), 572(0.039) MALDI-MS m/*z* Hf(TPPF20)OAc^{+1} calc. 1210, found 1210

Hf(TPyP)OAc_2 ^{1}H NMR (500MHz $CDCl_3$) δppm 9.04(s, 8H, pyrrole), 8.38(br s, 4H, phen-*o*), 8.13(br s,, 4H phen-*o*), 7.83(m, 4H, phen-*p*), 7.79(br s, 8H phen-*m*), 0.39(br s, 6H CH_3). UV-Vis MeOH λ_{max} nm(log ϵ) 3.96(4.60), 416(5.69), 500(2.84), 538(3.37), 570(3.49). Positive ESI-MS m/*z* Hf(TPyP)(HOAc)$(OMe)_2^{+1}$ calc. 918.2 found 918.2 MALDI-MS dithranol ($C_{14}H_{10}O_3$) matrix FW. 226, m/*z* Hf(TPyP)H$(C_{14}H_9O_3)_2^{+1}$ calc. 1246.6 found 1246.2.

Hf(T-Me-CPP)OAc$_2$ ^{1}H NMR (500MHz $CDCl_3$) δppm UV-Vis CH_2Cl_2 λ_{max} nm(log ϵ) 394(4.06), 416(5.12), 500(3.11), 540(3.89), 572(3.04) MALDI-MS dithranol matrix ($C_{14}H_{10}O_3$) m/*z* Hf(T-Me-CPP)($C_{14}H_9O_3)^{+1}$ calc. 1249 found 1250.

Hf[TCPP] 25 mg of the Hf(T-MeCPP)OAc_2 was dissolved in 2 mL of N-methyl pyrrolidone, NMP, and 1 g of pyridinium hydrochloride in a 10 mL screw cap vial. 0.1 mL of distilled water was added and the vial was purged with nitrogen gas. The cap was sealed and the solution was refluxed for three hours to cleave the esters. The vial was allowed to cool to room temperature and the solution was diluted with 8 mL of water, filling the vial. The porphyrin complex precipitated and was centrifuged in the vial. The supernatant contained a trace amount of free base porphyrin. Two additional washes and centrifugations from water followed by acetone effectively removed unwanted porphyrin and reaction solvents. The resulting complex was dried and weighed as 20 mg of Hf(TCPP), 93% yield. The complex does not formally have counter ligands as the carboxylates effectively bind to the hafnium ions of neighboring complexes rendering a coordination polymer that was very difficult to dissolve. The complex dissolves sparingly in DMF and moderately in MeOH, 10% NH_4OH. The UV-Vis in MeOH, 10% NH_4OH, (which may depolymerize the coordination polymer to some extent) λ_{max} nm (relative intensities) 418(1), 538(0.093) MALDI mass spectrum in dithranol matrix ($C_{14}H_{10}O_3$) found Hf(TCPP)($C_{14}H_9O_3)^{+1}$ 1192.25, calc. 1192.48

Hf(TTP)oct$_2$. About 1 mL of the Hf(TTP) reaction mixture from **method 2** was loaded onto a silica column in a Pasteur pipet. A small fraction of unreacted porphyrin was eluted with toluene along with the reaction solvent. The octinoate derivative, Hf(TTP)oct_2 was eluted with 3 mL of 70:25:5 CH_2Cl_2:EtOH:octanoic acid. The solvent

was removed by rotary evaporation, leaving behind only a small amount of octanoic acid. Methanol with 5% distilled H_2O was added wherein the product precipitated, and the solid consolidated by centrifugation. Two additional centrifugations from methanol with 10% distilled H_2O effectively rid the sample of excess octanoic acid. The sample was dried in an oven at 110 °C overnight. UV-Vis CH_2Cl_2 λ_{max} nm(log ϵ) 3.93(4.56), 416(5.69), 499(3.57), 539(4.38), 570(3.49). ^{1}H NMR (500 MHz, $CDCl_3$) δ ppm 0.34 (br s, 6 H, CH_3) 0.47 (t, 4 H, -CH_2) 0.82 (t, 4 H, -CH_2) 0.90 (t, 4 H, -CH_2) 1.03 (t, 4 H, -CH_2) 1.16 (t, 4 H, -CH_2) 2.73 (s, 12 H, phen-CH_3) 3.57 (d, 4 H, -CH_2) 7.67 (br s, 8 H, aryl-*m*) 8.05 (br s, 4 H, aryl-*o*) 8.23 (br s, 4 H, aryl-*o*) 9.03 (s, 8 H, pyrrole)

Hf(TPP)PABA$_2$ 100 mg of PABA was dissolved in10 mL of methanol. 0.5 mL of a 0.5M sodium methoxide solution was added. The resulting solution was combined with 20 mg of Hf(TPP)OAc_2 dissolved in 6 mL of toluene. The mixture was refluxed for ten minutes and the solvent was removed under vacuum. The residue was suspended in 10 mL of distilled H_2O and centrifuged. Two additional washings with 0.05 M KOH aqueous solutions removed most of the excess PABA. This was followed by two washings of distilled H_2O to remove residual KOH. After drying, the Hf(TPP)$PABA_2$ complex was dissolved in CH_2Cl_2 and filtered of any insoluble material. A final purification over silica was made possible by the stability of the complex. The PABA ligands bind well to the hafnium and do not exchange over a short silica column, 5 cm x 10 cm. The pure product was eluted with 1:1 CH_2Cl_2:MeOH. UV-Vis CH_2Cl_2 λ_{max} nm(relative intensities) 394(0.12), 414(1), 496(0.012), 539(0.074), 574(0.0085). See also crystallographic section.

$[Hf(TPP)]_2(\mu\text{-}\eta^2\text{-}O_2)_2$ 7 mg of $Hf(TPP)OAc_2$ was dissolved in 3 mL of $CHCl_3$ with 20% MeOH. One drop of conc. aq. HCl was added (to disassociate the acetate ligands), and 1 mL of methanol was layered over the solution. 0.05 mL of pyridine was added to the top of the methanol layer. The layers were allowed to slowly diffuse and evaporate. After two weeks, X-ray diffraction quality, square crystals of the $[Hf(TPP)]_2(\mu\text{-}\eta^2\text{-}O_2)_2$ complex formed on the walls of the glass. (See crystallographic discussion below).

A sample of the dissolved residue from **Method 2,** before silica purification, was submitted for ESI-MS. The product, most likely the $Hf(TPP)Cl_2$ complex, is hydrolyzed during the ESI-MS experiment to form multiple oxo-bridged species. UV-Vis CH_2Cl_2 λ_{max} nm(relative intensities) 378(0.064), 402(1), 497(0.0067), 535(0.053), 570(0.0052) ESI-MS found $[Hf(TPP)]_2[\mu\text{-}(O)(OH)]^{+1}$ *m/z* 1615, $[Hf(TPP)]_2(\mu\text{-}\eta^2\text{-}O_2)(\ \mu\text{-}OH)^{+1}$ *m/z* 1631, $[Hf(TPP)]_2(\mu\text{-}\eta^2\text{-}O_2)(OMe)]^{+1}$ *m/z* 1645.

The oxo-bridged crystal structure was found with the Hf(TTP) complex as well (see crystallographic discussion). These crystal were obtained unintentionally from a chloroform solution with 4% v/v conc. aq. HCl in attempts to make other derivatives. ESI-MS of the $Hf(TTP)OAc_2$ resulted in the oxo-bridged $[Hf(TTP)]_2[(\mu\text{-}O)H_3O^+$ calc. 1729 found 1729.2 (see appendix)

$[Hf(TTP)]_2[SO_4]_2$ and **$Hf(TPP)[HPO_4]_3^{-2}$** can both be achieved by preloading either $Hf(TPP)Cl_2$ from the dissolved residue of **method 2** (unreacted porphyrin must be eluted first before proceeding) or the pure $Hf(TPP)OAc_2$ complex onto silica. A 2% v/v solution of conc. sulfuric or phosphoric acid in 4:1 CH_2Cl_2:MeOH was passed over the column and the **$[Hf(TTP)]_2[SO_4]_2$** and **$Hf(TPP)[HPO_4]_3^{-2}$** complexes, respectively, were

eluted as one fraction. Again, we are able to purify and exchange the oxo-ligands in one easy step. The solutions are evaporated and suspended in water followed by centrifuge.

$[Hf(TPP)]_2[\mu\text{-}SO_4]_2$ elemental analysis found 2.7% for sulfur, 3.4% calculated for the pure compound, but this compound is known to be in equilibrium with the hydrated complex. UV-Vis. $CHCl_3$ λ_{max} nm(relative intensities) 388(0.078), 411(1), 493(0.0064), 536(0.045), 568(0.0060) ^{1}H NMR (500 MHz, dimethyl sulfoxide-d_6) δ ppm 7.88 (m, 12 H), 8.14 (br s, 4 H), 8.40 (br s, 4 H), 8.97 (s, 8 H, *pyrrole*)

$[Hf(TPP)]_2[HPO_4]_3^{-2}$ UV-Vis CH_2Cl_2 λ_{max} nm(relative intensities) 378(0.073), 410(1), 498(0.0072), 538(0.055), 575(0.0064). We observed a sharp singlet at -9.96 ppm in the ^{31}P NMR (400MHz, chloroform-*d*) with an external aqueous H_3PO_4 standard at 0.0 ppm. The same sample was measured with an internal excess of H_3PO_4 showing a very broad peak centered at -10.06ppm, due to the exchange of phosphates around the hafnium ion, and a free phosphate peak at 0.25ppm. ^{1}H NMR (500 MHz, chloroform-*d*) δ ppm 7.62 (br s, 4 H, *m*) 7.76 (br s, 12 H,) 8.12 (br s, 4 H) 8.74 (br s, 8 H, pyrrole)

Table 6. UV-Vis data for $Hf(P)L_2$ derivatives

Complex	Solvent	Soret[a]	major[b] Q-band	low *E* Q-band
$Hf(TPP)OAc_2$	CH_2Cl_2	414	540	
$Hf(TPP)OAc_2$ reduced	CH_2Cl_2	414	538	628[c]
$Hf(TTP)OAc_2$	CH_2Cl_2	416	539	
$Hf(TPyP)OAc_2$	MeOH	416	538	
$Hf(TPPF_{20})OAc_2$	CH_2Cl_2	408	535[d]	572[d]
$Hf(T\text{-}Me\text{-}CPP)OAc_2$	CH_2Cl_2	416	540	
Hf(TCPP)	MeOH, 10% NH_4OH	418	538	
$Hf(TPP)PABA_2$	CH_2Cl_2	414	539	
$Hf(TTP)oct_2$	CH_2Cl_2	416	539	
$[Hf(TPP)]_2[\mu\text{-}\eta^2\text{-}(O_2)]_2$	CH_2Cl_2	402	535	
$[Hf(TTP)]_2[SO_4]_2$	$CHCl_3$	411	536	
$Hf(TPP)]_2[HPO_4]_3^{-2}$	CH_2Cl_2	410	538	

[a]additional absorption band found as high energy shoulder of the Soret
[b]additional Q-bands are found as low and high energy shoulders of the major Q-band
[c]Low energy absorbance of reduced Hf(P) complexes are of greater intensity than the Q-band near 540
[d]Hf(TPPF20) Q-bands are of similar intensity

Conclusions:

The methods we have developed has expanded the range of tetra- aryl porphyrinates that can be metalated with the Hf(IV) ion compared to the precedent literature. The piano-stool type geometry of these complexes allow a great variety of oxygen bearing ligands that can be easily exchanged by elution form silica using the corresponding acids. The fluorescence of the deriviatvies reported are very similar indicating a negligible effect of the counter ions on the fluorescence of the hafnium porphyrin unit. Crystallographic studies reveal the diverse geometries, including dimeric structures, that these complexes are capable of, and possess great potential for future supramolecular architectures.

References

1. Spek, A. L., *J. Appl. Crystallogr* **2003,** 36, 7-13.

2. Ryu, S.; Whang, D.; Kim, J.; Yeo, W.; Kim, K., *J. Chem. Soc., Dalton Trans.* **1993**, 205-209.

3. Ryu, S.; Kim, J.; Yeo, H.; Kim, K., *Inorg. Chim. Acta* **1995,** 228, (12), 233-236.

4. Afzal, D.; Baughman, R.; James, A.; Westmeyer, M., *Supramol. Chem.* **1996,** 6, (3-4), 395-399.

5. Huhmann, J. L.; Rath, N. P.; Corey, J. Y., *Acta Crystallogr., Sect. C: Cryst. Struct. Commun.* **1996,** 52, (10), 2486-2488.

6. Knor, G.; Strasser, A., *Inorg. Chem. Commun.* **2002,** 5, (11), 993-995.

7. Tipugina, M. Y.; Lomova, T. N., *Russ. J. Inorg. Chem.* **2004,** 49, (6), 961-965.

8. Martin, P. C.; Amold, J.; Bocian, D. F., *J. Phys. Chem.* **1993,** 97, 1332-1338.

9. Brand, H.; Capriotti, J. A.; Arnold, J., *Organometallics* **1994,** 13, (11), 4469-4473.

10. Huhmann, L. J.; Corey, J. Y.; Rath, N. P.; Campana, C. F., *J. Organomet. Chem.* **1996,** 513, (1-2), 17-26.

11. Ryu, S.; Whang, D.; Kim, H. J.; Kim, K.; Yoshida, M.; Hashimoto, K.; Tatsumi, K., *Inorg. Chem.* **1997,** 36, (20), 4607-4609.

12. Thorman, J. L.; Guzei, I. A.; Jr, V. G. Y.; Woo, L. K., *Inorg. Chem.* **1999,** 38, (17), 3814-3824.

13. Thorman, J. L.; Guzei, I. A., *Inorg. Chem.* **2000,** 2344-2352, (11), 23.

14. Tomachynski, L. A.; Chernii, V. Y.; Volkov, S. V., *J. Porphyrins Phthalocyanines* **2001,** 5, (10), 731-734.

15. Tomachynski, L. A.; Chernii, V. Y.; Volkov, S. V., *Russ. J. Inorg. Chem.* **2002,** 47, (2), 208-211.

16. Gerasymchuk, Y. S.; Chernii, V. Y.; Tomachynski, L. A.; Legendziewicz, J.; Radzki, S., *Opt. Mater.* **2005,** 27, (9), 1484-1494.

17. Knor, G.; Strasser, A., *Inorg. Chem. Commun.* **2005,** 8, (5), 471-473.

18. Brand, H.; Arnold, J., *Organometallics* **1993,** 12, (9), 3655-3665.

19. Brand, H.; Arnold, J., *J. Am. Chem. Soc.* **1992,** 114, (6), 2266-2267.

20. Shibata, K.; Aida, T.; Inoue, S., *Tetrahedron Lett.* **1992,** 33, (8), 1077-1080.

21. Kim, H. J.; Whang, D.; Kim, K.; Do, Y., *Inorg. Chem.* **1993,** 32, (3), 360-362.

22. Kim, H.-J.; Whang, D.; Do, Y.; Kim, a. K., *Chem. Lett.* **1993,** 22, (5), 807-810.

23. Buchler, J. W.; Heinz, G., *Chem. Ber.* **1996,** 129, (2), 201-205.

24. Collman, J. P.; Kendall, J. L.; Chen, J. L.; Eberspacher, T. A.; Moylan, C. R., *Inorg. Chem.* **1997,** 36, (24), 5603-5608.

25. Fryzuk, M. D.; B.Love, J.; Rettig, S. J., *Organometallics* **1998,** 17, (5), 846-853.

26. Kim, H. J.; Jung, S.; Jeon, Y. M.; Whang, D.; Kim, K., *Chem. Commun.* **1999**, (11), 1033-1034.

27. Stulz, E.; Burgi, H. B.; Leumann, C., *Chem.-Eur. J.* **2000,** 6, (3), 523-536.

28. Witowska-Jarosz, J.; Gorski, L.; Malinowska, E.; Jarosz, M., *J. Mass Spectrom.* **2002,** 37, (12), 1236-1241.

29. Pistorio, B. J.; Nocera, D. G., *J. Photochem. Photobiol., A* **2004,** 162, (2-3), 563-567.

30. Du, G.; Woo, L. K., *Organometallics* **2003,** 22, (3), 450-455.

31. Collman, J. P.; Kendall, J. L.; Chen, J. L., *Inorg. Chem.* **2000,** 39, (8), 1661-1667.

32. Guilard, R.; Barbe, J.-M.; Ibnlfassi, A.; Zrineh, A.; Adamian, V. A.; Kadish, K. M., *Inorg. Chem.* **1995,** 34, (6), 1472-1481.

33. Girolami, G. S.; Milam, S. N.; Suslick, K. S., *Inorg. Chem.* **1987,** 26, (3), 343-344.

34. Bernstein, P. A.; Lever, A. B. P., *Inorg. Chem.* **1990,** 29, (4), 608-616.

35. Johnson, T. J.; Disselkamp, R. S.; Su, Y.-F.; Fellows, R. J.; Alexander, M. L.; Driver, C. J., *J. Phys. Chem. A* **2003,** 107, (32), 6138-6190.

36. Ryu, S.; Kim, J.; Yeo, H.; Kim, K., *Inorg. Chim. Acta* **1995,** 228, (2), 233-236.

37. Arnold, J.; Hoffman, C. G.; Dawson, D. Y.; Hollander, F. J., *Organometallics* **1993,** 12, 3645-3654.

38. Gomila, R. M.; Quinonero, D.; Rotger, C.; Garau, C.; Frontera, A.; Ballester, P.; Costa, A.; Deya, P. M., *Org. Lett.* **2002,** 4, (3), 399-401.

39. Ojadi, E.; Selzer, R.; Linschitz, H., *J. Am. Chem. Soc.* **1985,** 107, 7783-7784.

40. Buchler, J. W.; Schneehage, Z., *Naturforsch* **1973,** B28, 433.

41. Ghiladi, R. A.; Ju, T. D.; Lee, D.-H.; Moenne-Loccoz, P.; Kaderli, S.; Neuhold, Y.-M.; Zuberbuhler, A. D.; Woods, A. S.; Cotter, R. J.; Karlin, K. D., *J. Am. Chem. Soc.* **1999,** 121, (42), 9885-9886.

42. Drain, C. M.; Gentemann, S.; Roberts, J. A.; Nelson, N. Y.; Medforth, C. J.; Jia, S.; Simpson, M. C.; Smith, K. M.; Fajer, J.; Shelnutt, J. A.; Holten, D., *J. Am. Chem. Soc.* **1998,** 120, (15), 3781-3791.

43. Retsek, J. L.; Drain, C. M.; Kirmaier, C.; Nurco, D. J.; Medforth, C. J.; Smith, K. M.; Sazanovich, I. V.; Chirvony, V. S.; Fajer, J.; Holten., D., *J. Am. Chem. Soc.* **2003,** 125, 9787-9800.

44. Wilkinson, C. a., *Advanced Inorganic Chemistry*. John Wiley & Sons: 1999.

45. Bym, M. P.; Curtis, C. J.; Hsiou, Y.; Khan, S. a. d. I.; Sawin, P. A.; Tendick, S. K.; Terzis, A.; Strouse, C. E., *J. Am. Chem. Soc.* **1993,** 115, 9480-9497.

46. Engdahl, A.; Nelander, B., *Phys. Chem. Chem. Phys.* **2000,** 2, 3967-3970.

Hafnium porphyrinate appendix

Contents:

Methods

All UV-Visible were taken in 1 cm quartz or glass cuvettes unless otherwise indicated, on a Carey Bio 3 spectrophotometer. Mass spectrometry was done as a service by the University of Illinois, Urbana-Champaign or on an Agilent 1100 LC/MSD instrument. NMR were run on a 500 MHz Varian Inova. Fluorescence spectra were taken on a Spex Tau-3 fluorometer in 1 cm quartz cuvettes. Gasses, reagents, and solvents were used as received unless otherwise noted. Porphyrins were obtained from Aldrich or from Frontier Scientific.

Figure 1.

$Hf(TPP)OAc_2$ 50 µmol in CH_2Cl_2 1mm glass cuvette

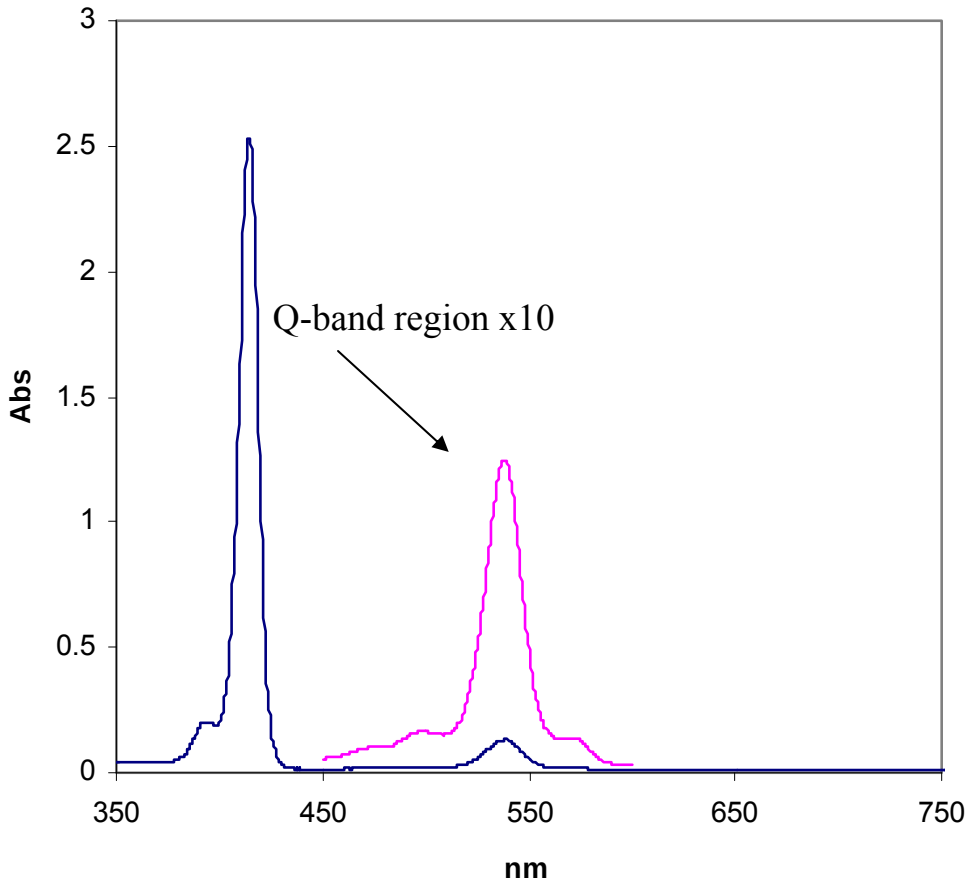

Figure 2a.

$Hf(TPP)OAc_2$ ^1H-NMR aromatic region in $CDCl_3$

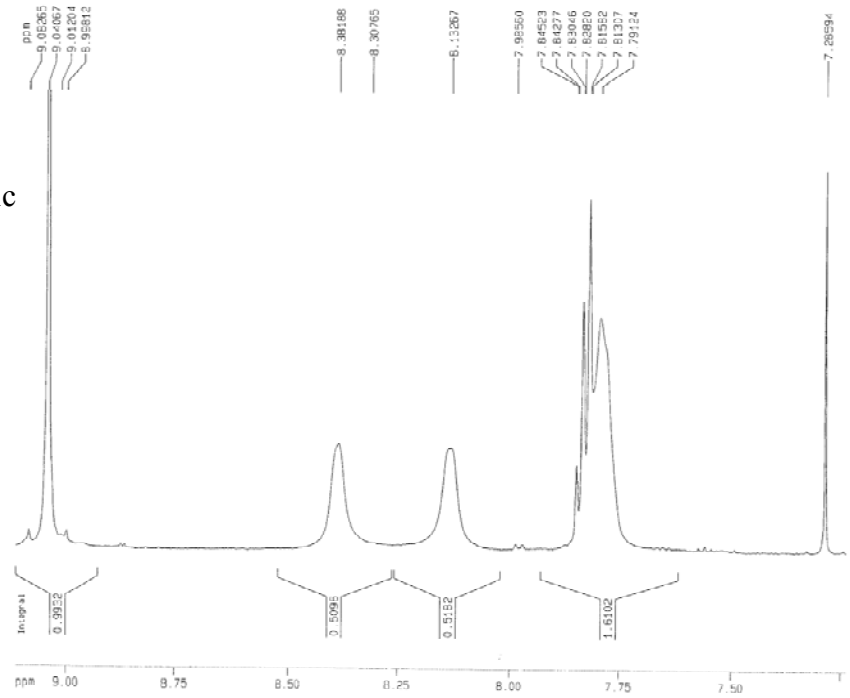

Figure 2b.

$Hf(TPP)OAc_2$ ^1H-NMR full spectrum in CDCl3

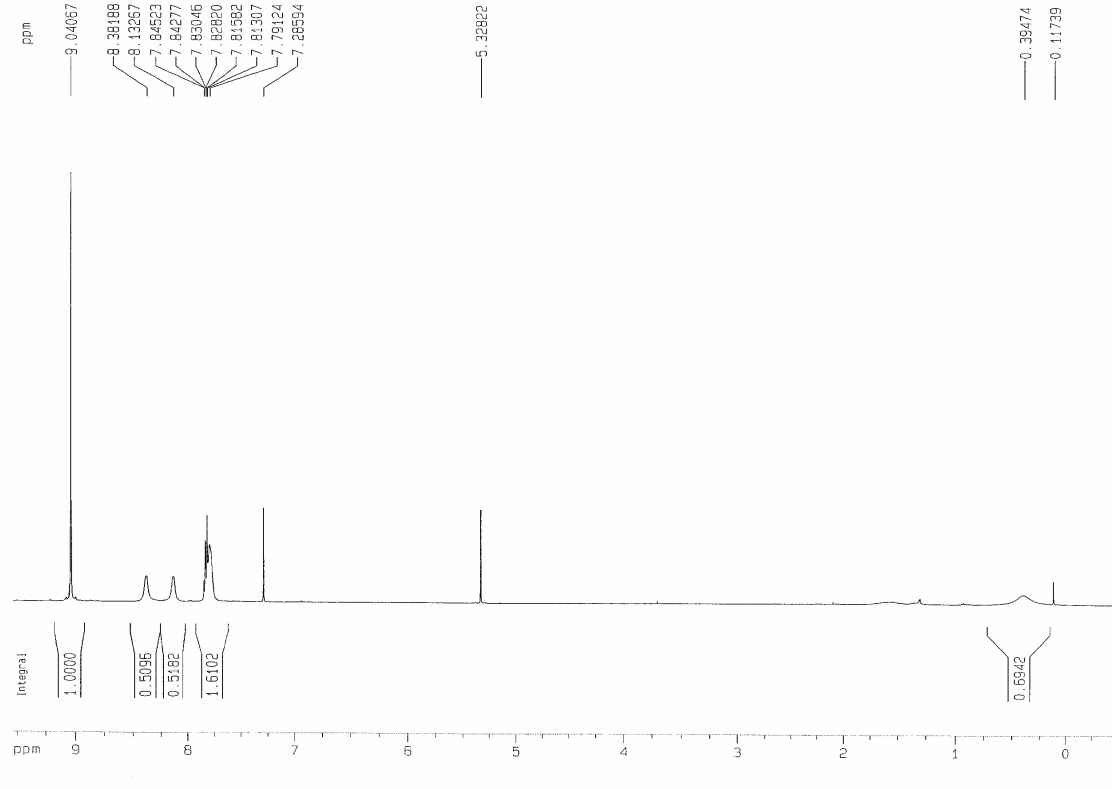

Figure 3.

$Hf(TPP)OAc_2$ COSY NMR

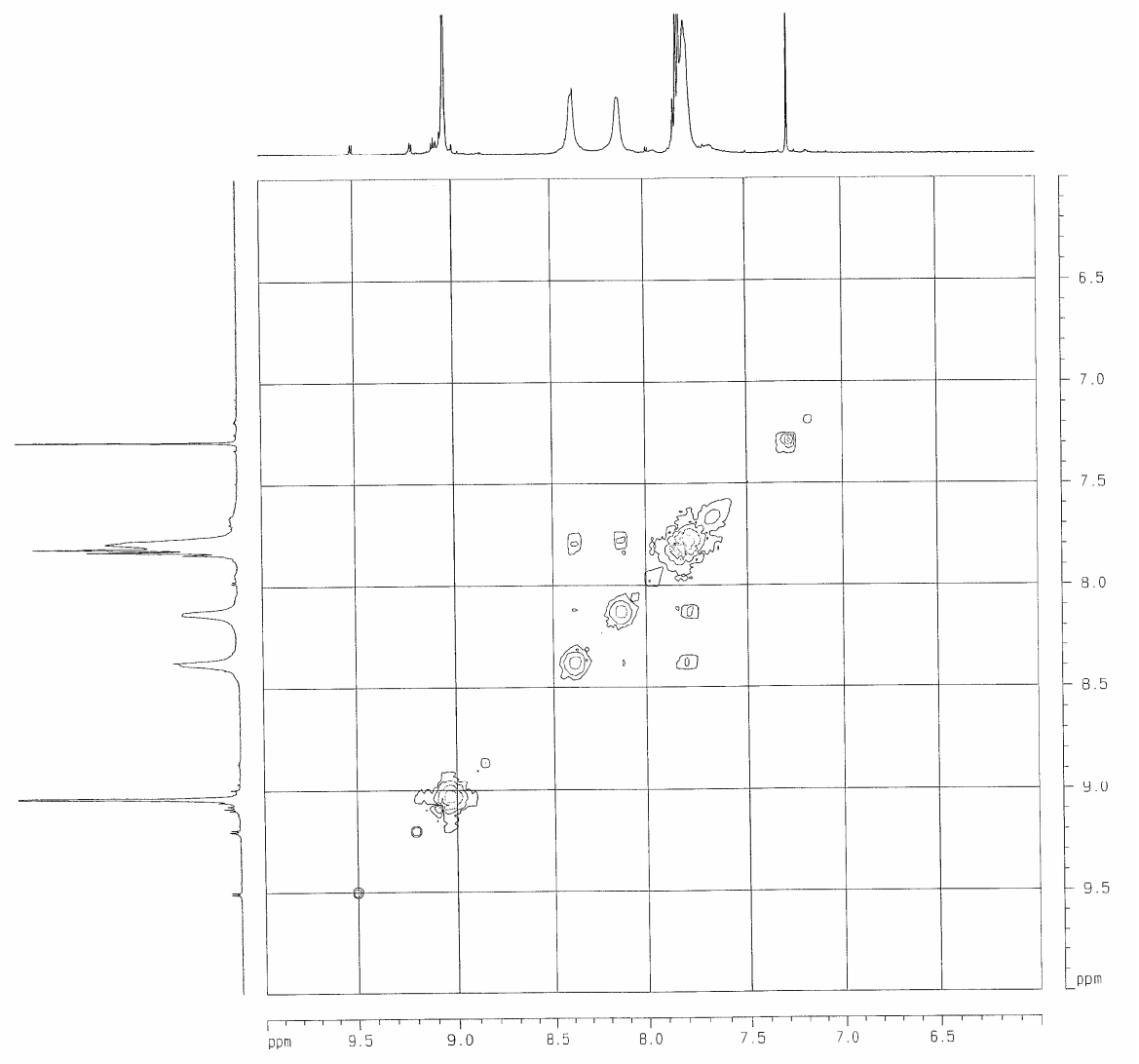

Figure 4. Hf(TPP)OAc_2 MALDI mass spectrum

Hf(TPP)OAc_2 MALDI, dithranol matrix FW 226
Hf(TPP)dithranate^{+1} FW 1017

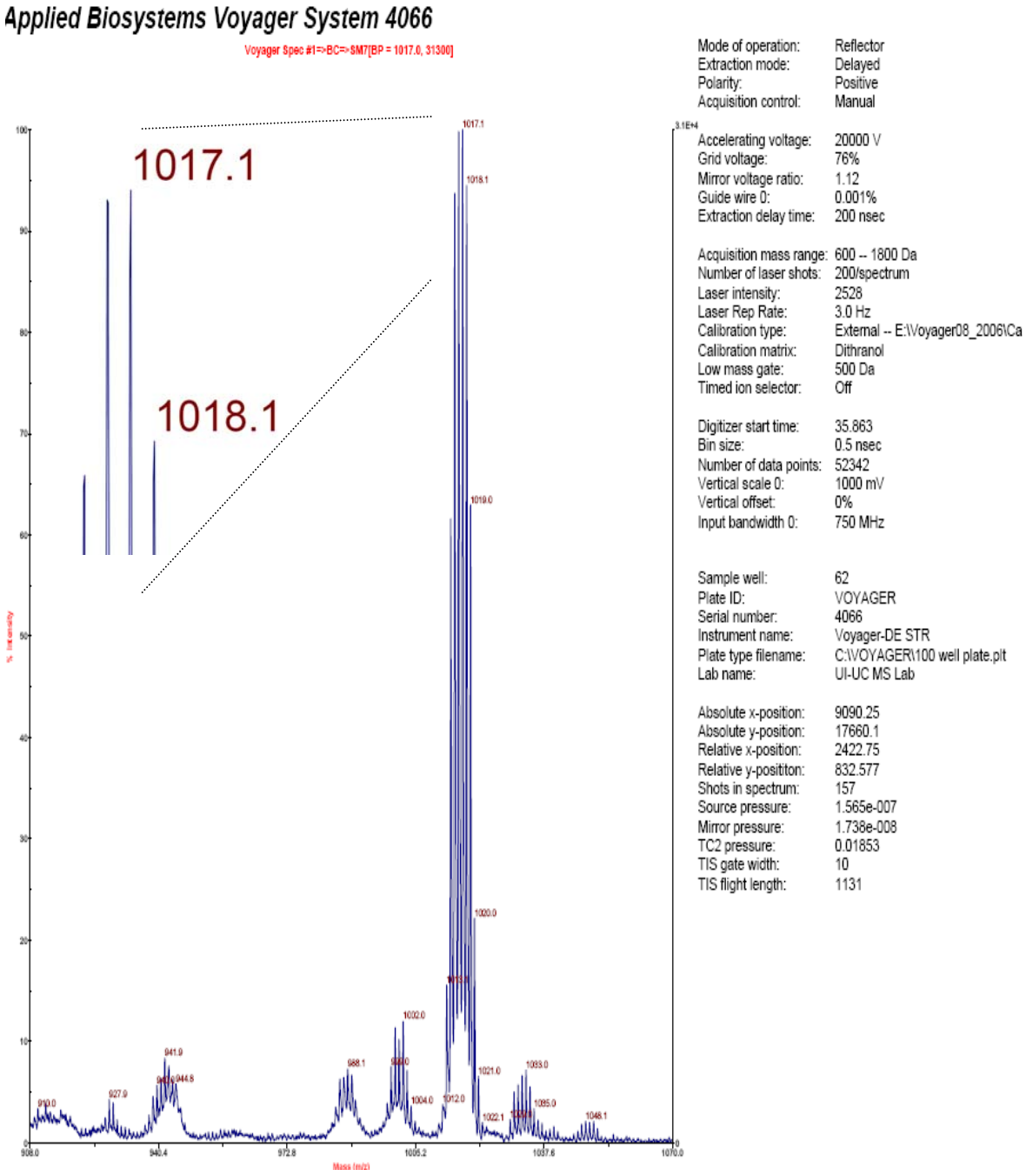

Figure 5. ESI-MS of $Hf(TPP)OAc_2$ positive ion mode

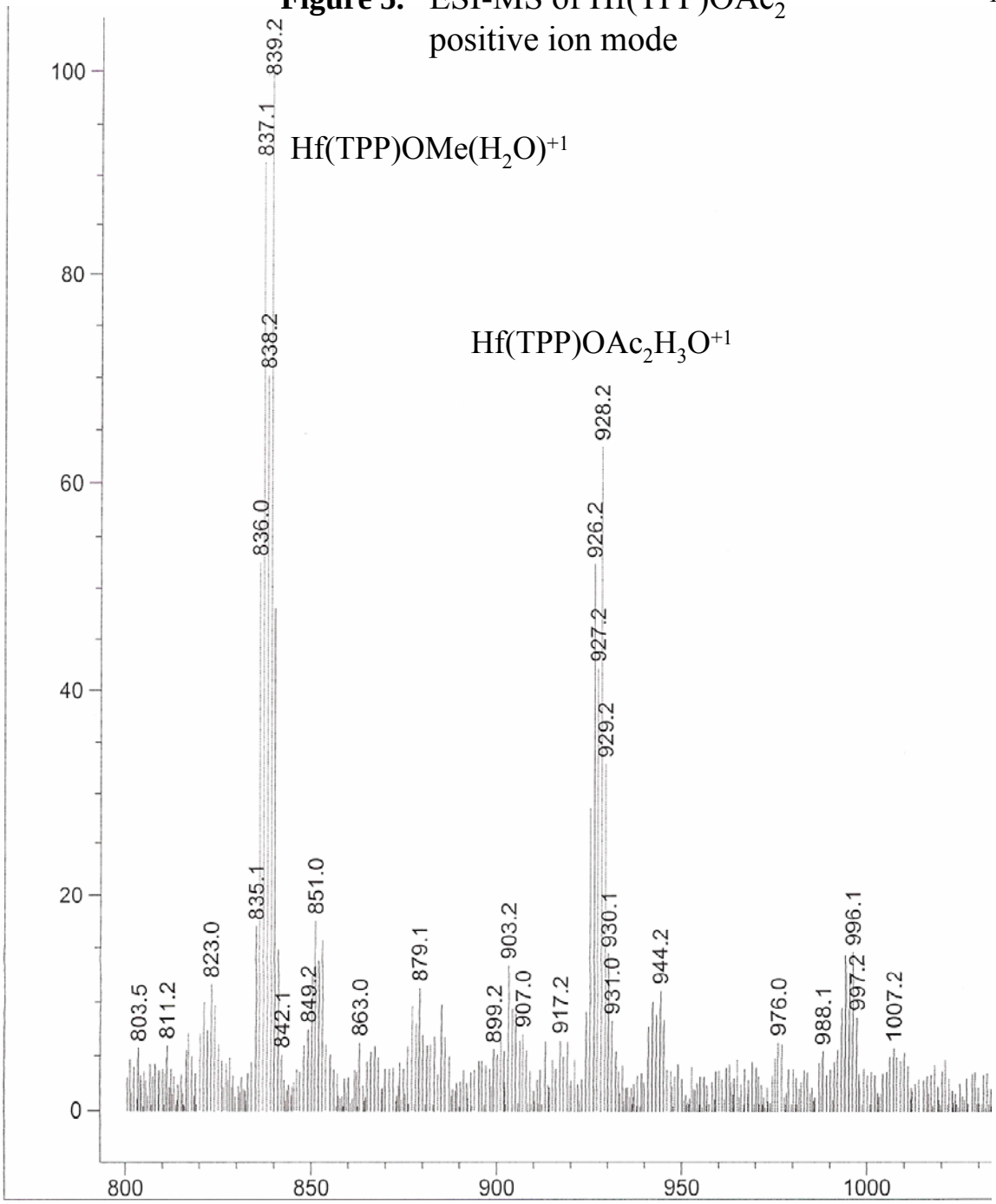

Figure 6a. Hf(TPP)OAc_2 emission spectrum

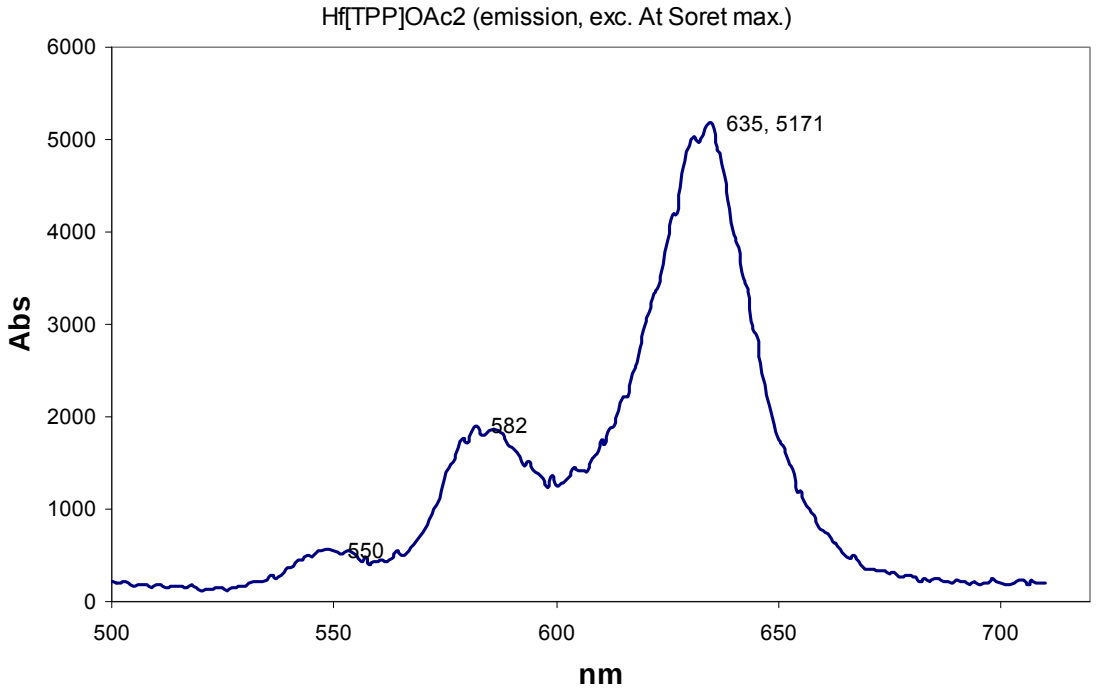

Figure 6b Hf(TPP)OAc_2 excitation spectrum

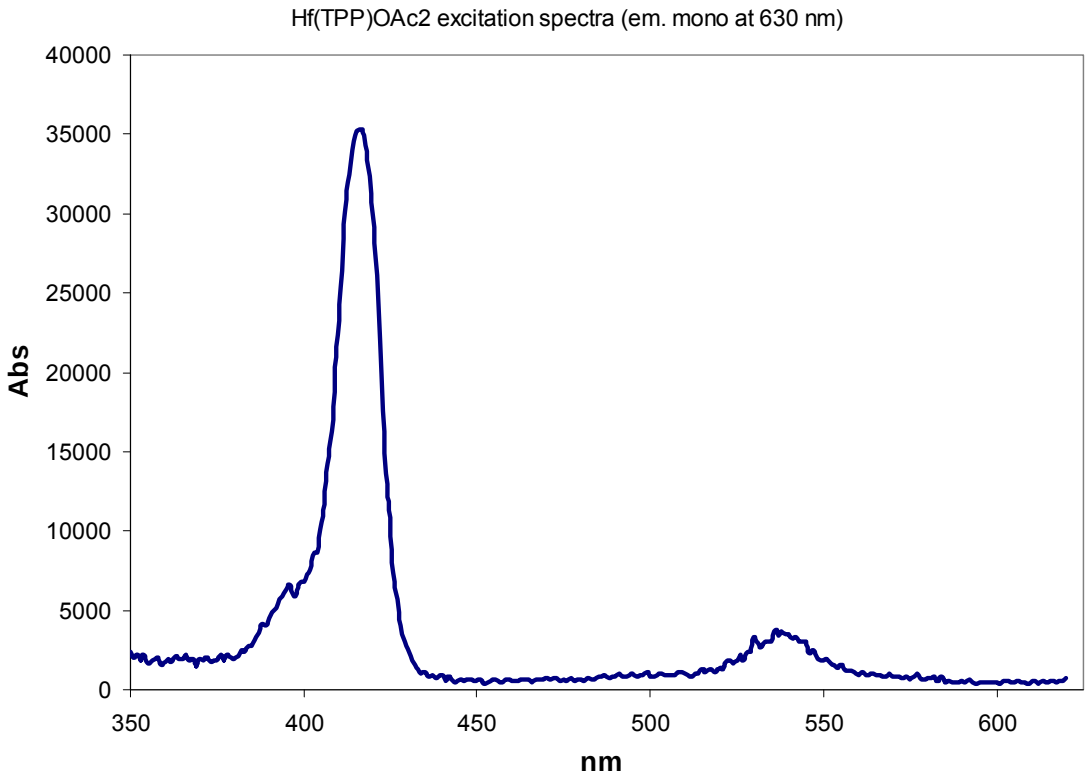

Figure 7.

Hf(TPP)OAc_2 reduced-chlorin from **method 4** UV-Vis spectrum

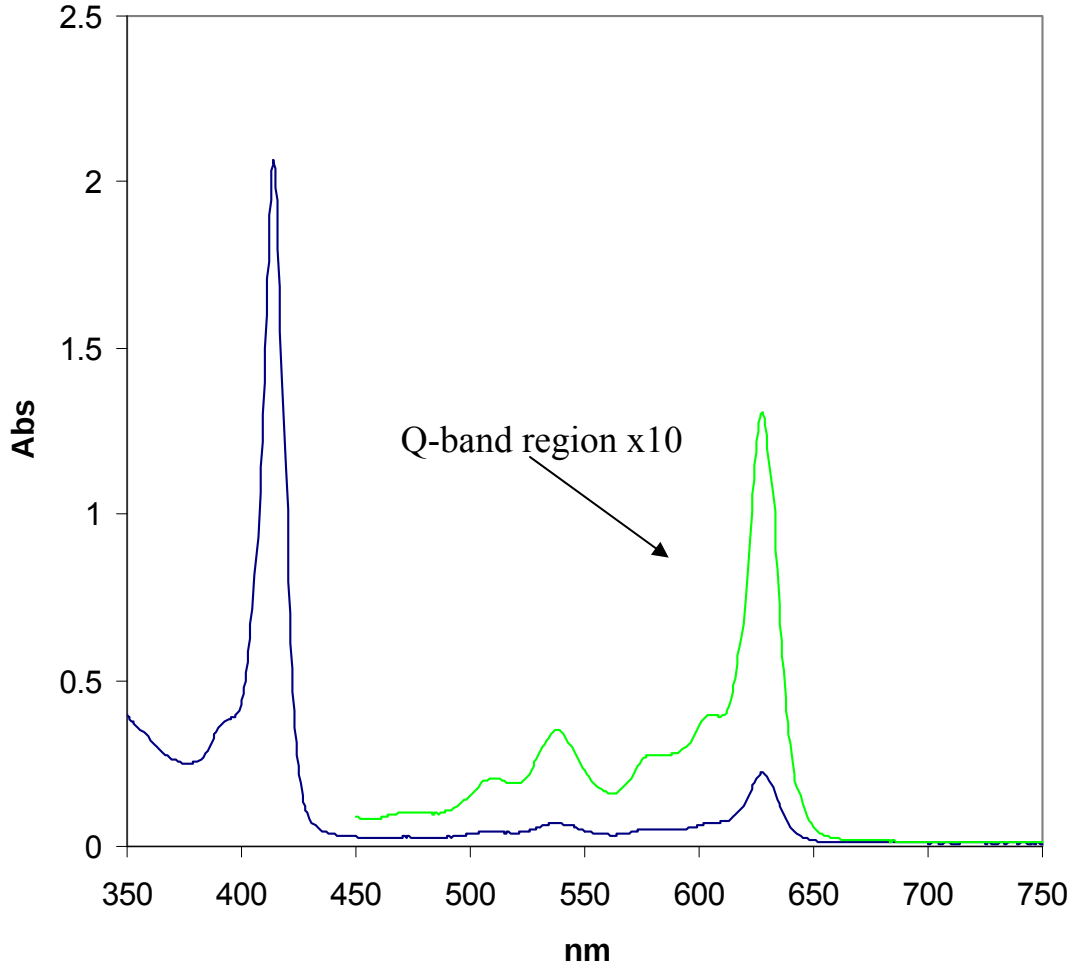

Figure 8a. $Hf(TPP)OAc_2$ reduced-chlorin from **method 4** ^1H- NMR spectrum; aromatic region in CDCl3

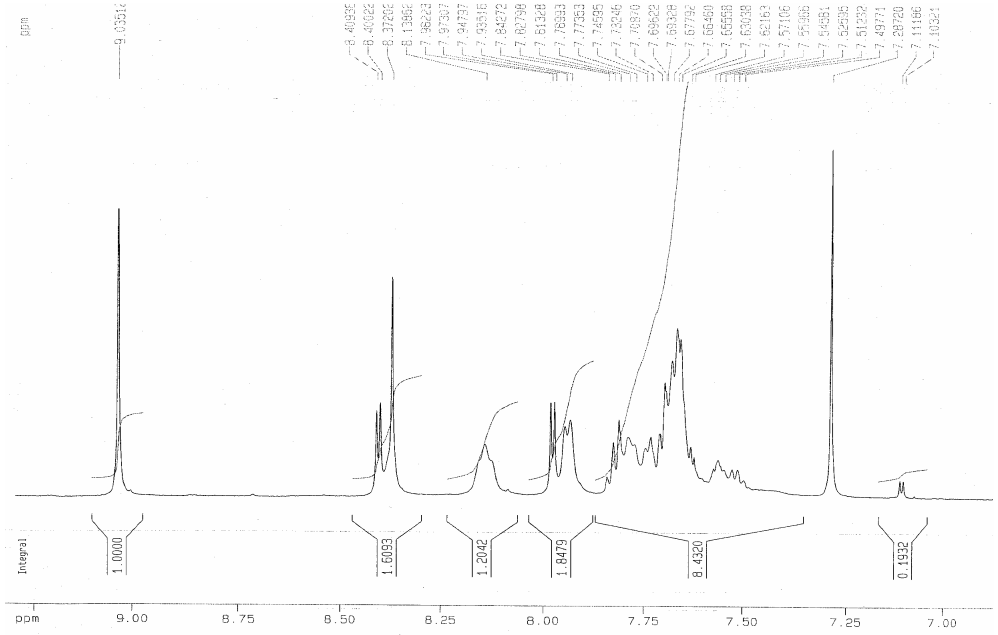

Figure 8b. $Hf(TPP)OAc_2$ reduced-chlorin from **method 4** ^1H- NMR spectrum; full spectrum in CDCl3

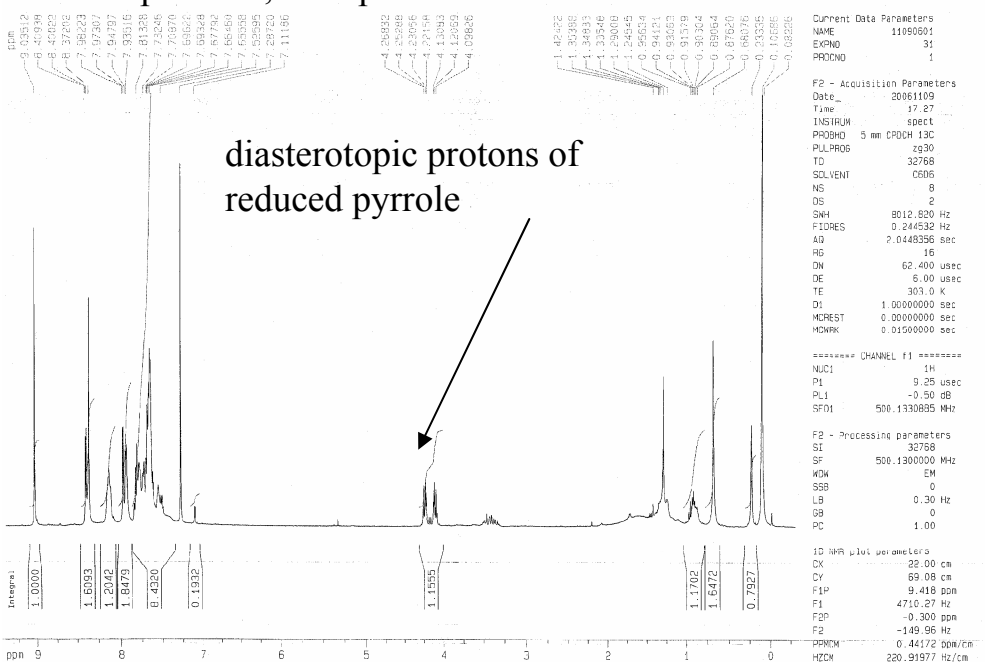

Figure 9.

Hf(TPP)OAc_2 reduced-chlorin from **method 4** COSY spectrum

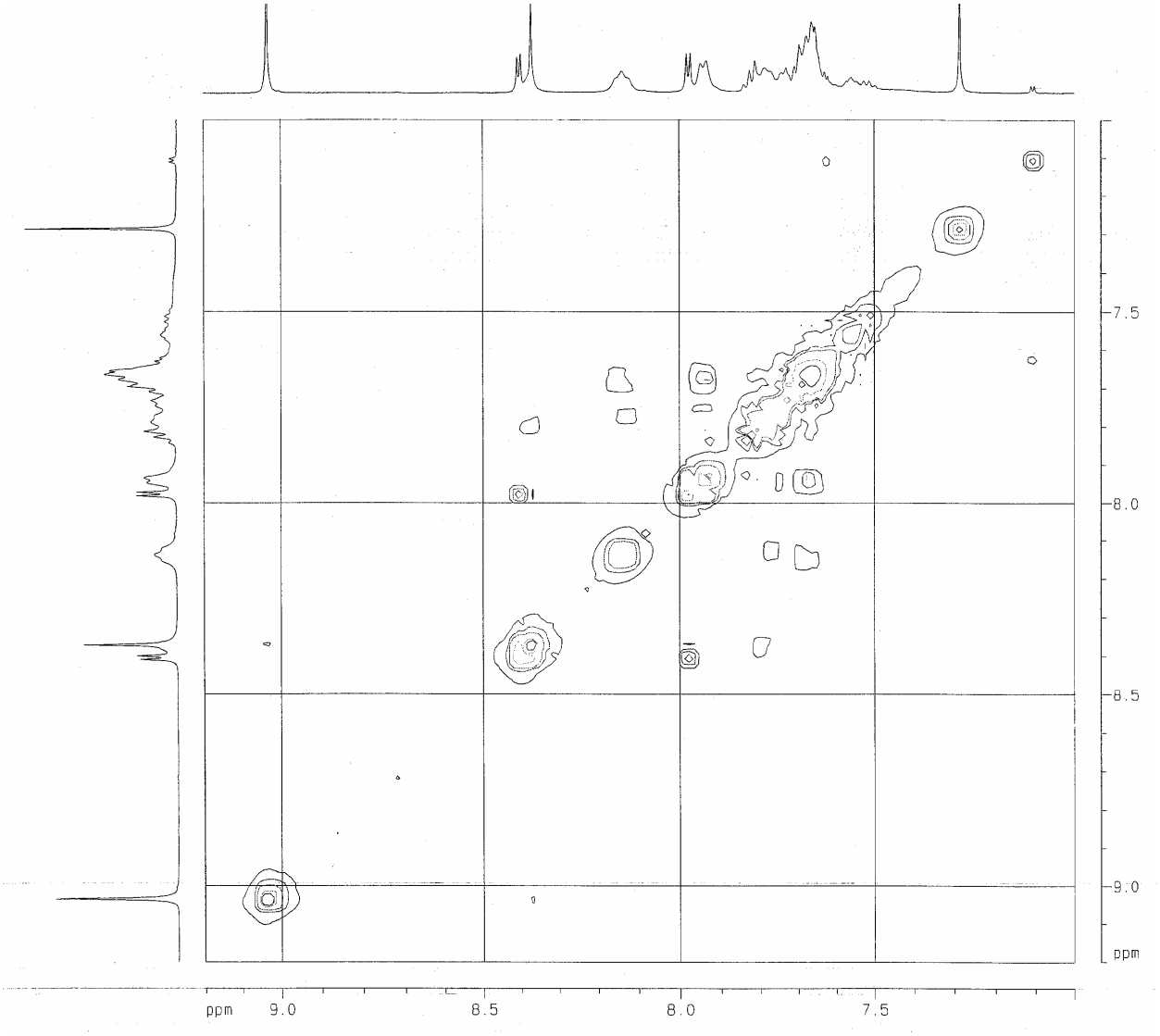

Figure 10. Positive ESI-MS of chlorin formed by Mg/HOAc

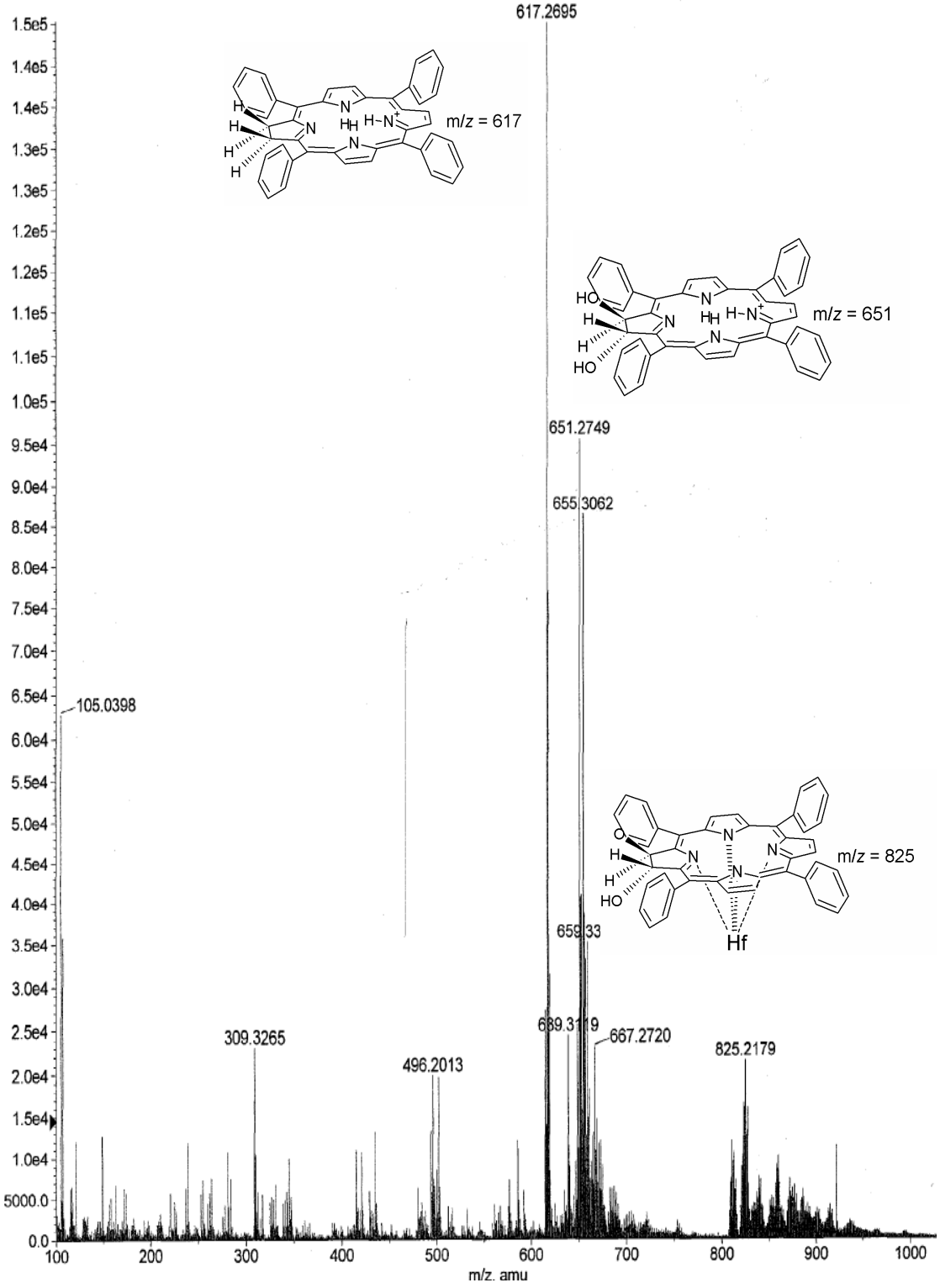

Figure 11.

Mg/HOAc reduction of Hf(TPP)OAc_2 UV-Vis spectrum in CH_2Cl_2 displays a mixture of chlorins

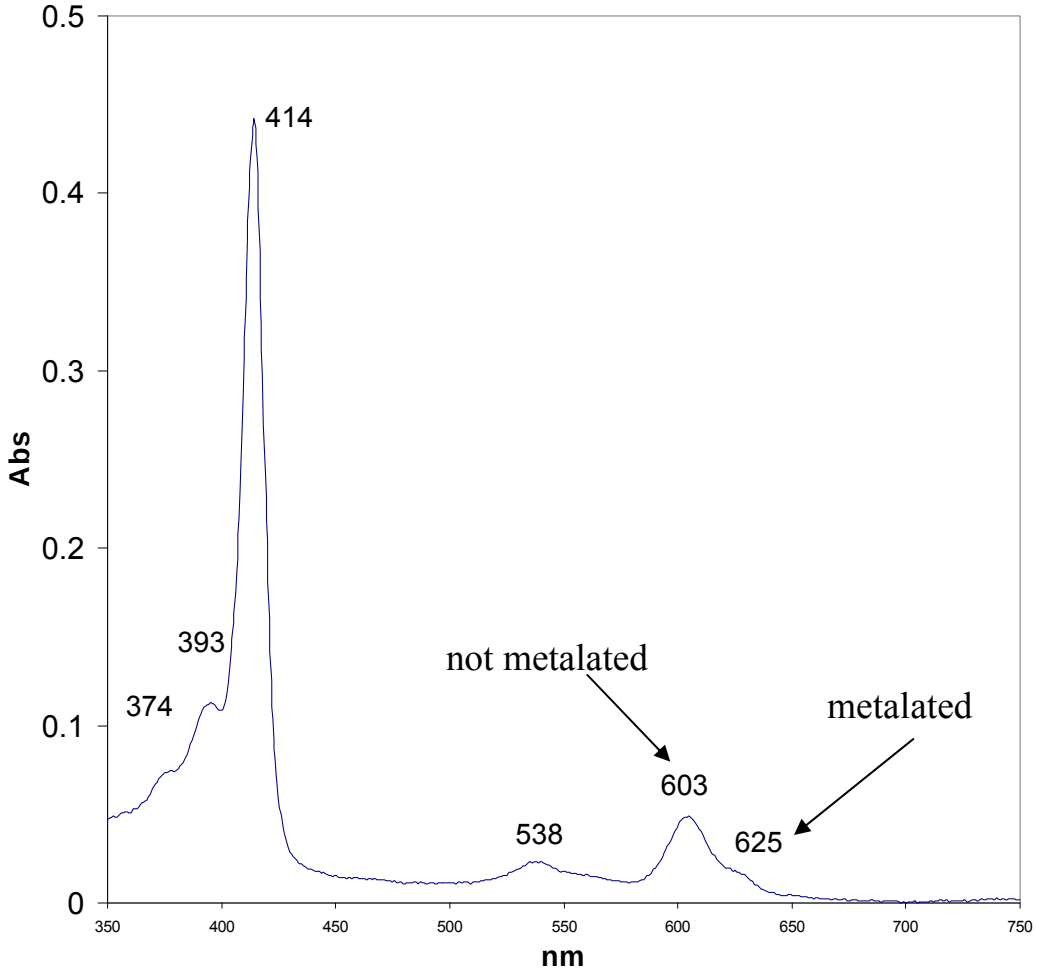

Figure 12. Hf(TPP)$PABA_2$ UV-Vis

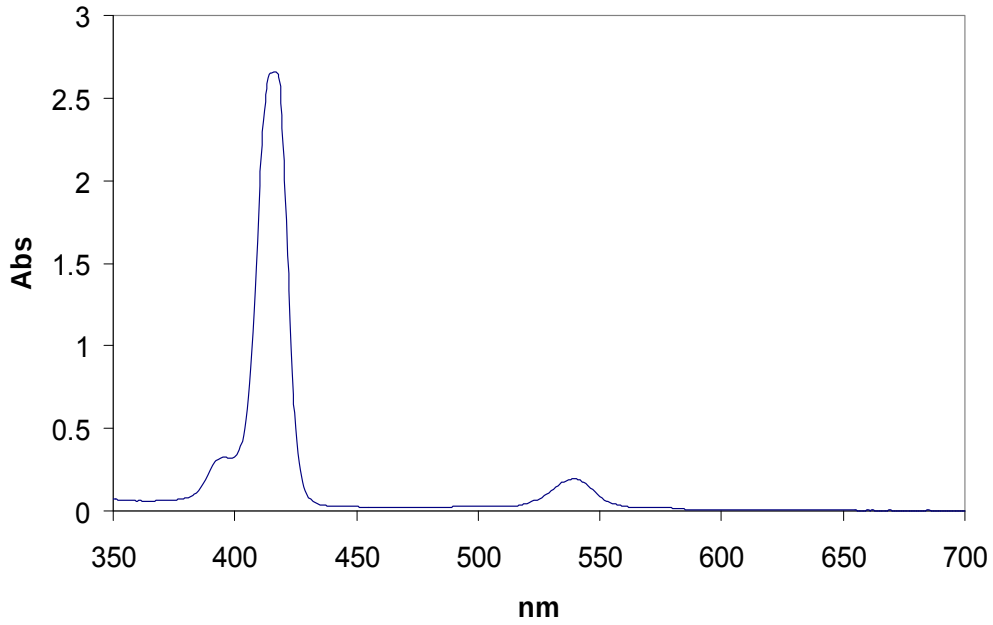

Figure 13. $[Hf(TPP)]_2(\mu\text{-}\eta^2\text{-}O_2)_2$ UV-Vis

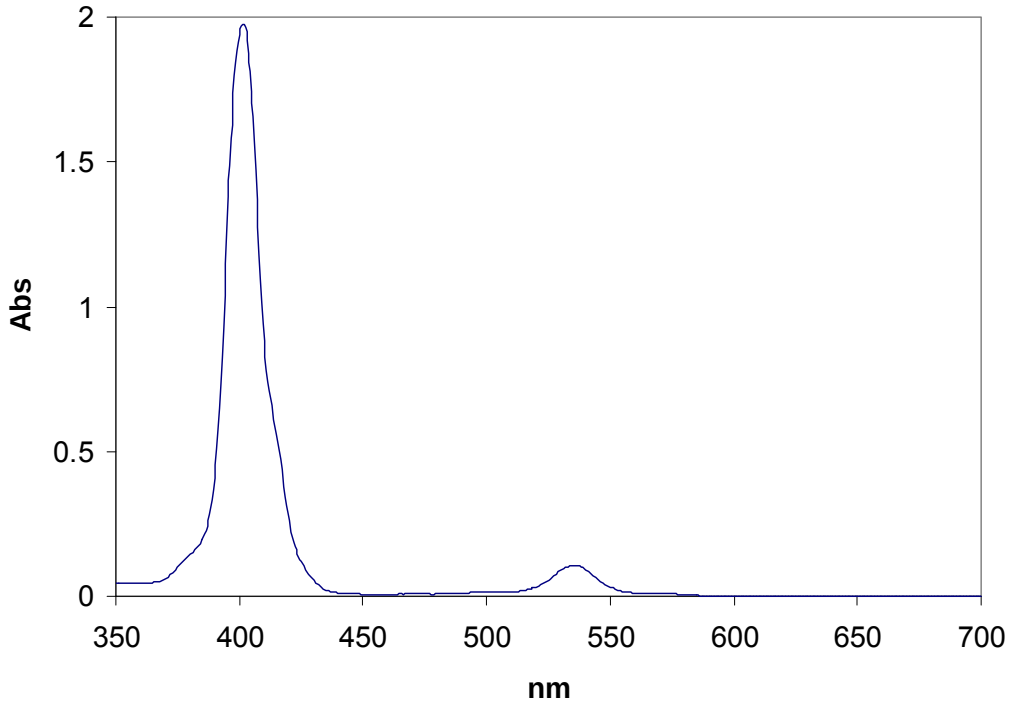

Figure 14. $[Hf(TPP)]_2(\mu\text{-}\eta^2\text{-}O_2)_2$ ESI-MS positive ion mode

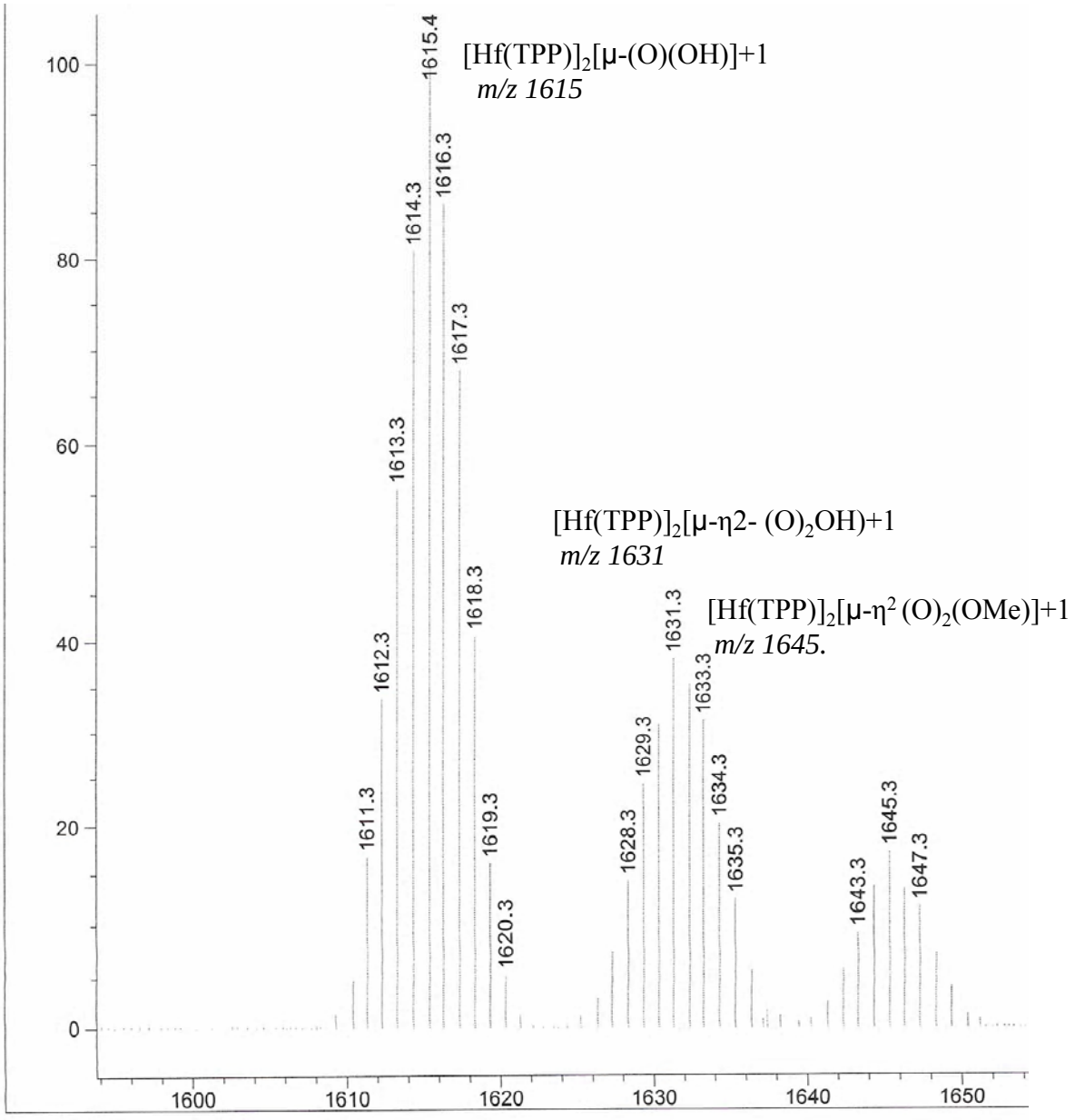

Figure 15a. crystal structure of $[Hf(TPP)]_2(\mu\text{-}\eta_2\text{-}O_2)_2$

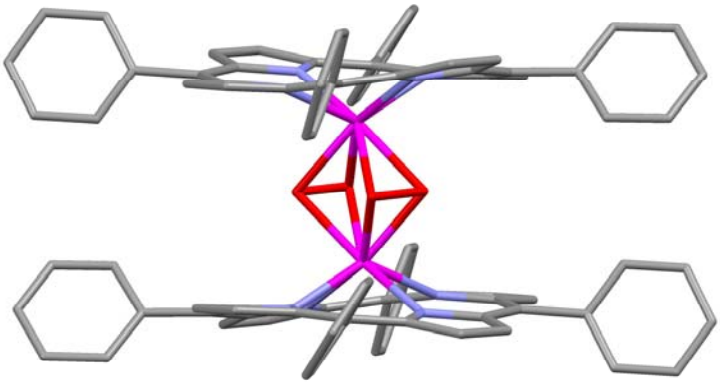

Figure 15b. crystal packing of $[Hf(TPP)]_2(\mu\text{-}\eta_2\text{-}O_2)_2$

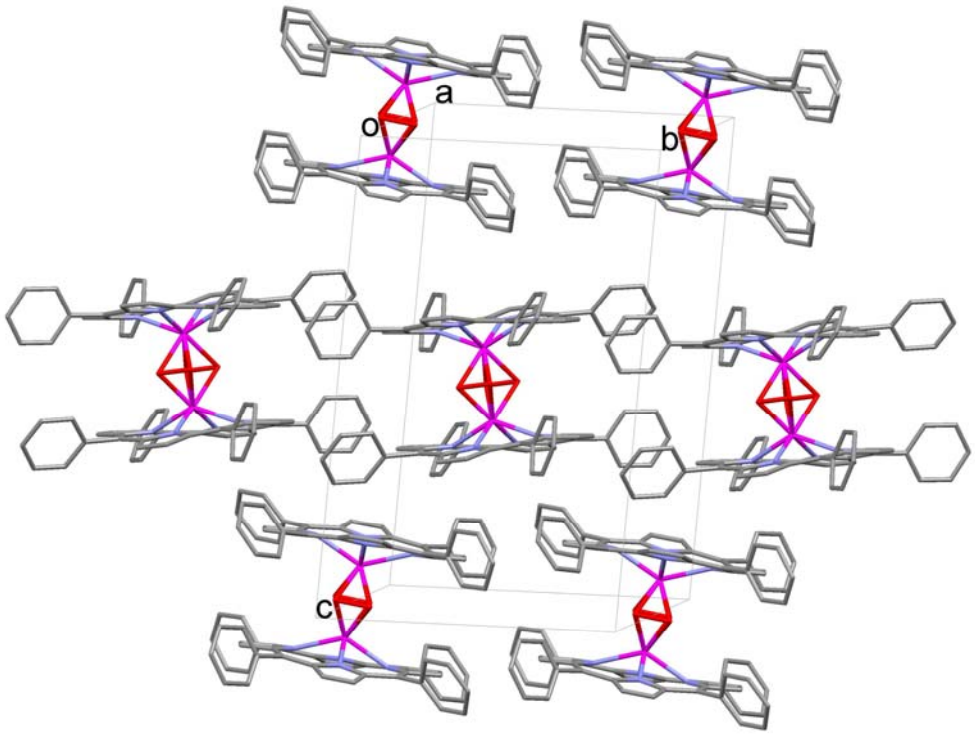

Figure 16.

$[Hf(TPP)]_2(SO_4)_2$ UV-Vis in CH_2Cl_2

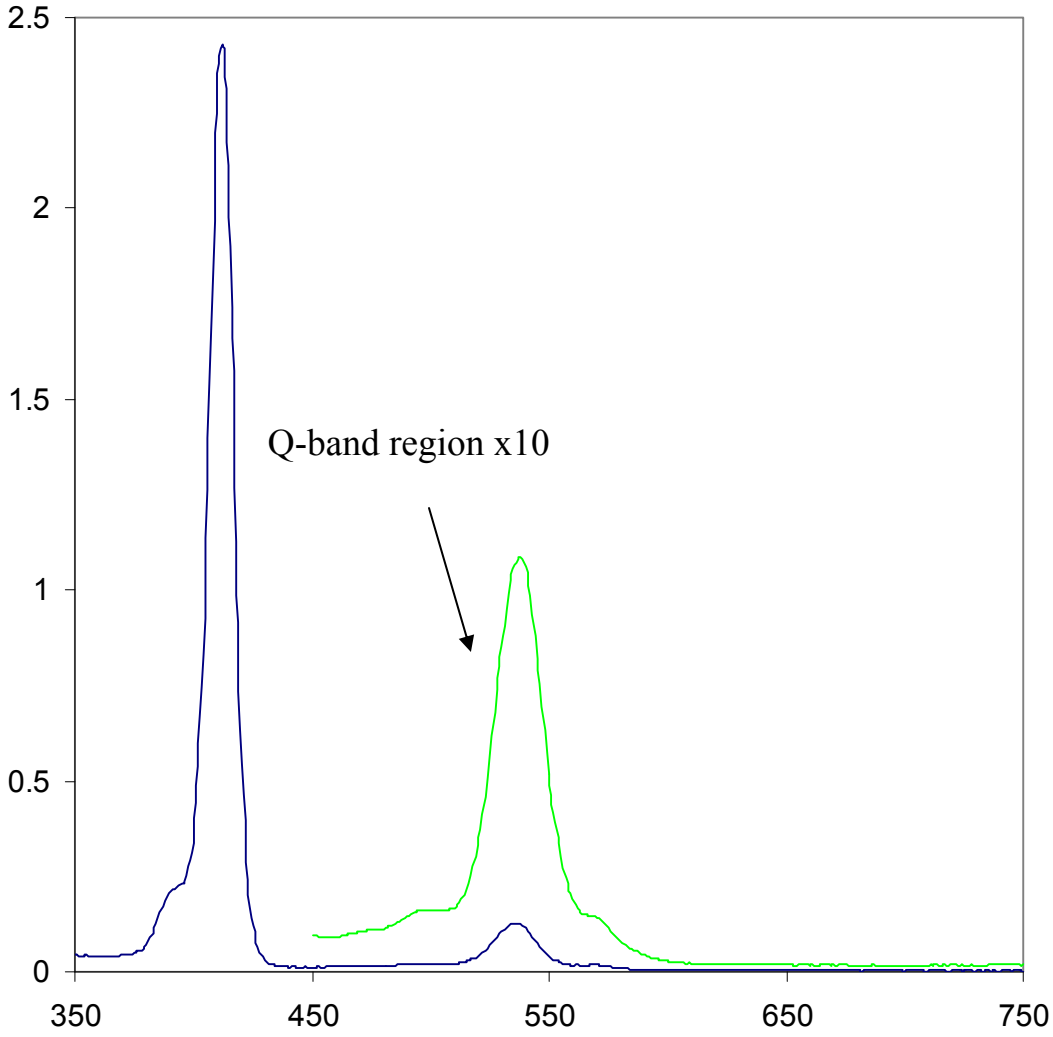

Figure 17a.

$[Hf(TPP)]_2(SO_4)_2$ ^1H NMR full spectrum in DMSO-d_6

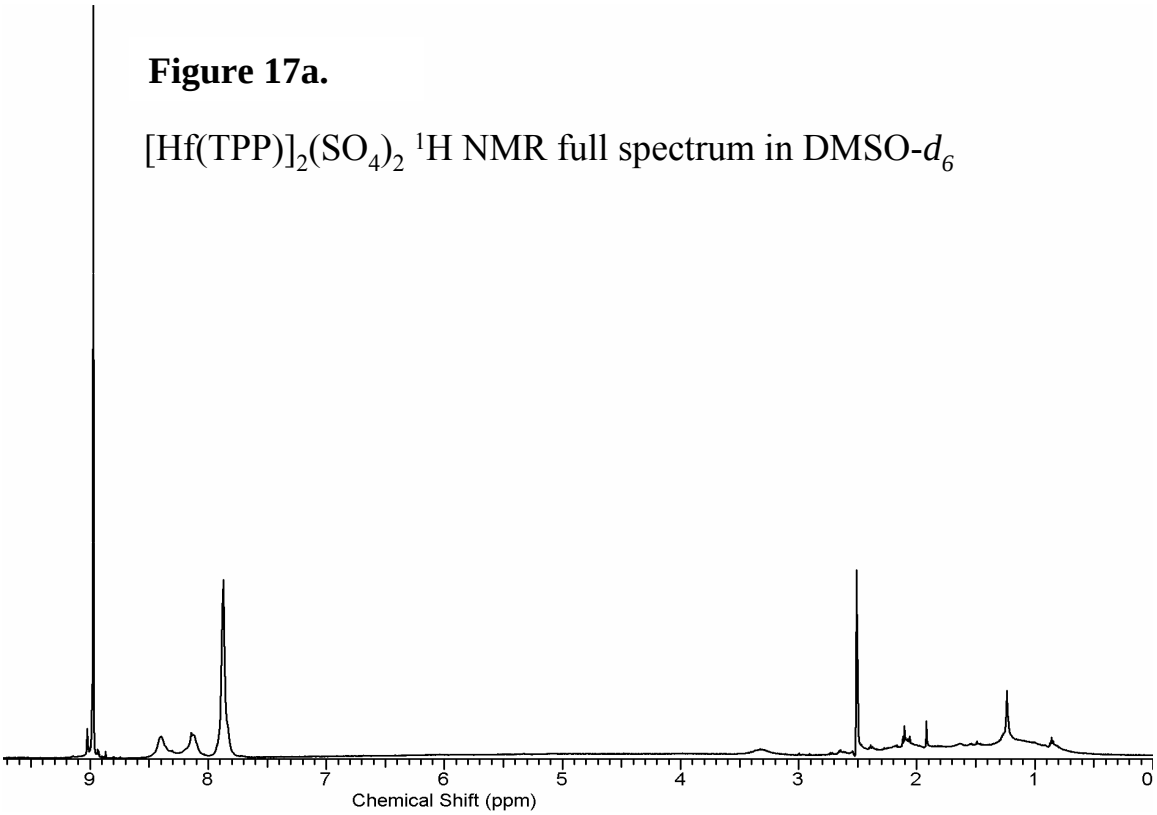

Figure 17b.

$[Hf(TPP)]_2(SO_4)_2$ ^1H NMR aromatic region in DMSO-d_6

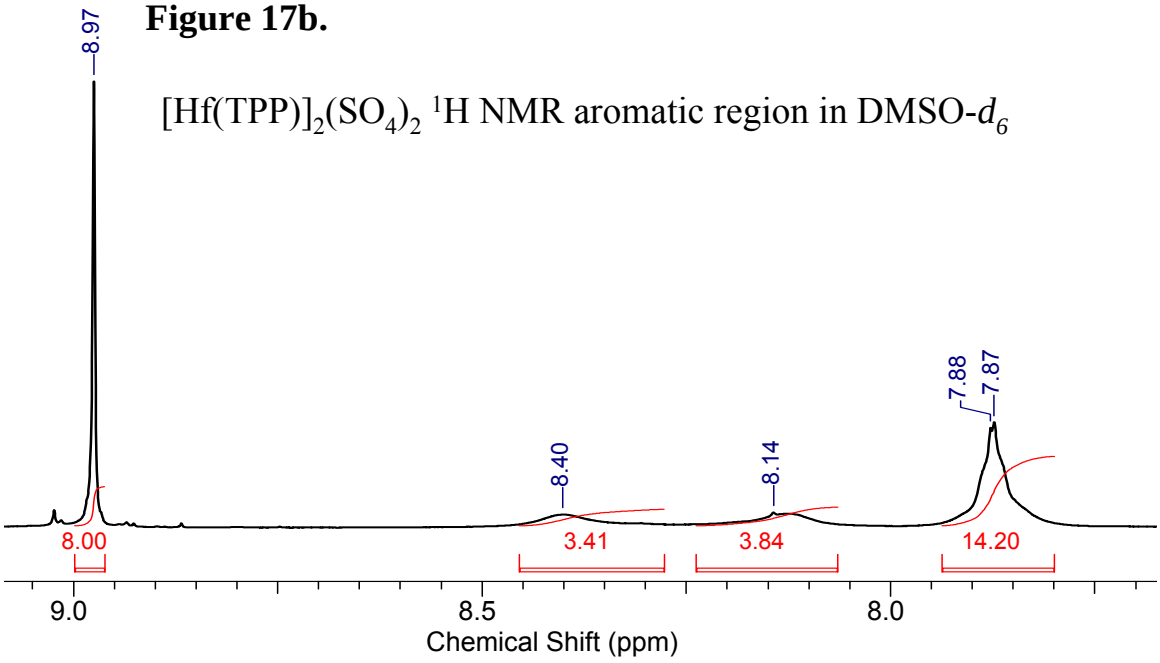

Figure 18.

$[Hf(TPP)]_2(SO_4)_2$ elemental analysis, presence of sulfur is verified but percent is low due to partial hydrolysis of the sample before submission for elemental analysis

RESULTS OF ANALYSIS

Sample Number	Schwarzkopf Number	% Sulfur
HF (TPP) S04	E78905	2.87
NaCl	E78906	<10 ppm
Aq.HCl	E78907	<10 ppm

Figure 19.

$[Hf(TPP)]_2(HPO_4)_3^{-2}$ UV-Vis

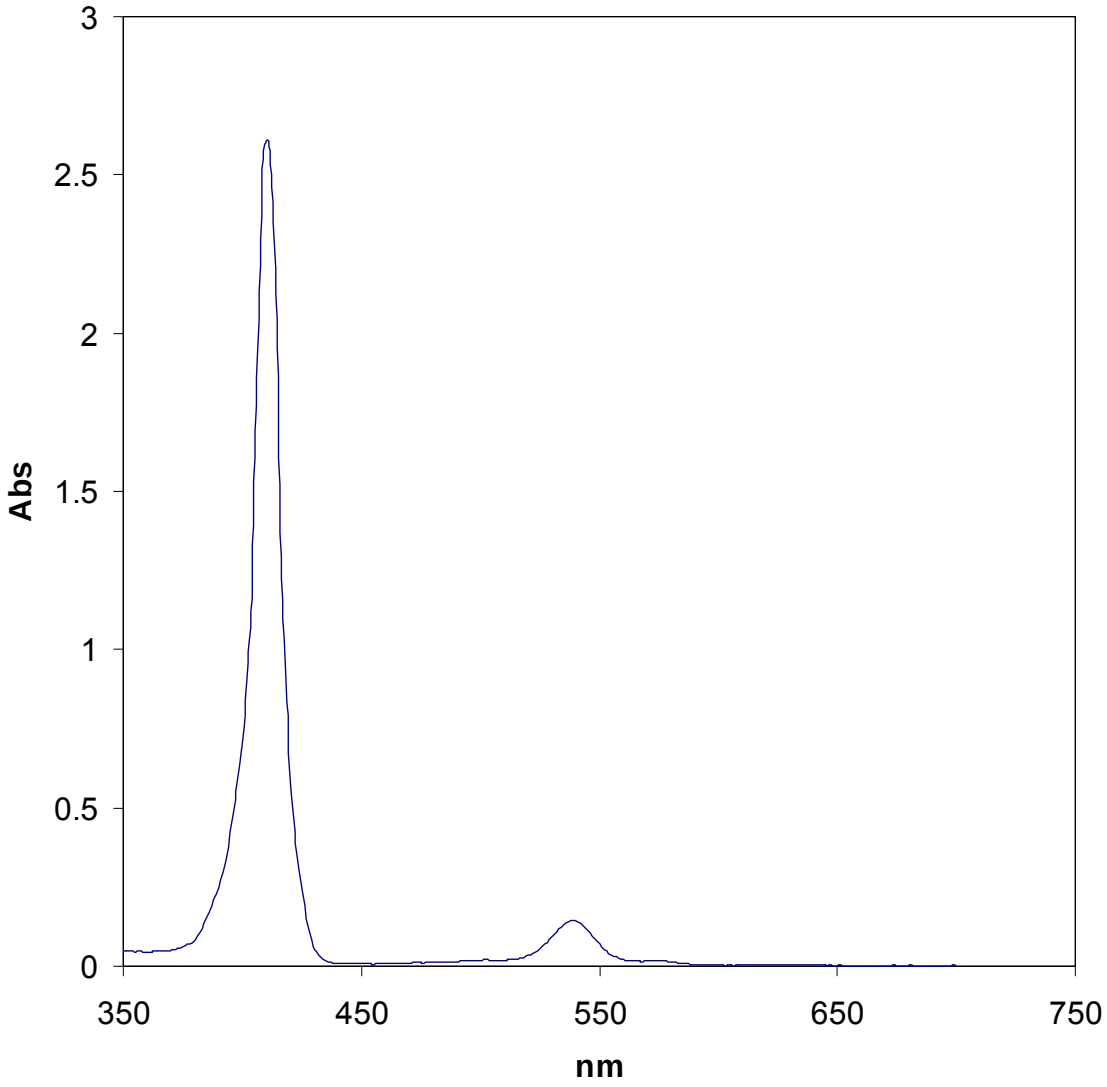

Figure 20a.

$[Hf(TPP)]_2(HPO_4)_3^{-2}$ full spectrum ^1H NMR in $CDCl_3$

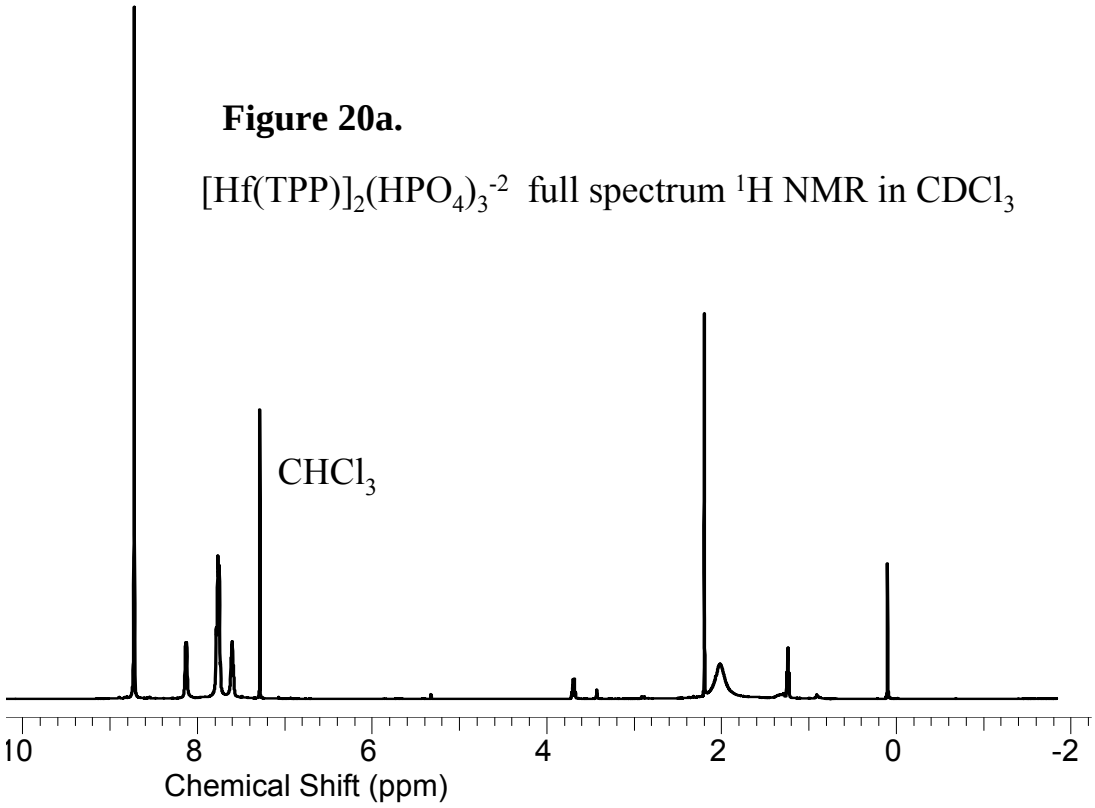

Figure 20b.

$[Hf(TPP)]_2(HPO_4)_3^{-2}$ aromatic region ^1H NMR in $CDCl_3$

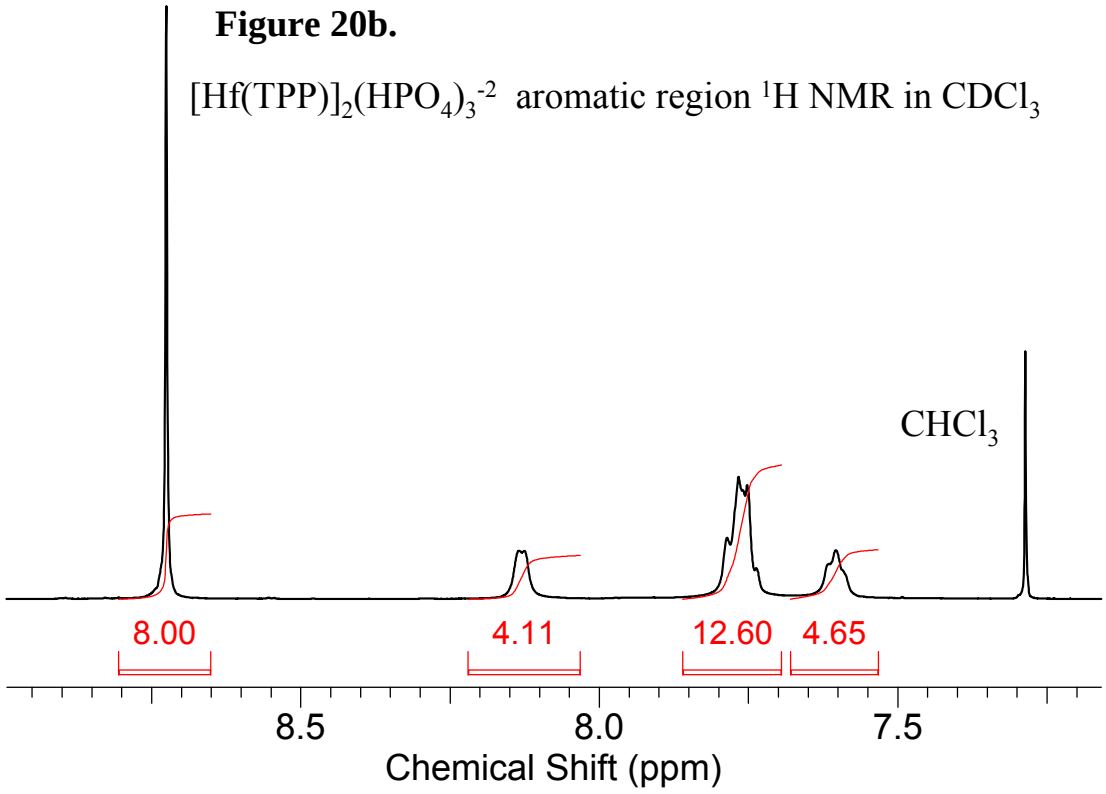

Figure 21a.
$Hf(TPP)(HPO_4)_3^{-2}$ ^{31}P NMR in $CDCl_3$ w/out H_3PO_4 standard

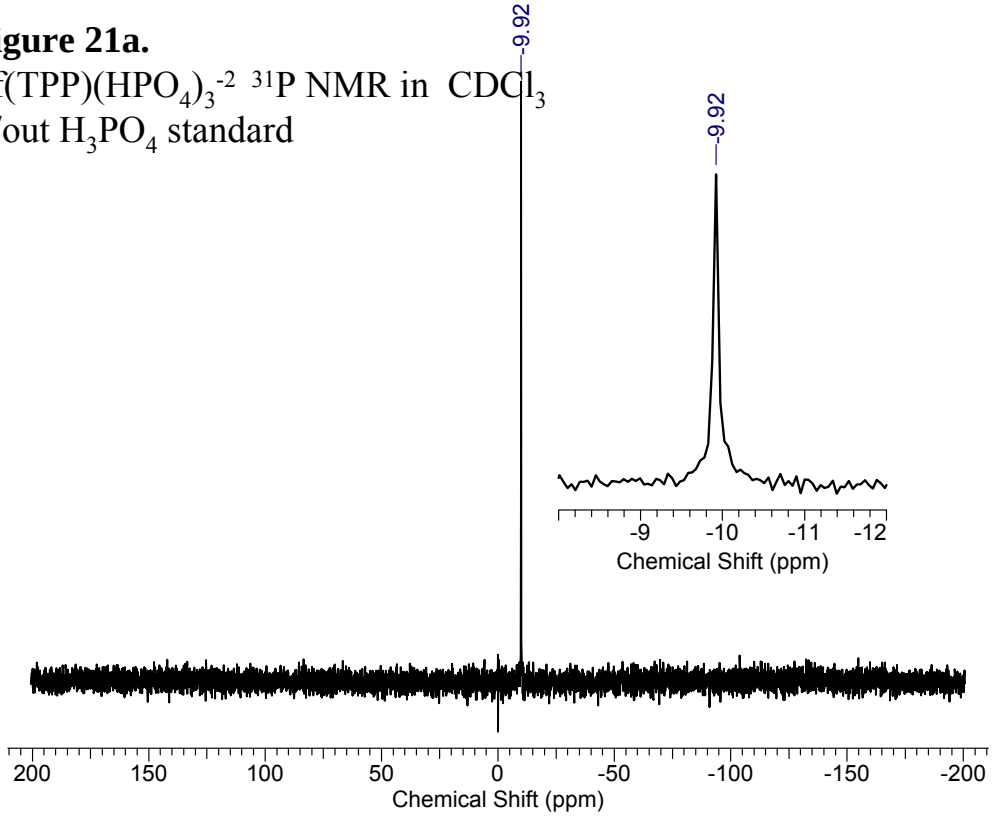

Figure 21b.
external H_3PO_4 standard

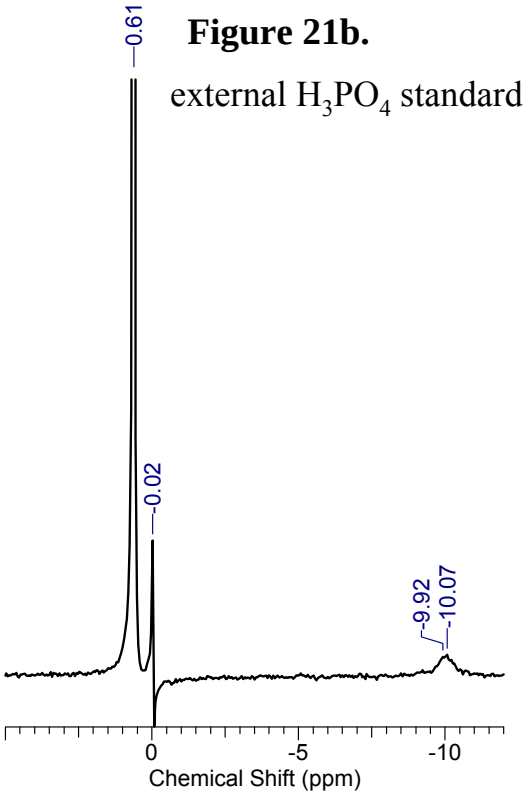

Figure 21c.
internal H_3PO_4 standard

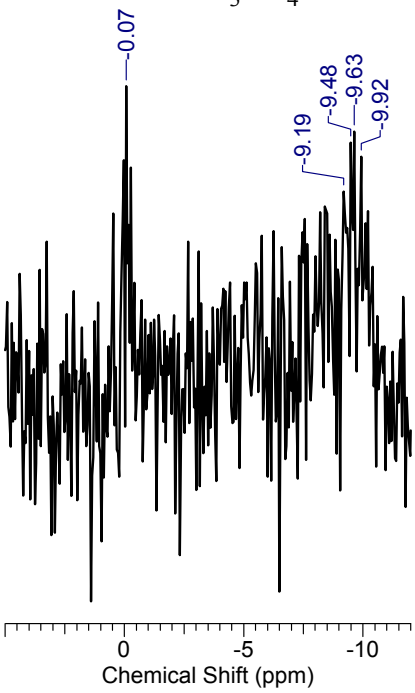

Figure 22.

$Hf(TTP)OAc_2$ UV-Vis in CH_2Cl_2

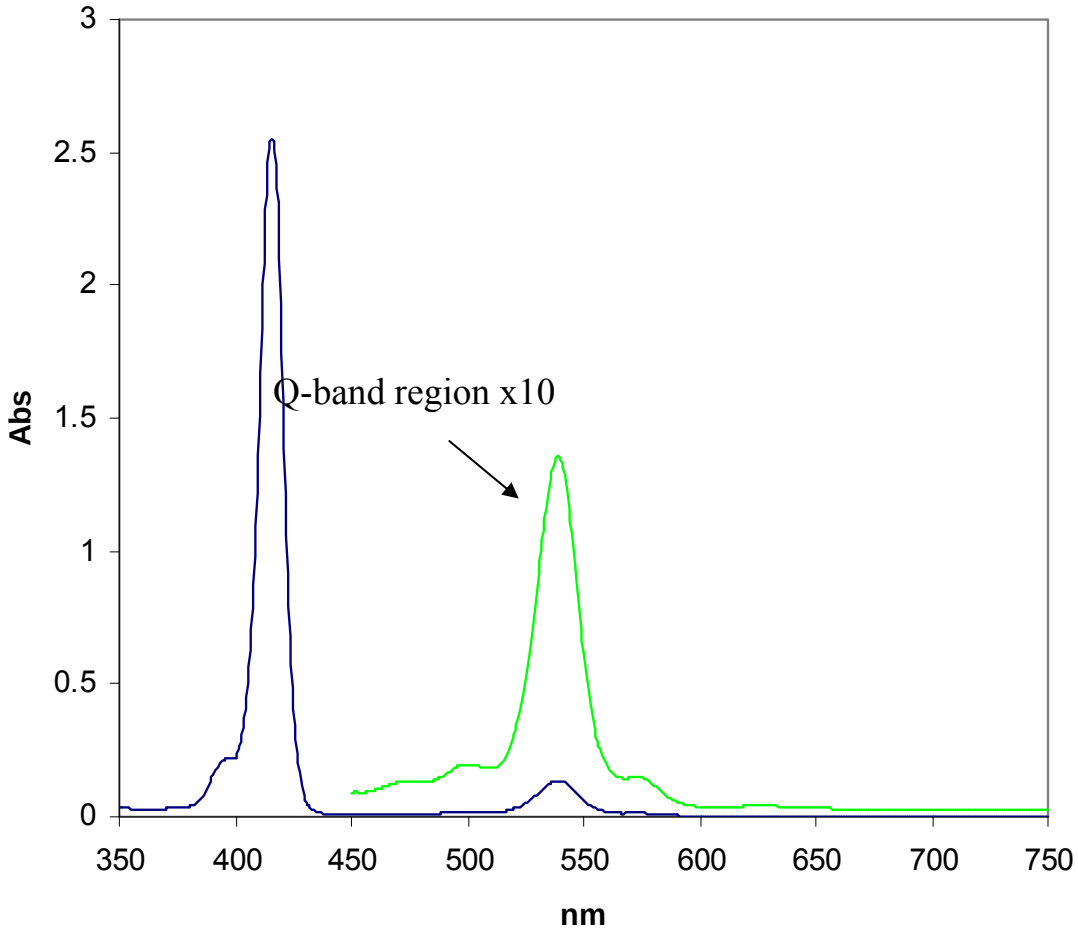

Figure 23a. $Hf(TTP)OAc_2$ full spectrum ^1H NMR in $CDCl_3$

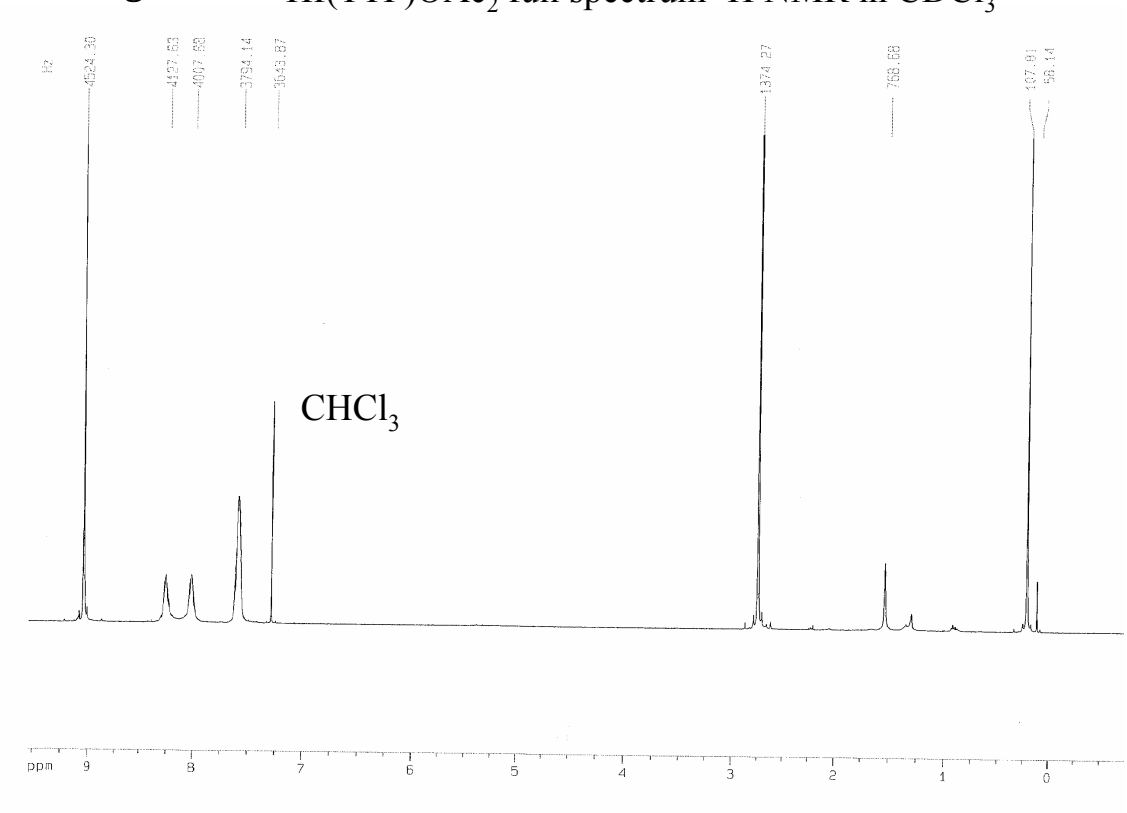

Figure 23b. $Hf(TTP)OAc_2$ showing acetate singlet at 0.26ppm integrating correctly with the tolyl CH_3 singlet at 2.75ppm

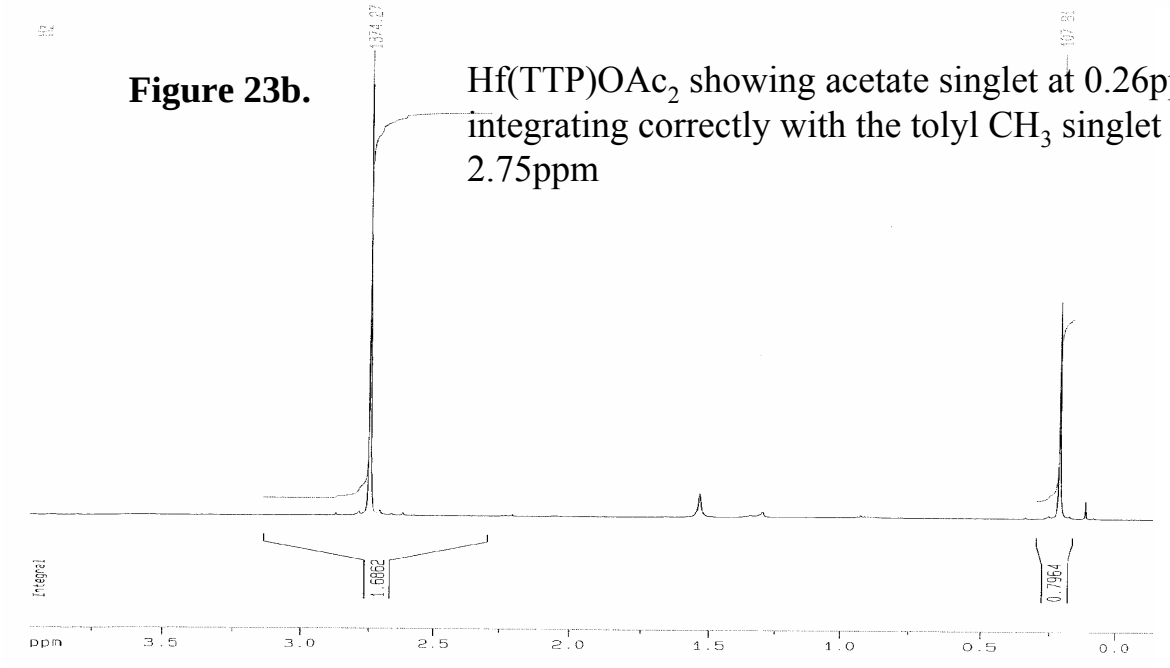

Figure 24.

MALDI-MS of $Hf(TTP)OAc_2$ in dithranol matrix

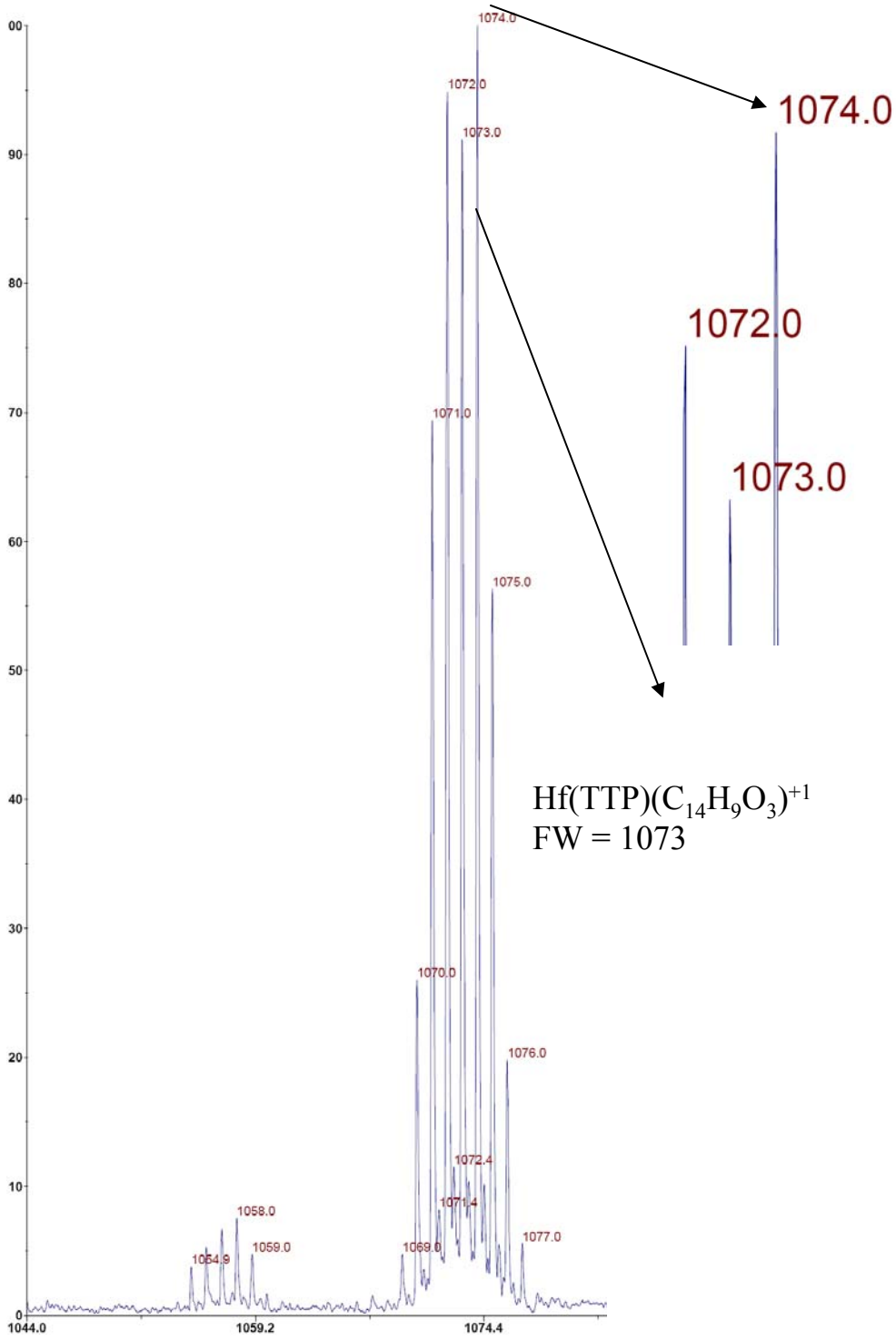

Figure 25.

$[Hf(TTP)]_2(\mu\text{-}\eta^2\text{-}O_2)_2$ ESI-MS, positive ion mode

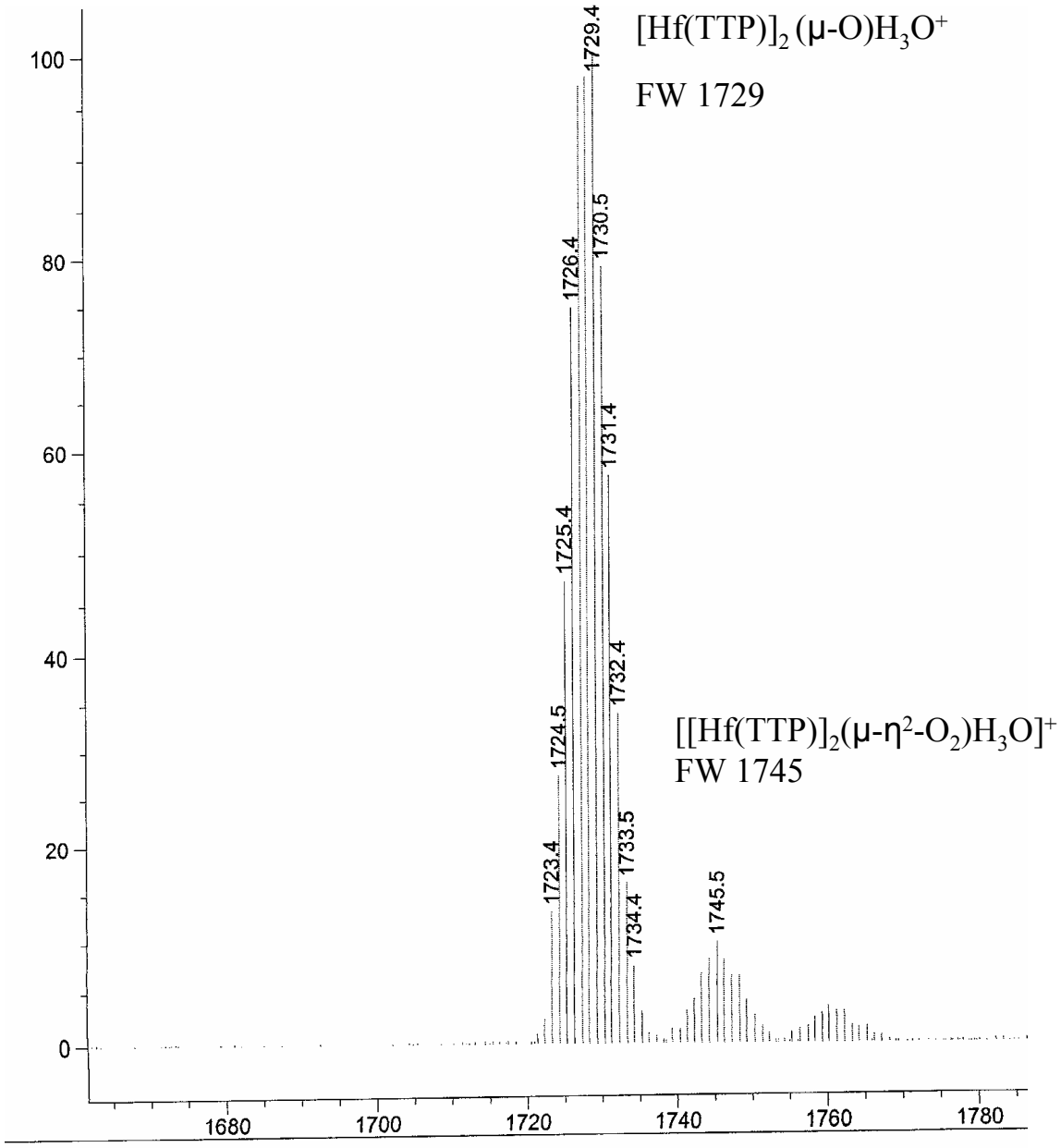

Figure 26.

Hf(TTP)oct$_2$ UV-Vis in CH_2Cl_2

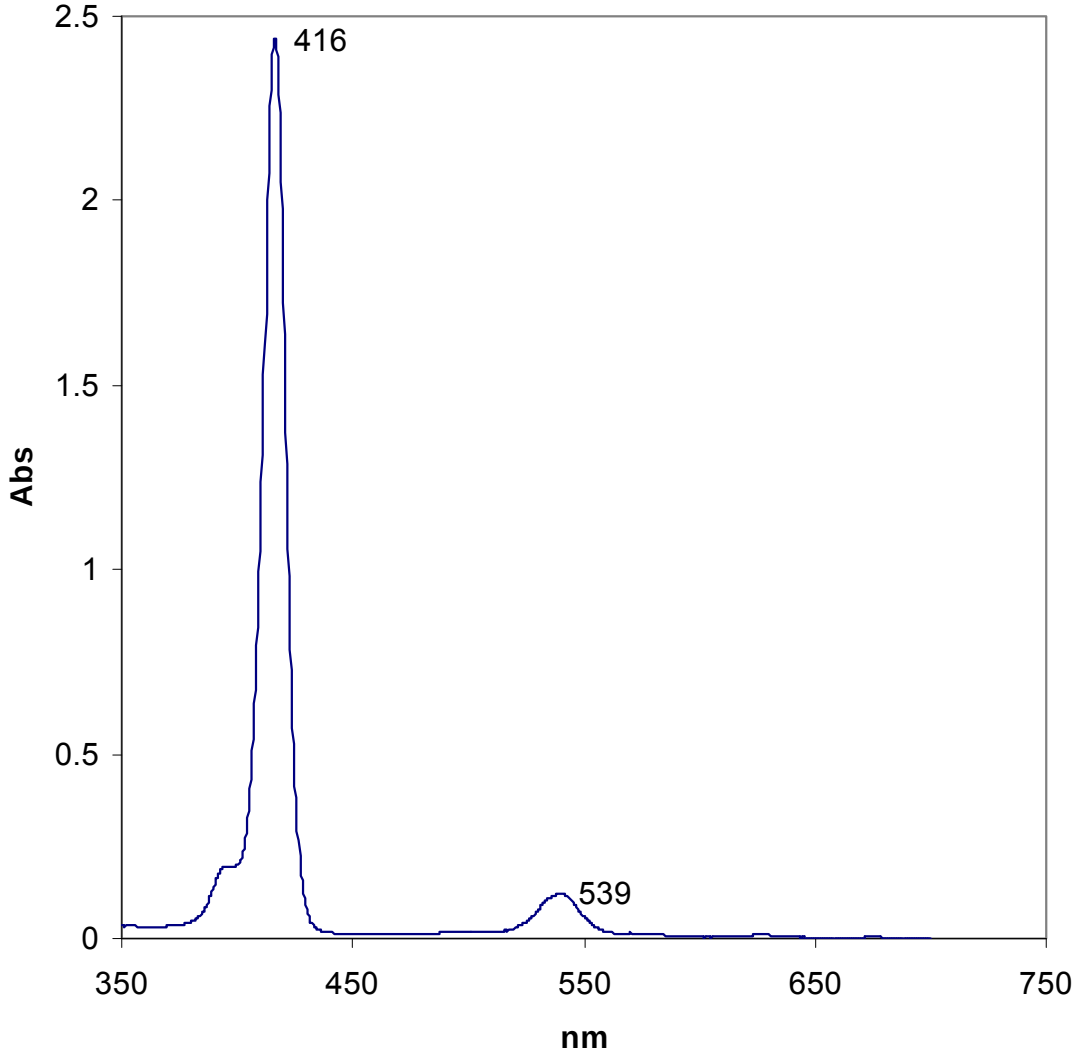

Figure 27a. Hf(TTP)oct$_2$ aliphatic region of the ^{1}H NMR spectrum in acetone-d_6

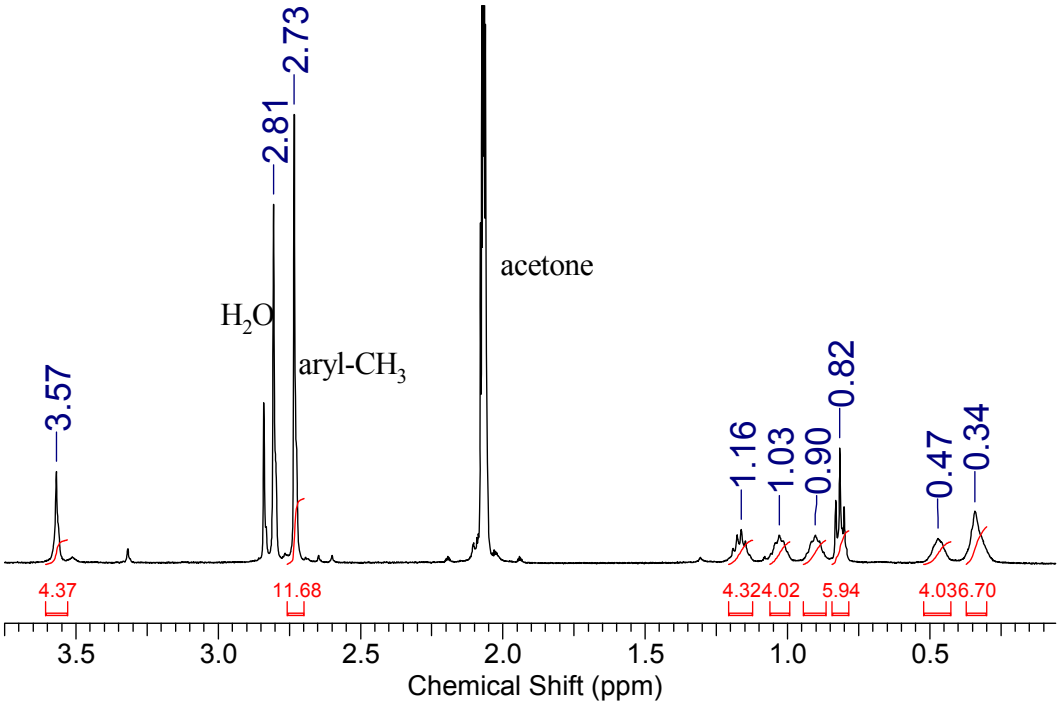

Figure 27b. Hf(TTP)oct$_2$ full spectrum ^{1}H NMR spectrum in acetone-d_6

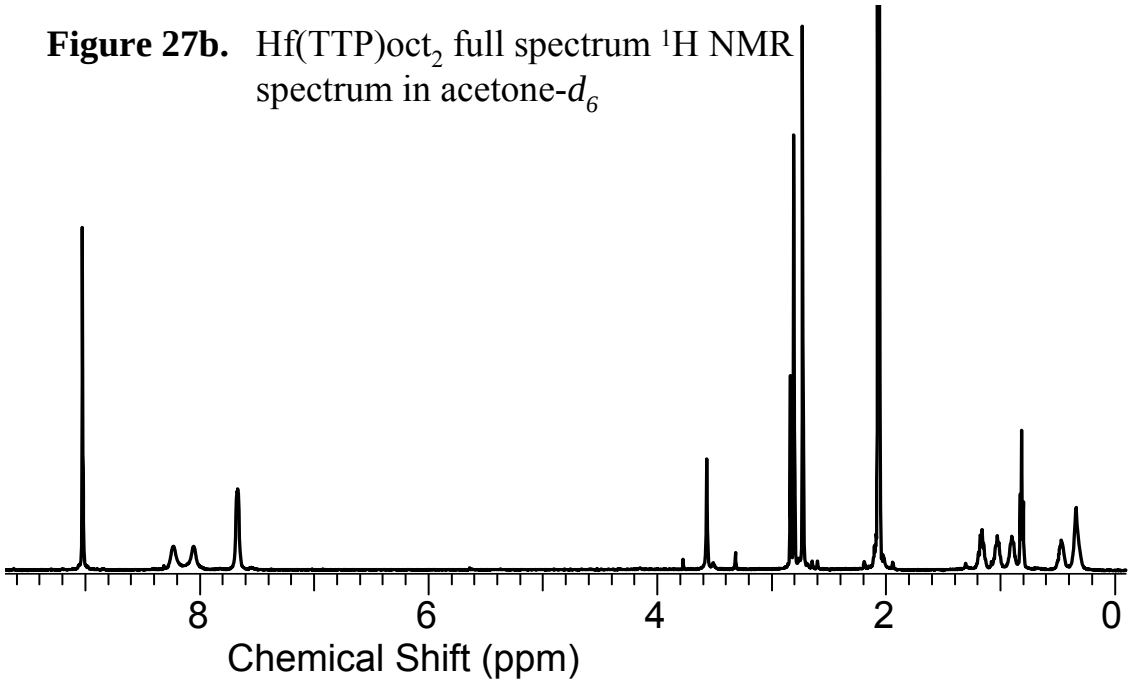

Figure 28.

$Hf(TPPF_{20})OAc_2$ UV-Vis

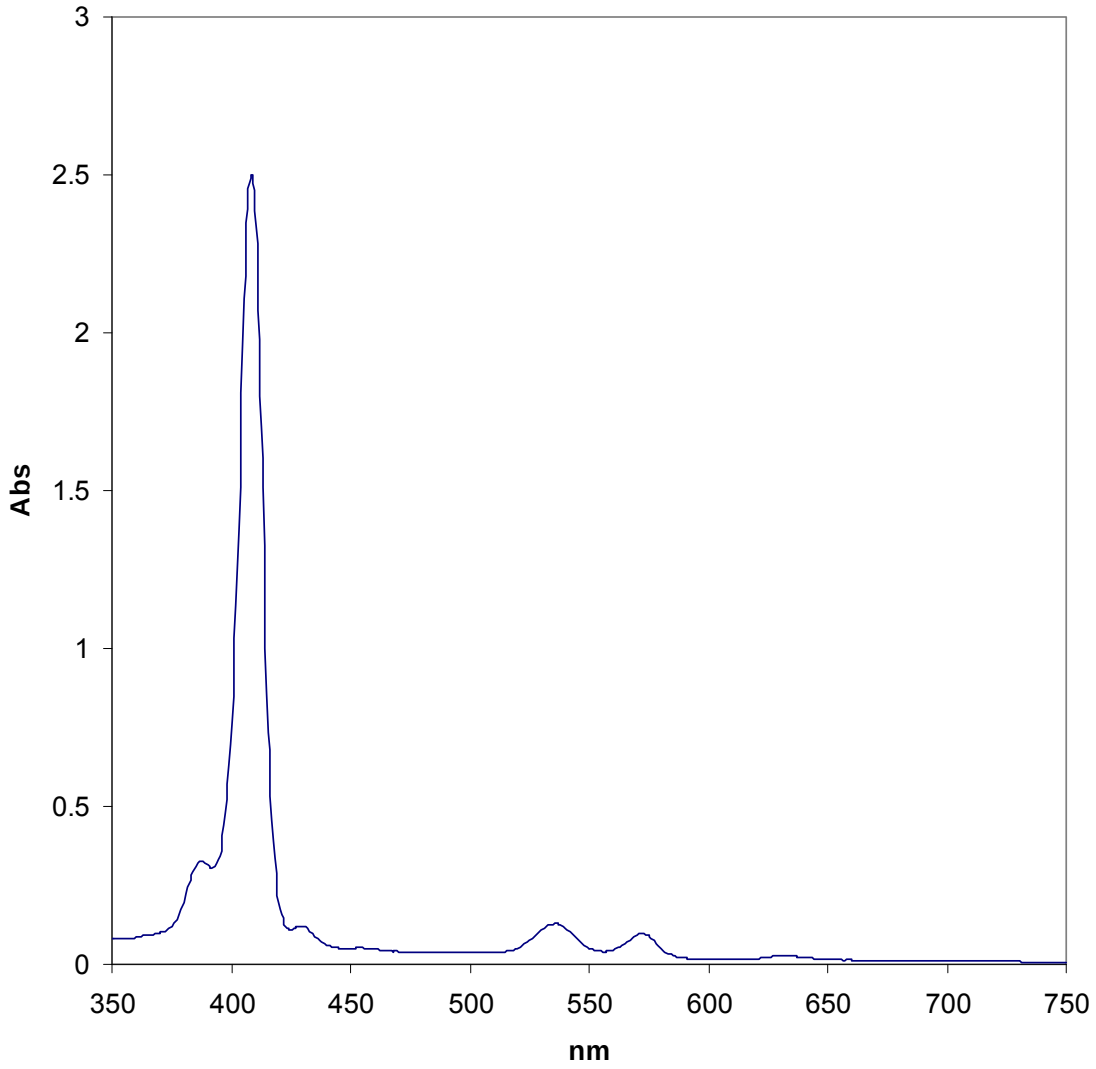

Figure 29.

$Hf(TPPF_{20})OAc_2$ ^1H NMR in $CDCl_3$

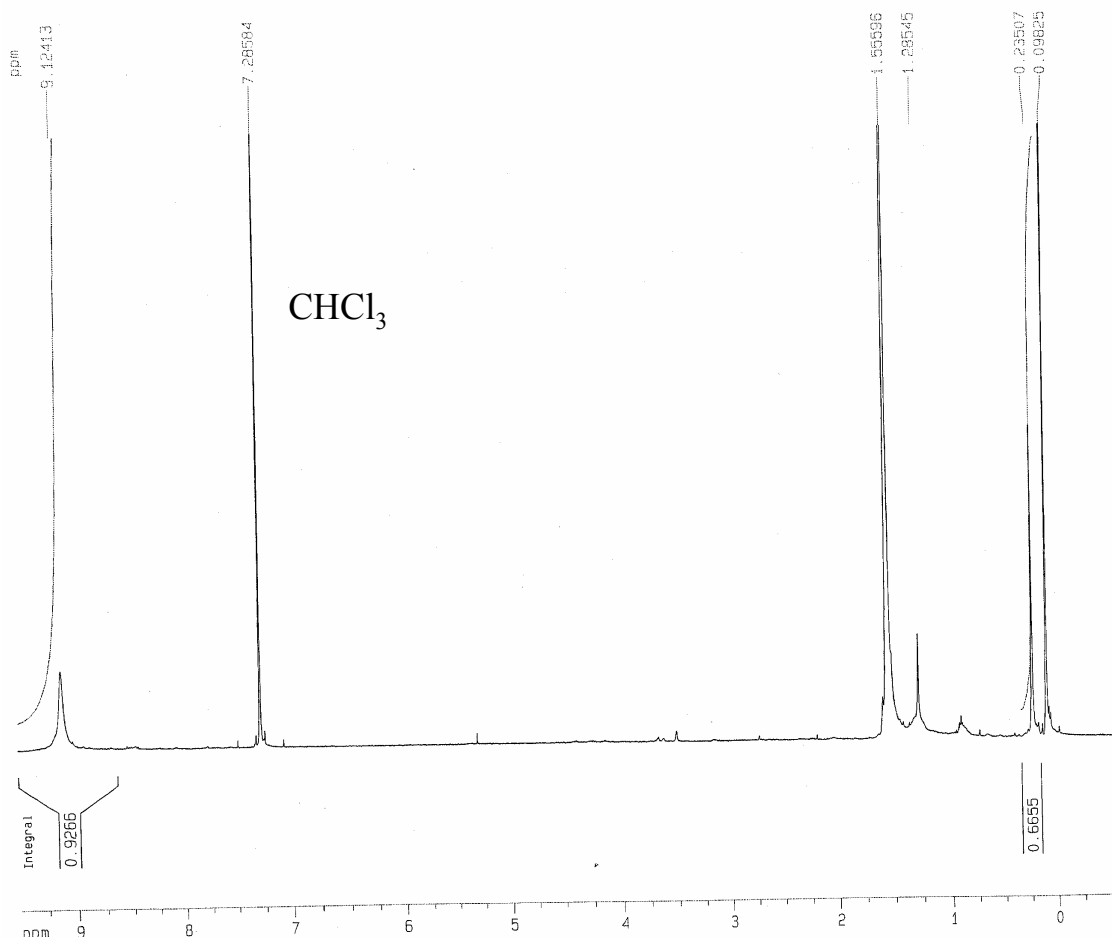

Figure 30.

$Hf(TPPF_{20})OAc_2$ MALDI-MS using dithranol matrix, acetate ligands are retained and not exchanged for the dithranol

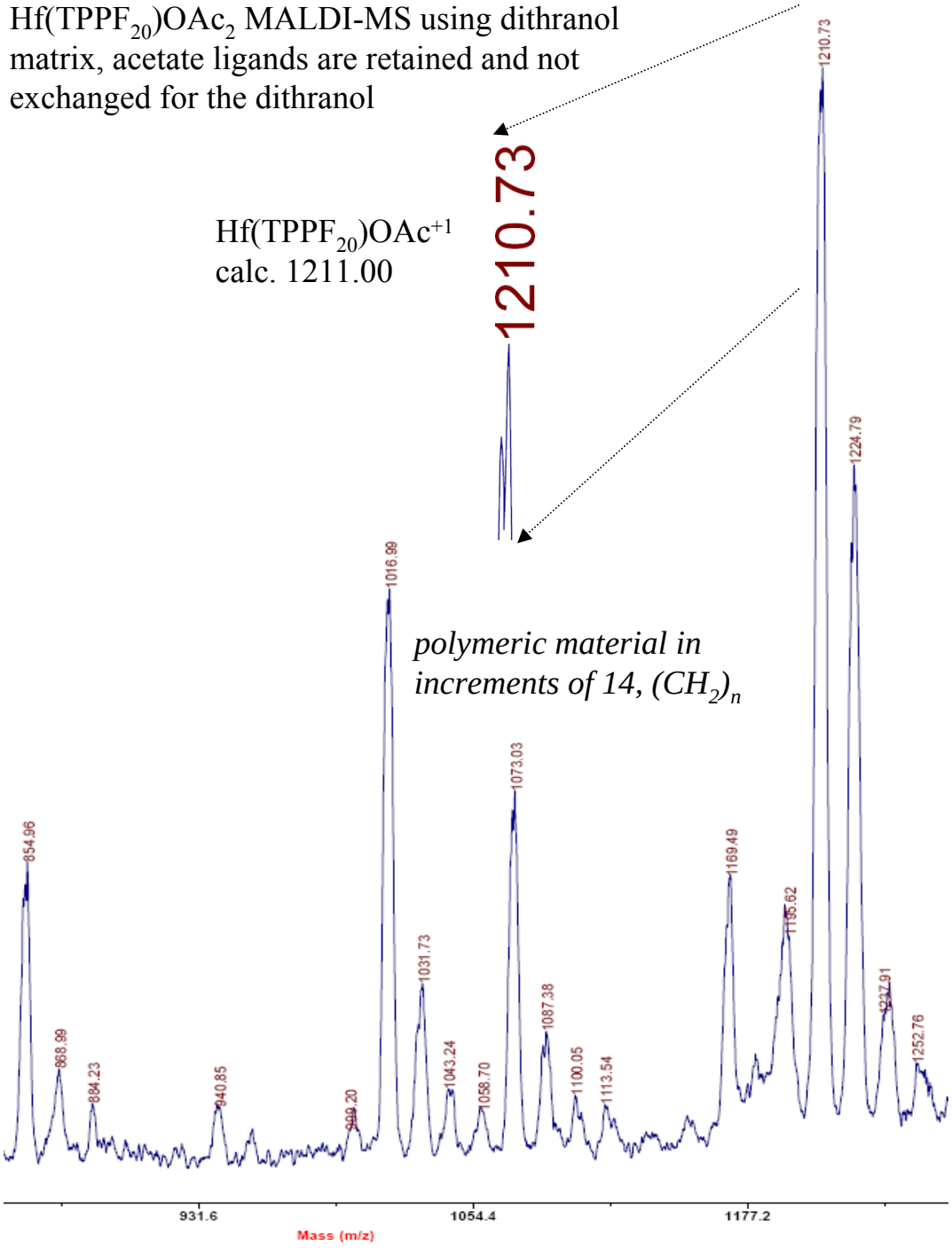

Figure 31.

$Hf(TPyP)OAc_2$ UV-Vis in CH_3OH

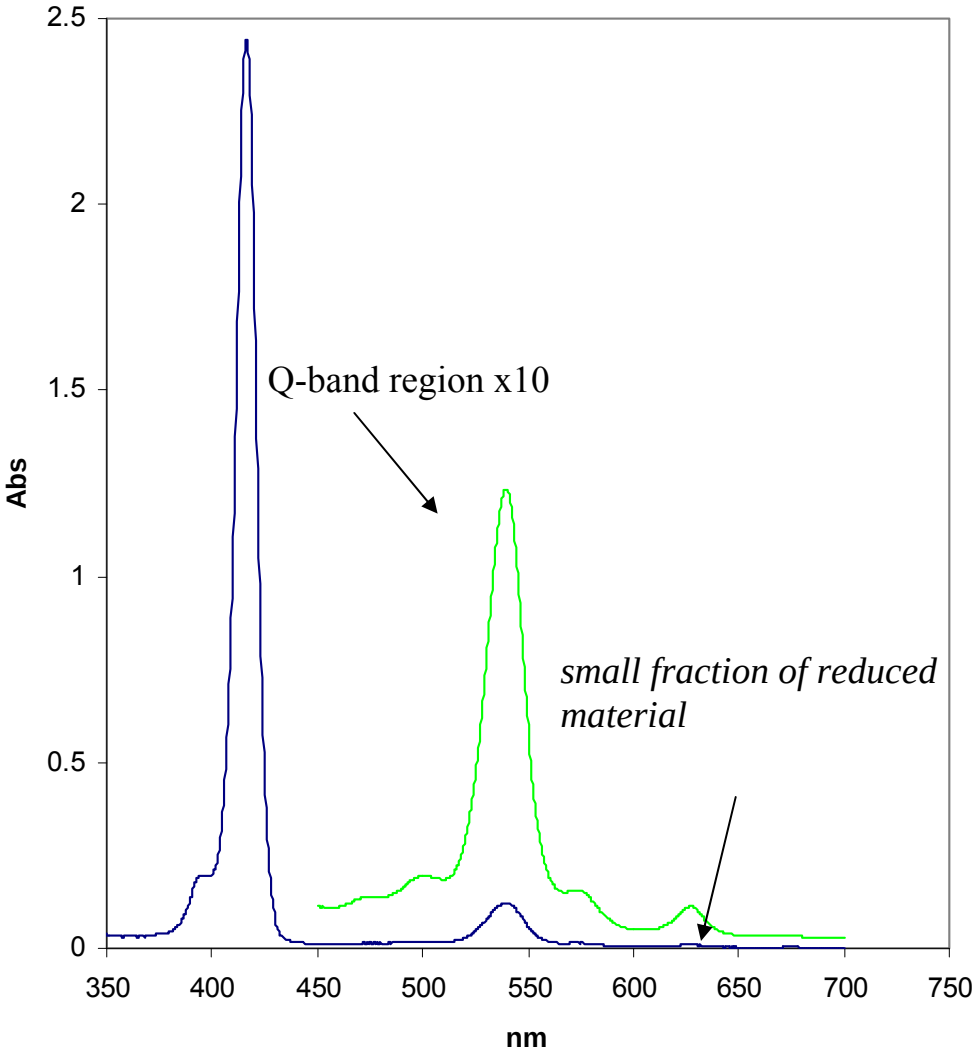

Figure 32a.

Hf(TPyP)OAc_2 Full spectrum ^{1}H NMR in CH_3OH-d_6

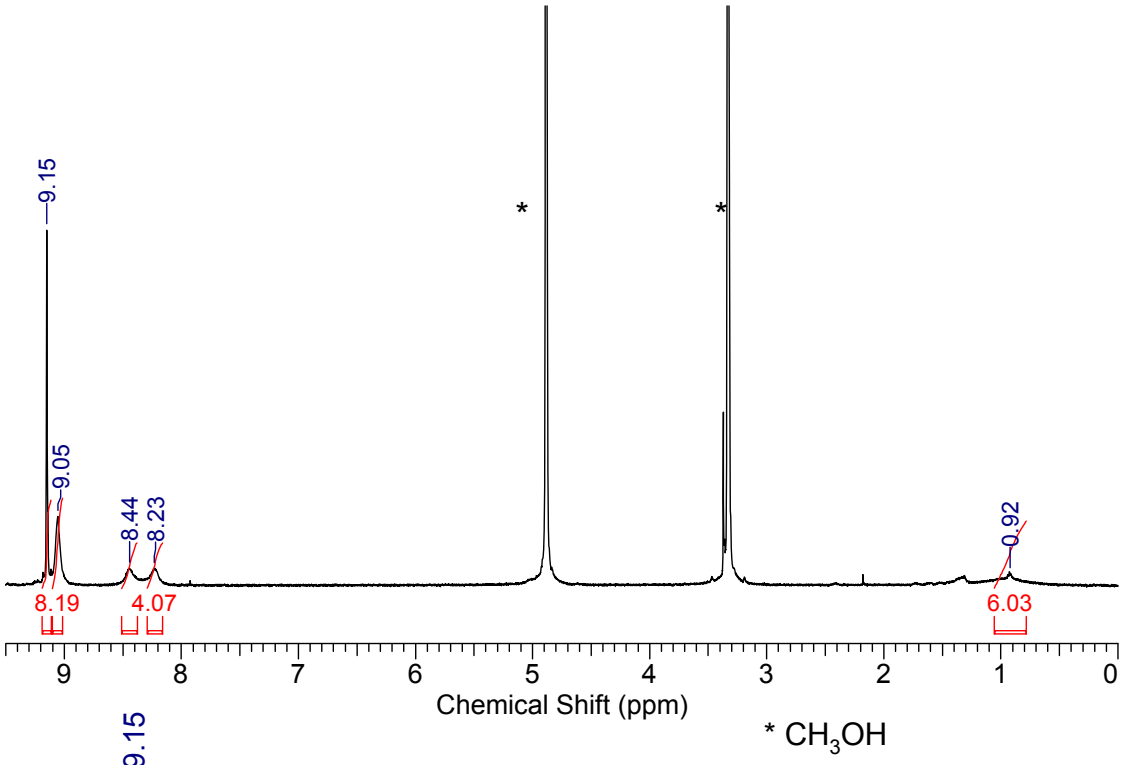

Figure 32b

Hf(TPyP)OAc_2 aromatic region ^{1}H NMR in CH_3OH-d_6

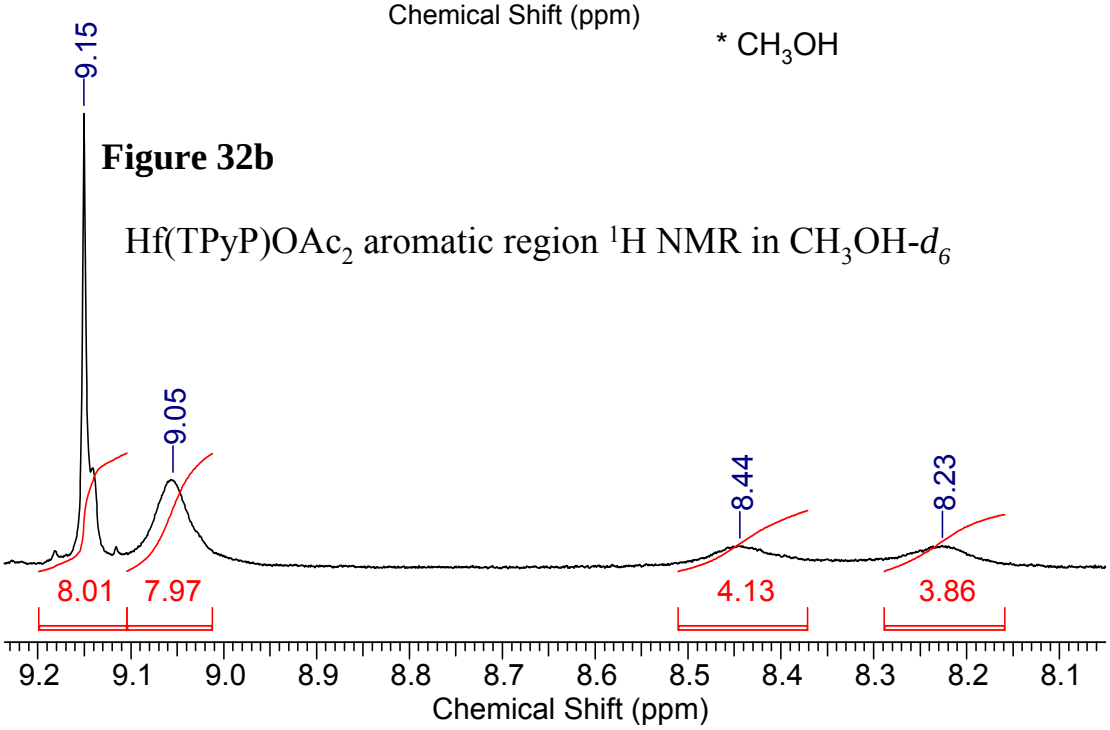

Figure 33.

ESI-MS, positive ion mode

$Hf(TPyP)OAc_2$

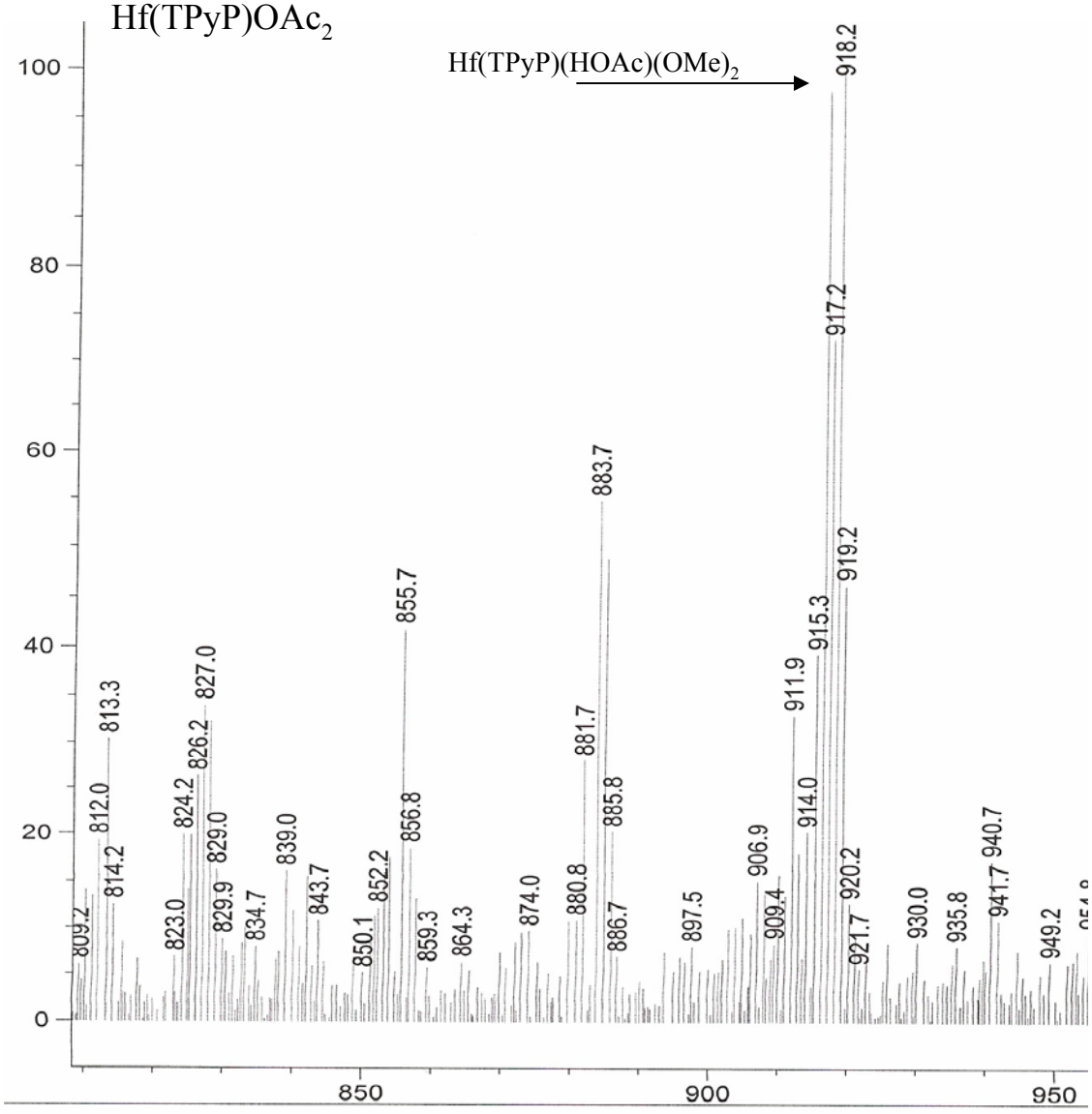

Figure 34.

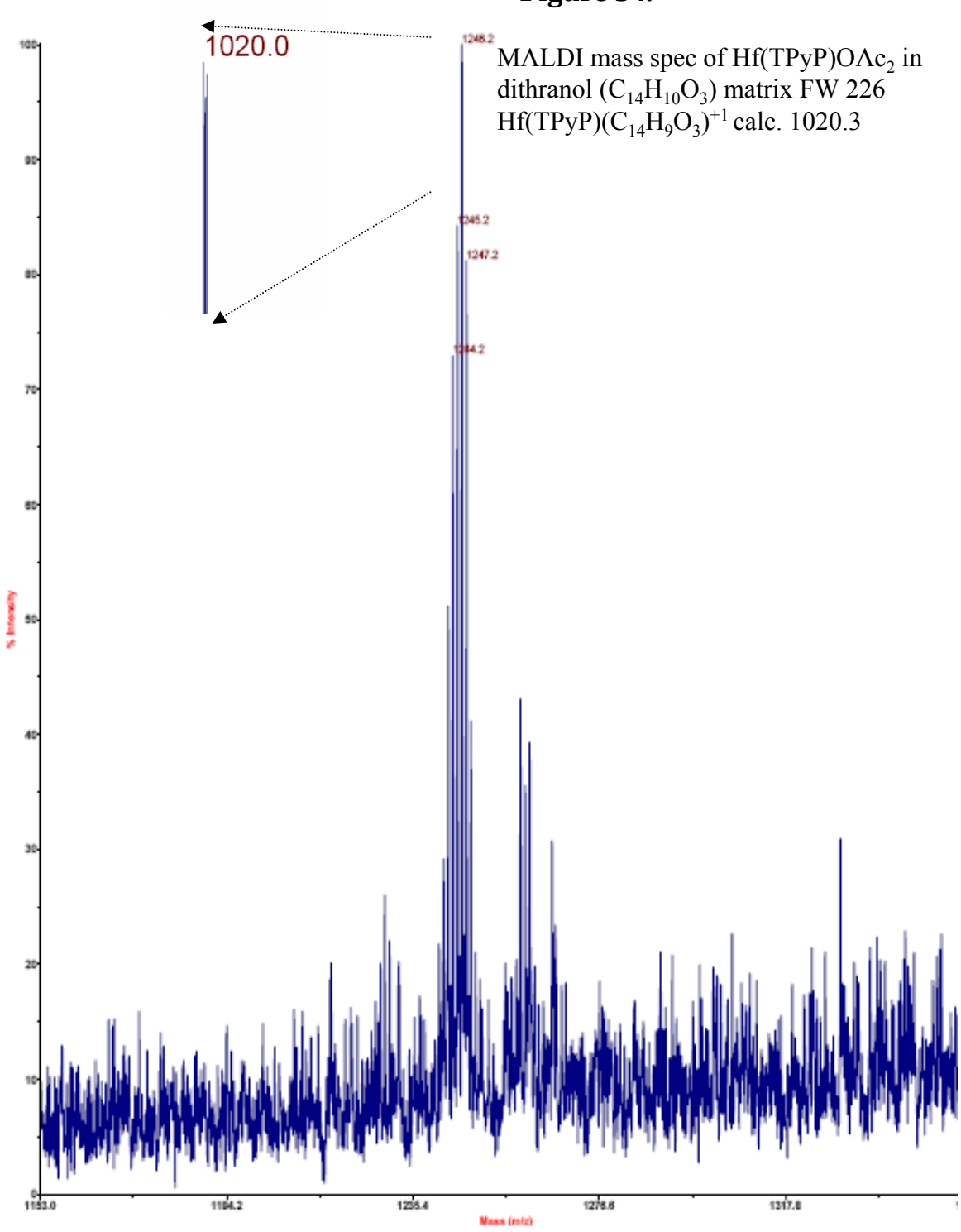

MALDI mass spec of $Hf(TPyP)OAc_2$ in dithranol ($C_{14}H_{10}O_3$) matrix FW 226 $Hf(TPyP)(C_{14}H_9O_3)^{+1}$ calc. 1020.3

Figure 35.

Hf(T-Me-CPP)OAc_2 UV-Vis and ^1H NMR after diazomethane reaction

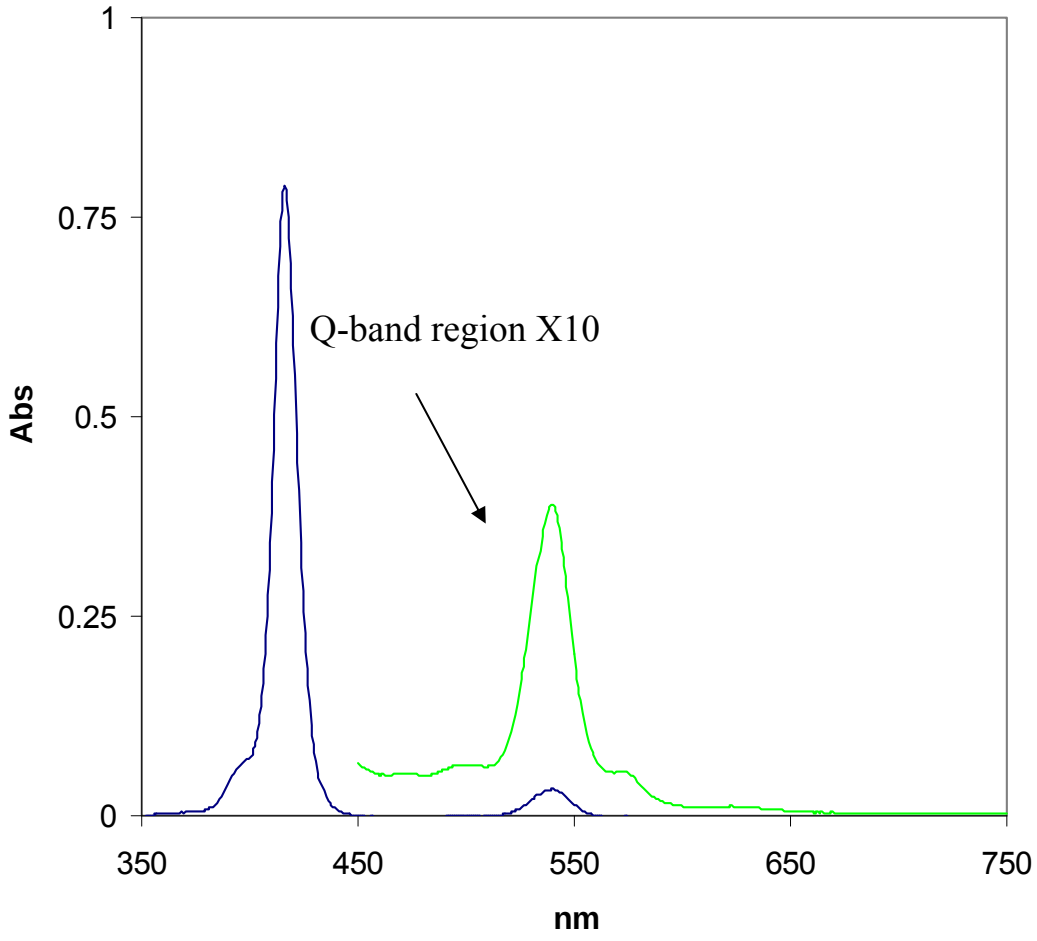

Figure 36.

Hf(T-Me-CPP)OAc_2 full spectrum ^1H NMR after diazomethane reaction in $CDCl_3$

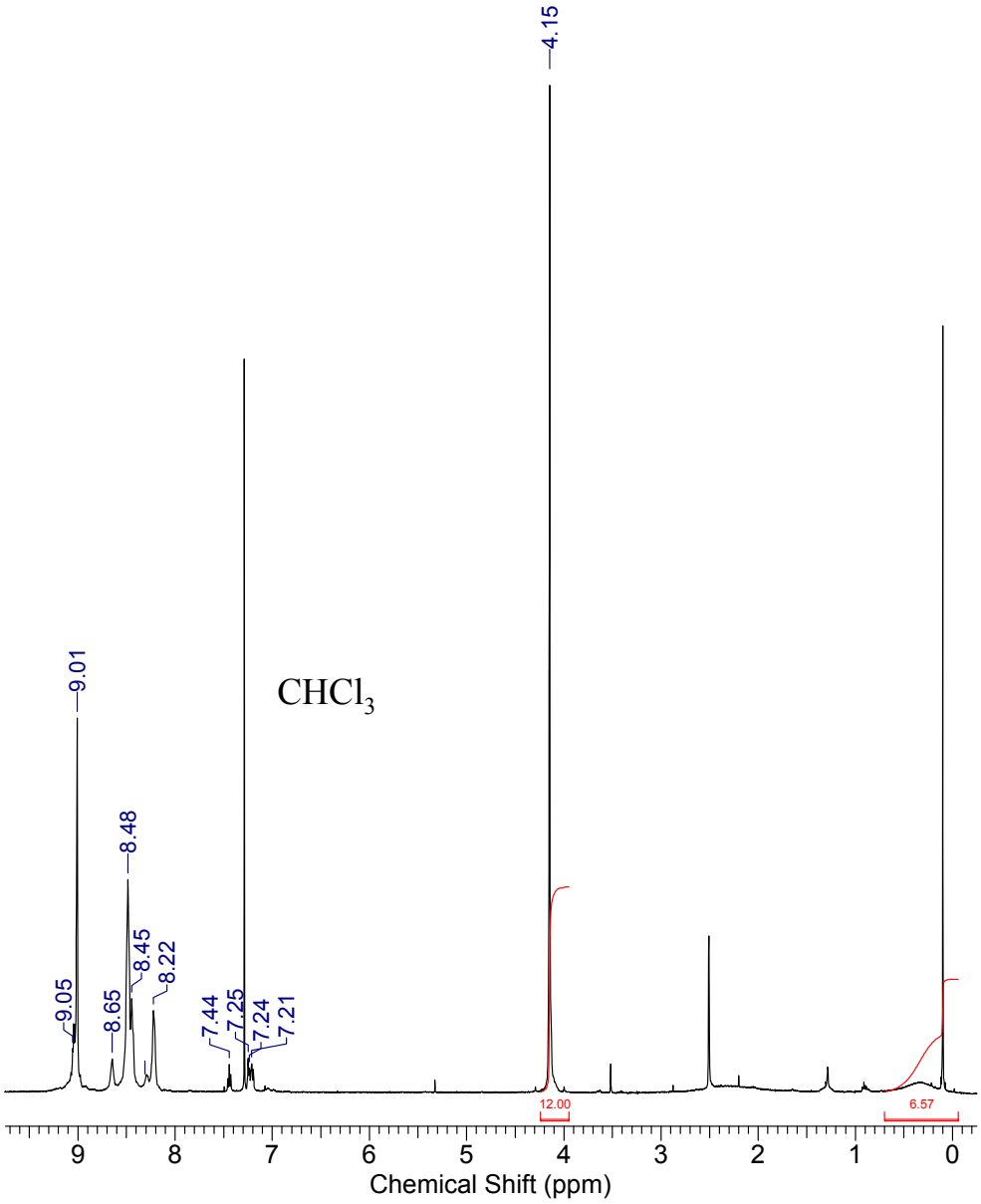

Figure 37.

Hf(T-Me-CPP)OAc_2 aromatic region ^1H NMR after diazomethane reaction in $CDCl_3$

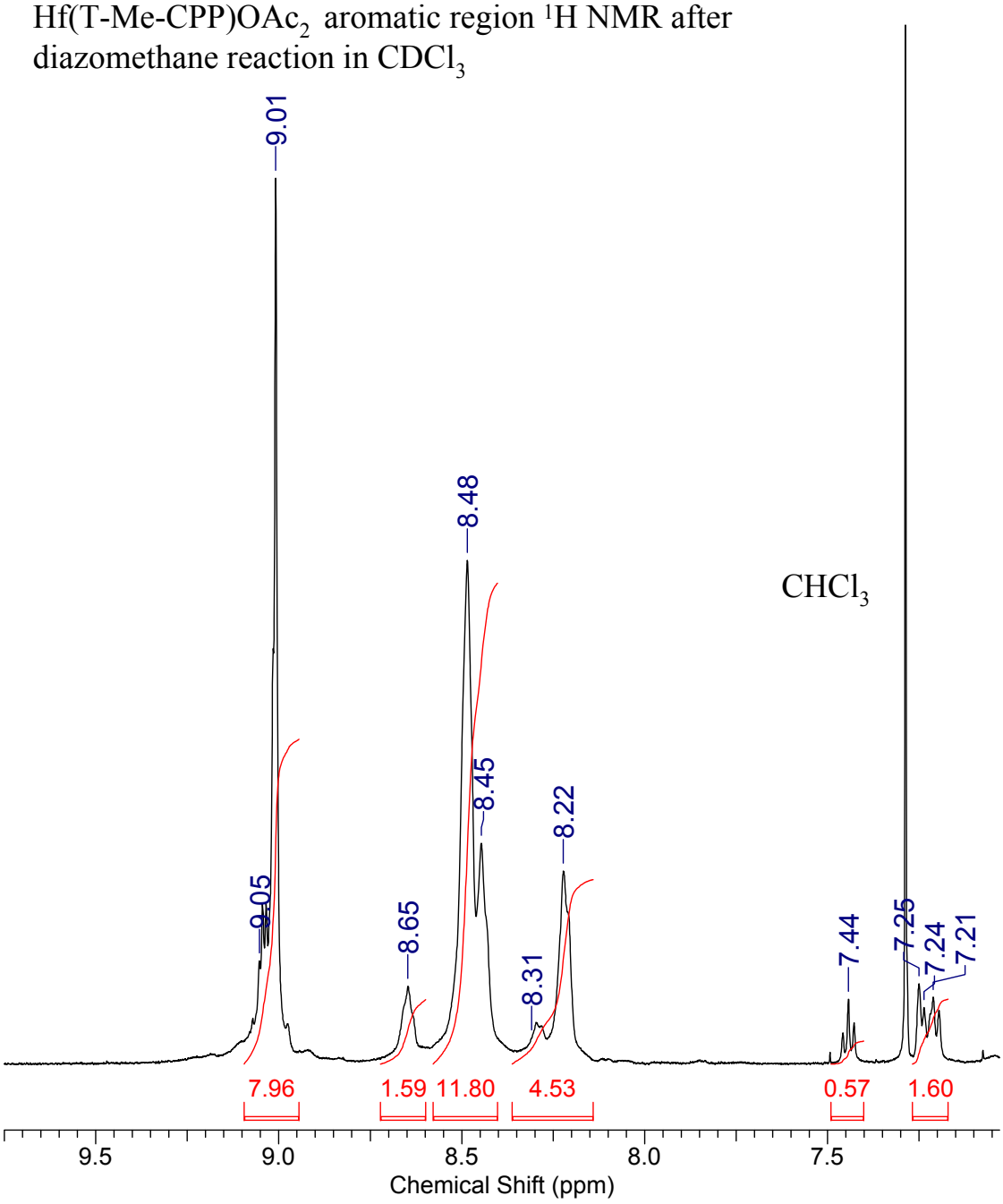

Figure 38.

Hf(T-Me-CPP)OAc_2 COSY NMR after diazomethane reaction

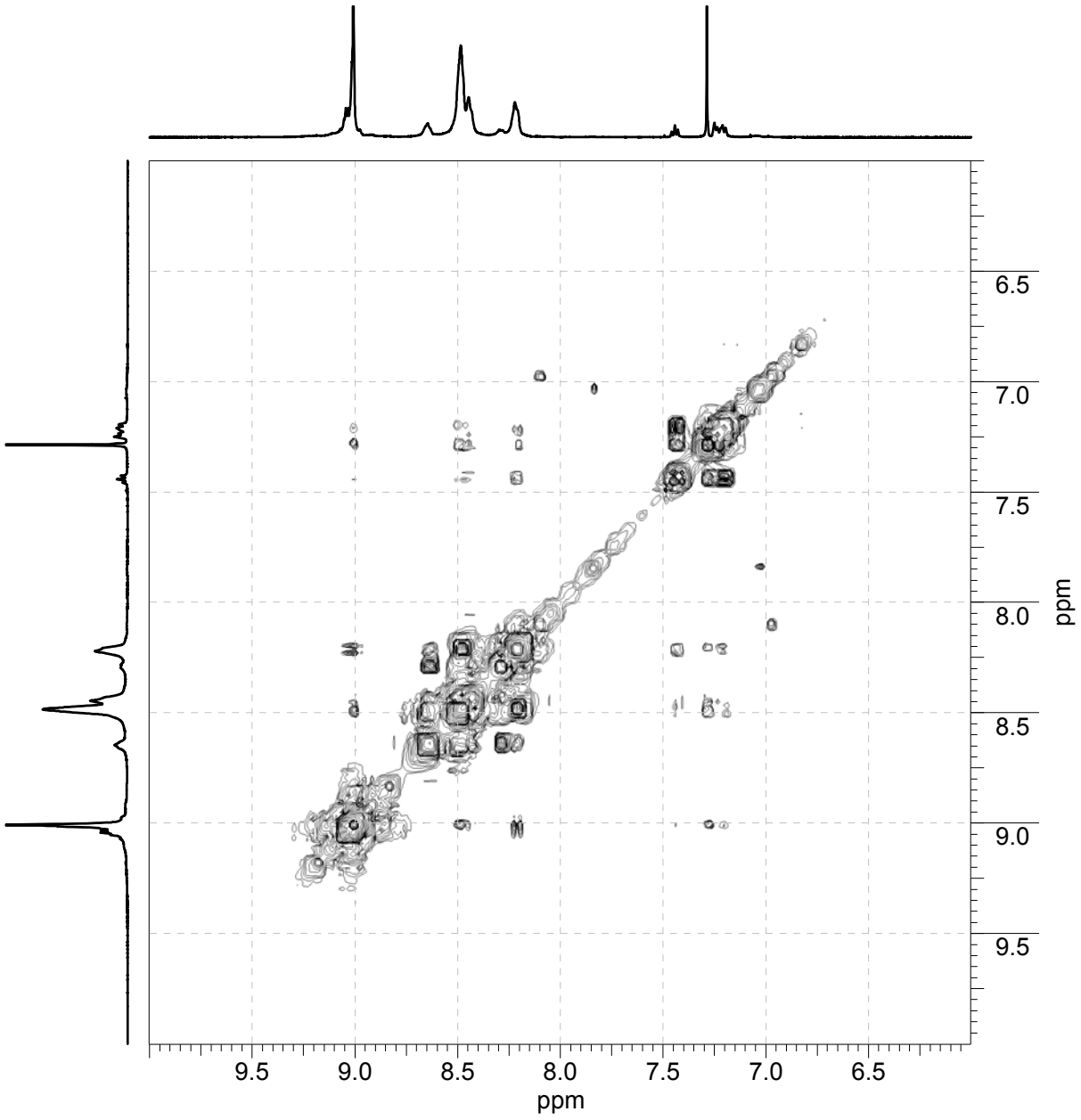

Figure 39.

High resolution MALDI-MS of Hf(T-Me-CPP)OAc_2 with partially cleaved esters and acetates replaced by dithranol matrix before diazomethane reaction

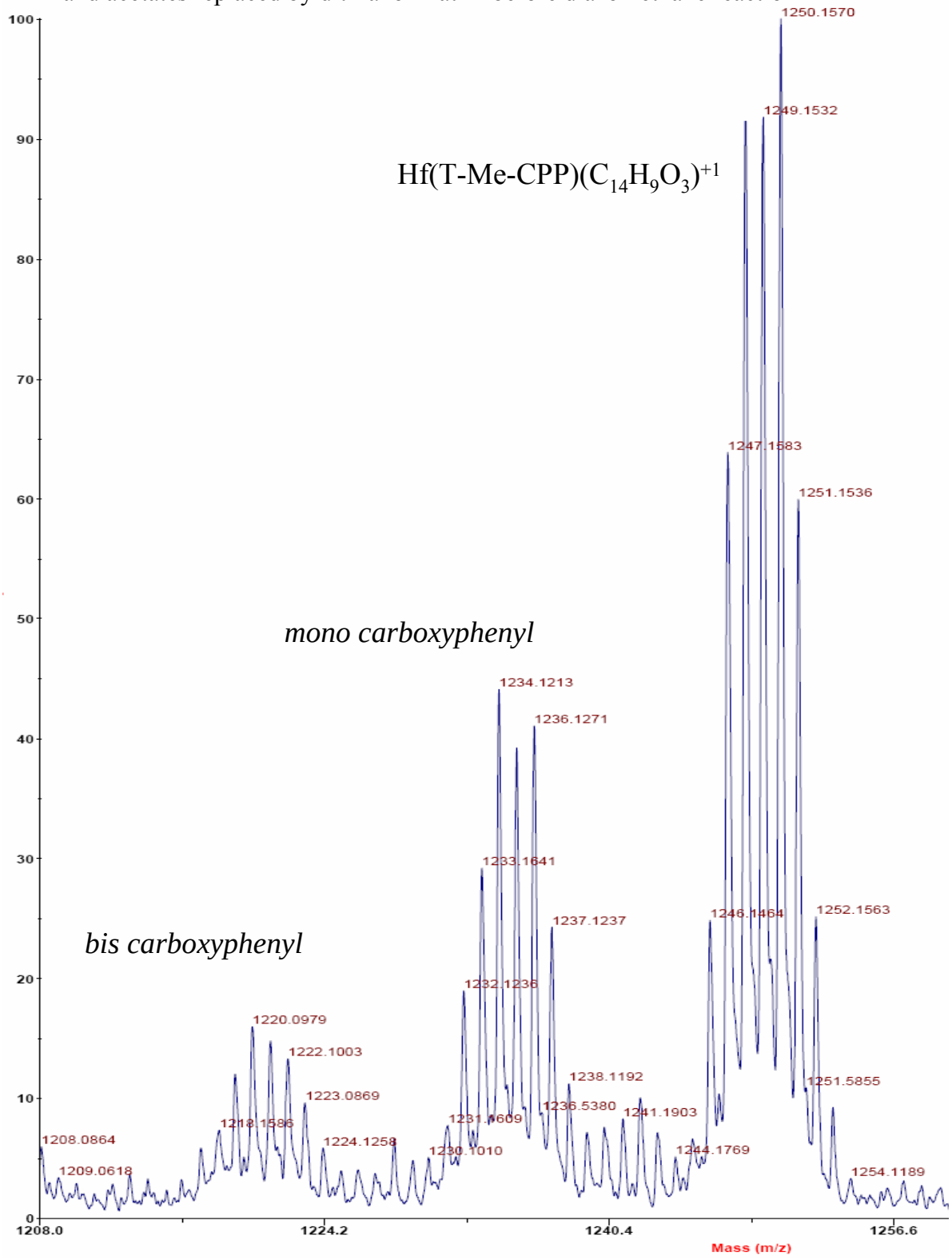

Figure 40.

Low resolution MALDI-MS of Hf(T-Me-CPP)OAc_2 with partially cleaved esters after diazomethane reaction; tetra-methyl ester fraction is increased but methylation remains slightly incomplete. Acetates replaced by dithranol matrix

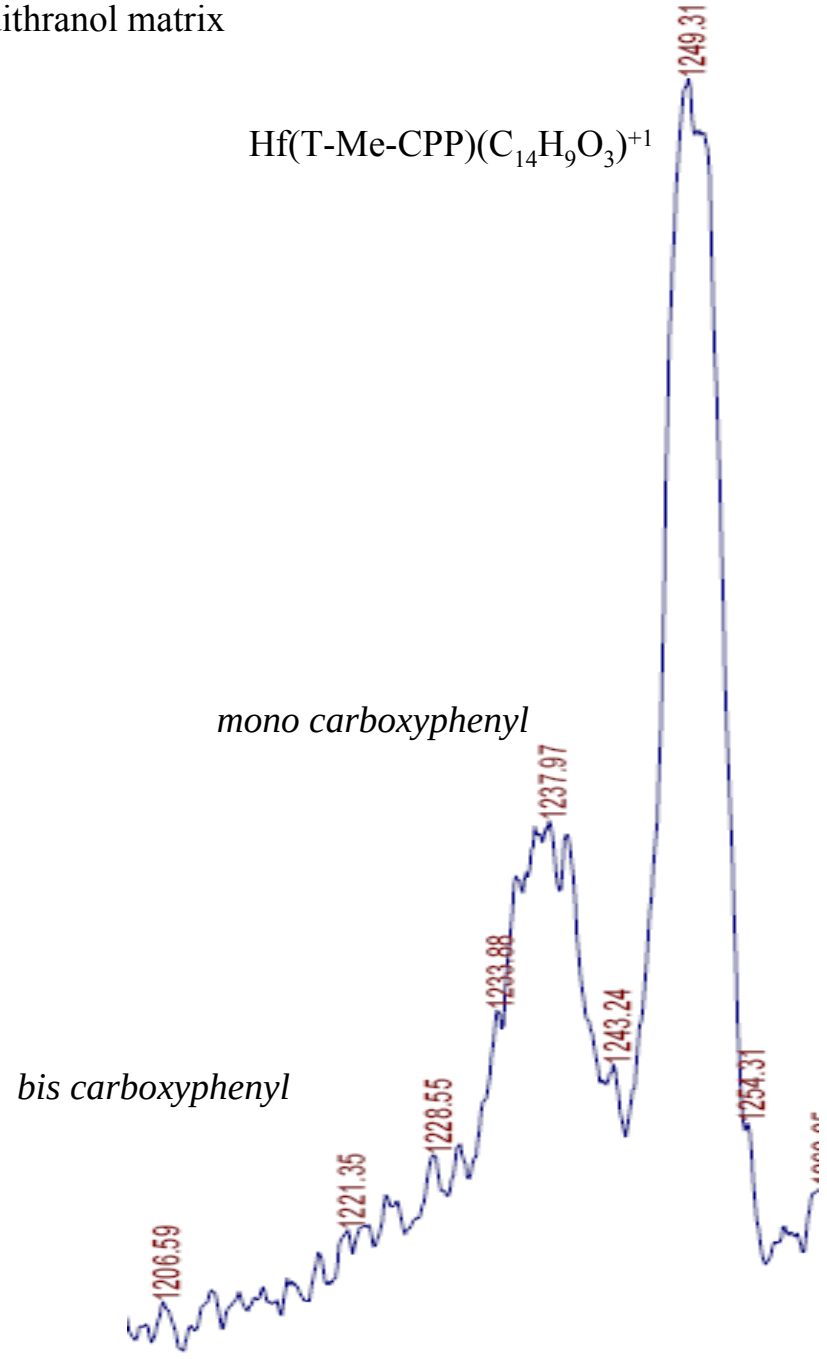

Figure 41.

ES-MS, positive ion mode, of $Hf(T\text{-}Me\text{-}CPP)_2OAc_2$ after diazomethane reaction

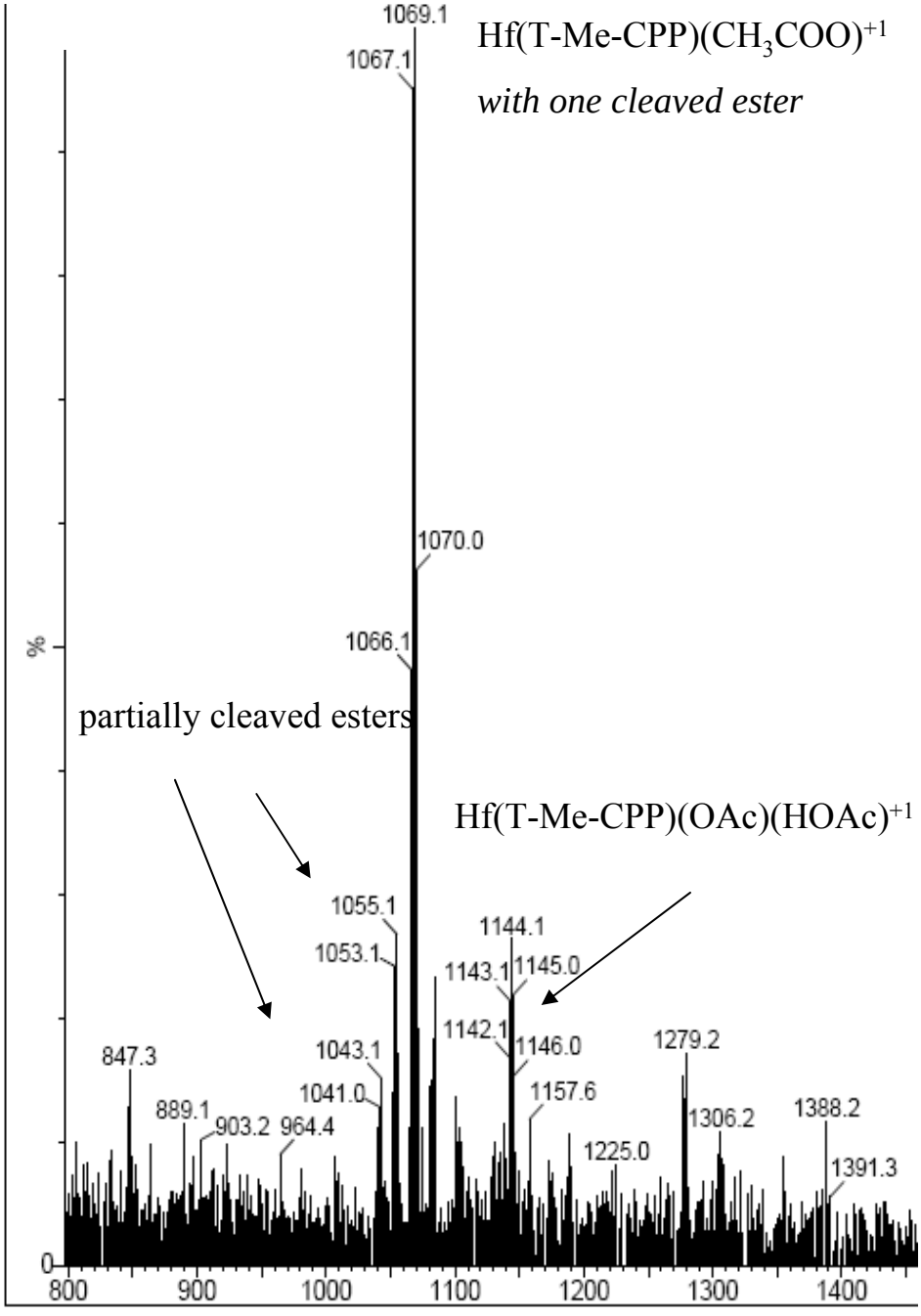

Figure 42.

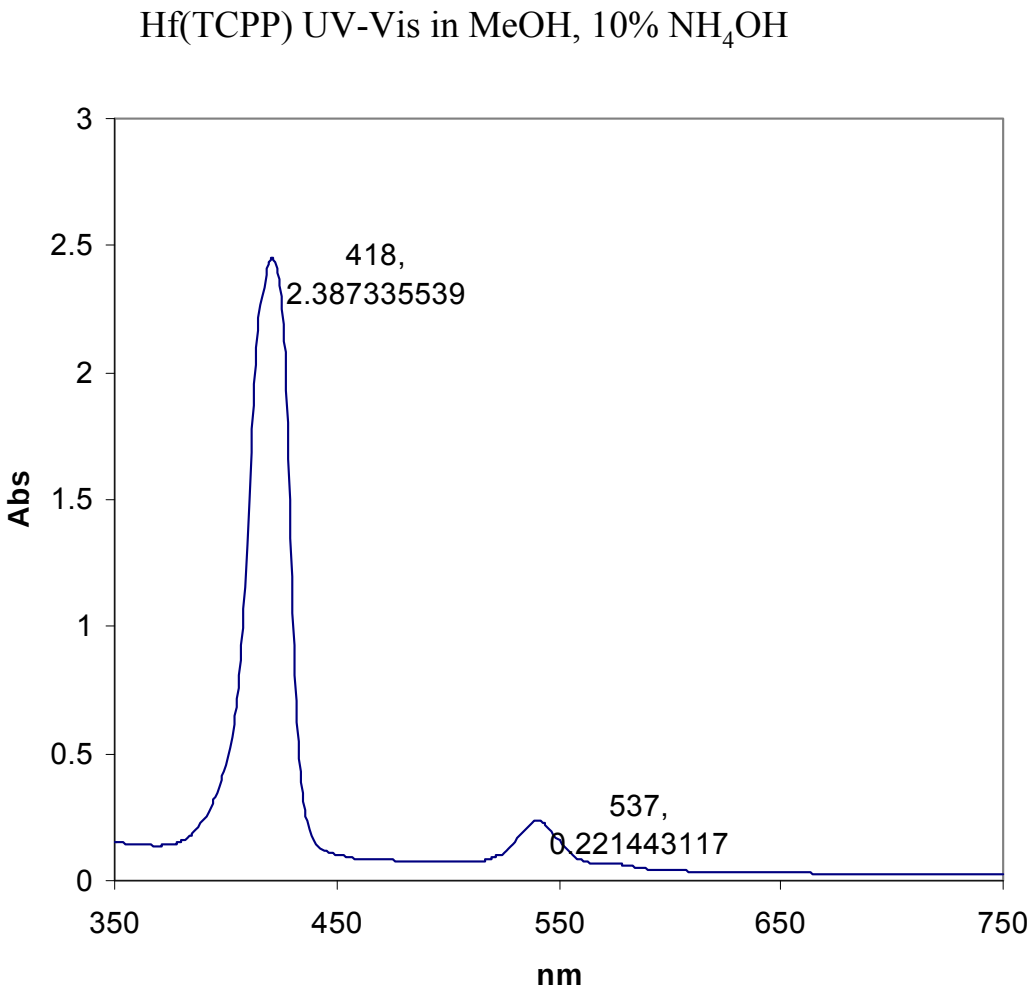
Hf(TCPP) UV-Vis in MeOH, 10% NH4OH
Abs
nm
418, 2.387335539
537, 0.221443117
3
2.5
2
1.5
1
0.5
0
350
450
550
650
750

Figure 43.

Hf(TCPP) MALDI-MS in dithranol matrix
as Hf(TCPP)$(C_{14}O_3H_9)^{+1}$

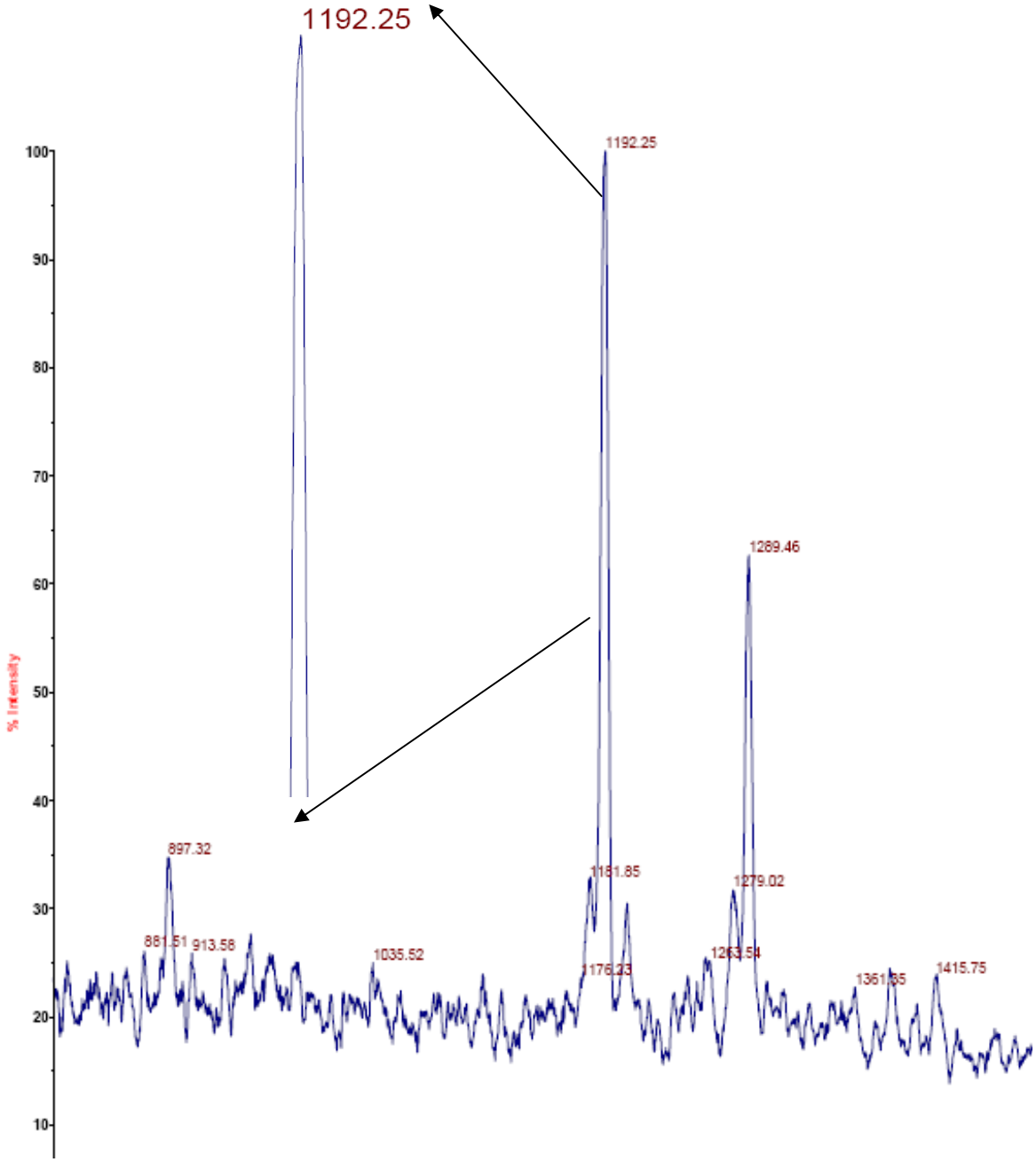

Figure 44.

Results of **Method 4** implemented on H_2TCPP and H_2TPyP

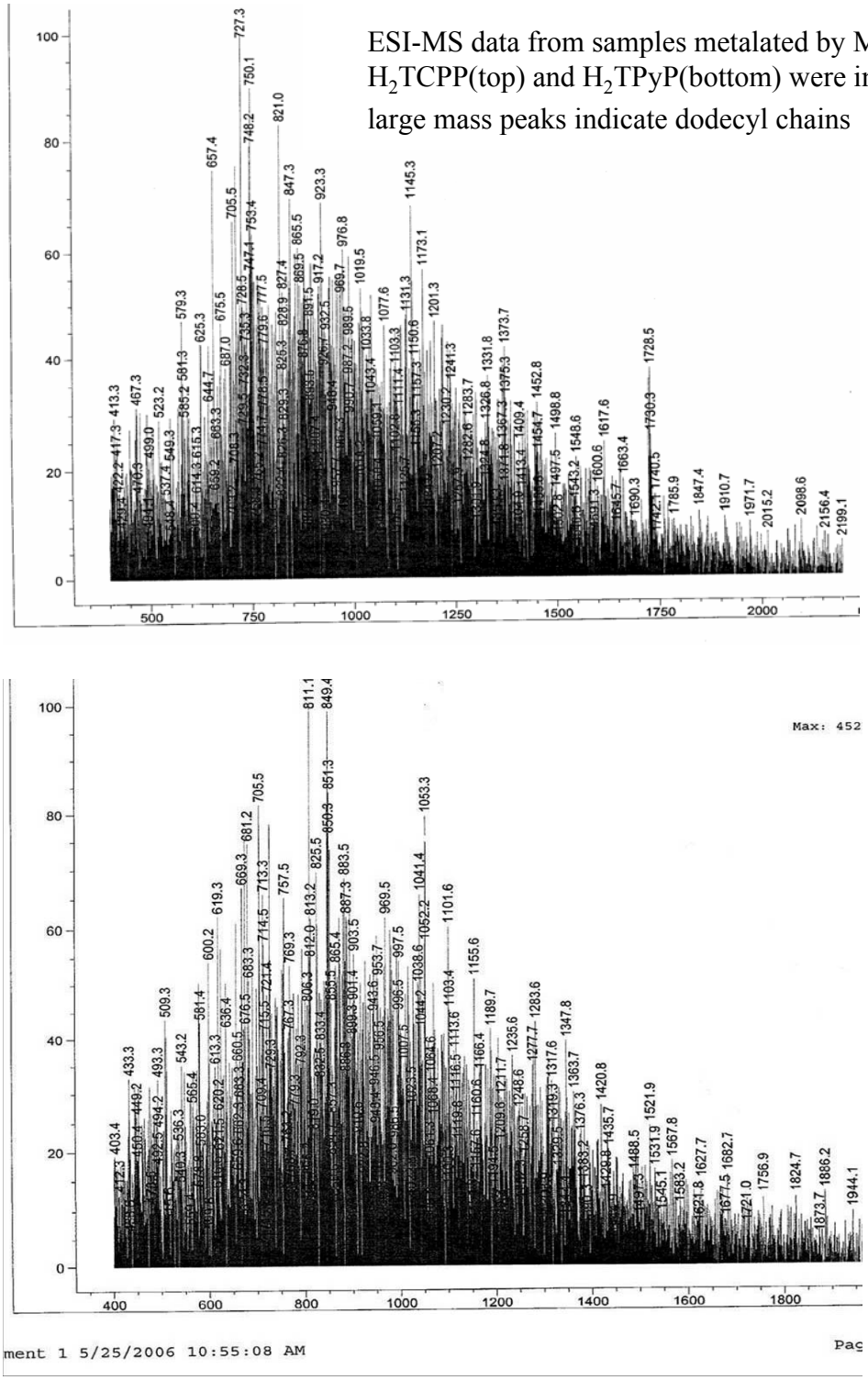

Figure 45a.

$[Hf(TPP)]_2(\mu\text{-}\eta^2\text{-}O_2)_2$ fluorescence emission spectra in CH_2Cl_2

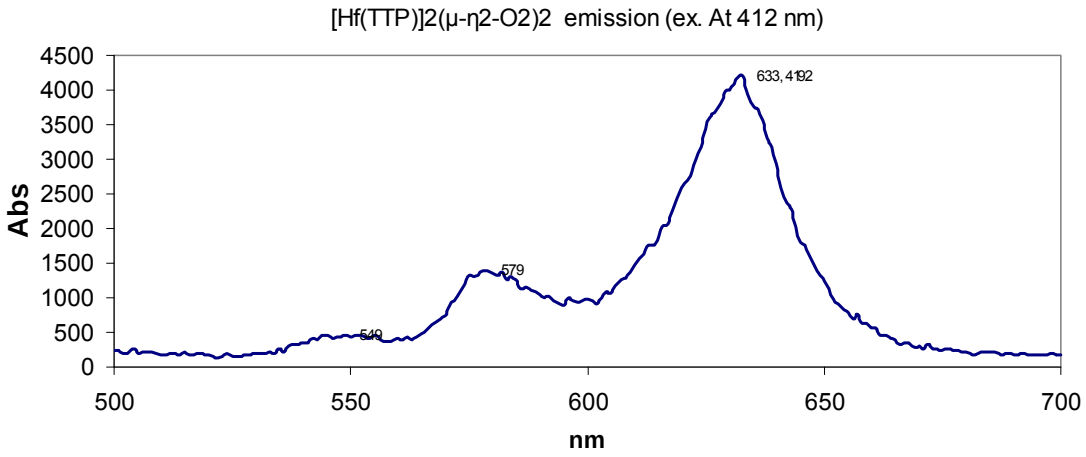

Figure 45b.

$[Hf(TPP)]_2(\mu\text{-}\eta^2\text{-}O_2)_2$ in CH_2Cl_2 excitation spectrum

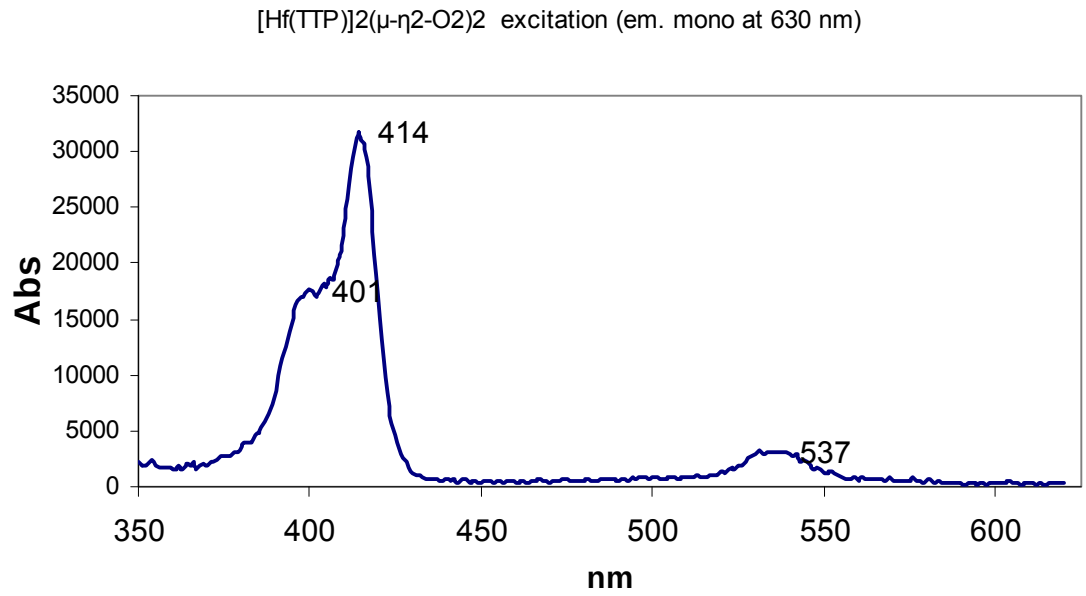

Figure 46a.

$[Hf(TPP)]_2(HPO_4)_2$ fluorescence spectrum

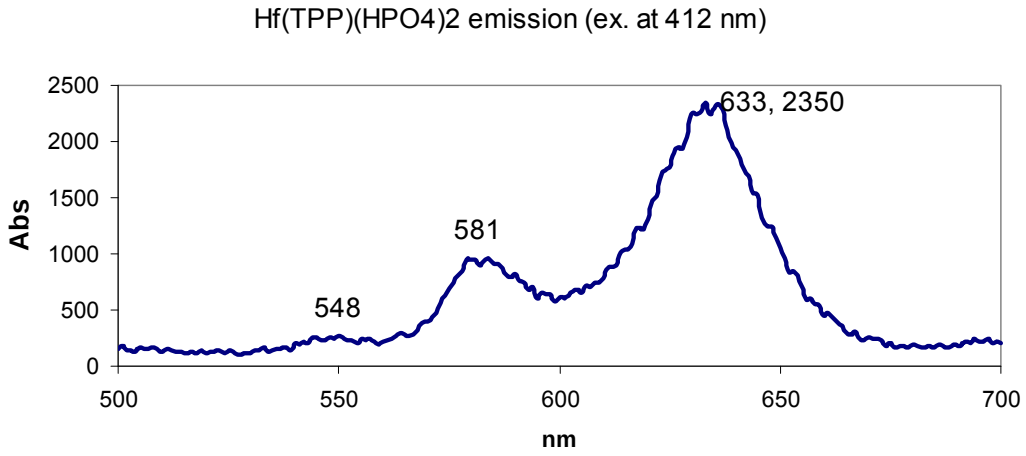

Figure 46b.

$[Hf(TPP)]_2(HPO_4)_2$ excitation spectrum

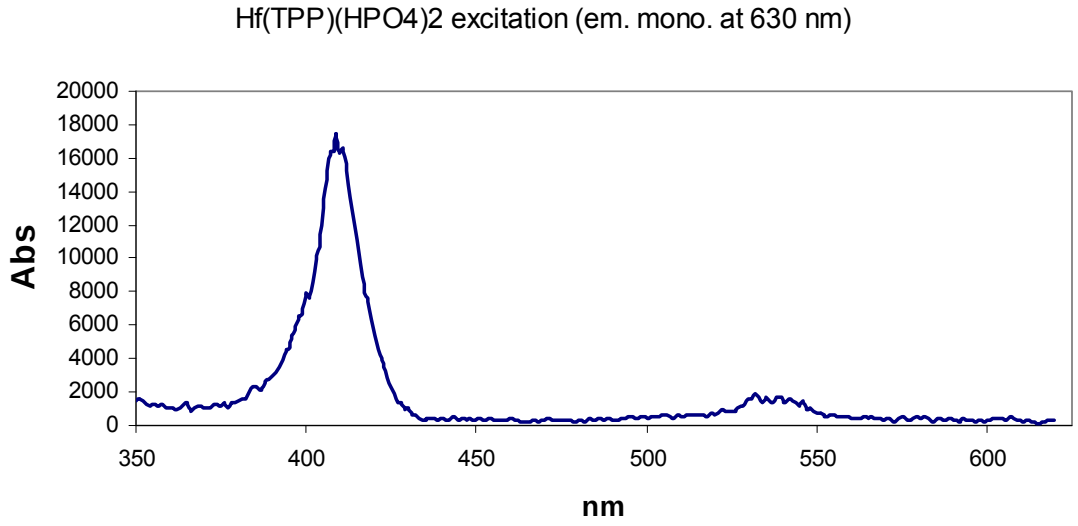

Figure 47. Hf(TPP)$(SO4)_2$ emission (ex. At 412 nm)

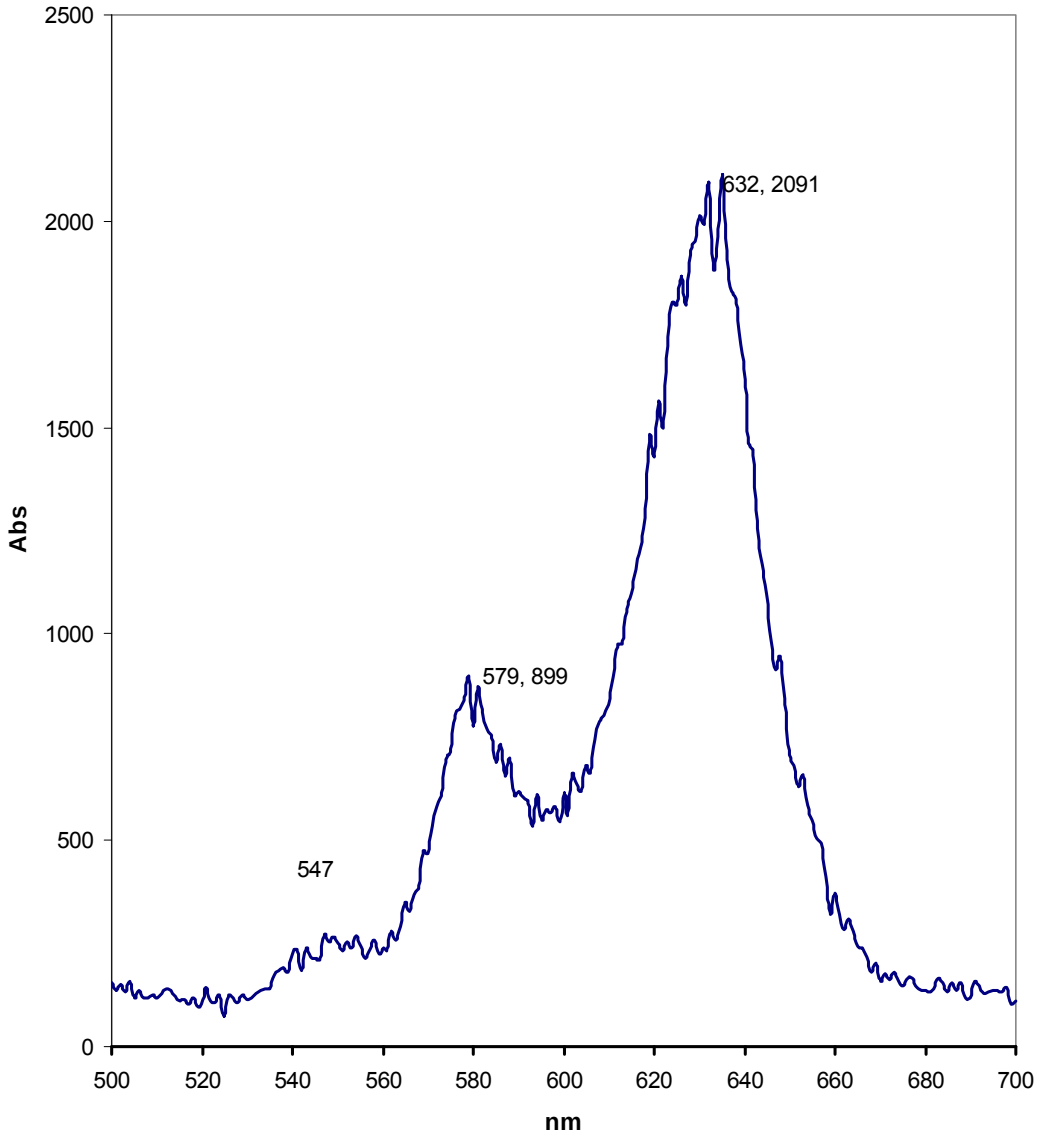

Chapter 3

Synthesis and Characterization of the First Porphyrinato Hafnium(IV) Lacunary, Keggin Polyoxometalate Ternary Complexes: Crystal Structure of the meso Tetra (4-pyridyl)-porphyrinato-Hafnium(IV)$PW_{11}O_{39}^{-5}$

Abstract

We report the synthesis and characterization of the first two porphyrinato-transition metal polyoxometalate ternary complexes, where the porphyrins are meso tetraphenylporphyrin (TPP), and meso tetra(4-pyridyl) porphyrin (TPyP), metalated with a hafnium(IV) ion. The polyoxometalate, POM, is the lacunary Keggin structure, $H_3PW_{11}O_{39}^{-4}$. The large hafnium ion rests outside the porphyrin core allowing the lacunary site on the POM to bind the remaining coordination sites of the hafnium to form (TPP)$HfPW_{11}O_{39}[TBA]_5$, **1** and (TPyP)$HfPW_{11}O_{39}[TBA]_5$, **2** where [TBA] is the tetrabutyl ammonium cation. The synthesis proceeds by a simple mixture of the Hf(por)OAc_2 starting complexes with $H_3PW_{11}O_{39}[TBA]_4$ in a mixed solvent of acetonitrile, CH_3OH and CH_2Cl_2. Characterization of the complexes shows distortion of the hafnium porphyrinate portion of the complex while the POM retains its rigid structure. This is displayed clearly in the NMR spectra and in the crystal structure of the (TPyP)$HfPW_{11}O_{39}^{-5}$ complex.

Introduction

Polyoxometalates (POMs) and porphyrins are the subject of study for many chemists, each having an enormous potential for structural variation and tuning of their electronic properties. POMs have been shown to have a wide range of applications such as catalysts,[1, 2] medical imaging agents,[3, 4] optical components, and electrochemical fuel cells, which utilize their rich redox chemistry,[5] to name a few. They are easy to make using inexpensive metal oxide salts.

Porphyrins have displayed a wide variety of uses as well. Their primary function as light absorbing dyes is readily observed in the form of chlorophyll in photosynthesis. Other natural porphyrins such as the heme, in hemoglobin, are efficient oxygen carriers in the blood and cyanocobalamin, B_{12}, is involved in crucial organometallic enzyme catalyzed reactions. Research with synthetic porphyrins extends into fields such as photovaltaics,[6, 7] supramolecular chemistry,[8-10] photodynamic light therapy in cancer research,[11] and molecular sieves in their crystalline form.[10, 12, 13] In addition, porphyrins are easily modified and a wide variety of meso tetra aryl porphyrins bearing various functional groups from biomolecules, such as sugars, to thiols, pyridyls, and carboxylic moieties are readily available.

In this work we report the synthesis and characterization of discrete, ternary metalloporphyrin-POM complexes where a transition metal ion is bound both to the porphyrin core and to the lacunary Keggin structure, $PW_{11}O_{39}^{-7}$. The premier examples of these new complexes use Hf(IV) to join meso tetraphenylporphyrin (TPP), and meso-

tetra (4-pyridyl) porphyrin to the Keggin framework to form (TPP)HfPW$_{11}$O$_{39}$[TBA]$_5$, **1**, and (TPyP)HfP$_{11}$O$_{39}$[TBA]$_5$, **2**. Previous research has shown electrostatic interaction between positively charged porphyrins and POMs.[14] This is especially interesting for the prospect of coupling the electronic properties of the porphyrin chromophore into the electron-rich Keggin PW$_{11}$O$_{39}^{-7}$ framework.

Previously, Keggin structures have been functionalized with cyclopentadienyl ligands at the lacunary site through Ti(IV), Zr(IV), and/or Hf(IV) metal ions.[3, 4, 15, 16] This provided some potential for functionalizing POMs with a range of biomolecules for applications such as transmission electron microscopy. The process of functionalizing these cyclopentadienyl ligands is exhaustive and results in low yields. Porphyrins offer a much greater potential to append a large range of multi-functional substituents. The synthesis is simple and procedes in higher yields.

There is a broad range of optical, photonic, and catalytic properties for porphyrins, and POMs are used as (photo)catalysts, ion conducting materials, and sensors. The hafnium metal center allows electronic coupling of the porphyrin and the POM. Since POMs are used as models for oxide surfaces, these complexes act as a model for some photovoltaic devices which function by charge injection into a semiconductor layer, such as TiO_2, from an organic dye in the excited state.[17, 18] Characterization of the binding moiety of the electron transport properties between the dye and the surface of the semiconductor is a key factor in engineering efficient solar energy conversion devices. Our structural studies of the porphyrin-POM ternary complexes have the potential to give insight into the nature of hafnium porphyrinate, Hf(P), binding to oxide surfaces.

Discussion

Synthesis:

The hafnium porphyrinate starting materials, $Hf(TPP)OAc_2$ and $Hf(TPyP)OAc_2$, can be synthesized according to literature methods[19] (for the TPP complex only) or as we have previously described.[20] The free lacunary Keggin polyoxometalate, $H_3PW_{11}O_{39}[TBA]_4$ was provided by the lab of Dr. Lynn Francesconi. Extensive characterization allows the spectroscopic properties of both the POM and porphyrinate portions of the complexes to be observed.

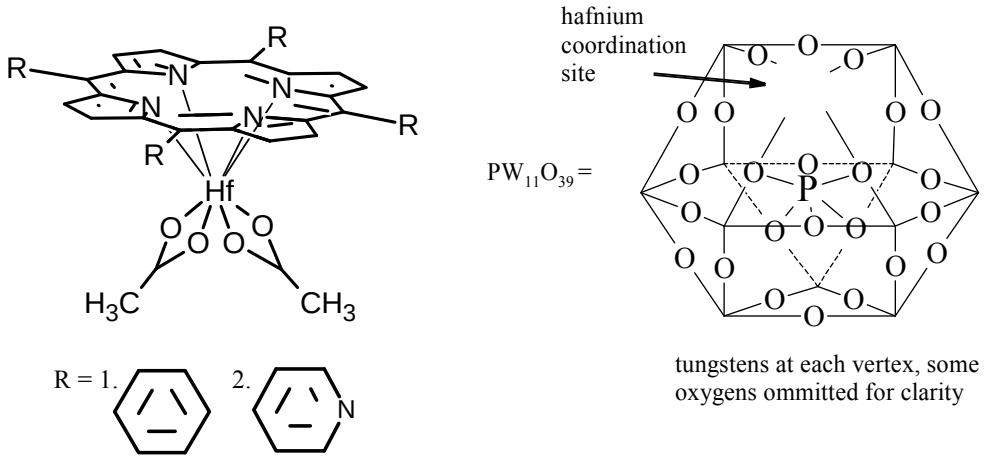

Figure 1 Illustration of the hafnium porphyrinate and POM starting complexes

The synthesis of the POM-porphyrin ternary complex is quite simple and only requires the exchange of the acetate ligands on the hafnium porphyrinate complex for the free oxygens on the lacunary site of the POM. The $Hf(P)OAc_2$ and POM starting complexes are dissolved separately and a stoichiometric amount of the POM solution is added dropwise to the porphyrin solution. The acidic protons on the binding oxygens in the lacunary site of the POM can cause some demetalation of the porphyrin, so the POM solution must be buffered by a base such as triethylamine before adding it to porphyrinate

solution. In addition, the formal charge of the ternary complex is +5 requiring one additional equivalent of [TBA]Br to be added to the mixture to yield the neutral (por)$HfPW_{11}O_{39}[TBA]_5$ complex. The binding of the POM is very strong as a result of the chelating effect of the four oxygens to the oxophilic Hf(IV) center. Addition of more than 1 equivalent of POM led to a high degree of porphyrin demetalation most likely leading to the $HfPW_{11}O_{39}^{-3}$ or the dimer $Hf(PW_{11}O_{39})_2^{-10}$ complexes. POM dimerization around lanthanides[21, 22] and zirconium[23] ions has been reported and is a significant factor in considering the general reaction equilibria of the products. ^{31}P NMR spectra of sample contaning excess POM shows multiple peaks near -10 ppm for the porphyrin free $HfPW_{11}O_{39}$ monomers and dimers in addition to the singlet peak for the target ternary complex at -16.2 ppm (see appendix). Thus, excess POM does not serve well to drive the desired reaction to completion.

In our previous work,[20] with $Hf(P)OAc_2$ complexes, the Hf-N bonds were observed to be very resistant to strong acids, bases, and high temperatures while the acetate ligands were easily exchanged. Thus it was surprising to observe the easy demetalation of the porphyrinates by an excess of POM. It is apparent from the large shift in the UV-Vs spectrum and physical characteristics of the crystal structure (*vide infra*) that the hafnium ion, which sits outside of the porphyrin core, is drawn even further from the mean plane of the pyrrolic nitrogens, thus, weakening the N-Hf bonds. Protic acids, such as dilute HCl, which do not demetalate the $Hf(P)OAc_2$ starting complex, instantly demetalates the porphyrin when added to a solution of the (P)Hf $PW_{11}O_{39}^{-5}$ complex.

In addition the (TPyP)Hf $PW_{11}O_{39}^{-5}$ complex appears to be more stable than the (TPP)Hf $PW_{11}O_{39}^{-5}$ complex. When 100 μMol, CH_2Cl_2 solutions of each complex was prepared and left out of direct light, the TPP complex completely demetalated within three weeks while only a fraction of the TPyP showed any sign of degradation. The peripheral pyridyl groups of the TPyP donate electron density to porphyrin which may strengthen the Hf-N bonds compared to the Hf(TPP) framework.

The unique solubility of the ternary complex in neat CH_2Cl_2 was surprising considering the highly charged POM framework. By dissolving the dried reaction residue in neat CH_2Cl_2 we are able to easily filter any impurities such as salts of the POM ($H_3PW_{11}O_{39}^{+4}$, Hf(IV)$PW_{11}O_{39}^{+3}$, or Hf(IV)$[PW_{11}O_{39}]_2^{-10}$). Precipitation of the CH_2Cl_2 solution, using a moderate amount of hexanes, leaves the trace amount of either free-base or hafnium porphyrinate not bound to a POM, in the supernatant. The UV-Visible spectra of the free-base porphyrin , hafnium-porphyrinate, and the target ternary complexes are readily distinguished.

Characterization:

The formation of the ternary complex was monitored by the UV-Vis absorption spectra of the porphyrinate portion of the complex. Both the Soret and Q-band regions of the spectrum displays a significant red shift as the reaction progresses. The Soret bands at 412 nm and 414 nm for the Hf(TPP)OAc_2 and Hf(TPyP)OAc_2 complexes shift to 425 nm and 426 nm for the ternary complex. The major Q-band near 540 nm shifts to 550 nm-548 nm. This indicates a structural change in the hafnium porphyrinate complex as the POM binds to the hafnium ion. As indicated by the NMR and crystal structure this

change includes a lengthening of the Hf-N bond and distortion of the porphyrin macrocycle as the POM encompasses a large portion of hafnium coordination sphere, drawing the metal center away from the porphyrin macrocycle.

The IR spectra for both complexes show distinctive features that indicate metalation of the lacunary site of the POM, most notably by the PO_4 region, 1000-1100 cm^{-1}.[15] For the unmetalated lacunary site, the reduced symmetry of the PO_4 results in two distinct bands, while metalation with hafnium forms an approximate symmetry similar to that of the $PW_{12}O_{40}$ and only a single band is observed for both the TPP and TPyP ternary complexes. The IR spectra of both ternary complexes match closely with those reported for the $[\eta^5\text{-}C_5(CH_3)_5]HfPW_{11}O_{39}^{4-}$ analogs [15].

Electrospray ionization mass spectroscopy, ESI-MS, was useful in identifying the complexes. The ionization process for both methods results in a cleavage of a O^{-2}unit, lost as a H_2O molecule, from the POM to alter the $(por)Hf[PW_{11}O_{39}]^{-5}$ complex to become a mono-protonated $(por)Hf[PW_{11}O_{38}]^{-3}$ complex displaying a peak at m/*z* of 3453/2 = 1726, and 3456/2 =1728, for the TPP and TPyP ternary complexes respectively. This type of decomposition has been observed in other polyoxometalate ESI-MS.[24]

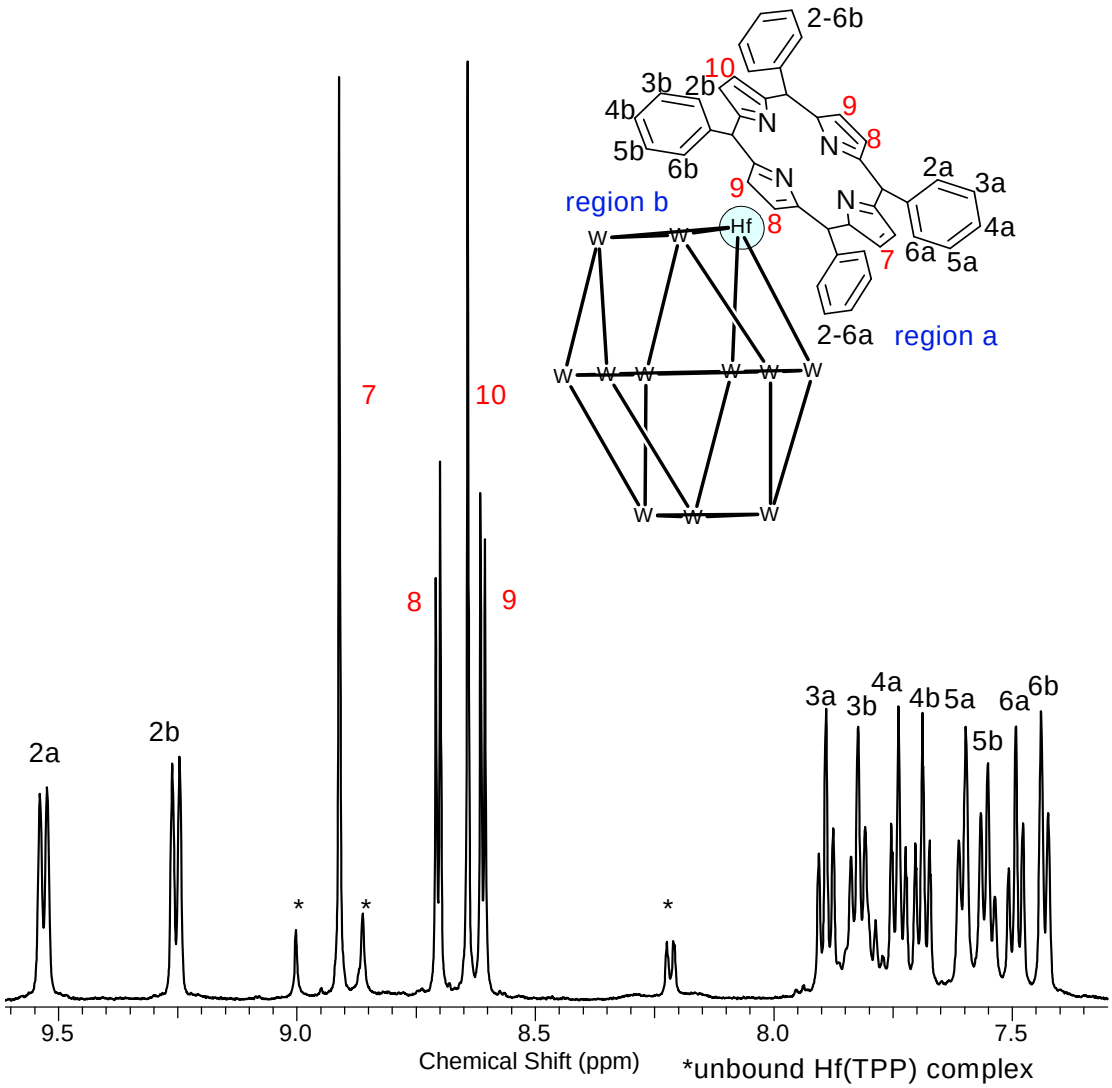

Figure 2. H^1 NMR of the (TPP)HfPW$_{11}$O$_{39}$[TBA]$_5$ complex aromatic region. Shifts are assigned according to the given chemical structure of the complex with the POM portion simplified for clarity.

H^1-NMR spectra for both complexes were taken in CD_3CN on a 500MHz Bruker NMR spectrometer. These spectra show a significant change in the proton resonances for the ternary

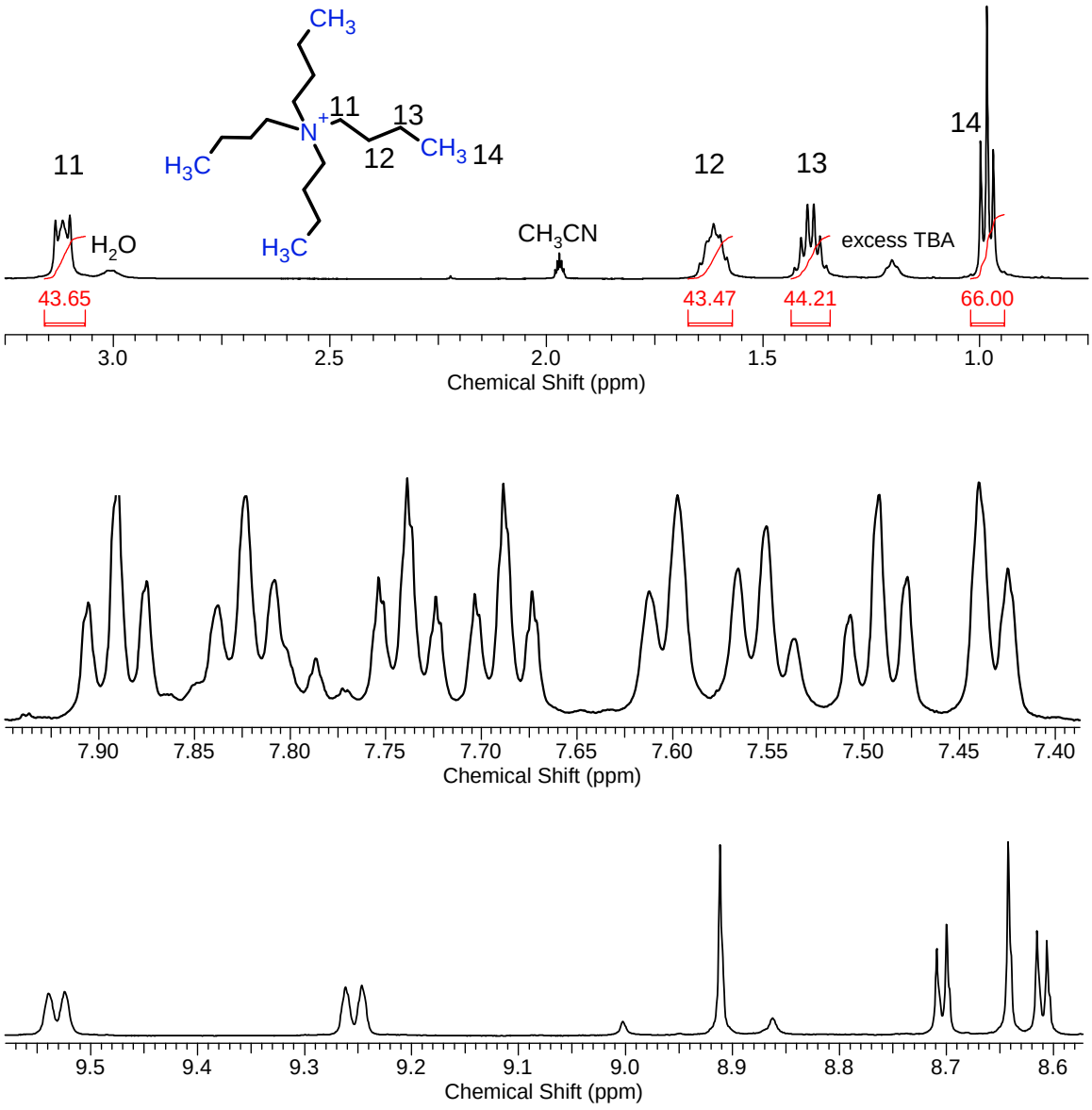

Figure 3. Aliphatic region(top) showing integral values of the methylene and methyl protons of the TBA counter cations displays appropriate values for 5 equivalents of TBA for the (TPP)HfPW$_{11}$O$_{39}$[TBA]$_5$ complex. Magnified display(middle and bottom) of the aromatic region showing well resolved peaks for all aryl proton resonances.

complexes compared to the Hf(P)OAc$_2$ starting complexes. Proton assignment was confirmed by COSY 2D spectra and comparison of data between the two complexes. **Figure 2** shows the H^1 NMR aromatic region of the TPP ternary complex. The two pairs of *ortho* and *meta* protons on each phenyl substituent are non-equivalent due to the

hafnium and POM complexation generating five distinct peaks. In addition, the phenyl substituents in region **a** compared to region **b** are not equivalent due to a non-parallel geometry between the porphyrin macrocycle and the mean O_4-plane of the lacunary oxygens, thus the four porphyrin phenyl groups display a total of 10 distinct peaks, 2a-6a and 2b-6b. Our assignment of the peaks where those protons facing to "outside" of the complex labeled 2a, 2b, 3a, and 3b are considered to be in the endo position similar to the proton assignment of $Ce(P)_2$ complexes[25, 26] where the porphyrin distortion turns these protons upwards into the ring current of the porphyrin causing a downfield shift. The distortion for the $(P)HfPW_{11}O_{39}[TBA]_5$ complexes are less severe than that found with $Ce(P)_2$ so the endo-*o* protons are the most affected while the endo-*m* protons are only moderately affected. The opposite protons, in the exo positions, are turned away from the ring current and are shifted upfield despite their more proximal position to the metal center and the POM. The *p*-positioned protons are neither shifted upfield or downfield, thus they are found directly between the endo and exo proton resonances. The integration shown in **Figure 3** verifies five TBA counter cations on the complex. The aryl and pyrrolic proton assignments are confirmed by the COSY spectrum of this complex (**figure. 4)** and our experience with metalloporphyrins coordinated to out-of-plane metal ions.[20, 27]

The four pyrrole regions also display non-equivalent peaks. The pyrrolic protons facing directly into region **a** display a singlet peak labeled **7**. The peak labeled **10** is a singlet peak for the pyrrolic protons facing directly into region **b**. The other two pyrroles straddle the division between region **a** and **b**, so the protons labeled **8** and **9** are split into a doublet of doublets.

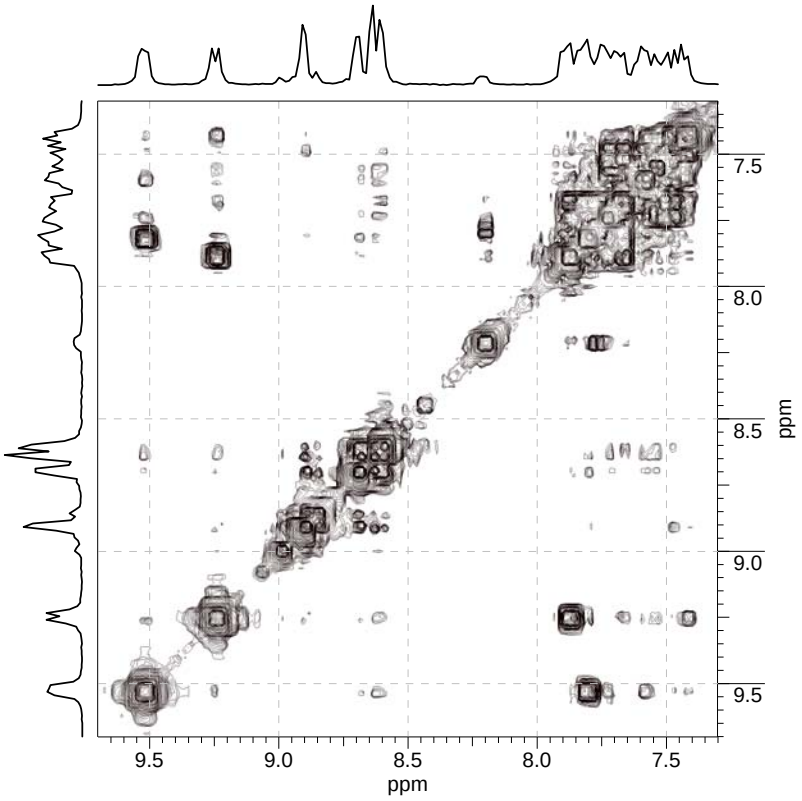

Figure 4. COSY spectrum of the (TPP)$HfPW_{11}O_{39}[TBA]_5$ complex

The ^1H NMR spectra of the (TPyP)$HfPW_{11}O_{39}[TBA]_5$ complex is very similar showing eight distinct aryl resonances and four pyrrolic resonances similar to those found with the TPP ternary complex (see appendix). The *meta*-proton resonances of the TPyP ternary complex are all shifted downfield in comparison to the *meta*- proton resonances of the TPP ternary complex due to their proximity to the pyridyl nitrogen.

^{31}P NMR for both the TPP and TPyP ternary complexes display a singlet peak at -16.20 and -16.25 ppm, respectively, in comparison to the cyclopentadienyl analog which displays a peak at -12.3 ppm.[15] There is a smaller peak at -16.59 ppm that may arise from exchange of TBA cations or porphyrin conformational changes (see appendix). This confirms that we find our phosphorus peak in the appropriate scale to other reported

ternary complexes of the $PW_{11}O_{39}$ framework. The porphyrin-free $HfPW_{11}O_{39}^{-3}$ complex displays a ^{31}P-NMR peak at -14.67 ppm.[20]

Crystallography

Suitable crystals for X-ray diffraction were obtained for the $(TPyP)HfPW_{11}O_{39}^{-5}$ complex. 50 mg of the complex was dissolved in 5 mL of a 1:1, CH_3CN:CH_3OH, solution in a 18 x150 mm test tube with a magnetic stir bar. Diethyl ether was added via pipet while stirring until the solution appeared cloudy. The solution was then placed in a warm water bath to evaporate just enough of the ether to make the solution *almost* clear of particulates. The solution was capped and placed in a freezer for four days after which time long, dark purple needles collected on the sides and bottom of the test tube.

The structure of the Hf(TPyP) portion of the ternary complex shows an interesting deviation from the structure of the $Hf(TPyP)OAc_2$ we reported earlier.[2] The porphyrin core adopts a saddle type distortion and the four inner pyrrole N-atoms deviate from the C_{20}-macrocycle towards the Hf ion, which lies above it. The distance of the hafnium from the mean N_4-plane is 1.218Å which is notably different than the 1.036Å deviation measured for the $Hf(TPyP)OAc_2$ complex. The average N-Hf bond length is 2.335Å compared to 2.264Å for the acetate derivative, further illustrating the affect of the POM on the hafnium coordination to the porphyrin core. These structural differences confirm our hypothesis that the large red shift in the UV-Visible spectrum is a result of the POM coordination drawing the hafnium ion further away, and a result of greater porphyrin distortion.

The structure of the $PW_{11}O_{39}$ portion of the complex is similar to previously reported structures of zirconium and hafnium Keggin and Wells-Dawson POMs.[15, 28] The

monovacant structure binds to the hafnium in a slightly asymmetrical fashion where the hafnium deviates from the mean O_4-plane by 1.145Å. The Hf-O bond varies between 2.20Å and 2.15Å, which is nearly identical to the reported $[(HfPW_{11}O_{39})_2]^{-10}$ dimer complex and clearly illustrates that the nature of lacunary site bonding to the hafnium ion is independent of the porphyrinate framework. There is no detectable structural perturbation in the POM as a result of the adjoining tetrapyrrole system.

The entire coordination around the hafnium ion assumes an antiprismatic geometry where the N_4 plane of the porphyrin and the O_4 plane of the lacunary site form the two square faces. The porphyrin is situated above the POM such that the four pyrroles are aligned with the spaces between the lacunary oxygens. There is, however, a 3.1° dihedral angle between the mean N_4 and O_4-planes which quantifies the amount by which these two planes are not perfectly parallel. Thus, the porphyrin is tilted towards the POM on one side. This tilt, in combination with the asymmetric coordination of the hafnium into the lacunary site on the POM, accounts for the non-equivalent aryl protons observed in the NMR spectra.

The packing scheme for the $(TPyP)HfPW_{11}O_{39}^{-5}$ complex is comprised of the complex forming zig-zag chains along the *a*-axis where the top surface of one porphyrin approaches the side of the POM of an adjacent complex. The porphyrin core is in line with the hafnium ion of the neighboring complex at an angle of approximately 78°. The pattern repeats itself by every two units along the chain, over a distance of 9.42Å. When viewing down the *a*-axis the distribution of the straight chains are observed to be widely spaced with solvent filled channels in between containing disordered CH_3CN, TBA^{+1}, CH_3OH, and Et_2O (**figure 6)**. We only find 2 TBA units for every ternary complex

which indicates that the charge balance is accounted for, in part, by protonation. This protonation may occur on the pyridyl groups themselves acting as a built in buffer system for the naturally acidic complex. This may also explain another reason why the (TPyP)HfPW$_{11}$O$_{39}^{-5}$ complex is more stable than the analogous TPP complex.

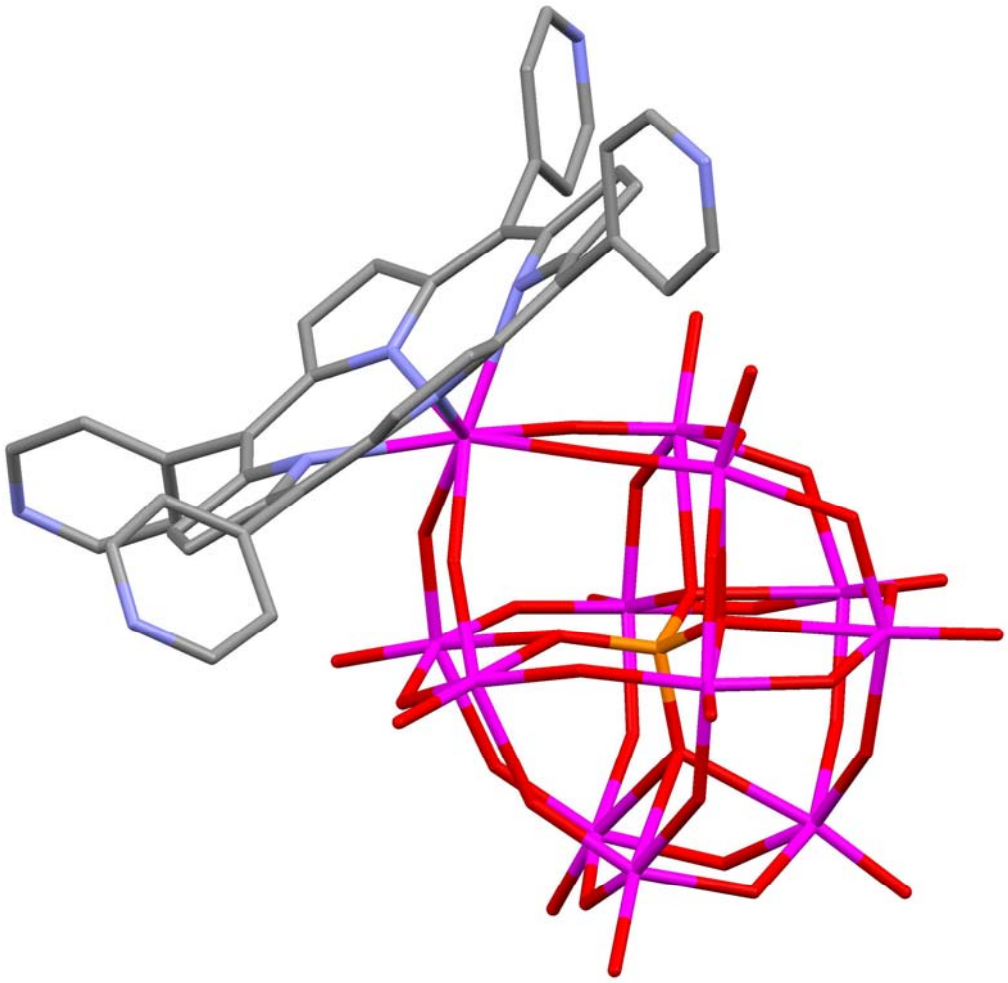

Figure 5 Crystal structure of the (TPyP)HfPW$_{11}$O$_{39}^{-5}$ complex. Note the asymmetric coordination of the hafnium ion to the lacunary site on the POM and the slight tilt of the porphyrin.

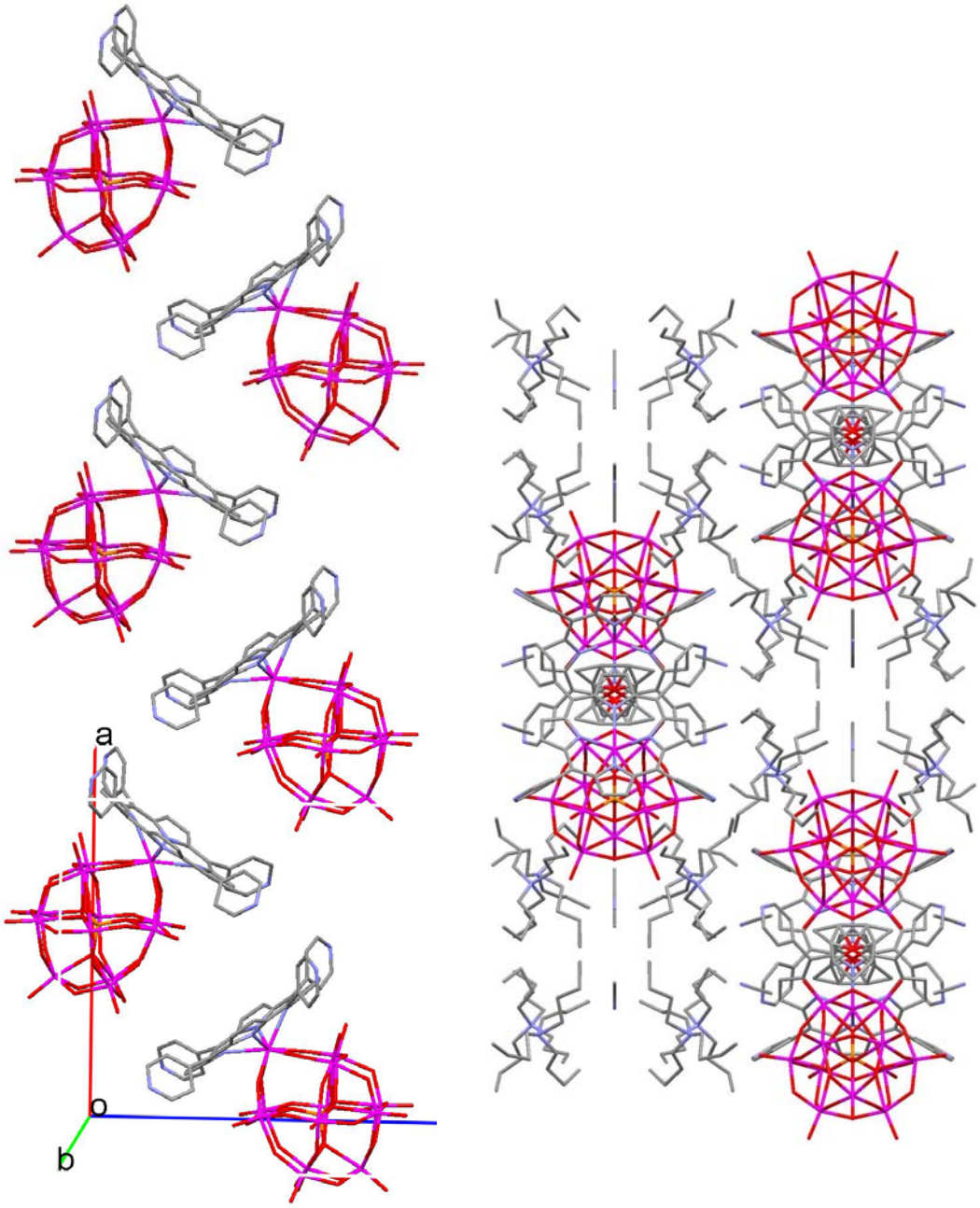

Figure 6 Crystal packing of the (TPyP)HfPW$_{11}$O$_{39}^{-5}$ complex shows formation of the zig-zag pattern along the *a*-axis, solvent omitted (left). Viewing down the *a*-axis (right) the distribution of the chains and the solvent filled channels between them can be seen.

Table 1 Crystallographic data, selected bond lengths, and deviation of the Hf(IV) ion from coordinating O_4 and N_4 planes for $Hf(TPyP)PW_{11}O_{39}$

Crystallographic data	
Compound	$(TPyP)HfPW_{11}O_{39}$
emp form	$C_{58.5}$ $H_{99.75}$ $Hf_{0.5}$ $N_{7.25}$ $O2_{0.50}$ $P_{0.5}$ $W_{5.5}$
formula wt.	2348.61
cryst. system	orthorhombic
space group	Pnma
unit cell	15632.(5)
a/ Å	19.419(4)
b/ Å	27.157(5)
α/ Å	29.642(6)
β/°	90
γ/°	90
V/ $Å^3$	90
Z	8
ρ_{calcd} [$Mgcm^{-3}$]	1.996
μ(MoKα) mm^{-1}	8.800
T/°K	100(2)
F(000)	8928
crystal size (cm)	0.3x0.18x0.18
Θ range[°]	1.73 to 27.50
index ranges	$-14 \le h \le 25$
	$-33 \le k \le 35$
	$-39 \le l \le 31$
reflns collected	74669
ind. reflections	18158
R(int)	0.1434
completeness to Θ_{max} [%]	99.0
reflns gt	10336
data/restraints/parameters	18158/14/719
final R indices [$I > 2\sigma(I)$]	
*R*1	0.0915
*wR*2	0.1729
R indices (all data)	
*R*1	0.1755
*wR*2	0.1729
largest diff. peak and hole [$eÅ^{-3}$]	3.169 and -1.669

Selected bond lengths (Å)	
Hf-N	2.344 – 2.327
Hf-O	2.203 – 2.150
$W\text{-}O_L$ [a]	1.758 – 1.784
W=O	1.684 – 1.724
$W\text{-}O_b$ [b]	1.844 – 2.087
$W\text{-}O_P$ [c]	2.296 – 2.459
P-O	1.501 – 1.567

Deviation of the Hf from the mean plane of the N_4(pyrrole) and O_4(lacunary)	
$Hf - N_4$	1.2177Å
$Hf - O_4$	1.1451Å

a $W\text{-}O_L$ bond length to the lacunary oxygen

b $W\text{-}O_b$ bond length to bridging oxygen

c $W\text{-}O_P$ bond length to oxygen from the central phosphate ion

Experimental

1. *meso-tetraphenylporphyrinato Hafnium(IV)$PW_{11}O_{39}$ tetra-butyl ammonium salt* **(TPP)Hf($PW_{11}O_{39}$)[TBA]$_5$** 20 mg of Hf(TPP)OAc_2 (910 g/mol, 0.022 mmol)was dissolved in 10 mL of a 1:1 mixture of CH_2Cl_2: CH_3OH in a 18 x150mm test tube with a magnetic stir bar at room temperature. 76 mg of $H_3PW_{11}O_{39}[TBA]_4$ (3650 g/mol, 0.021 mmol) and 5 mg of [TBA]Br was dissolved separately in 5 mL of acetonitrile, 1% v/v triethylamine. The resulting clear solution was added dropwise over the course of 5 minutes to the stirring hafnium porphyrinate solution. The reaction was monitored by UV-Visible spectroscopy, where the presence of the ternary complex is signified by a large red shift in the porphyrin Soret band from 414 nm to 425 nm, over the course of one hour. The solution was then removed under vacuum and the residue was dissolved in a minimal volume of CH_2Cl_2, ca. 4 mL, and filtered of a miniscule amount of insoluble salts. The product was precipitated with 25 mL of hexanes and collected on a filter. The product was allowed to dry initially in air and then under vacuum without heat to yield 91 mg, 98% yield, of **(**TPP)Hf$PW_{11}O_{39}[TBA]_4$**.** IR (Nujol NaCl) 1100-700 cm^{-1}, 1063(m, br.), 958 (m), 890 (wk), 816 (s., br.) 723 (m) UV-Vis CH_2Cl_2 λ_{max} nm (log ϵ) 403(4.51), 425(5.53), 508 (3.40), 548(4.21), 583 (3.30) H^1-NMR (ppm) CD_3CN, 30 $^{\circ}$C 9.53 (d, 2H- phen-*o*), 9.25 (d, 2H phen-*o*), 8.91(2H pyrrole), 8.71 (d, 2H pyrrole), 8.64 (s, 2H pyrrole), 8.61(d, 2H pyrrole), 7.89(t, 2H phen-*m*), 7.82 (t, 2H phen-*m*), 7.75 (t, 2H phen-*p*), 7.69(t, 2H phen-*p*), 7.60(d, 2H phen-*o*), 7.55(t, 2H phen-*m*), 7.49(t, 2H phen-*m*), 7.43(d, 2H phen-*o*), 3.12 (m. 40H N-CH_2-), 1.61 (m. 40H -CH_2-),

1.38 (m. 40 $–CH_2$-), 0.98 (t. 60H $–CH_3$) P^{31} NMR (CD_3CN) -16.29ppm Negative ES Mass spectroscopy for (TPP)Hf$(PW_{11}O_{38})^{-2}$ calc. m/*z* 1726.3 found 1726.4

2. *meso tetra-(4-pyridyl)-porphyrinato Hafnium(IV)$PW_{11}O_{39}$ tetra-butyl ammonium salt* **(TPyP)Hf$(PW_{11}O_{39})[TBA]_5$** 20 mg of Hf(TPyP)OAc_2 **(**914 g/mol, 0.022 mmol) was stirred with 75 mg of $H_3PW_{11}O_{39}[TBA]_4$ and 5 mg of [TBA]Br in the same solvents and procedure and described above. The reaction was complete after 20 minutes of stirring. The product was isolated by precipitating the target complex with 15 mL of hexanes from a 5 mL CH_2Cl_2 solution to yield 90 mg; 97% yield of the $H_3PW_{11}O_{39}[TBA]_5$. IR (Nujol NaCl) 1100-700 cm^{-1}, 1133 (wk.), 1076 (sh.), 1054 (s.), 949 (s), 880(m), 806 (vs. br.), 749 (sh) Vis CH_2Cl_2 λ_{max} nm (log ϵ) 402 (4.42), 426 (5.41), 505 (3.42), 550 (4.21), 582 (3.44) H^1-NMR (ppm),CD_3CN, 30 $^{\circ}C$ 9.50(br. s, 2H py-*o*), 9.18(d, 2H py-*o*), 9.08(d, 2H py-*m*), 9.02(d, 2H py-*m*), 8.94(s, 2H pyrrole), 8.78(br. d, 4H pyrrole and py-*m overlap*), 8.71(br. d., 4H pyrrole and py-*m overlap*), 8.68 (s. 2H pyrrole), 7.64(br.s., 2H py-*o*), 7.47(d, py-*o*), 3.14 (m. 40H N-CH_2-), 1.64 (m. 40H -CH_2-), 1.41 (m. 40 $–CH_2$-), 0.99 (t. 60H $–CH_3$) P^{31} NMR (CD_3CN) -16.25ppm, ESI-MS for (TPyP)Hf$PW_{11}O_{37}^{-1}$ calc. 3441 neg. ES found 3444.1; for (TPyP)Hf$PW_{11}O_{38}^{-2}$ calc. m/*z* 1728.2 neg. ES found 1728.7

Conclusions

The metalation of the lacunary $PW_{11}O_{39}^{-7}$ Keggin polyoxometalate with a hafnium(IV) porphyrinate complex yields a hybrid porphyrin-POM complex by a relatively simple procedure. The structure of the POM is the same as it appears in other reported structures of $HfPW_{11}O_{39}^{-3}$ complexes, indicating that the presence of the porphyrin has no effect on the rigid POM framework. The porphyrin chromophore is distorted into a domed structure and the Hf-N bonds are elongated relative to the parent $Hf(TPP)OAC_2$, these structural features shift the observed electronic transitions to lower energies as displayed by a red shifted UV-Visible absorption spectra. These complexes are the first of their kind to be reported and offer a potential venue to directly couple the light absorbing and electrochemical properties of porphyrinic systems with the complementary electrochemical and structural properties afforded by POMs.

References:

1. Dmitrenko, O.; Huang, W.; Polenova, T. E.; Francesconi, L. C.; Wingrave, J. A.; Teplyakov, A. V., *J. Phys. Chem. B* **2003,** 107, (31), 7747-7752.

2. Toth, J. E.; Anson, F. C., *J. Am. Chem. Soc.* **1989,** 111, 2444-2451.

3. Keana, J. F. W.; Ogan, M. D., *J. Am. Chem. Soc.* **1986,** 108, 7951-7957.

4. Keana, J. F. W.; Ogan, M. D.; LU, Y.; Beer, M.; Varkey, J., *J. Am. Chem. Soc.* **1986,** 108, 7957-7963.

5. Katsoulis, D. E., *Chem. Rev.* **1998,** 98, (1), 359-388.

6. Cherian, S.; Wamser, C. C., *J. Phys. Chem. B* **2000,** 104, (15), 3624-3629.

7. Tachibana, Y.; Haque, S. A.; Mercer, I. P.; Durrant, J. R.; Klug, D. R., *J. Phys. Chem. B* **2000,** 104, (6), 1198-1205.

8. Drain, C. M.; Chen., X., Self-Assembled Porphyrinic Nanoarchitectures. In *Encyclopedia of Nanoscience & Nanotechnology*, Nalwa, H. S., Ed. American Scientific Press: New York, 2004; Vol. 9, pp 593-616.

9. Drain, C. M.; Lehn, J.-M., *Chem. Commun.* **1994**, 2313-2315 (correction 1995, p503).

10. Drain, C. M.; Goldberg, I.; Sylvain, I.; Falber, A., *Top. Curr. Chem.* **2005,** 245, 55–88.

11. Chen, X.; Hui, L.; Foster, D. A.; Drain, C. M., *Biochem.* **2004,** 43, (34), 10918-10929.

12. Goldberg, I., *Chem. Comm.* **2005**, 1243-1254.

13. Goldberg, I., *Cryst. Eng. Comm.* **2002,** 4, 109-116.

14. Santos, I. C. M. S.; Rebelo, S. L. H.; Balula, M. S. S.; Martins, R. a. R. L.; Pereira, M. M. M. S.; Simoes, M. a. M. Q.; Neves, M. G. P. M. S.; Cavaleiro, J. e. A. S.; Cavaleiro, A. M. V.,*J. Mol. Catal. A: Chem.* **2005,** 231, (1), 35-45.

15. Babcock, L. M. Synthesis and Characterization of Group 4 Organometal Oxide Complexes. University of Illinois, Urabana-Champaign, 1988.

16. Kim, H. J.; Jung, S.; Jeon, Y. M.; Whang, D.; Kim, K.,*Chem. Comm.* **1997**, (22), 2201-2202.

17. K.Nazeeruddin, M.; Hunphry-Baker, R.; Officer, D. L.; Campbell, W. M.; Burrell, A. K.; Graetzel, M., *Langmuir* **2004,** 20, (15), 6514-6517.

18. Nazeeruddin, M. K.; Pèchy, P.; Renouard, T.; Zakeeruddin, S. M.; Humphry-Baker, R.; Comte, P.; Liska, P.; Cevey, L.; Costa, E.; Shklover, V.; Spiccia, L.; Deacon, G. B.; Bignozzi, C. A.; Graetzel, M., *J. Am. Chem. Soc.* **2001,** 123, (1613-1624).

19. Huhmann, J. L.; Corey, Y. J.; Rath, N. P.; Campana, C. F., *J. Organomet. Chem.* **1996,** 513, (1-2), 17-26.

20. Falber, A., Synthesis, Characterization, and Crystallography of Hafnium Porphyrinates. In Hunter College: New York, 2007; Vol. Chapter 2.

21. Luo, Q.; Howell, R. C.; Bartis, J.; Dankova, M.; William DeW. Horrocks, J.; Rheingold, A. L.; Francesconi, L. C., *Inorg. Chem.* **2002,** 41, 6112-6117.

22. Luo, Q.-H.; Howell, R. C.; Dankova, M.; Bartis, J.; Williams, C. W.; William DeW. Horrocks, J.; Victor G. Young, J., II; Rheingold, A. L.; Francesconi, L. C.; Antonio, M. R., *Inorg. Chem.* **2001,** 40, 1849-1901.

23. Gaunt, A. J.; May, I.; Collison, D.; Fox, O. D., *Inorg. Chem.* **2003,** 42, 5049-5051.

24. Boglio, C.; Lenoble, G.; Duhayon, C.; Hasenknopf, B.; Rene Thouvenot; Zhang, C.; Howell, R. C.; Burton-Pye, B. P.; Francesconi, L. C.; Lacote, E.; Thorimbert, S.; Malacria, M.; Afonso, C.; Tabet, J.-C., *Inorg. Chem.* **2006. ,** 45, (3), 1389-1398.

25. Buchler, J. W.; Nawra, M., *Inorg. Chem.* **1994,** 33, 2830-2837.

26. Davoras, E. M.; Spyroulias, C. A.; Mikros, E.; Coutsolelos, A. C., *Inorg. Chem.* **1994,** 33, 3440-3434.

27. Falber, A., New Methods for the Synthesis of Bis(Tetra-aryl Porphyrinato)cerium (IV) Complexes: Crystal Structures and NMR studies of Homeleptic and heteroleptic Complexes. In Hunter College: New York, 2007.

28. Kato, C. N.; Shinohara, A.; Hayashi, K.; Nomiya, K., *Inorg. Chem.* **2006,** 45, 8108-8119.

Porphyrinato-Hf(IV)-POM appendix

I. $(TPP)HfPW_{11}O_{39}[TBA]_5$

- A. UV-Vis and ESI-MS spectra
- B. IR spectrum
- C. ^{31}P NMR spectra

II. $(TPyP)HfPW_{11}O_{39}[TBA]_5$

- A. UV-Vis and ESI-MS spectra
- B. IR spectrum
- C. H^1 NMR 1D and COSY
- D. ^{31}P NMR spectrum

Figure 1.
UV-Vis spectrum of a 50 μM solution of (TPP)$HfPW_{11}O_{39}[TBA]_5$ in CH_2Cl_2 in a 1mm glass cuvette

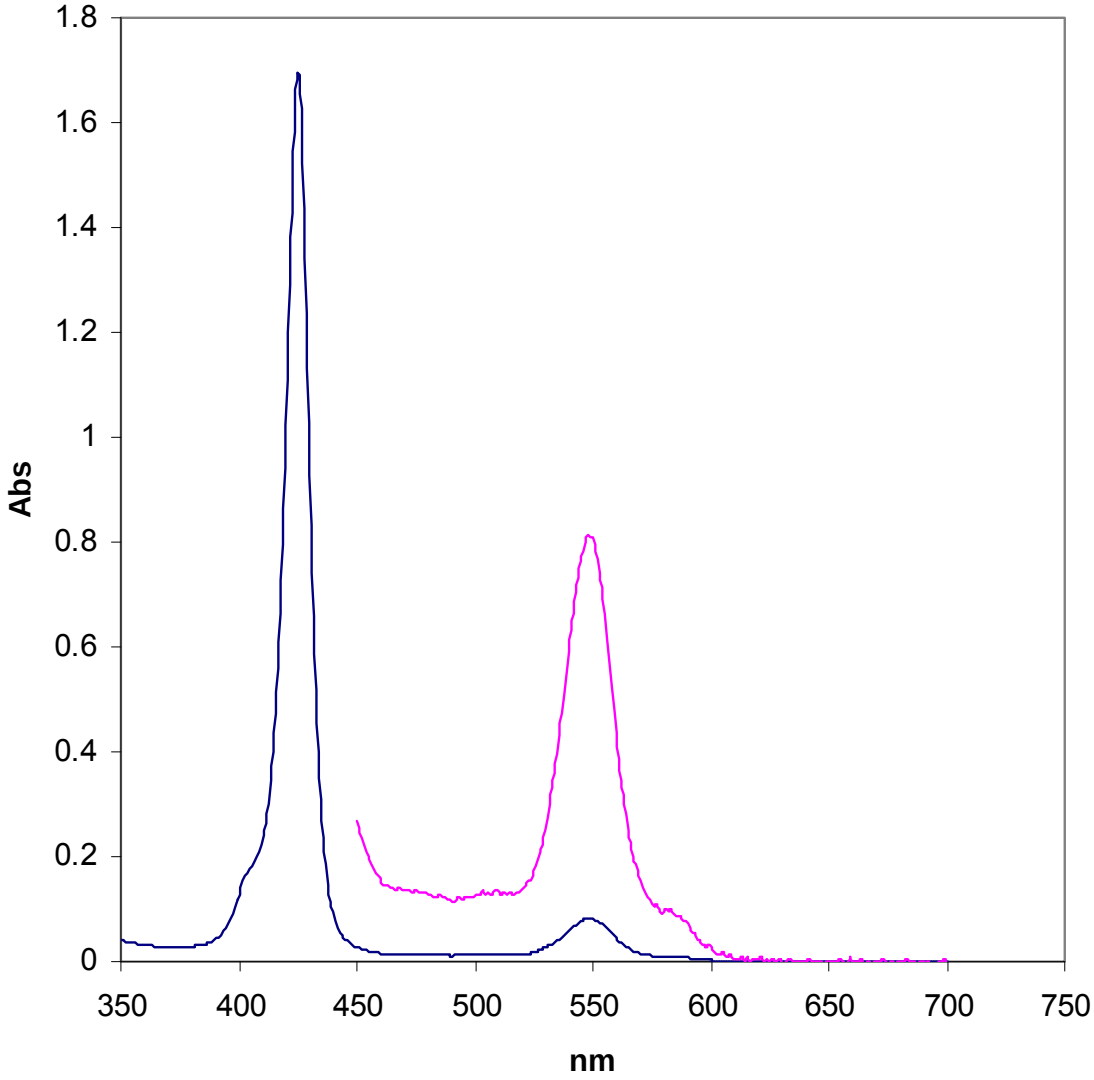

Figure 2.

ESI-MS of (TPP)$HfPW_{11}O_{39}$ with partial decomposition by loss of oxygen or demetalation of the porphyrin

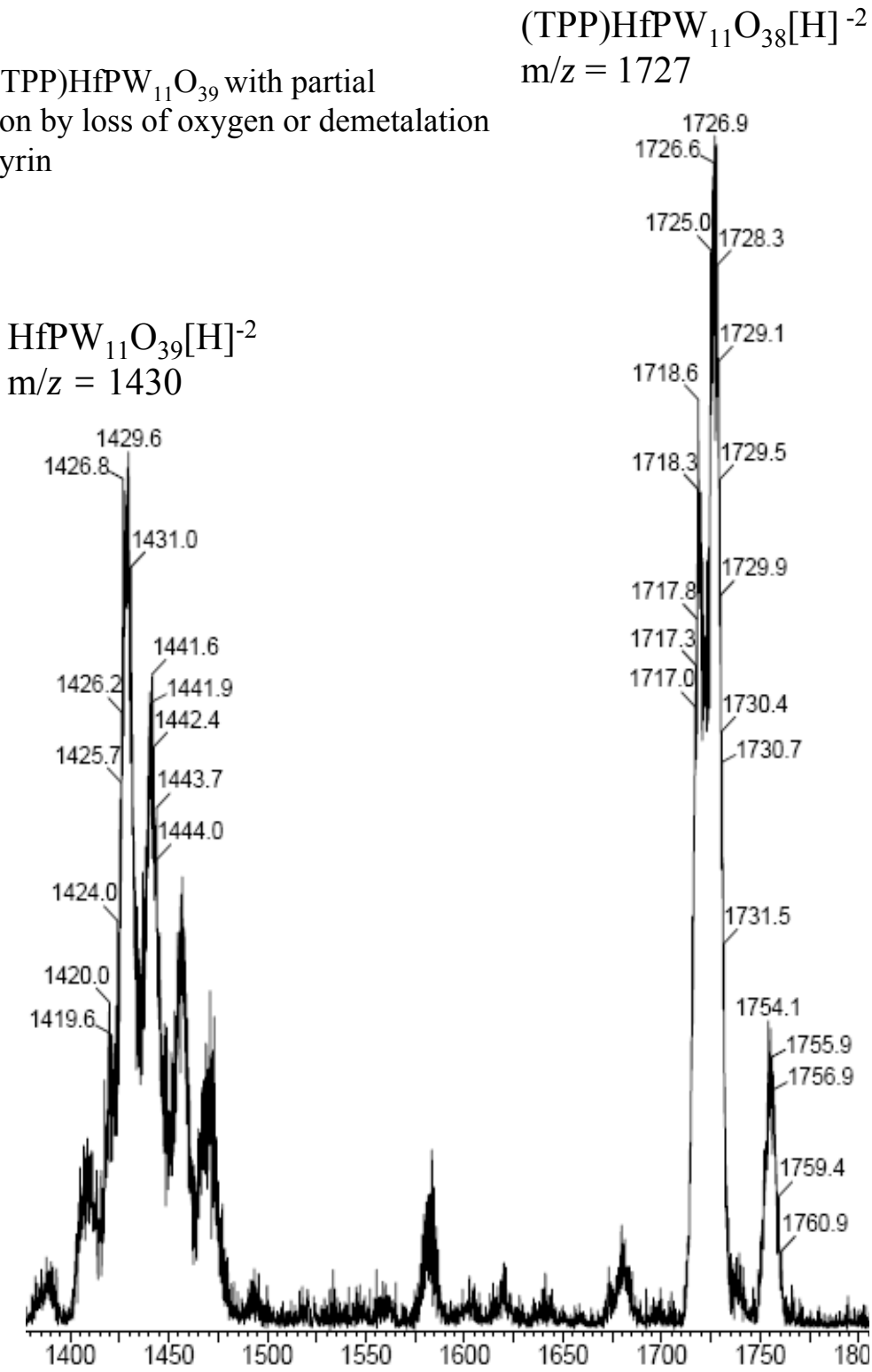

Figure 3. IR spectrum of (TPP)$HfPW_{11}O_{39}[TBA]_5$

Peak finding results for: pomtpp
Frequency: 644.61 - 1125.63, threshold: 94.371-94.929, sensitivity: 77.00
Peak finding result table:

Peak#	1	2	3	4	5	6	7	8	9
Position	1063.26	1002.37	993.53	958.46	890.43	816.23	753.54	723.63	701.68
Height	90.900	92.479	92.499	86.918	90.165	83.944	90.576	87.749	93.114

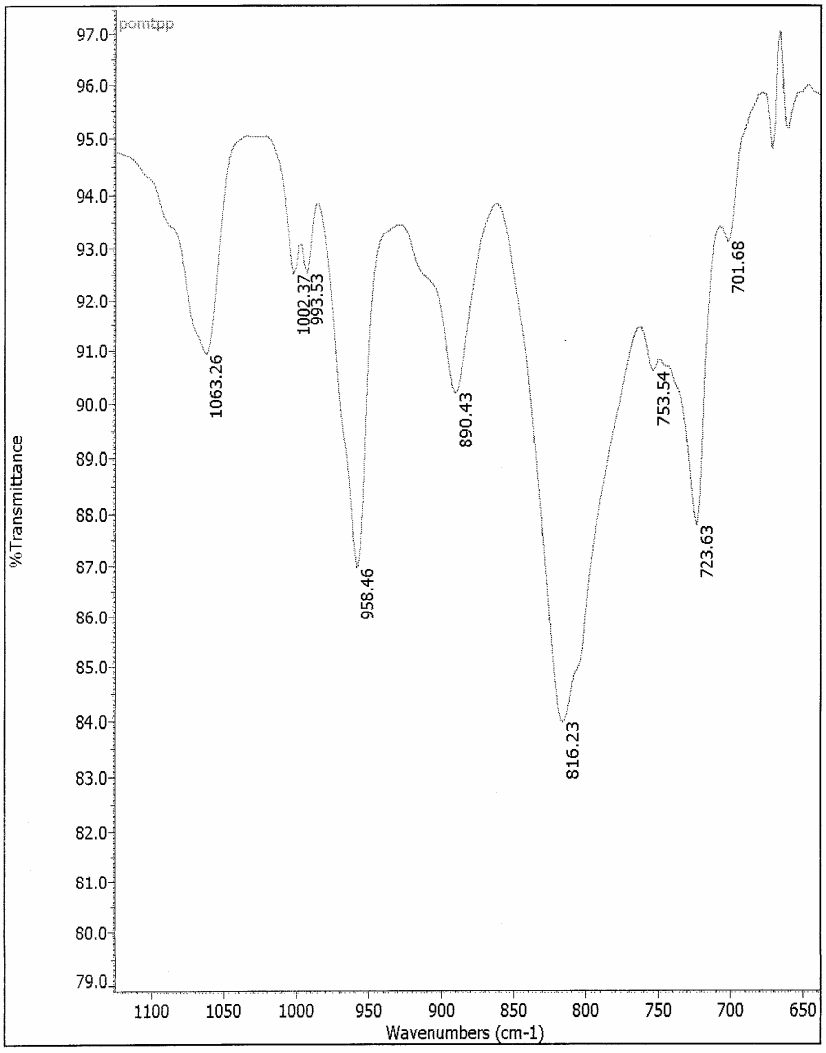

Figure 4. ^{31}P NMR of (TPP)$HfPW_{11}O_{39}[TBA]_5$ in CD_3CN, 20%CH_3CN

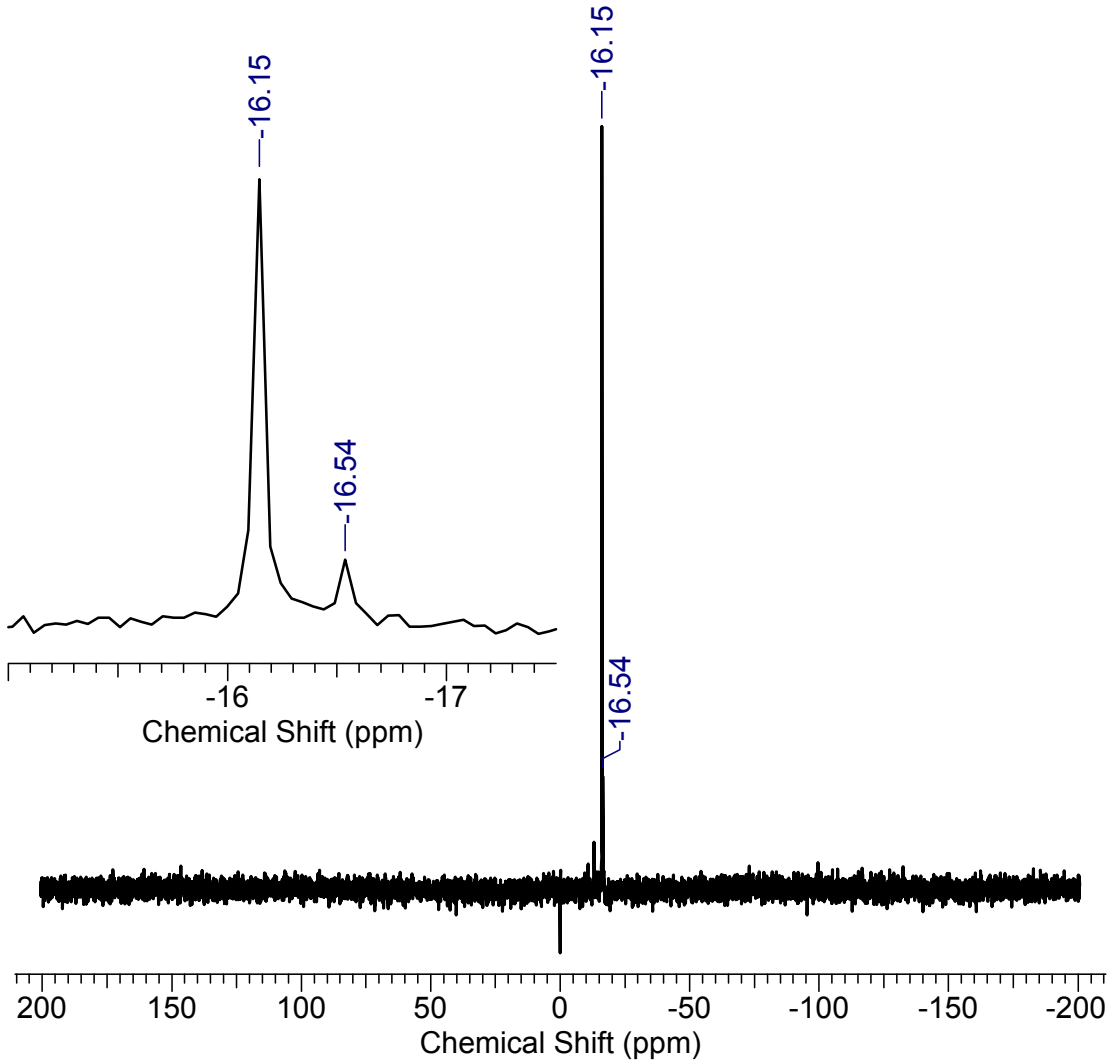

Figure 5. P^{31} NMR of (TPP)$HfPW_{11}O_{39}^{-5}$ with a 15% excess of POM showing peaks between -9.5 and -13.5 in addition to the peaks at -16.2 for the ternary complex. Demetallation of the porpyrin is apparent and distinction between the phosphate peak for the ternary complex and various $HfPW_{11}O_{39}$ complexes without porphyrin is shown

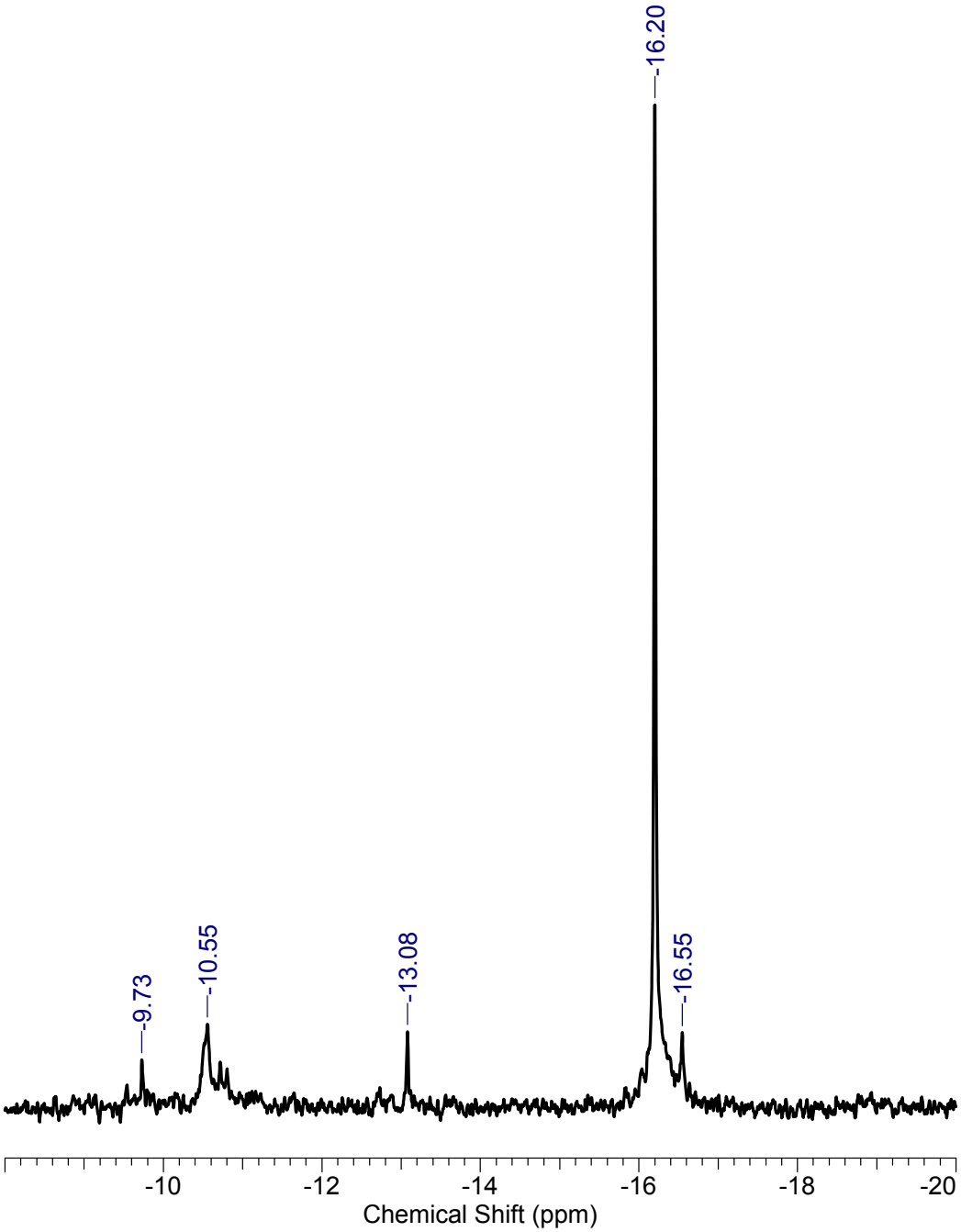

Figure 6.

UV-Vis spectrum of a 100 μM solution (TPyP)$HfPW_{11}O_{39}[TBA]_5$ in CH_2Cl_2 in a 1mm glass cuvette

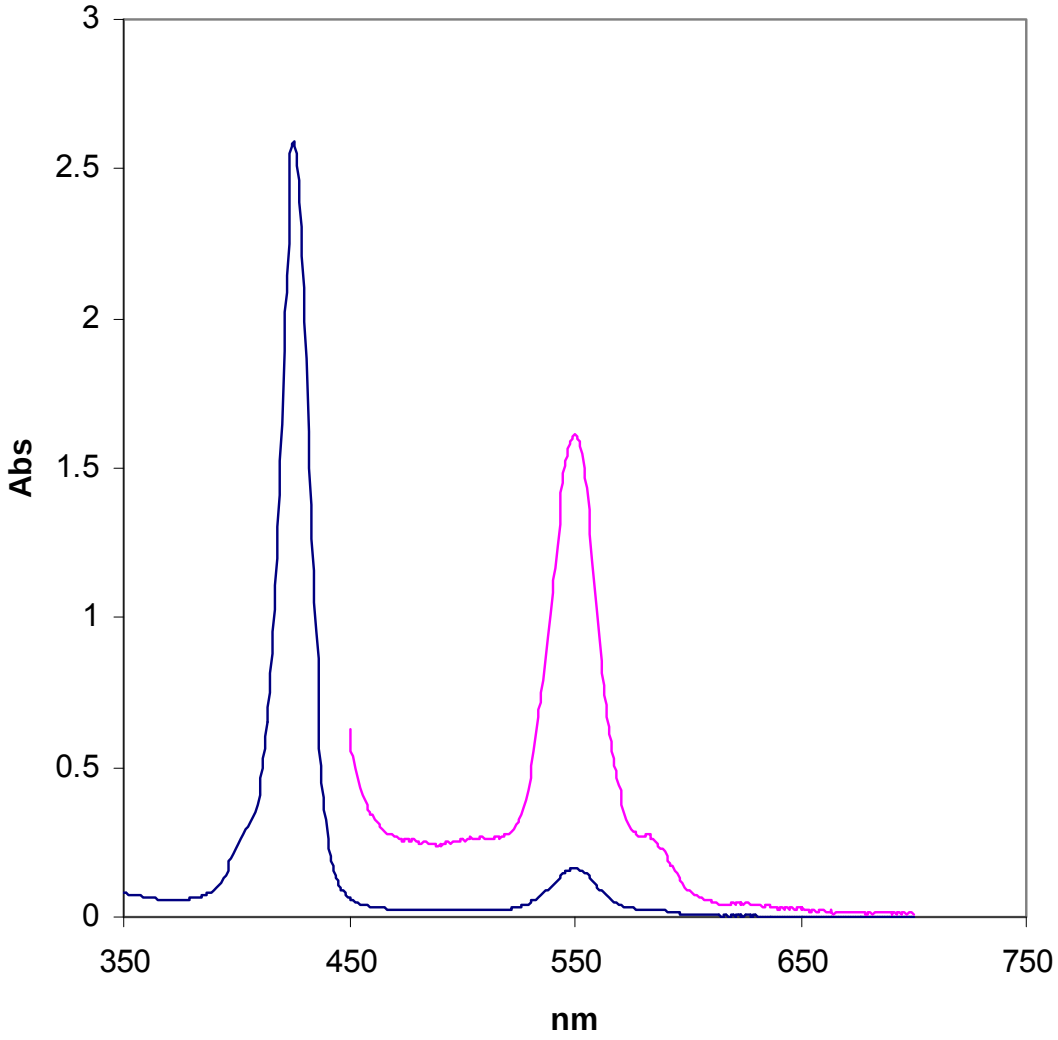

Figure 7.
ESI-MS spectrum of (TPyP)HfPW$_{11}$O$_{39}$[TBA]$_5$ with partial decomposition by loss of oxygen

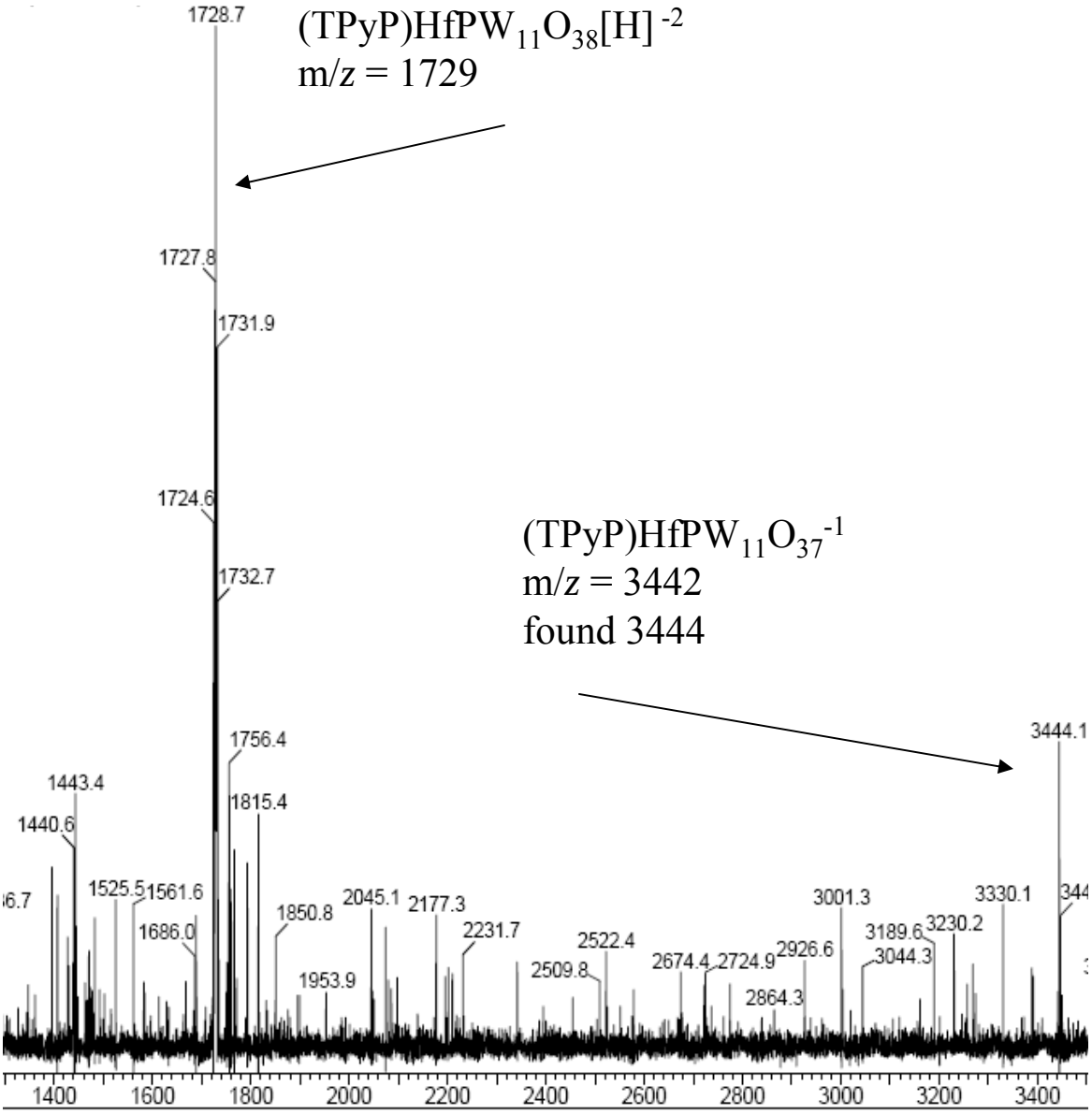

Figure 8. IR spectrum of (TPyP)HfPW$_{11}$O$_{39}$[TBA]$_5$

Peak finding results for: pom[tpyrp]
Frequency: 711.26 - 1188.74, threshold: 80.386-115.163, sensitivity: 100.00
Peak finding result table:

Peak#	1	2	3	4	5	6	7	8
Position	1132.98	1105.52	1076.79	1054.40	987.04	948.88	879.99	825.96
Height	99.674	106.525	100.258	79.793	99.877	56.058	68.277	41.679

Peak#	9	10	11					
Position	806.38	794.43	748.92					
Height	43.855	44.443	67.392					

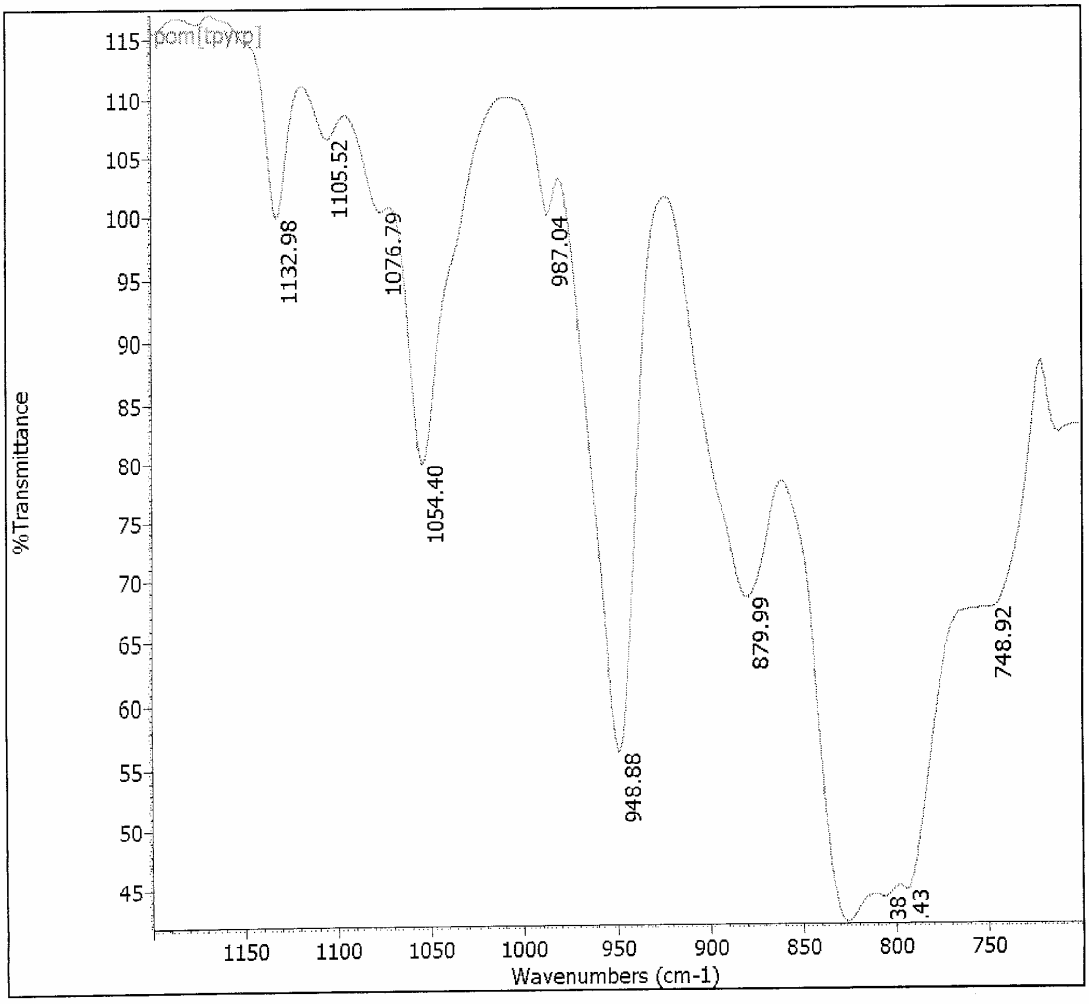

Figure 9. H^1 NMR of (TPyP)$HfPW_{11}O_{39}[TBA]_5$

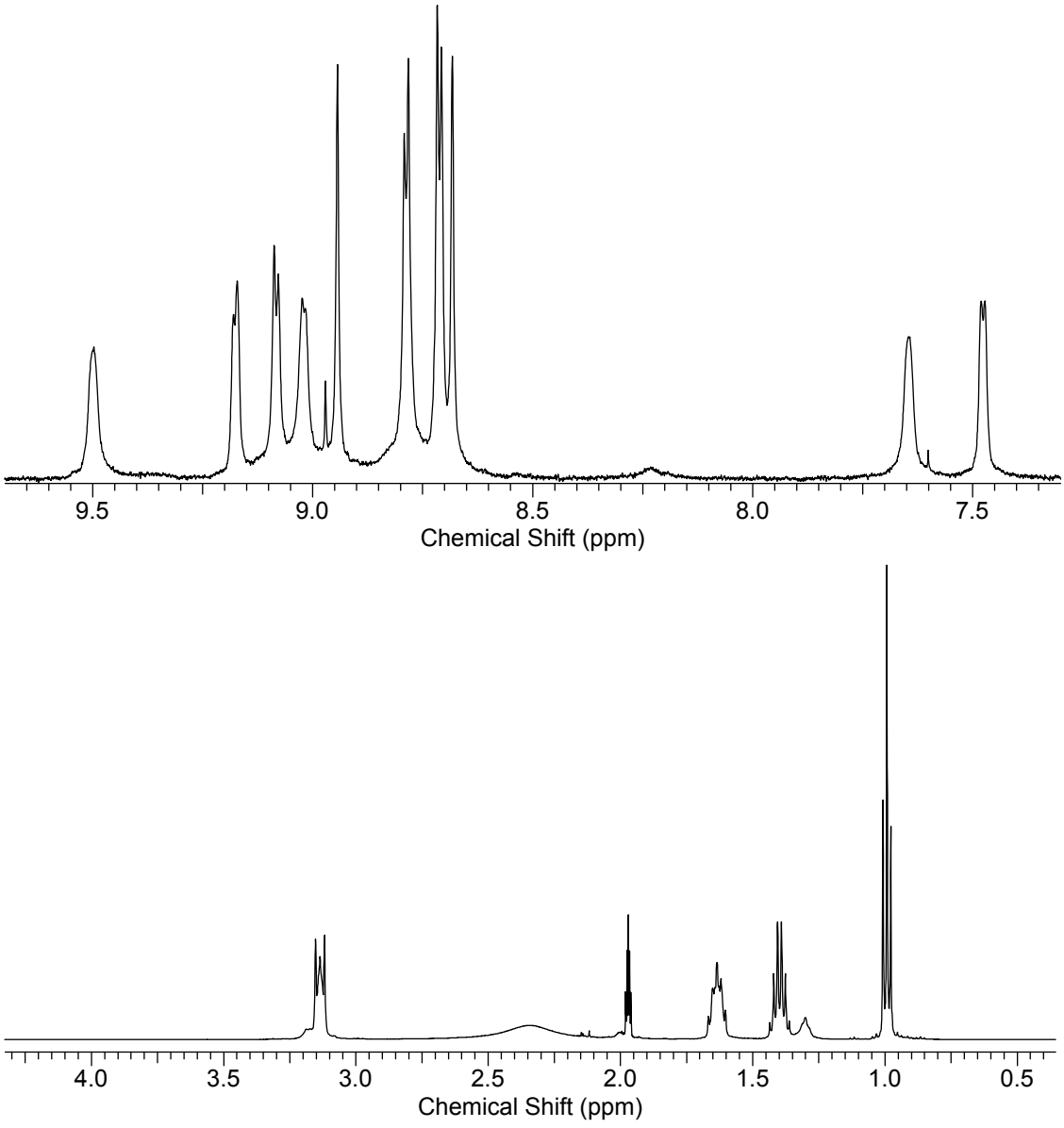

Figure 10. H^1 COSY NMR of $(TPyP)HfPW_{11}O_{39}[TBA]_5$

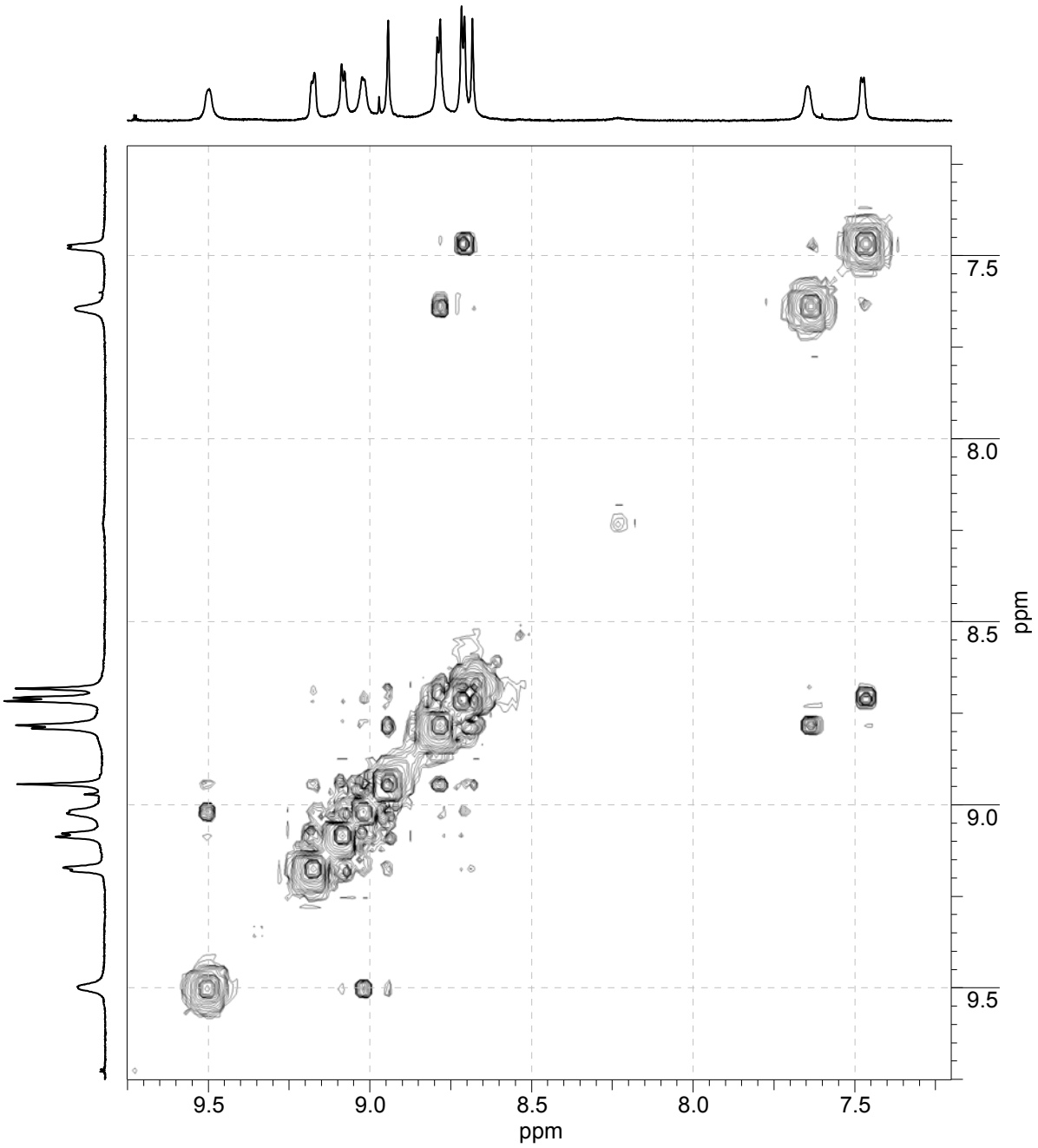

Figure 11. ^{31}P NMR of $(TPyP)HFPW_{11}O_{39}$ in CD_3CN, 20% CH_3CN

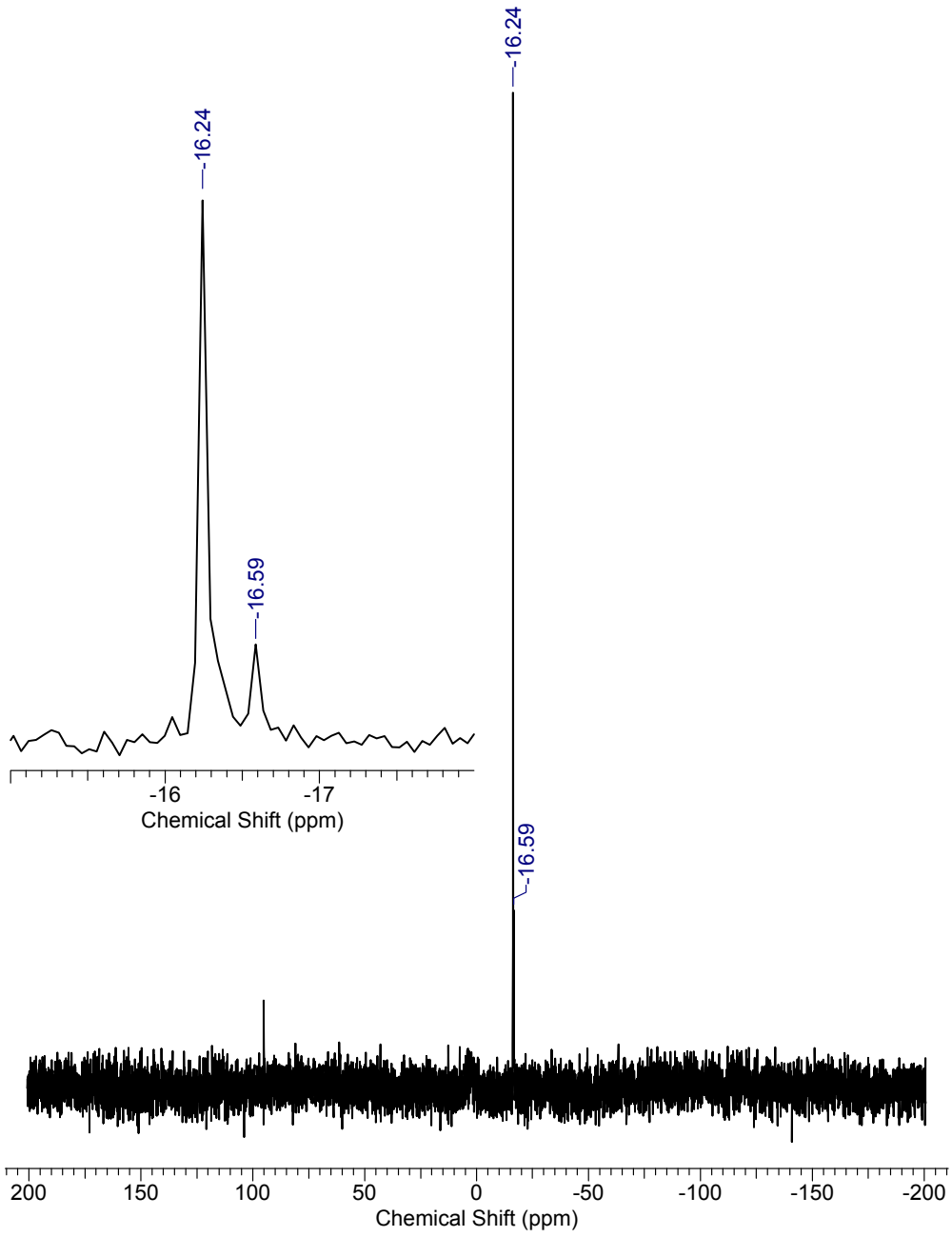

Bibliography

Introduction

1. Drain, C. M.; Shi, X.; Milic, T.; Nifiatis, F., *Chem. Commun.* **2001**, 287-288 (Adendum 1418).

2. Diskin-Posner, Y.; Dahal, S.; Goldberg, I., *Angew. Chem. Int. Ed.* **2000,** 39, (7), 1288-1292.

3. Buchler, J. W.; Ng, D. K. P., Metal Tetrapyrrole Double- and Triple-Deckers with Special Emphasis on Porphyrin Systems. In *The Porphyrin Handbook*, Kadish, K. M.; Smith, K. M.; Guilard, R., Eds. Academic Press:: San Diego, 2000; Vol. 3, pp 245-294.

4. Kadish, K. M.; Smith, K. M.; Guilard, R., *The Porphyrin Handbook*. Academic Press: San Diego, 2000.

5. Mauzerall, D. C., *Clin. Dermatol.* **998,** 16, (6), 195-201.

6. Drain, C. M.; Fischer, R.; Nolen, E.; Lehn, J. M., *Chem. Commun.* **1993**, 243-245.

7. Drain, C. M.; Lehn, J.-M., *Chem. Commun.* **1994**, 2313-2315 (correction 1995, p503).

8. Drain, C. M.; Nifiatis, F.; Vasenko, A.; Batteas, J. D., *Angew. Chem. Int. Ed.* **1998,** 37, (17), 2344-2347.

9. Milic, T.; Garno, J. C.; Smeureanu, G.; Batteas, J. D.; C. M. Drain, *Langmuir* **2004,** 20, 3974-3983.

10. Drain, C. M.; Goldberg, I.; Sylvain, I.; Falber, A., *Top. Curr. Chem.* **2005,** 245, 55–88.

11. Goldberg, I., *Chem. Comm.* **2005**, 1243-1254.

12. Goldberg, I., *Cryst. Eng. Comm.* **2002,** 4, 109-116.

13. Diskin-Posner; Patra, G. K.; Goldberg, I., *Eur. J. of Inorg. Chem.* **2001,** 2001, (10), 2515-2523.

14. Yael Diskin-Posner, G. K. P. a. I. G., *Cryst. Eng. Comm.* **2002,** 4, 296-301.

15. Goldberg, I., *Chem. Eur. J.* **2000,** 6, (21), 3863-3870.

16. Shmilovits, M.; Diskin-Posner, Y.; Vinodu, M.; Goldberg, I., *Cryst. Growth Des.* **2003,** 3, (5), 855-863.

17. Diskin-Posner, Y.; Dahal, S.; Goldberg, I., *Angew. Chem. Int. Ed.* **2000,** 39, (7), 1288-1292.

18. Nazeeruddin, M. K.; Pèchy, P.; Renouard, T.; Zakeeruddin, S. M.; Humphry-Baker, R.; Comte, P.; Liska, P.; Cevey, L.; Costa, E.; Shklover, V.; Spiccia, L.; Deacon, G. B.; Bignozzi, C. A.; Graetzel, M., *J. Am. Chem. Soc.* **2001,** 123, (1613-1624).

Chapter 1

1. Buchler, J. W.; Ng, D. K. P., Metal Tetrapyrrole Double- and Triple-Deckers with Special Emphasis on Porphyrin Systems. In *The Porphyrin Handbook*, Kadish, K. M.; Smith, K. M.; Guilard, R., Eds. Academic Press:: San Diego, 2000; Vol. 3, pp 245-294.

2. Bian, Y.; Jiang, J.; Tao, Y.; Choi, M. T. M.; Li, R.; Ng, A. C. H.; Zhu, P.; Pan, N.; Sun, X.; Arnold, D. P.; Zhou, Z. Y.; Li, H. W.; Mak, T. C. W.; Ng, D. K. P., *J. Am. Chem. Soc.* **2003,** 125, (40), 12257-12267.

3. Gross, T.; Chevalier, F.; Lindsey, J. S., *Inorg. Chem.* **2001,** 40, (18), 4762-4774.

4. Gryko, D.; Li, J.; Diers, J. R.; Roth, K. M.; Bocian, D. F.; Kuhr, W. G.; Lindsey, J. S., *J. Mat. Chem.* **2001,** 11, (4), 1162-1180.

5. Clausen, C.; Gryko, D. T.; Yasseri, A. A.; Diers, J. R.; Bocian, D. F.; Kuhr, W. G.; Lindsey, J. S., *J. Org. Chem.* **2000,** 65, (22), 7371-7378.

6. Otsuki, J.; Kawaguchi, S.; Yamakawa, T.; Asakawa, M.; Miyake, K., *Langmuir* **2006,** 22, (13), 5708-5715.

7. Li, Q. L.; Surthi, S.; Mathur, G.; Gowda, S.; Zhao, Q.; Sorenson, T. A.; Tenent, R. C.; Muthukumaran, K.; Lindsey, J. S.; Misra, V., *Appl. Phys. Lett.* **2004,** 85, (10), 1829-1831.

8. Qian, D. J.; Liu, H. G.; Jiang, J., *Colloids Surf., A* **2000,** 163, (2-3), 191-197.

9. Buchler, J. W.; Scharbert, B., *J. Am. Chem. Soc.* **1988,** 110, (13), 4272-4276.

10. Ikeda, M.; Takeuchi, M.; Shinkai, S.; Tani, F.; Naruta, Y.; Sakamoto, S.; Yamaguchi, K., *Chem. Eur. J.* **2002,** 8, (24), 5541-5550.

11. Shinkai, S.; Ikeda, M.; Sugasaki, A.; Takeuchi, M., *Acc. Chem. Res.* **2001,** 34, (6), 494-503.

12. Takeuchi, M.; Imada, T.; Shinkai, S., *Angew. Chem. Int. Ed.* **1998,** 37, (15), 2096-2099.

13. Sugasaki, A.; Ikeda, M.; Takeuchi, M.; Shinkai, S., *Angew. Chem. Int. Ed.* **2000,** 39, (21), 3839-3842.

14. Goldberg, I., *Chem. Comm.* **2005**, 1243-1254.

15. Goldberg, I., *Cryst. Eng. Comm.* **2002,** 4, 109-116.

16. Drain, C. M.; Goldberg, I.; Sylvain, I.; Falber, A., *Top. Curr. Chem.* **2005,** 245, 55–88.

17. Drain, C. M.; Lehn, J.-M., *Chem. Commun.* **1994**, 2313-2315 (correction 1995, p503).

18. Drain, C. M.; Nifiatis, F.; Vasenko, A.; Batteas, J. D., *Angew. Chem. Int. Ed.* **1998,** 37, (17), 2344-2347.

19. Drain, C. M.; Hupp, J. T.; Suslick, K. S.; Wasielewski, M. R.; Chen, X., *J. Porph. Phthal.* **2002,** 6, (4), 241-256.

20. Montalban, A. G.; Michel, S. L. J.; Baum, S. M.; Vesper, B. J.; White, A. J. P.; Williams, D. J.; Barrett, A. G. M.; Hoffman, B. M., *J. Chem. Soc. Dalton Trans.* **2001**, 3269-3273.

21. Buchler, J. W.; Kapellmann, H.-G.; Knoff, M.; Lay, K.-L.; Pfeifer, S., *Z. Naturforsch* **1983,** 38b, 1339-1345.

22. Buchler, J. W.; DeCian, A.; Fischer, J.; M.Kihn-Botulinski; Paulus, H.; Weiss, R., *J. Am. Chem. Soc.* **1986,** 108, 3652-3659.

23. Girolami, G. S.; Milam, S. N.; Suslick, K. S., *J. Am. Chem. Soc.* **1988,** 110, 2012-2013.

24. Girolami, G. S.; Milam, S. N.; Suslick, K. S., *Inorg. Chem.* **1987,** 26, (3), 343-344.

25. Roberts, J. D.; Hammond, G. S.; Cram, D. J., *Annu. Rev. Phys. Chem.* **1957,** 8, 299-330.

26. Buchler, J. W.; Nawra, M., *Inorg. Chem.* **1994,** 33, 2830-2837.

27. Jiang, J.; Machida, K.-i.; Adachi, G.-y., *J. Alloys Compd.* **1993,** 192, (1-2), 296-299.

28. Buchler, J. W.; Dippell, T., *Eur. J. Inorg. Chem.* **1998**, (4), 445-449.

29. Bernstein, P. A.; Lever, A. B. P., *Inorg. Chem.* **1990,** 29, (4), 608-616.

30. Tashiro, K.; Konishi, K.; Aida, T., *J. Am. Chem. Soc.* **2000,** 122, (33), 7921-7926.

31. S.Radzki; Giannotti, C., *J. Chem. Soc., Dalton Trans.* **1993**, 675 - 679.

32. Drain, C. M.; Kirmaier, C.; Medforth, C. J.; Nurco, D. J.; Smith, K. M.; Holten, D., *J. Phys. Chem.* **1996,** 100, (29), 11984-11993.

33. Drain, C. M.; Gentemann, S.; Roberts, J. A.; Nelson, N. Y.; Medforth, C. J.; Jia, S.; Simpson, M. C.; Smith, K. M.; Fajer, J.; Shelnutt, J. A.; Holten, D., *J. Am. Chem. Soc.* **1998,** 120, (15), 3781-3791.

34. Retsek, J. L.; Drain, C. M.; Kirmaier, C.; Nurco, D. J.; Medforth, C. J.; Smith, K. M.; Sazanovich, I. V.; Chirvony, V. S.; Fajer, J.; Holten., D., *J. Am. Chem. Soc.* **2003,** 125, 9787-9800.

35. Bilsel, O.; Rodriguez, J.; Milam, S. N.; Corlin, P. A.; Girolami, G. S.; Suslick, K. S.; Holten, D., *J. Am. Chem. Soc.* **1992,** 114, 6528-6538.

36. Borovkov, V. V.; Lintuluoto, J. M.; Fujiki, M.; Inoue, Y., *J. Am. Chem. Soc.* **2000,** 122, (18), 4403-4407.

37. Ponomarev, G. V.; Borovkov, V. V.; Sugiura, K.; Sakata, Y.; Shul'ga, A. M., *Tetrahedron Lett.* **1993,** 34, (13).

38. Davoras, E. M.; Spyroulias, G. A.; Mikros, E.; Coutsolelos, A. G., *Inorg. Chem.* **1994,** 33, 3430-3434.

39. Ercolani, G., *Org. Lett.* **2005,** 7, (5), 803-805.

40. Sugasaki, A.; Ikeda, M.; Takeuchi, M.; Koumoto, K.; Shinkai, S., *Tetrahedron* **2000,** 56, (27), 4717-4723.

41. Takeuchi, M.; Imada, T.; Ikeda, M.; Shinkai, S., *Tetrahedron Lett.* **1998,** 39, (43), 7897-7900.

42. Tashiro, K.; Fujiwara, T.; Konishi, K.; Aida, T., *Chem. Comm.* **1998**, (10), 1121-1122.

43. Spek, A. L., *J. Appl. Crystallogr.* **2003,** 36, (1), 7-13.

44. Gorbunova, Y. G.; Lapkina, L. A.; Martynov, A. G.; Biryukova, I. V.; Tsivadze, A. Y., *Russ. J. Org. Chem.* **2004,** 30, (4), 245-251.

45. Adler, A. D.; Longo, F. R.; Finarelli, J. D.; Goldmacher, J.; Assour, J.; Korsakoff, L., *J. Org. Chem.* **1967,** 32, 476-480.

46. Drain, C. M., *Proc. Natl. Acad. Sci., USA* **2002,** 99, 5178-5182.

47. Drain, C. M.; Batteas, J. D.; Flynn, G. W.; Milic, T.; Chi, N.; Yablon, D. G.; Sommers, H., *Proc. Natl. Acad. Sci., USA* **2002,** 99, 6498-6502.

48. Drain, C. M.; Chen, X., Self-Assembled Porphyrinic Nanoarchitectures. In *Encyclopedia of Nanoscience & Nanotechnology*, Nalwa, H. S., Ed. American Scientific Press: New York, 2004; Vol. 9, pp 593-616.

49. Milic, T. N.; Chi, N.; Yablon, D. G.; Flynn, G. W.; Batteas, J. D.; Drain, C. M., *Angew. Chem., Int. Ed.* **2002,** 41, 2117-2119.

50. Drain, C. M.; Bazzan, G.; Milic, T.; Vinodu, M.; Goeltz, J. C., *Israel J. Chem.* **2005,** 45, 255-269.

Chapter 2

1. Spek, A. L., *J. Appl. Crystallogr* **2003,** 36, 7-13.

2. Ryu, S.; Whang, D.; Kim, J.; Yeo, W.; Kim, K., *J. Chem. Soc., Dalton Trans.* **1993**, 205-209.

3. Ryu, S.; Kim, J.; Yeo, H.; Kim, K., *Inorg. Chim. Acta* **1995,** 228, (12), 233-236.

4. Afzal, D.; Baughman, R.; James, A.; Westmeyer, M., *Supramol. Chem.* **1996,** 6, (3-4), 395-399.

5. Huhmann, J. L.; Rath, N. P.; Corey, J. Y., *Acta Crystallogr., Sect. C: Cryst. Struct. Commun.* **1996,** 52, (10), 2486-2488.

6. Knor, G.; Strasser, A., *Inorg. Chem. Commun.* **2002,** 5, (11), 993-995.

7. Tipugina, M. Y.; Lomova, T. N., *Russ. J. Inorg. Chem.* **2004,** 49, (6), 961-965.

8. Martin, P. C.; Amold, J.; Bocian, D. F., *J. Phys. Chem.* **1993,** 97, 1332-1338.

9. Brand, H.; Capriotti, J. A.; Arnold, J., *Organometallics* **1994,** 13, (11), 4469-4473.

10. Huhmann, L. J.; Corey, J. Y.; Rath, N. P.; Campana, C. F., *J. Organomet. Chem.* **1996,** 513, (1-2), 17-26.

11. Ryu, S.; Whang, D.; Kim, H. J.; Kim, K.; Yoshida, M.; Hashimoto, K.; Tatsumi, K., *Inorg. Chem.* **1997,** 36, (20), 4607-4609.

12. Thorman, J. L.; Guzei, I. A.; Jr, V. G. Y.; Woo, L. K., *Inorg. Chem.* **1999,** 38, (17), 3814-3824.

13. Thorman, J. L.; Guzei, I. A., *Inorg. Chem.* **2000,** 2344-2352, (11), 23.

14. Tomachynski, L. A.; Chernii, V. Y.; Volkov, S. V., *J. Porphyrins Phthalocyanines* **2001,** 5, (10), 731-734.

15. Tomachynski, L. A.; Chernii, V. Y.; Volkov, S. V., *Russ. J. Inorg. Chem.* **2002,** 47, (2), 208-211.

16. Gerasymchuk, Y. S.; Chernii, V. Y.; Tomachynski, L. A.; Legendziewicz, J.; Radzki, S., *Opt. Mater.* **2005,** 27, (9), 1484-1494.

17. Knor, G.; Strasser, A., *Inorg. Chem. Commun.* **2005,** 8, (5), 471-473.

18. Brand, H.; Arnold, J., *Organometallics* **1993,** 12, (9), 3655-3665.

19. Brand, H.; Arnold, J., *J. Am. Chem. Soc.* **1992,** 114, (6), 2266-2267.

20. Shibata, K.; Aida, T.; Inoue, S., *Tetrahedron Lett.* **1992,** 33, (8), 1077-1080.

21. Kim, H. J.; Whang, D.; Kim, K.; Do, Y., *Inorg. Chem.* **1993,** 32, (3), 360-362.

22. Kim, H.-J.; Whang, D.; Do, Y.; Kim, a. K., *Chem. Lett.* **1993,** 22, (5), 807-810.

23. Buchler, J. W.; Heinz, G., *Chem. Ber.* **1996,** 129, (2), 201-205.

24. Collman, J. P.; Kendall, J. L.; Chen, J. L.; Eberspacher, T. A.; Moylan, C. R., *Inorg. Chem.* **1997,** 36, (24), 5603-5608.

25. Fryzuk, M. D.; B.Love, J.; Rettig, S. J., *Organometallics* **1998,** 17, (5), 846-853.

26. Kim, H. J.; Jung, S.; Jeon, Y. M.; Whang, D.; Kim, K., *Chem. Commun.* **1999**, (11), 1033-1034.

27. Stulz, E.; Burgi, H. B.; Leumann, C., *Chem.-Eur. J.* **2000,** 6, (3), 523-536.

28. Witowska-Jarosz, J.; Gorski, L.; Malinowska, E.; Jarosz, M., *J. Mass Spectrom.* **2002,** 37, (12), 1236-1241.

29. Pistorio, B. J.; Nocera, D. G., *J. Photochem. Photobiol., A* **2004,** 162, (2-3), 563-567.

30. Du, G.; Woo, L. K., *Organometallics* **2003,** 22, (3), 450-455.

31. Collman, J. P.; Kendall, J. L.; Chen, J. L., *Inorg. Chem.* **2000,** 39, (8), 1661-1667.

32. Guilard, R.; Barbe, J.-M.; Ibnlfassi, A.; Zrineh, A.; Adamian, V. A.; Kadish, K. M., *Inorg. Chem.* **1995,** 34, (6), 1472-1481.

33. Girolami, G. S.; Milam, S. N.; Suslick, K. S., *Inorg. Chem.* **1987,** 26, (3), 343-344.

34. Bernstein, P. A.; Lever, A. B. P., *Inorg. Chem.* **1990,** 29, (4), 608-616.

35. Johnson, T. J.; Disselkamp, R. S.; Su, Y.-F.; Fellows, R. J.; Alexander, M. L.; Driver, C. J., *J. Phys. Chem. A* **2003,** 107, (32), 6138-6190.

36. Ryu, S.; Kim, J.; Yeo, H.; Kim, K., *Inorg. Chim. Acta* **1995,** 228, (2), 233-236.

37. Arnold, J.; Hoffman, C. G.; Dawson, D. Y.; Hollander, F. J., *Organometallics* **1993,** 12, 3645-3654.

38. Gomila, R. M.; Quinonero, D.; Rotger, C.; Garau, C.; Frontera, A.; Ballester, P.; Costa, A.; Deya, P. M., *Org. Lett.* **2002,** 4, (3), 399-401.

39. Ojadi, E.; Selzer, R.; Linschitz, H., *J. Am. Chem. Soc.* **1985,** 107, 7783-7784.

40. Buchler, J. W.; Schneehage, Z., *Naturforsch* **1973,** B28, 433.

41. Ghiladi, R. A.; Ju, T. D.; Lee, D.-H.; Moenne-Loccoz, P.; Kaderli, S.; Neuhold, Y.-M.; Zuberbuhler, A. D.; Woods, A. S.; Cotter, R. J.; Karlin, K. D., *J. Am. Chem. Soc.* **1999,** 121, (42), 9885-9886.

42. Drain, C. M.; Gentemann, S.; Roberts, J. A.; Nelson, N. Y.; Medforth, C. J.; Jia, S.; Simpson, M. C.; Smith, K. M.; Fajer, J.; Shelnutt, J. A.; Holten, D., *J. Am. Chem. Soc.* **1998,** 120, (15), 3781-3791.

43. Retsek, J. L.; Drain, C. M.; Kirmaier, C.; Nurco, D. J.; Medforth, C. J.; Smith, K. M.; Sazanovich, I. V.; Chirvony, V. S.; Fajer, J.; Holten., D., *J. Am. Chem. Soc.* **2003,** 125, 9787-9800.

44. Wilkinson, C. a., *Advanced Inorganic Chemistry*. John Wiley & Sons: 1999.

45. Bym, M. P.; Curtis, C. J.; Hsiou, Y.; Khan, S. a. d. I.; Sawin, P. A.; Tendick, S. K.; Terzis, A.; Strouse, C. E., *J. Am. Chem. Soc.* **1993,** 115, 9480-9497.

46. Engdahl, A.; Nelander, B., *Phys. Chem. Chem. Phys.* **2000,** 2, 3967-3970.

Chapter 3

1. Dmitrenko, O.; Huang, W.; Polenova, T. E.; Francesconi, L. C.; Wingrave, J. A.; Teplyakov, A. V., *J. Phys. Chem. B* **2003,** 107, (31), 7747-7752.

2. Toth, J. E.; Anson, F. C., *J. Am. Chem. Soc.* **1989,** 111, 2444-2451.

3. Keana, J. F. W.; Ogan, M. D., *J. Am. Chem. Soc.* **1986,** 108, 7951-7957.

4. Keana, J. F. W.; Ogan, M. D.; LU, Y.; Beer, M.; Varkey, J., *J. Am. Chem. Soc.* **1986,** 108, 7957-7963.

5. Katsoulis, D. E., *Chem. Rev.* **1998,** 98, (1), 359-388.

6. Cherian, S.; Wamser, C. C., *J. Phys. Chem. B* **2000,** 104, (15), 3624-3629.

7. Tachibana, Y.; Haque, S. A.; Mercer, I. P.; Durrant, J. R.; Klug, D. R., *J. Phys. Chem. B* **2000,** 104, (6), 1198-1205.

8. Drain, C. M.; Chen., X., Self-Assembled Porphyrinic Nanoarchitectures. In *Encyclopedia of Nanoscience & Nanotechnology*, Nalwa, H. S., Ed. American Scientific Press: New York, 2004; Vol. 9, pp 593-616.

9. Drain, C. M.; Lehn, J.-M., *Chem. Commun.* **1994**, 2313-2315 (correction 1995, p503).

10. Drain, C. M.; Goldberg, I.; Sylvain, I.; Falber, A., *Top. Curr. Chem.* **2005,** 245, 55–88.

11. Chen, X.; Hui, L.; Foster, D. A.; Drain, C. M., *Biochem.* **2004,** 43, (34), 10918-10929.

12. Goldberg, I., *Chem. Comm.* **2005**, 1243-1254.

13. Goldberg, I., *Cryst. Eng. Comm.* **2002,** 4, 109-116.

14. Santos, I. C. M. S.; Rebelo, S. L. H.; Balula, M. S. S.; Martins, R. a. R. L.; Pereira, M. M. M. S.; Simoes, M. a. M. Q.; Neves, M. G. P. M. S.; Cavaleiro, J. e. A. S.; Cavaleiro, A. M. V.,*J. Mol. Catal. A: Chem.* **2005,** 231, (1), 35-45.

15. Babcock, L. M. Synthesis and Characterization of Group 4 Organometal Oxide Complexes. University of Illinois, Urabana-Champaign, 1988.

16. Kim, H. J.; Jung, S.; Jeon, Y. M.; Whang, D.; Kim, K.,*Chem. Comm.* **1997**, (22), 2201-2202.

17. K.Nazeeruddin, M.; Hunphry-Baker, R.; Officer, D. L.; Campbell, W. M.; Burrell, A. K.; Graetzel, M., *Langmuir* **2004,** 20, (15), 6514-6517.

18. Nazeeruddin, M. K.; Pèchy, P.; Renouard, T.; Zakeeruddin, S. M.; Humphry-Baker, R.; Comte, P.; Liska, P.; Cevey, L.; Costa, E.; Shklover, V.; Spiccia, L.; Deacon, G. B.; Bignozzi, C. A.; Graetzel, M., *J. Am. Chem. Soc.* **2001,** 123, (1613-1624).

19. Huhmann, J. L.; Corey, Y. J.; Rath, N. P.; Campana, C. F., *J. Organomet. Chem.* **1996,** 513, (1-2), 17-26.

20. Falber, A., Synthesis, Characterization, and Crystallography of Hafnium Porphyrinates. In Hunter College: New York, 2007; Vol. Chapter 2.

21. Luo, Q.; Howell, R. C.; Bartis, J.; Dankova, M.; William DeW. Horrocks, J.; Rheingold, A. L.; Francesconi, L. C., *Inorg. Chem.* **2002,** 41, 6112-6117.

22. Luo, Q.-H.; Howell, R. C.; Dankova, M.; Bartis, J.; Williams, C. W.; William DeW. Horrocks, J.; Victor G. Young, J., II; Rheingold, A. L.; Francesconi, L. C.; Antonio, M. R., *Inorg. Chem.* **2001,** 40, 1849-1901.

23. Gaunt, A. J.; May, I.; Collison, D.; Fox, O. D., *Inorg. Chem.* **2003,** 42, 5049-5051.

24. Boglio, C.; Lenoble, G.; Duhayon, C.; Hasenknopf, B.; Rene Thouvenot; Zhang, C.; Howell, R. C.; Burton-Pye, B. P.; Francesconi, L. C.; Lacote, E.; Thorimbert, S.; Malacria, M.; Afonso, C.; Tabet, J.-C., *Inorg. Chem.* **2006. ,** 45, (3), 1389-1398.

25. Buchler, J. W.; Nawra, M., *Inorg. Chem.* **1994,** 33, 2830-2837.

26. Davoras, E. M.; Spyroulias, C. A.; Mikros, E.; Coutsolelos, A. C., *Inorg. Chem.* **1994,** 33, 3440-3434.

27. Falber, A., New Methods for the Synthesis of Bis(Tetra-aryl Porphyrinato)cerium (IV) Complexes: Crystal Structures and NMR studies of Homeleptic and heteroleptic Complexes. In Hunter College: New York, 2007.

28. Kato, C. N.; Shinohara, A.; Hayashi, K.; Nomiya, K., *Inorg. Chem.* **2006,** 45, 8108-8119.